A Novel Role for Activated Leukocyte Cell Adhesion Molecule (ALCAM) in Neurotrophin Signalling in Neurons

Anna Wade

University College London Institute of Neurology

and

Cancer Research UK London Research Institute

PhD Supervisors:

Linda Greensmith

Giampietro Schiavo

A thesis submitted for the degree of

Doctor of Philosophy

University College London

2011

Declaration

I Anna Wade confirm that the work presented in this thesis is my own. Where information has been derived from other sources, I confirm that this has been indicated in the thesis.

Abstract

The classical immunoglobulin family of cell adhesion molecules, known as the IgCAMs, have been characterised as having an important adhesive function at areas of cell-cell contact and from cell to extracellular matrix. Members of this family have been shown to participate in signal transduction and increasingly it seems that this could be a general feature of the IgCAM family rather than the exception. We aimed to determine whether IgCAMs that undergo retrograde axonal transport in neurons contribute to neuronal viability and co-operate with neurotrophin signalling.

Activated Leukocyte Cell Adhesion Molecule (ALCAM) was identified in cells of immune system as the binding partner of the T-cell glycoprotein CD6, where it contributes to normal T-cell activation. Additionally ALCAM has been shown to have an important role in the nervous system, where it is involved in neuron pathfinding and development of the neuromuscular junction.

We identified ALCAM as a protein associated with the axonal retrograde transport compartment containing neurotrophins and their receptors in primary ventral horn neurons. I found that ALCAM is bidirectionally transported in neurons, and predominantly cotransported with the neurotrophin receptor $p75^{NTR}$ toward the cell body. Furthermore, I found ALCAM could specifically potentiate neurotrophic signalling. ALCAM overexpression resulted in extension of longer neuritic processes in PC12 cells treated with nerve growth factor (NGF). The extracellular domain is both necessary and sufficient to potentiate NGF-induced neurite outgrowth, while the transmembrane and cytoplasmic domain have no effect. ALCAM overexpression only potentiated specific growth factor stimuli but had no effect on other pathways leading to differentiation or on undifferentiated PC12 cell morphology.

In conclusion, ALCAM appears to synergise with NGF signalling to induce neuronal differentiation and may have a role in the nervous system not only as an adhesion molecule but also in neurotrophin signalling.

Acknowledgement

First and foremost I would like to thank Giampietro Schiavo and Linda Greensmith for their input and support over the past three and a half years. I consider myself lucky to have had two supervisors, who have provided complementary expertise and supervision.

Secondly, I would like to thank all the members of both the Molecular Neuropathobiology laboratory, at the LRI and the Greensmith laboratory at the UCL Institute of Neurology for being helpful and enjoyable people to work with. In particular, I would like to thank Jim Dick, for his help maintaining my mouse colony and Bernadett Kalmar for her patience and time with the sprouting study *in vivo*. I also give special thanks to Matthew Golding and Claire Thomas for their wisdom, guidance, good spirits and constant help during my PhD. I would also like to thank David Attwell and the UCL Neuroscience Wellcome Trust committee for giving me the opportunity to take part in such a prestigious and interesting program, as well as Sally Leevers and CRUK for adopting me as a student of the LRI. I am incredibly fortunate that during my PhD I have been involved with such respected institutions as the Wellcome Trust, UCL and CRUK's LRI.

Finally I would like to thank my family, particularly my Mum and Dad for their support and many thanks to my friends, both old and new, who have been a great help to me over the past 4 years through the blood, sweat and tears. My PhD has been a worthwhile experience; I have learnt a lot, both of a scientific nature and some useful life lessons.

Table of Contents

Table of figures

List of tables

Abbreviations

°C	Degrees celsius
2D	Two dimensions
3D	Three dimensions
ADAM	A disintegrin and metalloprotease
ALCAM	Activated leukocyte cell adhesion molecule
ALCAM-D	ALCAM tagged at C-terminal with dendra
ANOVA	Analysis of variance
ATP	Adenosine triphosphate
au	Arbitrary units
BDNF	Brain-derived neurotrophic factor
BoNT/A	Botulinum toxin A
bp	Base pairs
BSA	Bovine serum albumin
C	Constant type-2 Ig domain
CAM	Cell adhesion molecule
cAMP	Cyclic adenosine monophosphate
CAR	Coxsackie virus and adenovirus receptor
CAV-2	Canine adenovirus serotype 2
CD6	CD6-glycoprotein
cDNA	Complementary DNA
CNS	Central nervous system
CNTF	Ciliary neurotrophic factor
CREB	cAMP response element binding protein
dbcAMP	Dibutyryl-cyclic adenosine monophosphate
Dendra	Dendra photoactivatable fluorescent protein
DMEM	Dulbecco's modified eagle's medium
DM-GRASP	Chick orthologue of ALCAM
DMSO	Dimethyl sulfoxide
DNA	Deoxyribonucleic acid
dNTPs	Deoxynucleotide triphosphates
DPT	Days post-transfection

DRG	Dorsal root ganglia
DRM	Detergent resistant membrane
Ec	Extracellular
EDL	Extensor digitorum longus muscle
EDTA	Ethylenediaminetetraacetic acid
EGF	Epidermal growth factor
ERK	Extracellular-signal regulated kinase
FAK	Focal adhesion kinase
Fc	Antibody fragment (cystallisable region) used in protein chimeras
FGF	Fibroblast growth factor
FGFR	Fibroblast growth factor receptor
FNIII	Fibronectin type-3
FYN	oncogene related to SRC
g	Gram
GDNF	Glial cell derived neurotrophic factor
GDP	Guanosine diphosphate
GFP	Green fluorescent protein
GFRa	GDNF family receptor-alpha
GPI	Glycosylphosphatidylinositol
GST	Glutathione S-transferase
Gt	Goat
GTP	Guanosine triphosphate
h	Hour(s)
Hc	C-terminal fragment of the tetanus toxin
HEPES	4-(2-hydroxyethyl)-1-piperazineethanesulfonic acid
His	Histadine
HRP	Horse-radish peroxidase
Hu	Human
Ic	Intracellular
IF	Immunofluorescence
Ig	Immunoglobulin
IgG	Antibody immunoglobulin
IP	Immunoprecipitation

IPTG	Isopropyl β-D-1-thiogalactopyranoside
kb	Kilo base pairs
kDa	Kilodaltons
Kidins220	Kinase D-interacting substrate 220 kDa
kV	Kilovolts
L1	L1 cell adhesion molecule
LAL	Levator auris longus muscle
LAMP2	Lysosomal-associated membrane protein 2
LC	Live-cell imaging
LRI	CRUK London Research Institute
MAPK	Mitogen-activated protein kinase
min	Minute(s)
MION	Amino-derivatised monocrystalline iron oxide nanoparticles
ml	Milliletre
mm	Millimetre
MMP	Matrix metalloprotease
MW	Molecular weight
NCAM	Neural cell adhesion molecule
ng	Nanogram
NgCAM	Chick orthologue of L1-CAM
NGF	Nerve growth factor
nm	Nanometres
nM	Nanomolar
NMJ	Neuromuscular junction
NSF	N-ethylmaleimide-sensitive factor
$p75^{NTR}$	p75 neurotrophin receptor
PBS	Phosphate buffered saline
PC12	Rat pheochromocytoma
PCR	Polymerase chain reaction
PFA	Paraformaldehyde
PKC	Protein kinase C
pM	Picomolar
PSA	Poly-sialylated

Rab	Ras analog in brain
Rb	Rabbit
RGC	Retinal ganglion cell
RGD	Arginyl-glycyl-aspartic
RNA	Ribonucleic acid
rpm	Revolutions per minute
RT-PCR	Reverse transcriptase polymerase chain reaction
s	Second(s)
SDS	Sodium dodecyl sulphate
SDS-PAGE	SDS-polyacrylamide gel electrophoeresis
SEM	Standard error of the mean
SNARE	Soluble NSF attachment protein receptor
TCA	Trichloroacetic acid
TeNT	Tetanus toxin
Tris	Tris(hydroxymethyl)aminomethane
TrkA	Tropomyosin receptor kinase A
V	Variable Ig domain
VH	Ventral horn
WB	Western blot
WT	Wild type
x g	g-force
µg	Mircogram
µl	Microlitre
µm	Micrometre
µM	Micromolar

Chapter 1. Introduction

The human brain is estimated to contain around 100 billion neurons and each one is required to make the necessary connections with other neurons or target tissues to build the networks required for life. Further complexity arises, as individual neurons are specialised cells with a highly polarised architecture and specific function. Neurons have a cell body that contains the nucleus, a dendritic compartment consisting of many dendrites that receive synaptic input, and a long axon that transmits electrical signals to target cells. The cell body contains only a fraction of the total cellular cytoplasm and organelles (1-10%), whilst the remaining proportion is localised in the dentritic tree and axon, possibly at great distances from the nucleus. This arrangement presents unique challenges to neuronal cells during development and maintenance of the nervous system.

The development of the nervous system was classically described as being dependent on soluble long-distance cues and membrane bound short-distance signposts. It was proposed that distinct molecules mediated these two guidance mechanisms. In recent years however, it has become increasingly apparent that not only do long and short-distance cues cooperate with each other, but that important players can actually have dual functions and participate in both pathways. In this thesis, I aimed to investigate whether activated leukocyte cell adhesion molecule (ALCAM) found in an axonal retrograde signalling endosome of ventral horn neurons, cooperated with neurotrophins, mediators of long-range signalling during development.

1.1 Neurotrophins, their receptors and retrograde signalling

The first neurotrophin to be described was nerve growth factor (NGF) discovered by Rita Levi-Montalcini as a result of work started in the 1950s (Aloe, 2004). Studies of the chick limb in Victor Hamburger's lab led to the observation that neurons were overproduced in development, and their subsequent survival depended on the presence of target tissues. While in Hamburger's lab, Levi-Montalcini noticed that mouse tumours implanted in the chick limb resulted in hyperinnervation of resident internal organs. She suggested that this unusual observation was because the tumours produced a diffusible agent stimulating neuron growth and differentiation (Levi-Montalcini and Hamburger, 1951). In 1960, Levi-Montalcini isolated the secreted protein, named NGF, in collaboration with Stanley Cohen, for which both shared the 1986 Nobel Prize for Physiology or Medicine. Since the initial identification of NGF, many studies on neurotrophins have shown that distinct neuronal populations use specific neurotrophin signalling pathways for axon guidance and cell survival during development (reviewed in Zweifel et al., 2005). To date, many other growth factors have been discovered and they are currently under intensive investigation since they provide potential therapies for many neurodegenerative conditions.

In addition to NGF there are 3 other members of the neurotrophin family: Brain derived neurotrophic factor (BDNF), neurotrophin-3 (NT3) and neurotrophin-4/5 (NT4/5). Neurotrophins bind to two types of receptors. They bind with ligand specificity to tropomyosin receptor kinases (Trk); NGF binds to TrkA, BDNF and NT4/5 bind TrkB, while NT3 binds to TrkC (Figure 1.1). Trk receptors dimerise on ligand binding, autophosphorylate, and this in turn activates downstream signalling cascades including the serine/threonine protein kinase (Akt) and mitogen-activated protein kinase (MAPK). On the other hand, all the neurotrophins as well as their immature forms

(proneurotrophins) can bind the $p75^{NTR}$ receptor. The $p75^{NTR}$ receptor is a member of the tumour necrosis family (TNF) receptor superfamily and has no intrinsic catalytic activity but through associations with other membrane partners it can elicit downstream signalling. Activation of the receptor can lead to diverse responses depending on the ligand bound and the co-receptor engaged (reviewed in Schecterson and Bothwell, 2010) and (Vilar et al., 2009). For example, $p75^{NTR}$ activation can lead to apoptosis when it binds proneurotrophins in complex with sortilin, can promote cell survival in the presence of TrkA, and can induce growth cone collapse when associated with the nogo receptor (Schecterson and Bothwell, 2010). The complexity and diversity of the interactions between neurotrophins and their receptors is important when considering the widespread and varied function of these factors during development that is tightly regulated in time and space.

The neurotrophin hypothesis states that neurons are overproduced during development and only those that successfully compete for limited target-derived factors survive (reveiwed in Zweifel et al., 2005). Critical to this proposal is the implication that retrograde signals need to be transmitted from target tissues to the neuron cell body. Initial evidence that neurons were indeed engaged in retrograde signalling was that neurotrophins could undergo retrograde transport e.g. radiolabelled NGF applied in the periphery was found in the neuron cell body (Hendry et al., 1974). More recently, signalling endosomes have been proposed to mediate the transport of activated neurotrophin receptors and the neurotrophins themselves to maintain neuron survival (reviewed in Ibanez, 2007). Introduction of neurotrophins directly into the cytoplasm of the PC12 cells did not sustain survival, and suggested that neurotrophins need to bind to membrane receptors to elicit the survival response (Heumann et al., 1981). Subsequent studies found that the receptors had to undergo internalisation and transport to sustain survival and that following transport at least some receptors need

to remain bound to their ligand to fulfil their trophic function (Watson et al., 1999, Ye et al., 2003).

Another important aspect of long-distance growth factor signalling in neurons is that ligand and receptor have to undergo the appropriate sorting upon internalisation and entry into the endocytic system. TrkA has been reported to undergo both clathrin-dependent and clathrin-independent mechanisms of endocytosis, and following NGF stimulation has been predominantly found in multivesicular bodies and within compartments associated with the small GTPases Rab5 and Rab7 (reviewed in Moises et al., 2007). The Rab family of small GTPases are regulators of intracellular trafficking events, and they recycle between a predominantly cytosolic GDP-bound form and an active GTP-bound membrane-associated form (reveiwed by Ng and Tang, 2008). Dominant-negative mutants of dynamin and Rab7 show that Trk internalisation is important in regulating neurotrophin signalling, cell survival and differentiation (Saxena et al., 2005, Zhang et al., 2000).

Although common themes are emerging, the exact nature of the signalling endosome as it undergoes axonal transport remains controversial, because findings change depending on the cell type and stimulation paradigm used (reviewed by Ibanez, 2007 and Cosker, 2008 #214). Although most studies investigating TrkA endocytosis have been conducted in cell lines, similar endocytic proteins have been observed associated with neurotrophin receptor-containing endosomes in primary neurons (e.g. Rab5 and Rab7) (Ibanez, 2007). In Deinhardt (2006b) the $p75^{NTR}$ neurotrophin receptor was found to undergo constitutive clathrin-independent endocytosis, recycling back to the plasma membrane in basal conditions and only in the presence of NGF was $p75^{NTR}$ directed into a clathrin-dependent endocytic pathway linked to the retrograde transport route (Deinhardt et al., 2007). This illustrates that the fate of the receptor depends on

the presence of ligand and its type. Endosomes undergoing microtubule associated fast axonal transport in neurons have been reported to travel at rates ranging from 0.5-5 μm/s. The speeds of axon transport observed *in vitro* are consistent with, and could account for, the observed times taken between neurotrophin exposure at axon terminals and their appearance in cell bodies *in vivo*, e.g. 2.5 mm/hour (Hendry et al., 1974).

Interestingly, following retrograde transport, the signalling cascades activated in the cell body can be distinct to that observed after direct activation of the soma. Local application of NGF to cell bodies or axons in compartmentalised chambers activated both extracellular-signal-regulated kinases 1/2 (ERK1/2) and ERK5 MAPK pathways (Watson et al., 2001). However, upon NGF stimulation of distal axons, only ERK5 was phosphorylated in the cell soma and this was necessary for survival and the phosphorylation of transcription factors e.g. cyclic-AMP response element binding protein (CREB) (Watson et al., 2001).

It is noted that other retrograde signalling mechanisms, independent of signalling endosomes, have been proposed in recent years (reviewed in Ibanez, 2007). Firstly, it has been suggested that lateral propagation of receptor phosphorylation at the cell surface and waves of increased intracellular calcium could transmit quick retrograde signals. However evidence is currently lacking on whether these mechanisms are relevant to neuronal signal transduction where propagation has to travel for long distances, and it is unresolved how the directionality of the signal could be maintained. Secondly, there is evidence for direct association of signalling molecules with the transport machinery, independent of signalling endosomes. After injury, Fainzilber and colleagues found that axonal importins bind cytoplasmic dynein and retrogradely transport various proteins with nuclear localisation sequences (reviewed in Hanz and

Fainzilber, 2006). Nevertheless, it appears that retrograde transport is an important aspect of delivering signals from the periphery to the cell body.

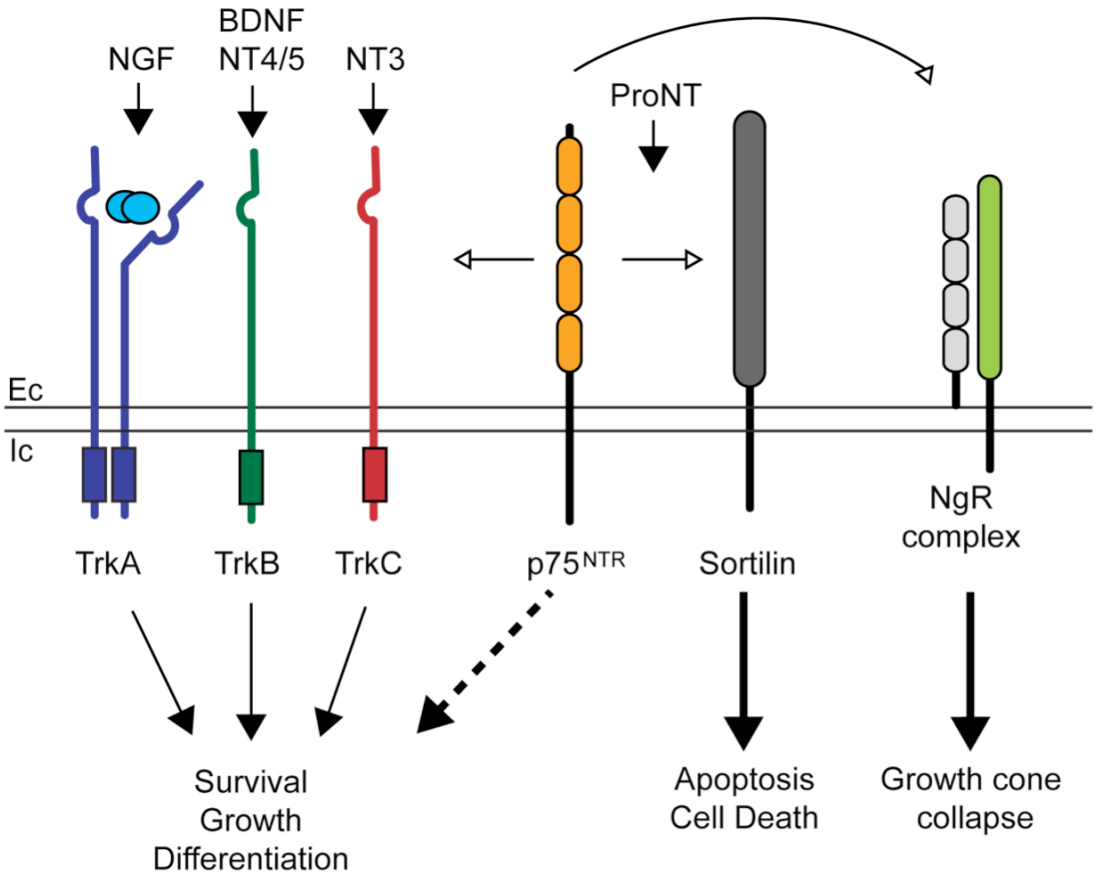

Figure 1.1 Neurotrophins and their receptors

Two TrkA receptors are depicted binding an NGF dimer to activate downstream signalling for survival, growth and differentiation. The other Trk receptors and their relative preference for neurotrophins are shown, with BDNF and NT4/5 binding TrkB, while NT3 binds TrkC. The $p75^{NTR}$ receptor can interact with Trk receptors and contributes to survival signalling as indicated (dotted arrow). The $p75^{NTR}$ receptor can also bind proneurotrophins (ProNT) in complex with sortilin to activate apoptosis and cell death pathways, or bind to the Nogo receptor (NgR) complex to induce growth cone collapse.

1.2 Axonal transport

The unique architecture of neurons results in the majority of their cytoplasm being contained within their axon and dendrites, some at great distance from the cell soma. For example for a motor neuron, whose cell body is around 50 μm in diameter, its axon could reach over 1 metre in humans, e.g. for those innervating the lower limb muscles – which is equivalent to 20,000 times the diameter of the cell body. This makes neurons particularly dependent on active transport, since organelles, proteins, energy and signals are required to travel over great distances (reviewed in Salinas et al., 2008, Perlson et al., 2010). A schematic illustrating the process of axonal transport is shown in Figure 1.2. Newly synthesised material is transported anterogradely, away from the cell body towards the cell periphery, e.g. protein and membrane components, mitochondria and mRNAs required for local translation. Simultaneously, proteins and organelles targeted for degradation are transported back to the soma. Importantly, as well as maintaining synthetic and degradative processes, axonal transport is involved in regulating cell signalling. For example, as explained in section 1.1, neurotrophins secreted from target tissues need to be retrogradely transported to the cell body to elicit their full survival response. Axonal transport requires molecular motors to move along the cytoskeleton using energy from ATP hydrolysis. Anterograde axonal transport is predominantly associated with kinesin motors that move towards the plus ends of microtubules, while cytoplasmic dynein is the main retrograde motor and travels towards the microtubule minus ends. In axons, unlike dendrites, microtubules are almost all oriented so that the plus ends are located at the nerve terminal while the minus ends are toward the cell body (reviewed in Salinas et al., 2008)

Disruption in axonal transport has been associated with many neurodegenerative conditions supporting the view that this process is of particular importance to neuronal

survival (reviewed by De Vos et al., 2008). Mutations in the kinesin motors KIF5a and KIF1Bβ have been associated with neurodegeneration in families with hereditary spastic paraplegia and charcot-marie-tooth type 2A neuropathy respectively (Xia et al., 2003, Zhao et al., 2001). Furthermore, mutations in the $p150^{Glued}$ subunit of dynactin, a component of the retrograde dynein motor complex, cause spinal and bulbar muscular atrophy (SBMA) in human patients (Puls et al., 2005).

Further evidence from animal models suggests that mutations disrupting axonal transport are sufficient to cause neurodegeneration. Defects in axonal transport have been observed in affected neurons in Drosophila and mouse models of Huntington's disease following overexpression of mutant huntingtin, a motor-associated protein (Gunawardena et al., 2003, Her and Goldstein, 2008). Mice that express a dominant negative form of dynactin, known to disrupt dynein function, have progressive motor neuron loss (LaMonte et al., 2002), and mice with mutations within the heavy chain of cytoplasmic dynein (*cra* and *loa)*, show axonal transport defects and a sensory neuron degenerative phenotype (Hafezparast et al., 2003, Chen et al., 2007).

Defects in axonal transport have also been observed in neurodegenerative conditions even when the primary causative mutation is not directly linked to axonal transport. A defect in retrograde axonal transport is one of the earliest pathogenic events observed in the SOD^{G93A} mouse model of amyotrophic lateral sclerosis (Williamson and Cleveland, 1999, Kieran et al., 2005, Bilsland et al., 2010). This suggests that disruption of axonal transport is a common contributing factor to neurodegeneration. When SOD^{G93A} mice are crossed with *loa* mice, with a mutation in cytoplasmic dynein, the axonal transport deficits are no longer observed and the mice survive significantly longer than their SOD^{G93A} littermates (Kieran et al., 2005). Although the mechanism by which the dynein mutation alleviated SOD^{G93A} neurodegeneration remains unknown, it

has recently been associated with alleviation of the SOD^{G93A} mitochondrial pathology (El-Kadi et al., 2010). The study by Kieran et al (2005) indicates that axonal transport is directly involved in the disease process since improvement in transport correlated with delayed disease progression.

It has not yet been determined how defects in axonal transport can lead to neurodegeneration but it is likely to involve several pathways (reviewed by Perlson et al., 2010). As illustrated in Figure 1.2, axonal transport is required to balance general house keeping functions between the periphery and cell body. Evidence of aberrant mitochondrial transport and localisation in neurodegenerative diseases suggest that the energy supply of neurons is disrupted (De Vos et al., 2007). As well as aberrant energy supplies, there is evidence of disruption in degradation of proteins and organelles in neurodegenerative conditions. Defects in the distribution and transport of lysosomes has been observed e.g. in a model of motor neuron disease (Chevalier-Larsen et al., 2008). Mice with loss of autophagy (a process for bulk protein degradation) specifically in neurons have poly-ubiquitinated protein accumulations and show neurodegeneration (Komatsu et al., 2006).

Since neurotrophic signalling requires retrograde transport to maintain neuronal survival, defects in axonal transport are likely to result in misregulation of signalling. In mouse models of neurodegeneration exogenous supply of growth factors can only delay, but cannot prevent, disease progression (Dodge et al., 2010) and neurotrophins have had limited success in treatment of human disease (Thoenen and Sendtner, 2002). This would suggest that additional signals to neurotrophic factors are required for motor neuron survival. Similar defects in axonal transport were observed in embryonic neurons from two distinct mouse models of neurodegeneration with very different rates of disease progression (Kieran et al., 2005), and this can be partially

explained by differences in the transport of death signals in the two models (Perlson et al., 2010). However, neurodegenerative conditions do not only concern pathological processes within neurons, but also involve interactions with their environment through non-cell autonomous processes e.g. that involve the surrounding glial cells (Boillee et al., 2006). In view of the complexity of neurodegenerative diseases, which involve multiple cell types and pathological mechanisms, it is likely that other retrograde factors that contribute to neuron viability and function have yet to be identified.

Axonal transport was initially studied in squid giant axoplasm preparations, where the movement of motors along microtubules could be recorded in the presence of various inhibitors and pathogenic proteins (for example Brady et al., 1993). However, this system is limited in its physiological relevance since it is quite far removed from the environment of a mammalian intact axon. To follow retrograde transport *in vivo*, the endogenous properties of infective viruses and bacterial toxins known to undergo internalisation and transport to the central nervous system, have been used (reviewed by Salinas et al., 2010). Alternatively, protein and organelle accumulation can be examined both proximally and distally to nerve ligations. This has been used to examine the transport of anterograde and retrograde cargoes *in vivo* and to determine the relative transport efficiency in various pathological states (for a recent study see Perlson et al., 2009). However, these methods inferred transport by analysing the accumulation of labelled toxin, virus or protein of interest *ex vivo*, rather than directly measuring transport dynamics. More recently, cellular and molecular biology techniques have allowed analysis of transport in living neurons *in vitro* e.g. transport of TrkB and NgCAM cell adhesion molecule using fluorescent tags or antibodies to these proteins (Ascano et al., 2009, Yap et al., 2008). However, in these studies the proteins of interest were transfected into differentiated neuronal cell lines and primary neurons that could potentially alter endogenous trafficking processes. In our laboratory, we

have taken advantage of the endogenous properties of the binding fragment of the tetanus toxin to make a fluorescent probe that allows axonal retrograde transport to be examined in living neurons *in vitro* and *in vivo* (Lalli and Schiavo, 2002, Bilsland et al., 2010).

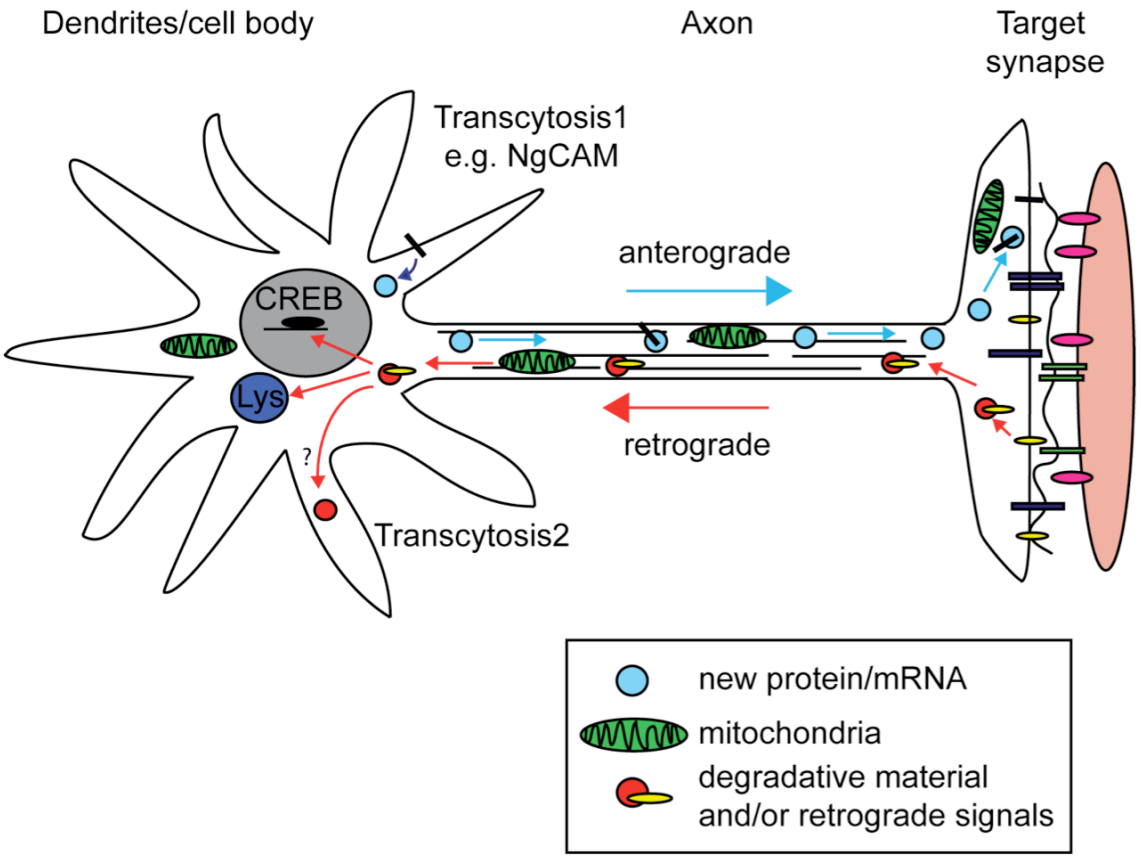

Figure 1.2 Axonal transport and its functions

The dendrites and cell body of a typical neuron are shown on the left, with the axon projecting to the target synapse on the right. Newly synthesised proteins, mitochondria, mRNA, and proteins from the dendritic plasma membrane (indicated by Transcytosis1) and are all transported anterogradely toward the target synapse (blue arrows). Mitochondria, proteins targeted for degradation and retrograde signals are transported from the synapse to the cell body (red arrows). Once in the soma the retrograde cargoes are sorted to their next destination. This could be to the nucleus to activate transcription, e.g. CREB transcription, or activate signalling in the cytosol. Cargoes could be targeted to lysosomes for degradation (Lys), or transcytosed to the plasma membrane (Transcytosis2).

1.3 The binding fragment of the tetanus toxin labels a retrograde axonal transport compartment

Toxigenic strains of bacteria of the genus *Clostridia* produce the tetanus toxin (TeNT) and the seven serotypes of botulinum toxins (BoNT). These neurotoxins bind neurons with high affinity and cause spastic or flaccid paralysis respectively (reviewed in Lalli et al., 2003a). Both TeNT and BoNT are internalised in motor neurons at the neuromuscular junction (NMJ). Several serotypes of BoNT bind to proteins of synaptic vesicles, such as synaptotagmin and SV2A-C and remain at the NMJ where they cleave soluble N-ethylmaleimide-sensitive factor (NSF) attachment protein receptor (SNARE) proteins and block exocytosis of acetylcholine. In certain circumstances BoNT/A was shown to undergo retrograde transport and reach distant sites in the central nervous system (CNS) (Antonucci et al., 2008). Following clathrin-dependent endocytosis (Deinhardt et al., 2006a) TeNT is not retained at the NMJ but directed to a long-range transport pathway to the motor neuron cell body in the spinal cord. Here, TeNT is transcytosed to inhibitory interneurons where it cleaves the SNARE protein VAMP/synaptobrevin and blocks neurotransmission. This results in the excessive stimulation of motor neurons, which in turn causes spastic paralysis in their target muscles. The route of internalisation and transport of TeNT is shown in Figure 1.3. It is known that the carboxy-terminal fragment (Hc) of clostridial neurotoxins are responsible for neuron binding specificity and therefore members of our laboratory previously designed this atoxic Hc fragment to follow the internalisation and retrograde transport route used by the TeNT holotoxin (reviewed by Lalli et al., 2003a).

The Hc fragment has been engineered with several molecular tags i.e. a vesicular stomatitis virus protein G epitope (VSVG) (Herreros et al., 2000) and a cysteine-rich region (Lalli et al., 2003b). This allows for the atoxic toxin fragment to be easily and

specifically modified with fluorophores, such as Alexa Fluor dyes, to visualise the transport of Hc in live neurons in live-cell imaging experiments (Lalli and Schiavo, 2002). The Hc-containing endosome undergoes long-range retrograde axonal transport that is dependent on dynein function and the myosin Va motor (Lalli et al., 2003b). Further studies found that the Hc-labelled endosome also contained neurotrophins such as BDNF and NGF, and neurotrophin receptors $p75^{NTR}$ and TrkB (Lalli and Schiavo, 2002, Deinhardt et al., 2006b). This retrograde axonal transport compartment is considered to be a non-degradative compartment as it is non-acidic (Bohnert and Schiavo, 2005), and does not label with LysoTracker (Lalli and Schiavo, 2002). The Hc-containing endosome associates with Rab5 and Rab7 GTPases (Deinhardt et al., 2006b), which as discussed in section 1.1, are associated with neurotrophin signalling endosomes. It is thought that this is a sequential process, with Rab5 involved in the early steps of internalisation, while Rab7 activity is required for long-distance vectorial transport along the axon (Deinhardt et al., 2006b). Interestingly, mutations in Rab7 are associated with Charcot-Marie-Tooth type 2B neuropathy (Verhoeven et al., 2003), consistent with the idea that this small GTPase has an important role in neurons.

In our laboratory a method to purify the axonal retrograde transport compartment using the Hc fragment conjugated to monocrystalline iron oxide nanoparticles (MION) was developed (Deinhardt et al., 2006b). It was shown that the Hc-MION undergo endocytosis and transport in living ventral horn neurons in culture. By harvesting the neurons in the absence of detergent and mechanically breaking the plasma membrane it was possible to purify the endosomes containing Hc-MION by passing post-nuclear supernatants through a magnet. A schematic illustrating the experiment is shown in Figure 1.4. Using this technique, it was demonstrated biochemically that the Hc-labelled endosome contained the neurotrophin receptor $p75^{NTR}$ and the small GTPases

Rab5 and Rab7, confirming the associations observed in live-cell imaging experiments (Deinhardt et al., 2006b).

In a similar experiment performed by K. Deinhardt in our laboratory, these purified Hc-labelled organelles were analysed by mass spectrometry (unpublished data). This allowed for large-scale analysis of the proteins associated with the axonal retrograde transport compartment. Several proteins found in this proteomic analysis were known to be associated with the Hc endosome by western blot and live-cell imaging, and served as positive controls. These included several motor complexes, such as myosins and cytoplasmic dynein subunits, as well as the small GTPases Rab5 and Rab7. Of the 348 proteins identified, the majority (216) were classified as cytoplasmic/membrane proteins, i.e. not mitochondrial, nuclear or ribosomal. Of the cytoplasmic/membrane proteins, around 12% were plasma membrane proteins, which included ion channels and transporters and many cell recognition molecules. All the major classes of cell adhesion molecules (CAM) were represented including selectins, integrins, and members of the immunoglobulin cell adhesion molecule (IgCAM) superfamily. Although cadherins were not directly identified, junction plakoglobin, an intracellular protein associated with the E-cadherin/catenin complex, was found in the mass-spectrometry proteomic analysis. Additionally cadherin13 had been identified in a previous proteomic screen undertaken in the laboratory, of proteins that immunoprecipitated with Hc within lipid raft fractions (unpublished data). Table 1 provides a list of the cell recognition molecules identified in the Hc proteome.

I was particularly interested in whether the CAMs present in the Hc-labelled axonal retrograde transport compartment were undergoing long-range transport, and if so whether these were distinct carriers from the neurotrophin containing endosomes. Considering that in recent years CAMs have been shown to have diverse roles in

signalling, I also wanted to see whether the CAMs present in the axonal transport compartment are involved in the modulation of neurotrophin signal regulation.

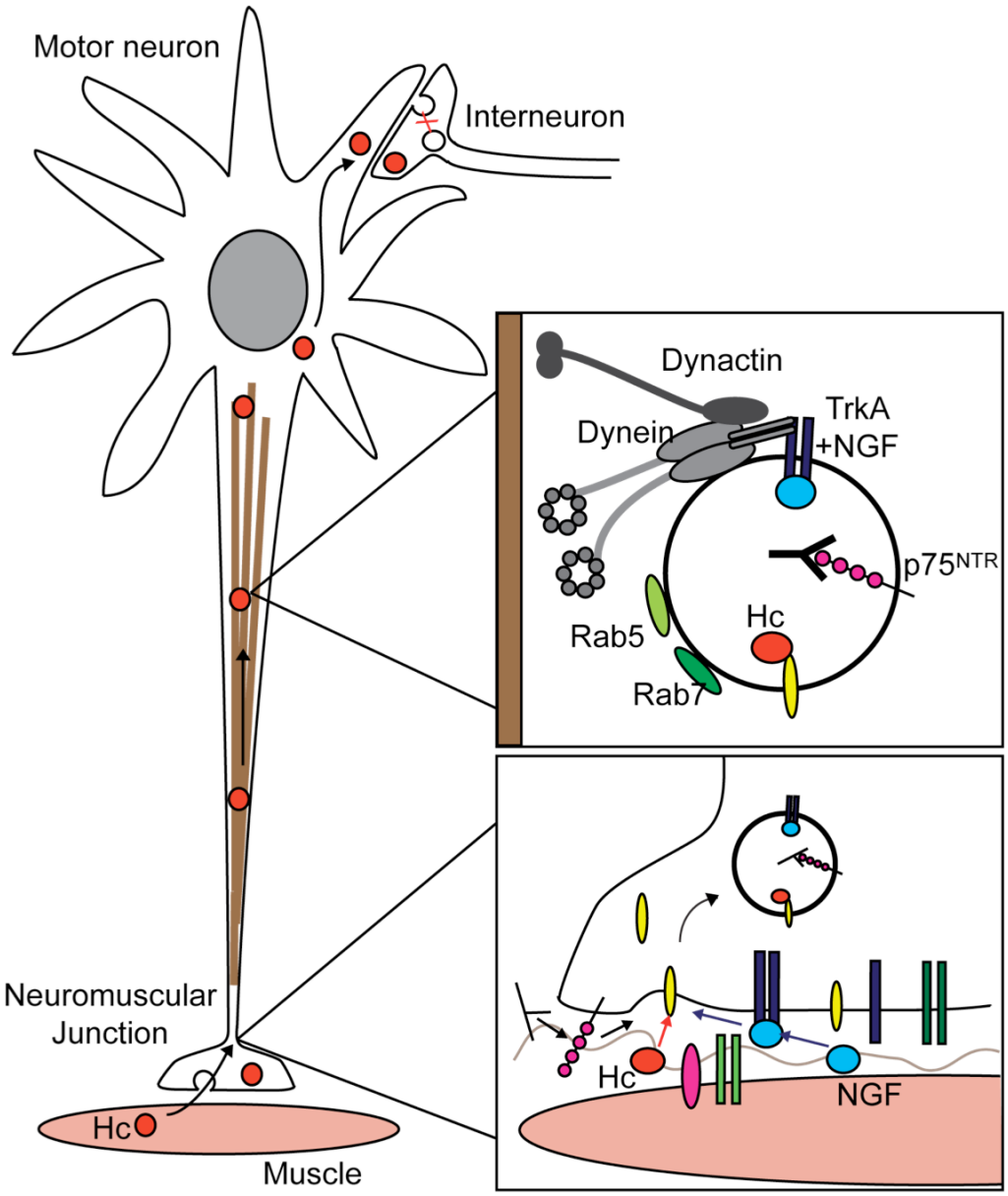

Figure 1.3 TeNT Hc internalisation and transport

TeNT Hc is endocytosed from the plasma membrane at the neuromuscular junction and is retrogradely transported along microtubules (brown) to the cell soma, where it is transcytosed to inhibitory interneurons to block their exocytosis. Hc binds to polysialo-gangliosides on the cell surface, as well as some GPI-anchored (e.g. Thy1.1) and transmembrane receptors (yellow) (Herreros et al., 2000). In the retrograde transport compartment neurotrophin receptors TrkA and $p75^{NTR}$ and their ligands (antibodies (Y) or neurotrophins, NGF blue circle) are found (lower inset). The retrograde axonal compartment is also associated with the GTPases Rab5 and Rab7 and the retrograde motor complex dynein and dynactin (upper inset).

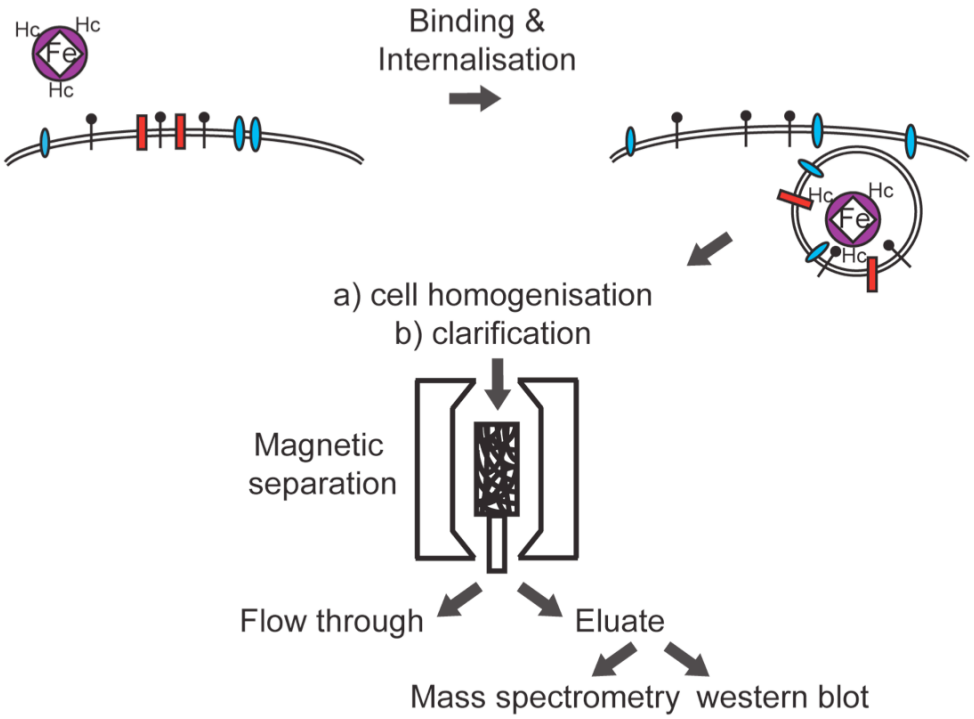

Figure 1.4 Endosome purification using Hc-MIONs

This scheme shows the binding and subsequent internalisation of Hc-coupled MIONs. Cells were then homogenised, samples clarified by centrifugation and postnuclear supernatant separated using a magnetic column. Protein eluted from the beads was used for mass-spectrometry or western blot. Samples were compared to the flow through that contains proteins not associated with the beads.

Protein	Accession Number	Score (∝ peptide number)	Confirmation
Integrin, beta-1 precursor	P09055	93.13	
Integrin, beta 6	Q6AYF4	39.01	
E-selectin ligand 1	Q61543	64.08	
Junction plakoglobin (Desmoplakin-3) (Desmoplakin III)	Q02257	38.08	RP, IF
Neural cell adhesion molecule 1, 140 kDa isoform precursor	P13596	63.28	RP, IF
Coxsackievirus and adenovirus receptor homolog precursor (CAR)	P97792	43.66	LC, IF, WB
Poliovirus receptor-related protein 2 precursor (Murine herpesvirus entry protein B) (Nectin-2)	P32507	35.89	
CD166 antigen precursor (Activated leukocyte cell adhesion molecule)	**O35112**	**51.14**	
CD147 antigen; Basigin precursor (OX-47 antigen) (Glycoprotein CE9);	P26453	41.22	
Reticulon-4 (Neurite outgrowth inhibitor) (Nogo protein)	Q9JK11	97.98	
Nidogen-1 precursor (Entactin);	P10493	56.94	
Erythrocyte band 7 integral membrane protein (Stomatin) (Protein 7.2b)	P54116	38.54	
Glypican-4 precursor (K-glypican);	P51655	54.2	

Table 1 Cell surface proteins associated with the Hc-labelled axonal retrograde transport compartment

Components of integrin, selectin and cadherin binding complexes are coloured in orange, green and yellow respectively. IgCAM superfamily members are coloured in blue and ALCAM, which has been investigated in this thesis, is in bold. Other cell membrane proteins identified are also shown (uncoloured) and include reticulon-4 a protein associated with neurite outgrowth inhibition. NCAM, CAR and junction plakoglobin had already been confirmed by other techniques to associate with the Hc-endosome (RP- Hc-raft proteome; LC live-cell imaging; IF immunofluorescence; WB western blot).

1.4 Cell adhesion molecules (CAM)

Cell adhesion molecules (CAMs) are critical for the development and maintenance of tissue architecture necessary for multicellular life. These cell surface proteins are responsible for cell to cell, and cell to extracellular matrix interactions and comprise of the cadherin, integrin, selectin and immunoglobulin (Ig) families. None of these proteins have intrinsic enzymatic activity and therefore were not defined as receptors. However, extensive evidence now exists that CAMs are capable of signalling and have important roles in growth factor signalling regulation (reviewed in Schmid and Maness, 2008, Maness and Schachner, 2007).

The IgCAM superfamily, are transmembrane proteins with large extracellular domains and shorter cytoplasmic tails responsible for interactions with the cytoskeleton. It is one of the largest protein families. For example, over 1% of the predicted genes in the Drosophila genome are Ig-domain-containing proteins suggesting that they have important, diverse, though perhaps redundant functions (Kamiguchi and Lemmon, 2000). L1 and neural cell adhesion molecule (NCAM) are two prototypical proteins from this family and are the best characterised (reviewed in Schmid and Maness, 2008). The properties of these two proteins as examples of the diverse interactions and functions that members of the IgCAM superfamily have are discussed below. Figure 1.5 is a schematic representing the protein structures and some of their known properties.

NCAM was the first identified cell adhesion molecule in the nervous system (reviewed in Maness and Schachner, 2007). The three major NCAM isoforms have identical extracellular domains that contain 5 Ig domains, followed by 2 fibronectin type-III (FN III) repeats. There are two transmembrane isoforms of NCAM that differ by a 261 amino acid insertion in the cytoplasmic domain (NCAM-140 and NCAM-180 without

and with the insert respectively) and a Glycosylphosphatidylinositol (GPI) anchored form (NCAM-120) that is expressed predominantly on glial cells. The relative expression of these isoforms changes throughout development, with the 180 kDa form increasing with age and being associated with the stabilisation of synapses. Post-translational modification generates an alternative NCAM form that is glycosylated on its 5th Ig domain with poly-sialylated acid side chains (PSA). This is thought to inhibit homophilic interactions causing decreased adhesion. NCAM-PSA is also developmentally regulated, and decreases in adulthood when it is only found at sites of neuritogenesis and where it has been linked to synaptic plasticity.

Apart from its role in cell adhesion, NCAM has been shown to have diverse functions in growth factor signalling and its regulation. NCAM interacts with the fibroblast growth factor receptor (FGFR) signalling pathways in several ways. NCAM homophilic binding can potentiate neurite outgrowth in a FGFR-dependent manner, the mechanism of which is not yet fully understood (Saffell et al., 1997). NCAM can also bind directly to FGFR, and peptides either interfering or mimicking NCAM-FGFR binding can inhibit or activate FGFR downstream signalling respectively, leading to changes in differentiation and survival (Neiiendam et al., 2004, Anderson et al., 2005). Interestingly their co-signalling is context-dependent; NCAM signalling in neurite outgrowth is independent of FGFR when resident in lipid rafts, while FGFR-dependent when in non-raft membranes (reviewed in Maness and Schachner, 2007). Furthermore, NCAM can act as the co-receptor for GDNF in the presence of GDNF family receptor alpha (GFRα), and acts as an alternative co-receptor in GDNF signalling in cells that do not express the classical GDNF receptor RET (Paratcha et al., 2003). Recently the intracellular domain of NCAM has been shown to interact directly with the kinase domain of TrkB (Cassens et al., 2010). The authors of this study found that TrkB activation results in

NCAM phosphorylation, which in turn regulates NCAM-mediated neurite outgrowth, suggesting that a functional relationship exists between NCAM and TrkB signalling.

The L1-CAM family consists of L1, Close-Homolog of L1 (CHL1), NrCAM and Neurofascin. All members have 6 Ig domains, followed by 4 or 5 FN III domains, which only show around 35-45% overall homology, but are more highly conserved within their cytoplasmic tails. L1 is known to bind several proteins in the cytoplasm, which are important for its function. L1 binds to ankyrin via a conserved FIGQ/AY motif that is responsible for anchorage to the actin cytoskeleton. Tyrosine phosphorylation within the L1 motif inhibits ankyrin binding and interactions with the cytoskeleton, which in turn increases migration and neurite outgrowth (Whittard et al., 2006). L1 also plays a role in axon guidance, where it can mediate growth cone collapse by acting as a co-receptor for Semaphorin 3a with Neuropilin-1 (Castellani et al., 2002). Similarly to NCAM, L1 can cooperate with growth factor signalling cascades, for example transfection of L1 increased sustained ERK1/2 activation in response to serum or Platelet derived growth factor (PDGF) (Silletti et al., 2004).

Both L1 and NCAM cooperate with integrin signalling. Integrins are another family of CAMs important for cell to extracellular matrix interactions and are capable of inside-out and outside-in signalling (reviewed in Ivaska and Heino, 2010). L1 has a conserved arginyl-glycyl-aspartic acid (RGD) motif in its extracellular 6th Ig with which it interacts with αvβ5-integrin (Mechtersheimer et al., 2001). A second motif in the 3rd FN III domain can also recruit integrins in a non-RGD-dependent manner (Silletti et al., 2000). Interactions between integrins and L1 have also been shown to cooperate with growth factor signalling. Phosphorylation of the L1 cytoplasmic domain can alter its extracellular conformation (Chen et al., 2010). These alternative L1 extracellular domain conformations show differential binding to specific integrins, and in turn this

has been associated with altered L1 proteolysis and migration (Chen et al., 2010). The way in which NCAM interacts with integrins is less well resolved but they have been shown to converge on the same downstream MAPK pathway and this ability depends on FYN and FAK kinases downstream of NCAM (Maness and Schachner, 2007).

Integrin functions are intimately linked to their endocytic recycling (Caswell et al., 2009). In Pellinen et al (2006) integrins were found to associate directly with the Rab GTPase Rab21. Rab21 activity regulated integrin internalisation, which in turn altered integrin mediated adhesion and migration. Similarly, evidence suggests that endocytosis also contributes to IgCAM function and regulation. The neuron specific isoform of L1 encodes a RSLE motif that recruits the AP2 clathrin adaptor, which is required for endocytosis of L1 at the growth cone and is important for axon growth (Kamiguchi et al., 1998). This interaction is also regulated by the phosphorylation state of the tyrosine residue immediately adjacent to the AP2 binding motif (YRSLE) (Schaefer et al., 2002). On dephosphorylation, L1 is preferentially endocytosed at specific areas of cell-cell contact e.g. rear of the growth cone and its endocytosis is necessary for neurite outgrowth on L1 substrate. NCAM can also undergo regulated endocytosis in neurites. NCAM was shown to be endocytosed after antibody-induced clustering on the plasma membrane of cell bodies followed by recycling back to the plasma membrane (Diestel et al., 2007). In this study the authors found NCAM in a mono-ubiquitinated form on the plasma membrane after antibody clustering and suggested that this could be the endocytosis signal. It is noted that this study was performed using transfected protein in primary neurons and cell lines, and that the process has yet to be reported *in vivo*. Interestingly, NCAM was found to be associated with the Hc axonal retrograde transport vesicle by mass spectrometry (see Table 1), as well as in the Hc-associated raft proteomic screen, which may suggest that endogenous NCAM undergoes endocytosis in ventral horn neurons.

There is growing evidence to suggest that IgCAMs can undergo a specialisation of the endocytic pathway known as transcytosis, where proteins can be transported from the plasma membrane of one compartment and travel to another. Transcytosis has been characterised in endothelial cells where proteins are transported from basolateral membrane to the apical membrane or vice versa. In neurons a similar process has been observed for proteins transcytosed from the plasma membrane of the dendritic compartment to the axon and vice versa (see Figure 1.2 for examples). Work by Winckler and colleagues have shown that the chick homolog of L1, NgCAM, undergoes a regulated process of transcytosis, whereby the protein is targeted to the soma/dendritic compartment plasma membrane before internalisation and targeting to the axon (Wisco et al., 2003). It is suggested that transcytosis is important for the maintenance of the compartmentalisation of proteins within the polarised architecture of the neuron. Indeed, it has been found that the process is regulated by the neuron-enriched endosomal protein of 21 kDa (NEEP21), and if this is disrupted, L1 loses its restriction to the axon and is also erroneously found within the plasma membrane of the dendritic compartment (Yap et al., 2008). Transcytosis is of particular interest in the context of the Hc-labelled axonal retrograde transport compartment, because transcytosis has been observed for neurotrophins, neurotrophin receptors and the tetanus toxin itself (Rind et al., 2005, Ascano et al., 2009), and could be a destination of other endogenous proteins within the Hc-positive endosome.

Another important property of L1 and NCAM is that both proteins are substrates for disintegrin and metalloprotease (ADAM) membrane proteolysis. Ectodomain shedding can downregulate CAM dependent migration and adhesion but can also result in autocrine stimulation. NCAM ectodomain shedding has been shown to inhibit cortical neuron outgrowth, while it stimulates hippocampal neuron outgrowth (Hubschmann et al., 2005, Hinkle et al., 2006). This again illustrates the context-dependence of IgCAM

signalling. L1 is not only cleaved by ADAM17 and ADAM10 but also undergoes regulated intramembrane proteolysis by γ-secretase, to produce an intracellular cytoplasmic domain (Maretzky et al., 2005). In this study, upon inhibition of L1 shedding, neurite outgrowth of cerebellar neurons from explants grown on an L1-substrate was also decreased. Interestingly, the authors found that ADAM10 was responsible for constitutive L1 cleavage, as well as in response to a glutamate receptor agonist, while ADAM17 was responsible for L1 cleavage to different stimuli, including cholesterol depletion or phorbol ester stimulation (PMA). It should also be noted that in the explant experiments used in this study, ADAM17 inhibition had a greater effect than ADAM10 inhibition, suggesting that other ADAM17 substrates, including the growth factor receptors $p75^{NTR}$ and TrkA (Ahmed et al., 2006, Diaz-Rodriguez et al., 1999), could contribute to the decreased neurite outgrowth observed.

The importance of L1 and NCAM in the maintenance of tissue integrity and growth factor signalling is illustrated by their associations with disease. L1 and NCAM are both upregulated in brain tumours (Schmid and Maness, 2008) and mutations in both proteins are associated with neuropsychological conditions. L1 is mutated in an X-linked form of mental retardation and NCAM misregulation has been associated with schizophrenia and bipolar disorder (reviewed by Schmid and Maness, 2008). However it is noted that there is considerable redundancy within the IgCAM superfamily, illustrated by the mild phenotypes observed in knockout mice. For instance both the NCAM and L1-CAM knockout mice are viable and fertile (Cremer et al., 1994, Cohen et al., 1998). Mice lacking L1 expression show defects in corticospinal tract development and hyperfasciculation in the brain (Wiencken-Barger et al., 2004). NCAM knockout mice also have subtle defects including learning difficulties and alterations in neurotransmitter release at the neuromuscular junction (Polo-Parada et al., 2001).

In summary, members of the IgCAM superfamily are involved in a diverse array of functions by interacting with many different partners as co-receptors, or co-operating with common signalling cascades. IgCAM endocytosis and regulated proteolysis are common properties involved in regulating their function, as well as their interaction with other signalling pathways. In this thesis, I examined ALCAM, a protein found among the associated IgCAMs in the proteomic screen of the Hc-positive compartment Table 1. As a member of the IgCAM superfamily and possessing some of the interesting properties outlined in this section, ALCAM was a good candidate to investigate for a novel role in neurotrophic signalling.

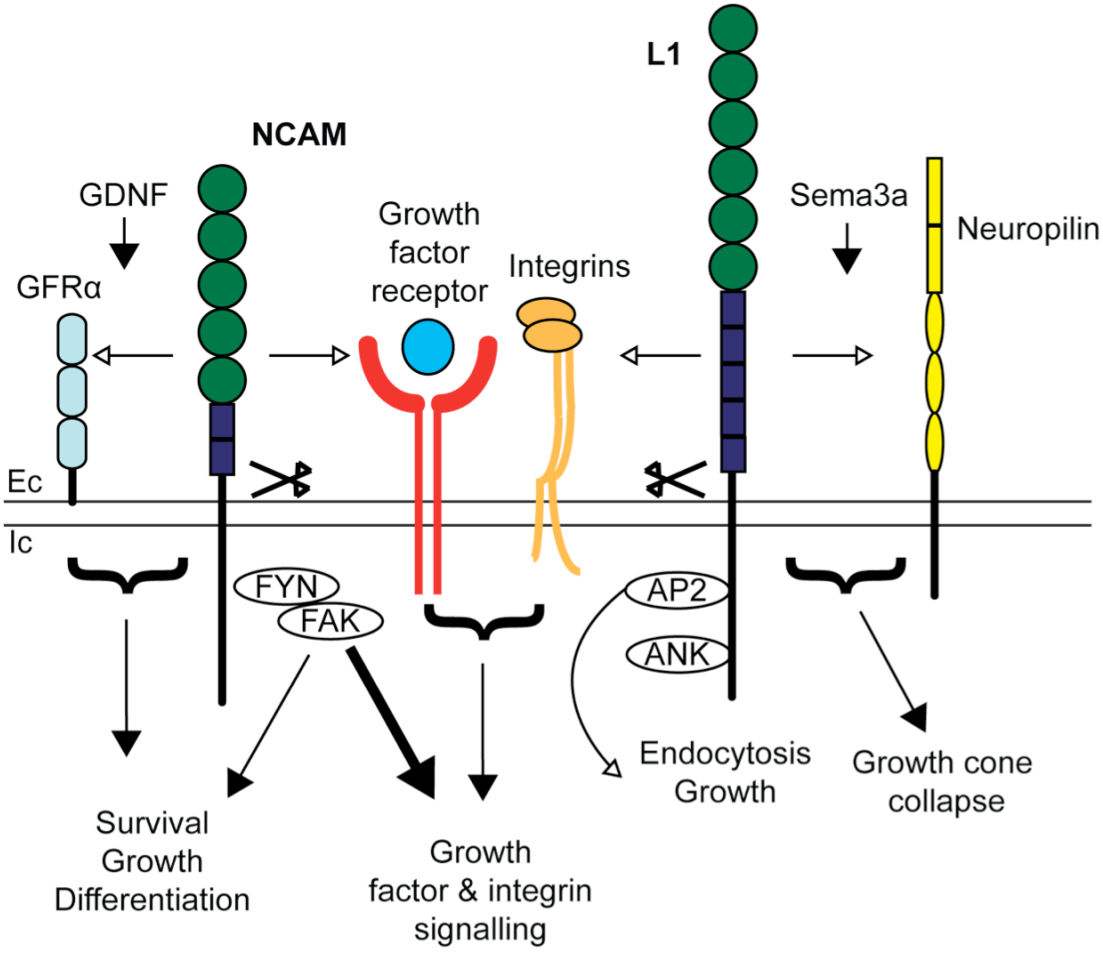

Figure 1.5 IgCAM interactions with growth factor signalling

Structurally, NCAM and L1 contain fibronectin type-III domains (dark blue boxes) and Ig domains (green circles). Sites of metalloprotease cleavage are indicated by scissors in the NCAM and L1 juxtamembrane regions. NCAM is known to interact with GDNF family receptor α (GFRα) as a co-receptor for GDNF and activates neuronal survival, growth and differentiation. NCAM can also activate downstream signalling on its own via its intracellular interaction with FYN and FAK kinases. L1 is depicted interacting with neuropilin, with which it mediates repellent sema3a signalling and induces growth cone collapse. Intracellularly, L1 binds the AP2 clathrin adaptor to mediate endocytosis and ankyrin (ANK) through which it interacts with the actin cytoskeleton. NCAM and L1 both cooperate with integrin and growth factor signalling pathways (e.g. EGF and FGF). This can happen via direct interactions with these receptors at the membrane or by activating the same downstream signalling cascades and therefore potentiating their response (large arrow).

1.5 Activated Leukocyte Cell Adhesion Molecule (ALCAM)

ALCAM is a classical IgCAM, that is a member of the subfamily defined by having 5 extracellular domains, two variable type Ig domains and 3 constant type-2 domains (i.e.$V_1V_2C_1C_2C_3$), followed by a transmembrane region and a cytoplasmic tail (Figure 1.6). ALCAM is expressed in many different tissues, for instance in the nervous system, the immune system and in haematopoietic stem cells (reviewed in Swart, 2002). ALCAM expression is highly temporally and spatially regulated and is found on cells undergoing dynamic cellular interactions, e.g. neurons during axonal outgrowth, immune cells during T-cell activation and cancer cells during migration (reviewed in Swart, 2002). ALCAM has been independently found in different species and tissues. Its synonyms include BEN/MuSC in mice, CD166/ALCAM in humans, DM-GRASP/SC1 in chick, and neurolin in fish to name but a few (for an extensive list see Swart, 2002). Throughout this thesis, I will refer to the protein as ALCAM.

The other members of the $V_1V_2C_1C_2C_3$ subfamily are BCAM/lutheran (basal cell adhesion molecule/lutheran blood group antigen), a laminin receptor, and MUC18/CD146. BCAM and MUC18 show low similarity with the ALCAM sequence (34.7% and 37.4% respectively). The greatest homology between the three receptors is in their extracellular domains, while similarities are lost in their cytoplasmic domains (Swart, 2002). ALCAM has a very short cytoplasmic domain of only 34 amino acids, while BCAM and MUC18 have bigger cytoplasmic domains. This is an important consideration in the study of ALCAM because so far no interaction motifs have been identified in its cytoplasmic tail and there is only limited evidence for intracellular interactors, such as actin (Te Riet et al., 2007) and ubiquitin (Thelen et al., 2008). Within higher vertebrates, ALCAM is strongly conserved, with around 95% similarity between mouse, rat, rabbit and human (Swart, 2002). This suggests that ALCAM may

have similar functions across these species. This is important in the context of my thesis where both mouse and rat cells were examined.

Three isoforms of human ALCAM have been reported and are shown schematically in Figure 1.6. ALCAM-1 and ALCAM-2 are products of alternative splicing, with ALCAM-2 missing a short 13 amino acid sequence in the juxtamembrane region. No functional differences have been reported for the two isoforms. A third ALCAM variant, consisting of just the most distal extracellular V_1 domain, has been isolated from endothelial cells and is suggested to be the product of alternative splicing (Ikeda and Quertermous, 2004). In this study, it was shown that the soluble isoform could inhibit ALCAM homophilic interactions and could increase cell migration in both an ALCAM-dependent and independent manner. The equivalent splicing region of exon 3 is present in the ALCAM locus of the mouse genome and a transcript coding for soluble ALCAM was found by 3'-rapid amplification from mouse endothelial cell cDNA suggesting that this isoform is conserved between humans and mice.

ALCAM was identified as the heterophilic binding partner of the glycoprotein CD6 expressed on lymphocytes (Bowen et al., 1995, Skonier et al., 1997). Mapping studies have shown that the N-terminal V_1 domain of ALCAM binds to the membrane proximal scavenger receptor cysteine rich (SRCR) domain of CD6, as illustrated in Figure 1.7 (Skonier et al., 1997, Bowen et al., 1997). Their interaction is important for the stabilisation of the immunological synapse, and is required to elicit T-cell activation (Zimmerman et al., 2006, Gimferrer et al., 2004). The interaction of ALCAM and CD6 is highly conserved and displays cross-species binding with mouse and human ALCAM both capable of binding mouse and human CD6 (Bowen et al., 1997). ALCAM can also engage in homophilic interactions (Bowen et al., 1995). Structure-function analysis using antibodies to specific ALCAM domains and N-terminal truncated mutants

identified that the most distal ALCAM domains are responsible for ligand binding in *trans*, whereas the membrane proximal domains are responsible for ALCAM binding in *cis,* and leads to clustering (van Kempen et al., 2001).

Surface-plasmon-resonance experiments determined that the ALCAM-CD6 complex has a 100 fold higher affinity than the homotypic interaction between two ALCAM proteins (Hassan et al., 2004). ALCAM interactions have been further characterised using single-molecule force spectroscopy to compare homophilic binding and the heterophilic interaction to CD6 (Te Riet et al., 2007). The two interactions show very different properties, the ALCAM-CD6 interaction having a 100 fold lower dissociation rate and greater resistance to mechanical stress (i.e. more resistant to applied force), while the homotypic interaction displayed greater lability (Te Riet et al., 2007). The homophilic bonds lability could have functional importance because ALCAM is often expressed in migrating cells.

The ALCAM transmembrane region and cytoplasmic domain interact with the cytoskeleton. ALCAM co-immunoprecipitates with β-actin and interestingly disruption of the cytoskeleton enhances ALCAM avidity without affecting the affinity (Te Riet et al., 2007). These findings are consistent with data from Nelissen et al (2000), where cytochalasin D treatment (which inhibits actin polymerisation) resulted in increased ALCAM lateral mobility, clustering and cell adhesion. Since ALCAM adhesion is modulated by cytoskeletal rearrangements it was examined whether, similar to integrin and cadherin adhesion, Rho-like GTPases were involved. However, it was found that ALCAM adhesion regulation is independent of these proteins and is instead associated with PKCα activity (Zimmerman et al., 2004).

Interestingly, a second ALCAM soluble form, lacking the transmembrane and cytoplasmic domains is produced as a product of metalloprotease cleavage and

ALCAM was identified in a proteomic screen as a substrate for ADAM17 (Bech-Serra et al., 2006). Furthermore, the soluble ALCAM extracellular domain was immunoprecipitated from growth medium of epithelial ovarian cancer cells in culture and evidence of the cleaved fragment was found *in vivo* from patient ascites and sera (Rosso et al., 2007). In this study, the authors found that ALCAM cleavage was stimulated by EGF receptor activation and was ADAM-dependent. This has important implications for cancer, because inhibitors of ADAM cleavage decreased motility of these cells. Recently it has been proposed that targeting of ADAM17 cleavage and inhibiting of soluble ALCAM release may be a promising cancer therapy (Nuti et al., 2010). This is of particular interest considering that ADAM17 has been also shown to cleave the neurotrophin receptors $p75^{NTR}$ and TrkA as well as L1 (Ahmed et al., 2006, Diaz-Rodriguez et al., 1999, Maretzky et al., 2005).

Alterations in ALCAM expression as well as cleavage have been associated with many forms of cancer, poor prognosis and with tumour progression and metastasis (reviewed by Ofori-Acquah and King, 2008). Swart and colleagues have suggested that ALCAM may function as a cell density sensor and may act at the interface between growth and metastasis (Swart et al., 2005). As described earlier, ALCAM can bind homophilically in *trans* or in *cis*, and these authors propose that the resulting ALCAM network is important in sensing cell-cell interactions. A schematic representation of this model is shown in Figure 1.8. Upon expression of an amino-terminal truncated ALCAM (ΔN-ALCAM) mutant, the ALCAM network is disrupted and this interferes with cell adhesion without effecting soluble ligand binding (van Kempen et al., 2001). Further work on the ΔN-ALCAM showed that expression in adherent melanoma cells inhibited metalloprotease activation in 2D and 3D cultures, as well as in *ex vivo* tumours from mice (Lunter et al., 2005). These experiments found that despite the inhibition of metalloprotease activity, there was an increase in metastasis, which interestingly

invalidated the previous assumption that metastasis is always accompanied with increased metalloprotease activity.

Swart's group has since compared truncated ALCAM expression with its soluble ALCAM form (V_1 domain alone)(van Kilsdonk et al., 2008). This study revealed that although both ALCAM forms could disrupt the ALCAM network (Figure 1.8), they had both similar and opposite consequences. Expression of soluble ALCAM inhibited metalloprotease activity similarly to ΔN-ALCAM, but in contrast to ΔN-ALCAM, it actually decreased migration and metastasis (van Kilsdonk et al., 2008). The difference in metastatic potential was reflected by concomitant changes in L1-CAM expression and it was proposed that this could account for the differential effect on metastasis. L1-CAM was increased in ΔN-ALCAM cells but decreased in soluble ALCAM expressing cells, suggesting L1 expression was linked to metastatic potential.

As well as undergoing regulated proteolysis and having a regulatory role in metalloprotease activity, another interesting property of ALCAM is that it has also been shown to undergo endocytosis (Piazza et al., 2005). In this study, full-length ALCAM was identified as a potential therapeutic target for antibody-based immunotherapy in cancer. In a phage display library screen, human single chain antibody fragments were selected on the basis of whether they could be internalised in ovarian cancer cell lines (Piazza et al., 2005). The authors found that upon ligand binding (either CD6-Fc or I/F8 minibody) ALCAM was internalised in a clathrin-dependent compartment and recycled back to the plasma membrane. Furthermore, stimulation of ALCAM endocytosis increases epithelial ovarian cancer cell migration in a wound-healing assay (Rosso et al., 2007). Since ALCAM can undergo ligand-dependent internalisation in cancer cells, it was a good candidate to investigate its internalisation and axonal transport in neurons.

ALCAM is expressed in the nervous system and its expression is developmentally regulated (Dillon et al., 2005, Fournier-Thibault et al., 1999). It is associated with axon fasciculation and neurite outgrowth in several systems. In lower vertebrates, it was shown that ALCAM is important for motor neuron outgrowth and fasciculation. In fish, antibodies blocking ALCAM adhesion result in the misprojection and defasciculation of axons that express ALCAM as they exit the spinal cord (Ott et al., 2001). In chick, DM-GRASP, the orthologue of ALCAM, was shown to support neurite extension from distinct subsets of neurons by homophilic interactions (DeBernardo and Chang, 1995). Furthermore, using affinity chromatography, DM-GRASP was shown to interact with NgCAM (L1 chick orthologue) and antibodies blocking this interaction inhibited neurite extension on an NgCAM substrate (DeBernardo and Chang, 1996).

DM-GRASP expression is dynamically regulated during neuromuscular junction formation in the chick limb (Fournier-Thibault et al., 1999). The authors found that ALCAM is expressed on muscle cells and fibres and is downregulated upon innervation with motor neurons that also express ALCAM. In the mature limb ALCAM expression is only localised to the neuromuscular junction, but interestingly, this process is reversible. After muscle dennervation ALCAM is re-expressed on mature muscle fibres, as well as in regenerating motor neurons. Upon reinnervation, ALCAM expression is again confined to the neuromuscular junction (Fournier-Thibault et al., 1999). These results suggest that ALCAM homophilic interactions are important in neuromuscular junction maintenance, which is of particular interest in my investigation of CAMs contained in the axonal retrograde transport compartment in motor neurons. It is possible that ALCAM homophilic interactions between axon terminal and muscle could provide a muscle contact signal.

Further studies on DM-GRASP in chick have focussed on its role in the retina, where ALCAM expression is also spatiotemporally regulated. Avci et al (2004) found ALCAM is concentrated on retinal ganglion cell (RGC) axons during their outgrowth from the retina. RGCs showed a preference to grow along DM-GRASP/laminin substrates and this was inhibited by addition of blocking antibody fragments to ALCAM of its heterophilic binding partner NgCAM. In flatmount retina cultures, antibodies to DM-GRASP resulted in misprojections of the RGC axons at the point of the optic fissure where the axons grow into the optic nerve (Avci et al., 2004), suggesting that DM-GRASP adhesion is important in RGC outgrowth from the retina. More recent work from Pollerberg and colleagues reported that DM-GRASP is endocytosed at RGC growth cones (Thelen et al., 2008). They found that DM-GRASP endocytosis is clathrin-dependent and dynein-dependent, and is altered upon inhibition of MAPK and PI3K activity. In this study, a yeast-2-hybrid screen was conducted to look for interactors with the DM-GRASP cytoplasmic domain that could drive endocytosis. The authors found evidence that DM-GRASP's cytoplasmic domain has ubiquitin-binding activity, and is also a site of ubiquitination. The details of this interaction, however has not been clarified, and it has not been resolved whether DM-GRASP ubiquitination alters DM-GRASP internalisation or function (Thelen et al., 2008).

In the mouse, ALCAM expression has also been identified in the nervous system during development e.g. ALCAM specifically labels a subset of cranial sensory ganglia (Sekine-Aizawa et al., 1998). ALCAM is downregulated at points of defasciculation of primary vestibulo-cerebellar afferents and ALCAM substrates promote axonal outgrowth of these cells (Kawauchi et al., 2003). In further studies, it has been shown that ALCAM specifically labels spinal accessory motor neurons and their axons from E9.5-E12.5 and subsequently is also expressed in motor neurons in the ventral horn of

the spinal cord (Dillon et al., 2005). This suggests that ALCAM may be expressed on motor neurons in the ventral horn neuron cultures used in our experiments.

Since ALCAM is expressed in many cells of the murine nervous system, immune system and haematopoietic stem cells, it is perhaps surprising that mice lacking endogenous ALCAM ($ALCAM^{-/-}$) do not have an overt phenotype (Weiner et al., 2004). The mice are viable and fertile, and show only subtle defects in the nervous system. Problems with fasciculation are observed in their motor thoracic nerves and their RGCs (Weiner et al., 2004). RGCs have also been shown to misproject in the optic tectum of $ALCAM^{-/-}$ mice (Buhusi et al., 2009). The authors of this study suggest that ALCAM in the tectum is required for the successful targeting of RGC expressing L1, and is consistent with the finding that the two proteins interact (DeBernardo and Chang, 1996).

In summary, ALCAM possesses properties that make it of particular interest to study as a candidate protein transported in the axonal retrograde transport compartment and that could have a function related to neurotrophic signalling in neurons. Firstly, it is expressed in motor neurons during development and its expression is regulated by innervation of target muscles. Secondly, ALCAM is endocytosed and can be cleaved by metalloproteases and these properties are important in the ability of L1 and NCAM to cooperate in growth factor signalling. In this thesis, I examine whether ALCAM undergoes retrograde axonal transport in neurons and whether ALCAM, similarly to other IgCAMs, cooperates with neurotrophic signalling in the nervous system.

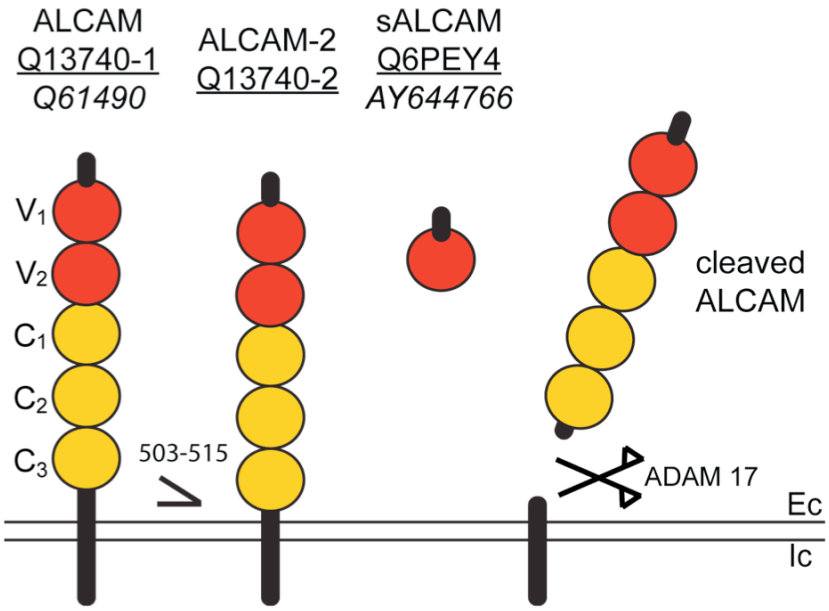

Figure 1.6 ALCAM forms in human and mouse

All reported ALCAM forms are shown (Accession numbers: human, underlined and mouse, italics). ALCAM consists of five extracellular domains, two variable immunoglobulin (IgG) domains (V_1 and V_2) and three constant type-2 IgG domains (C_{1-3}). ALCAM-2 has 13 amino acids removed in the juxtamembrane region by alternative splicing (indicated by the wedge). The soluble form is the V_1 domain alone, while another soluble form consisting of the entire extracellular domain is produced as a result of juxtamembrane cleavage by the disintegrin and metalloprotease, ADAM17 (scissors).

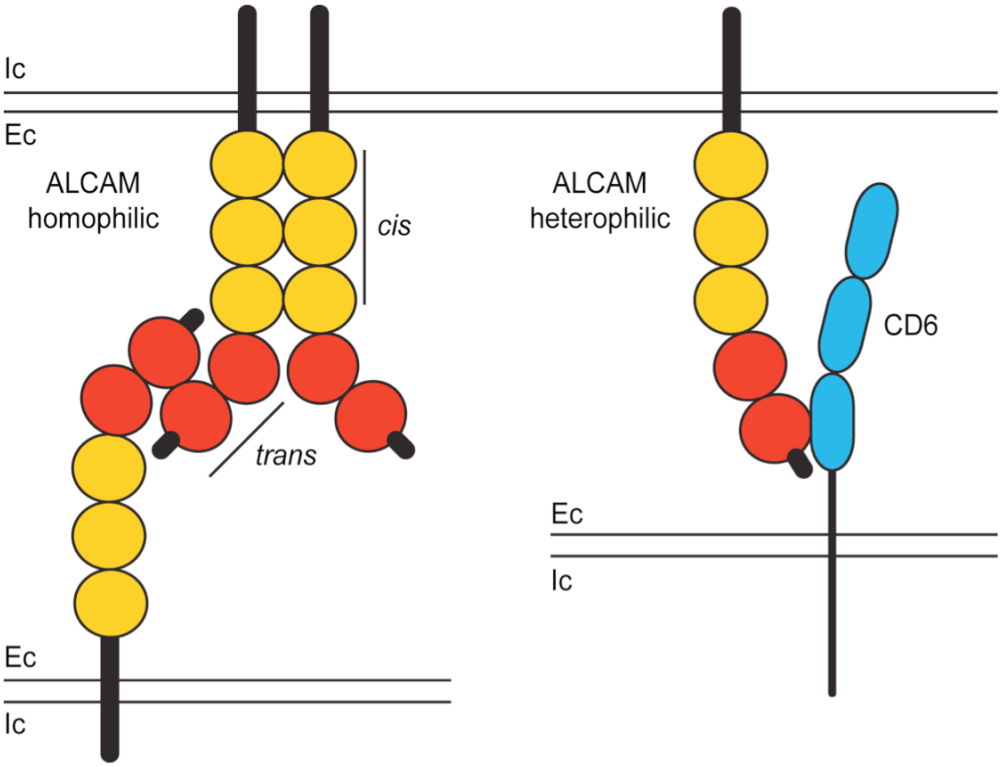

Figure 1.7 ALCAM engages in both homophilic and heterophilic interactions

Homophilic ALCAM binding can occur both in *cis* interactions via domain C_{1-3} and in *trans* via V_1 and V_2. ALCAM heterophilic binding to the juxtamembrane scavenger receptor cysteine rich (SRCR) domain of T-cell glycoprotein CD6 is mediated by its V_1 domain. The two forms of binding have very different properties, homophilic binding increases with avidity and has high lability, while heterophilic binding is of much higher affinity.

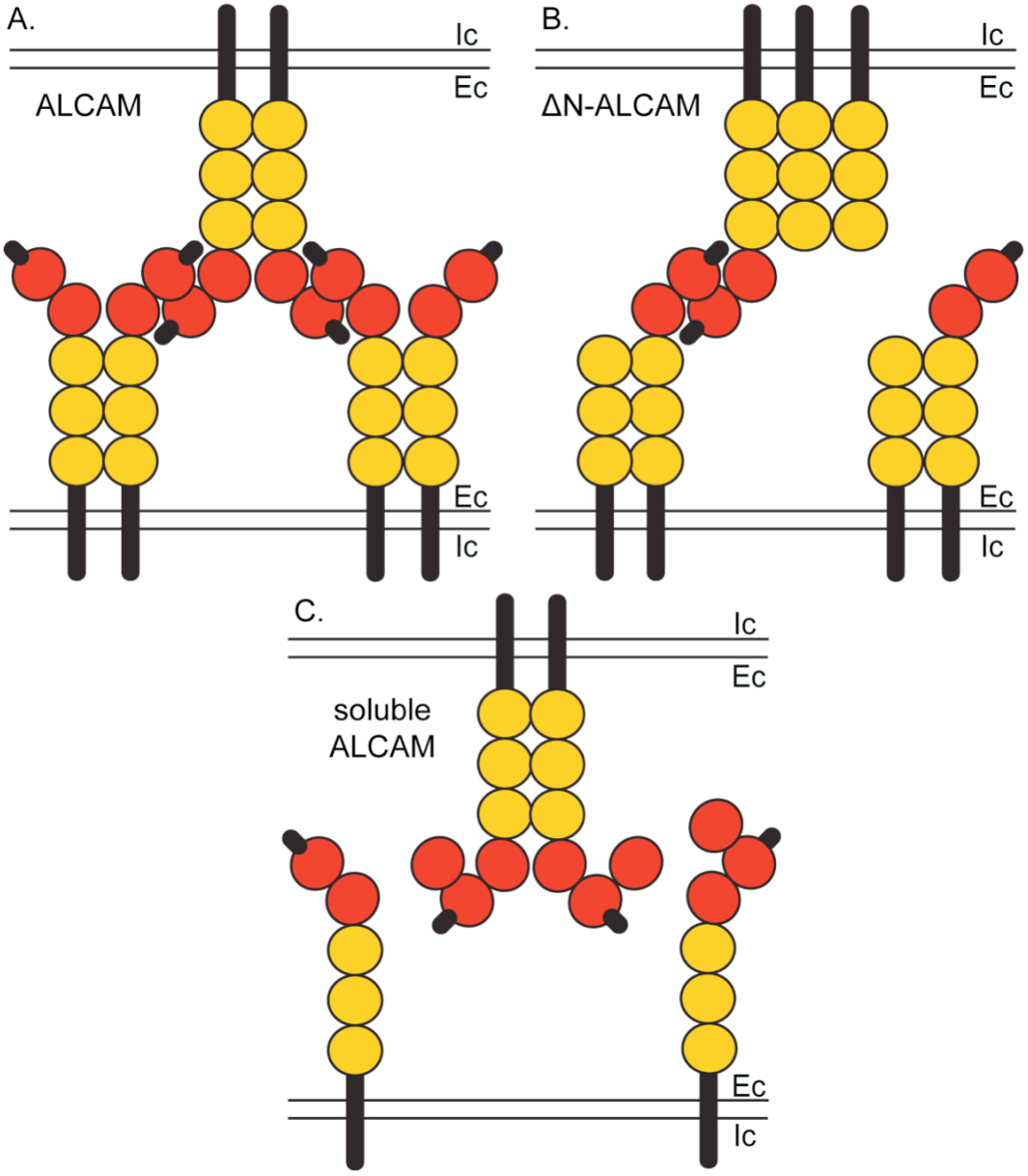

Figure 1.8 Model of ALCAM function

ALCAM can engage in homophilic interactions both in *trans* and *cis*, and thus forming an ALCAM network between two ALCAM expressing cells as shown in A. It has been proposed by Swart and colleagues that ALCAM lacking V_1 and V_2 (ΔN-ALCAM), disrupts formation of the network by disrupting binding in *trans*. However ΔN-ALCAM expression would still promote binding in *cis* and may partially compensate for loss of the network. In contrast, expression of soluble ALCAM would disrupt network formation without promoting *cis* interactions. The schematic illustrates the various ways in which ALCAM network formation can be interfered with and may explain differences in the effects of expressing mutant ALCAM constructs. (modified from (van Kilsdonk et al., 2008)

.

Chapter 2. Materials and Methods

2.1 Materials

2.1.1 Reagents

Laboratory chemicals were obtained from Sigma, Invitrogen, BDH-Prolabo or Fischer Scientific unless otherwise stated. Molecular biology reagents were obtained from Qiagen and restriction enzymes and DNA enzymes were from New England Biolabs. Fluorophore-conjugated secondary antibodies and LysoTracker Red DND-99 were supplied by Molecular Probes, while horseradish peroxidase (HRP)-coupled secondary antibodies were all from DAKO. Reagents for western blot visualisation by enhanced chemiluminescence (ECL) were supplied from GE Healthcare, while Kodak provided autoradiographic films.

2.1.2 Cell lines

Rat pheochromocytoma (PC12) cells were obtained from Dr T. B. Rogers, University of Washington USA (Herreros et al., 2000). Rat mammary adenocarcinoma (MTLN3) cells were a kind gift from Prof. E. Sahai, CRUK's London Research Institute (LRI). U251MG astrocytoma cells and mouse neuroblastoma (Neuro2A) were obtained in house from LRI cell services.

2.1.3 Bacteria

XL1Blue, TG1, BL21 competent bacteria were from LRI stocks and made in house. XL10-gold® ultracompetent bacteria were from Stratagene.

2.1.4 Vectors and expression plasmids

The pDendra-2N vector was obtained from Evrogen. The His_6-tag containing vector, pET30b-hERCC1 was a kind gift from Prof. N. McDonald, LRI. The CD8-CI-MPR pIRES-neo2 vector was the kind gift of Prof. M. Seaman, University of Cambridge.

2.1.5 Recombinant Proteins

The following proteins were obtained from R&D systems:

Rat GDNF family receptor alpha Fc chimera (GFRa-1/GDNF Ra-1 Fc chimera)

Mouse ALCAM/CD166 Fc Chimera (ALCAM-Fc)

Mouse CD6 Fc Chimera (CD6-Fc)

Human immunoglobulin IgG1 Fc (Hu-Fc)

Fluorescently labelled canine adenovirus serotype 2 (CAV-2-cy3) was a kind gift provided by Prof. E. Kremer, Institut de Génétique Moléculaire de Montpellier and was used in live-cell imaging experiments as described in (Salinas et al., 2009).

2.1.6 Primers for construct insert amplification

Table 2 lists the primers used for cloning ALCAM constructs in this study.

2.1.7 Antibodies

See Table 3 for primary antibodies used for immunofluorescence, western blot and live-cell imaging.

Table 2 Primers used for cloning

Insert Name	Primers	Digest
ALCAM-FL	MNP278ALCAMxho1start AAACTCGAGACCATGGCATCTAAGGTGTCC MNP285ALCAMbamh1stop AAAGGATCCTCGGCTTCTGTTTTGTGATT	Xho1 BamH1
Signal sequence	MNP278ALCAMxho1start AAACTCGAGACCATGGCATCTAAGGTGTCC MNP301_revpEcoR1_ssAL AAAAGAATTCACAGTGTACCATCCAAGGCCTGG	Xho1 EcoR1
ΔD1-ALCAM	MNP303_forpDeltaD1_AL AAAGTGAATTCTCCTACCCTAGTCAAGGTGTT MNP285ALCAMbamh1stop AAAGGATCCTCGGCTTCTGTTTTGTGATT	EcoR1 BamH1
ΔD1D2-ALCAM	MNP304_forpDeltaD1D2_AL AAAGTGAATTCTCCTACAGAGCAGGTGACA MNP285ALCAMbamh1stop AAAGGATCCTCGGCTTCTGTTTTGTGATT	EcoR1 BamH1
ΔC-ALCAM	MNP278ALCAMxho1start AAACTCGAGACCATGGCATCTAAGGTGTCC MNP302_revpDeltaCYMKK_AL AAAGGATCCTCCTTCTTCATGTACAGCCAGTAG	Xho1 BamH1
CD8Ec	MNP323_CD8startXho1 AAACTCGAGACCATGGCCTTACCAGTGACC MNP324_CD8revEcoR1 AAAGAATTCCCCCTCGTGTGCACTGCGCC	Xho EcoR1
ΔEc-ALCAM	MNP309_forpDeltaEc_AL AAAGTGAATTCTGACCAGGCAAAACTGATT MNP285ALCAMbamh1stop AAAGGATCCTCGGCTTCTGTTTTGTGATT	EcoR1 BamH1
ALCAM-Ec	MNP288_alcam_d1d5_Sfo1f AAGGCGCCATGGGATGGTACACTGTCAAC MNP282_alcam_d1d5_Xho1 AAACTCGAGTTTTGCCTGGTCATTCACCTT	Sfo1 Xho1
ALCAM-C	MNP283alcam_cyt_Nde1 AAACATATGTACATGAAGAAGTCCAAAACTGCA MNP284alcam_cyt_Xho1 AAACTCGAGGGCTTCTGTTTTGTGATTGTT	Nde1 Xho1

Table 3 Primary antibodies

Dilutions for western blot (WB), immunofluorescence (IF), -cell imaging (LC).

Antigen	Name & Supplier	Species	Dilution
ALCAM (mouse extracellular domain)	AF1172, R&D Systems	Goat	WB 1:500 IF 1:150 LC 1:500
ALCAM (mouse cytoplasmic domain)	In house ALCAM-C 4682	Rabbit	WB 1:250 (serum) or 1:100 (IgG) IF 1:600
ALCAM (mouse cytoplasmic domain)	In house ALCAM-C 4683	Rabbit	WB 1:250 (serum)
Dendra2	AB822, Evrogen	Rabbit	WB 1:10,000
His_6	6X His tag® HRP ab1187, Abcam	Rabbit	WB 1:1000
Kidins 220	In house 1F8 (Bracale et al., 2007)	Mouse	IF 1:400
LAMP2	A L-93, BD PharmingenTM	Rat	IF 1:500
P44/42 MAPK (ERK1/2)	Cell Signalling Cat No 9102	Rabbit	WB 1:1000
Phospho-p44/42 MAPK (ERK1/2)	Cell Signalling Cat No 9106	Mouse	WB 1:1000-1:2000
NCAMic	Cat 556323, BD PharmingenTM	Rat	IF 1:400
Thy1.1	MRC OX-7 BD PharmingenTM	Mouse	WB 1:1000
PanTrk	C-14, Santa Cruz	Rabbit	WB 1:500
PanTrk	B-3, Santa Cruz	Mouse	WB 1:500
Phospho-TrkA	Cell Signalling Cat No 9141	Rabbit	WB 1:1000
Tubulin	Tuj1, Covance	Mouse	WB 1:10,000
$p75^{NTR}$Ec	In house (Deinhardt et al., 2006b)	Rabbit	WB 1:1000 IF 1:1000 LC 1:500
$p75^{NTR}$Ic	In house (Deinhardt et al., 2006b)	Rabbit	WB 1:1000

2.2 Methods

2.2.1 DNA techniques and cloning

I designed ALCAM constructs tagged with Dendra (Gurskaya et al., 2006), a photoactivatable fluorescent protein for expression experiments in mammalian cells. I also designed His_6-tagged ALCAM protein fragments to be expressed in bacteria and the protein purified. The cloning strategies used to produce the ALCAM-Dendra and ALCAM-His_6 constructs are illustrated in Figure 2.1 and Figure 2.2 respectively.

2.2.1.1 Amplification of DNA fragments

Primers were designed to amplify full length ALCAM or its fragments from the image clone IMGCLO3501215, or the CD8 fragment from the CD8-CIMPR vector, a kind gift of Prof. M. Seaman, University of Cambridge. For each reaction, 10 ng of template DNA was used with 200 µM deoxynucleoside triphosphates (dNTPs), 0.5 µM of the appropriate forward and reverse primers, 1 µl PfuTurbo DNA polymerase and made up to a final reaction volume of 40-50 µl with MilliQ water.

The following PCR program was used adjusting the annealing temperature and elongation time according to what fragment was being amplified:

1. 95°C for 2 min
2. 95°C for 60 s
3. Annealing temperature for 30 s (approximately 10°C less than the melting temperature of forward and reverse primers)
4. 72°C for elongation time (approximated 60 s per Kb amplified)
5. Back to step 2, 29 times
6. 72°C for 10 min
7. 12°C thereafter

2.2.1.2 Insert and vector digests

The amplified insert and 2-4 µg of vector were digested with appropriate restriction enzymes, enzyme buffer and 1% Bovine Serum Albumin (BSA) in MilliQ water as

required, for 2 h at 37°C followed by 20 min at 65°C to inactivate the restriction enzymes. Digested vector DNA was then incubated with alkaline phosphatase for 1 h at 37°C to remove the reactive 5'-phosphates from the DNA fragment ends to minimise potential self-annealing of the vector.

To purify the DNA from the reaction mix, digested vectors were ran on 1% agarose gels, bands corresponding to the linearised vector were cut out and purified using the Qiagen QIAquick® Gel extraction kit. Inserts were purified directly after the digest using the Qiagen QIAquick® PCR purification kit.

The ALCAM extracellular domain (ALCAM-Ec) DNA sequence contains an internal Nde1 restriction site therefore the Nde1 enzyme was avoided when digesting the insert. Instead the insert was cut with Sfo1, to produce a blunt-end. Therefore, the Nde1 digested vector underwent an additional step to convert the Nde1 sticky-end into a blunt-end so that the Sfo1 digested ALCAM-Ec insert could ligate with the vector. This was undertaken in sequential steps as shown in Figure 2.2 and the restriction sites are represented in Figure 2.3. The pET-ERCC1 vector was digested for 2 hours at 37°C with Nde1 and heat inactivated for 20 minutes at 65°C. The vector DNA was then incubated with 1 µl of T4 polymerase and 30 µM dNTPs for 30 minutes at 15°C. The polymerase fills in the 5' overhang to convert the Nde1 sticky end into a blunt-end. The now blunt linearised vector was then purified using the Dyex® 2.0 Spin Kit and eluted in 35 µl required for the next digest with Xho1, BSA and its corresponding enzyme buffer for 2 h at 37°C, followed by heat inactivation at 65°C for 20 min. The pET Vector was separated from the ERCC1 insert on a 1% agarose gel, the digested vector band was cut out and vector DNA was purified using the Qiagen QIAquick® Gel extraction kit as before. The process is represented in Figure 2.2.

2.2.1.3 Ligation

Digested insert and vector were ligated by T4-ligase overnight at 16°C with a vector to insert ratio of 1:3 to 1:5. All reactions were conducted with a control sample, containing vector alone without insert.

2.2.1.4 Transformation of bacteria

Bacteria were transformed by adding 2 µl ligation mix to 100 µl bacteria for 10 min then by electroporating the mix at 2.5 kV. Bacteria were recovered by adding 900 µl of Super Optimal broth with Catabolite repression (SOC) medium. Transformants were selected by plating the bacteria on agar plates containing 50 µg/ml Kanamycin or 100 µg/ml Ampicillin, as appropriate.

For the more complicated ligations (i.e. ΔD1D2-ALCAM-D and CD8-ALCAM-D), supercompetent XL10-gold® bacteria were transformed by heat shock. Bacteria and ligation mix were incubated with β-mercaptoethanol for 30 min, heat shocked for 30 s at 42°C, kept on ice for 2 min then recovered with NZY+ broth (10 g NZ amine, 5 g NaCl, 5 g yeast extract in 1 litre deionised water was obtained from LRI media services and supplemented with 12.5 mM $MgCl_2$, 12.5 mM $MgSO_4$ and 20% w/v glucose before use) for 1 hour at 37°C. Transformants were plated on agar plates, with appropriate resistance as above.

2.2.1.5 Preparation of plasmid DNA

Bacteria from picked colonies were grown in lysogeny broth (LB, from LRI media services) at 37°C overnight. Plasmid DNA was isolated using Qiaprep® spin miniprep or Qiafilter® plasmid maxi kits as appropriate. Isolated plasmid DNA was analysed by diagnostic digests with restriction enzymes and ran on an agarose gel, followed by plasmid sequencing.

2.2.1.6 Plasmid sequencing

Approximately 200-300 ng of plasmid DNA was added to 3.2-5 pM of appropriate primers spanning around 400 base pairs (bp), BigDye Terminator (BDT) reaction mix and made up to 20 µl with MilliQ to undergo a sequencing PCR reaction:

1. 95°C for 2 min
2. 95°C for 30 s
3. 60°C for 4 min
4. Back to step 2, 29 times
5. 12°C thereafter

Samples were then purified by Dyex® 2.0 Spin Kit and sent for sequencing (LRI equipment park).

For all pDendra-2N constructs the following vector primers were used:

MNP279pdendraNforward AGGCGTGTACGGTGGGAG

MNP280pdendraNreverse GGTGTTCATGGTGGCGAC

For sequencing ALCAM image clone and subsequent constructs the following internal primers were used as appropriate:

MNP273ALCAMint1 GCATTCCGATCTTCTACGA

MNP274ALCAMint2 GCCATTCACCTGTTCTGTG

MNP275ALCAMint3 CGCGACTGTGGTGTGGATG

MNP276ALCAMint4 CCAGAGCACGATGAGGCAG

MNP277ALCAMint5 GCAGTTCATTCTACCAAGC

2.2.1.7 RNA isolation

TRIzol® Reagent (Invitrogen) was used to isolate RNA from 35 mm cell culture plates according to the manufacturers instructions. Briefly, cells were directly lysed in 1 ml of TRIzol reagent and incubated for 5 min at room temperature for dissociation of nucleoprotein complexes. Then 0.2 ml of chloroform was added per sample, tubes were shaken, incubated at room temperature for a further 2 min before centrifugation at 12,000 x g for 15 min at 4°C. The samples separated into two phases, a lower red phenol-chloroform phase and an upper aqueous phase that contains RNA. The aqueous phase was transferred to a new eppendorf and the RNA precipitated by mixing with 0.5 ml isopropanol at room temperature for 10 min followed by centrifugation at 12,000 x g 10 minutes at 4°C. The RNA pellet was washed in 1 ml 75% ethanol, vortexed and centrifuged for 5 minutes at 7,500 x g 4°C. Finally, pellets were left to dry and then resuspended in water. The concentration and integrity of the RNA was verified using the Nanodrop 1000 spectrophotometer (Thermo Scientific). Absorbance is measured at 260 nm and 280 nm (represented as if recorded with a conventional 10mm light path). The absorbance ratio 260/280 is a measure of the RNA purity. Ideally the ratio should be ~2 for RNA, if it is lower it may indicate the presence of contaminants such as proteins. I also analysed RNA samples by electrophoresis on a 1% agarose gel where preserved RNA should resolve into 2 distinct bands.

2.2.1.8 cDNA synthesis and analysis

I used the Superscript® Vilo cDNA synthesis Kit (Invitrogen) to amplify cDNA samples from purified RNA. In subsequent PCR reactions 2 µl of the resulting cDNA preparation was used with the appropriate primers (ALCAM or CD6 forward and reverse primers) and MegaMix (Microzone Ltd).

ALCAM	MNP274ALCAMint2	GCCATTCACCTGTTCTGTG
	MNP308ALCAMin3_rev	CACCACAGTCGCGTTCCTAC
CD6	MNP338_CD6forwardprimer	GTGTGTAAGCAACTGAAGTG
	MNP339_CD6revprimer	TGAGGGCGGGCTCCTGTCCT

2.2.2 Mouse breeding and genotyping

Mice lacking ALCAM were a kind gift from Dr. J. Weiner at the University of Iowa. The mice were generated using knock-in techniques, by homologous recombination, to introduce a GFP followed by a stop codon into the endogenous ALCAM locus (Weiner et al., 2004). There is no evidence of ALCAM transcription downstream of the insertion and there is no evidence of ALCAM protein expression in the knockout mice. In the original paper, the mice are named $BEN^{-/-}$ mutant mice. BEN is one of the many names used for the ALCAM protein (names are reviewed by Swart, 2002). Throughout this thesis I will refer to these mice as ALCAM knockout animals ($ALCAM^{-/-}$).

The colony is maintained by breeding heterozygous ($ALCAM^{+/-}$) animals to generate all three genotypes; wild type, $ALCAM^{+/-}$ and $ALCAM^{-/-}$. Mice and embryos are identified by genotyping with the following PCR program using DNA extracted from adult ear snips, tail snips or embryonic tissue, using Viagen DirectPCR® lysis reagent. The forward primer binds to the ALCAM locus upstream of the knockout insertion and differential reverse primers are used, which bind to the wild type sequence or the EGFP sequence in the knockout allele.

Primers	BEN-SA:	5’ CTA AGG CGA GAC CCA CAA GCG 3’
	BEN-Leader-Rev2:	5’ GAT CAA GAG GCA GAA AAC CAG 3’
	EGFP-Rev	5’ GTC GTC CTT GAA GAA GAT GG 3’

ALCAM genotyping PCR programme

1. 95°C for 3 min
2. 95°C for 30 s
3. Annealing temperature 58°C for 30 s
4. 72°C for elongation 45 s
5. Back to step 2, 24 times
6. 72°C for 10 min
7. 12°C thereafter

Genotyping was run as two separate reactions: BEN-SA + BEN-Leader-Rev2 for wild type and BEN-SA + EGFP-Rev for knockout reactions, using 2-5 pM of each primer, 1.5 µl of DNA and 15 µl of MegaMix (Microzone Ltd). Samples were run on a 1.5% agarose gel to resolve a 150 bp wild type band and a 400 bp knockout allele (Weiner et al., 2004).

2.2.3 Cell culture

2.2.3.1 Primary ventral horn neuron cultures

Pregnant CD1 female mice were euthanised using CO_2 or intraperitoneal injection of pentobarbitone and E12.5-13.5 embryos were removed by hysterectomy. Embryonic spinal cords were dissected out and the meninges and dorsal root ganglia (DRG) were carefully removed. The dorsal portions of the spinal cords were cut away to isolate the ventral horn, which were dissociated by DNAase incubation and centrifugation at 370 x g through a 4% BSA cushion (Arce et al., 1999). Cells were resuspended in complete medium composed of Neurobasal medium (GIBCO®, Invitrogen), 2% B-27 Supplement (Invitrogen), 2% horse serum, 0.5 mM glutamine (CRUK Cell Services), 0.05% β-mercaptoethanol, 10 ng/ml ciliary neurotrophic factor (CNTF) (Invitrogen), 0.1 ng/ml glial cell-derived neurotrophic factor (GDNF) (Invitrogen), 50 units/ml penicillin, 50 µg/ml streptomycin solution. Cells were plated onto poly-D,L-ornithine/laminin-coated 35 mm glass-bottom dishes (MatTek) or coverslips at a density of 75,000-

100,000 cells/plate and maintained in culture for 5-10 days at 37°C and 7.5% CO_2. Ventral horn neuron cultures are enriched for motor neurons, but also contain interneurons and glia. Previous characterisation of ventral horn neuron cultures in the laboratory established by immunofluorescence that 30-40% of neurons in these cultures are motor neurons, using peripherin as a marker. No sensory neurons are present because the dorsal part of the spinal cord is removed.

For dissections of ALCAM knockout litters an additional genotyping step from embryo tail and feet was carried out during isolation of the ventral horns. Ventral horns of the same genotype were then pooled before dissociation.

2.2.3.2 Magnetic isolation of Hc retrograde carriers

For Hc endosome purification Hc-MIONs were used, as previously described in (Deinhardt et al., 2006b) and is represented schematically in the Introduction, Figure 1.3. Ventral horn neurons were isolated from 10 mouse embryos and plated on to 100 mm dishes. Ventral horn neuron cultures were incubated with MION beads either for 30 min on ice followed by two washes in Hanks buffered salt solution (HBSS - obtained from LRI media services) supplemented with 0.4% BSA and then shifted to 37°C for 1 hr in complete medium, or added directly to ventral horn neuron cultures incubated at 37°C in complete medium for 1-2 h. After cooling on ice, cells were scraped in HBSS supplemented with a protease inhibitor cocktail (Roche), and centrifuged at 170 x g for 5 min at 4°C. Cells were resuspended in breaking buffer (0.25 M sucrose, 10 mM HEPES-KOH, pH 7.2, 1 mM ethylenediaminetetraacetic acid (EDTA), 1 mM MgOAc, complete protease inhibitors). Ventral horn neurons were passed 15 times through a cell cracker (18 µm clearance; EMBL) and clarified at 690 x g for 10 min at 4°C to remove nuclear membranes. AS columns (Miltenyi Biotech) were equilibrated with breaking buffer supplemented with 0.4% BSA. The column was placed inside the magnetic field of the SuperMACS II (Miltenyi Biotech), and the postnuclear supernatant

was loaded two times onto the column. After washing with 15 ml breaking buffer, the column was removed from the magnetic field and elution was carried out with 5.5 ml of breaking buffer containing 300 mM KCl. Proteins were precipitated (see 2.2.4.3) before solubilisation in Laemmli sample buffer. Proteins were separated by SDS-PAGE (4-12%).

2.2.3.3 Primary astrocyte cultures

Astrocytes were isolated from decapitated CD1 neonate pups at 2 days after birth (P2). The spinal cord was isolated and meninges were removed then transferred to HBSS. Two working solutions, A and B were prepared and kept at 37°C: Solution A comprised of Eagle's balanced salt solution (LRI media Services), supplemented with 1% penicillin/streptomycin, 0.3% BSA and 20 µg/ml DNAse. Solution B is comprised of solution A supplemented with 0.25 mg/ml trypsin and 0.15 mg/ml DNAse.

Spinal cords were chopped into small pieces, then transferred to solution A and triturated. The suspension was centrifuged at 4°C for 5 min at 800 x g. The supernatant was discarded and the pellet resuspended in 10 ml of solution B and incubated for 10 min at 37°C with 5% CO_2, followed by a second centrifugation for 5 min at 800 x g. The supernatant was discarded and the pellet resuspended in solution A, followed by a final centrifugation for 5 min 800 x g. The final pellet was resuspended in Dulbecco's modified eagle medium (DMEM) (from LRI media services) supplemented with 10% fetal bovine serum and 1% penicillin/streptomycin. Before plating, the solution was passed through a N70 filter to remove large debris and aggregates. Cells were maintained in culture for 7 days at 37°C and 7.5% CO_2 to reach confluency before preparing cell lysates.

2.2.3.4 PC12 cell culture

PC12 cells were maintained in Dulbecco's modified eagle medium (DMEM) (GIBCO®, Invitrogen) supplemented with 7.5% horse serum, 7.5% fetal bovine serum, 4 mM glutamine and 1% penicillin/streptomycin. PC12 cells were frozen in 45% horse serum, 45% fetal bovine serum and 10% sterile dimethyl sulfoxide (DMSO), frozen at -80°C and stored in liquid nitrogen.

2.2.3.5 PC12 cell transfection

Cells were transfected at 30% confluency one day after plating on 0.1 mg/ml polylysine-coated coverslips. Lipofectamine 2000 transfection reagent was used at a ratio of 0.5 µg DNA to 1.5 µl lipofectamine per coverslip in a 12 well plate. After 5 min incubation of DNA and lipofectamine in 100 µl Optimem (GIBCO®, Invitrogen) respectively, DNA and transfection reagent were incubated for a further 20 min before addition dropwise to cells in DMEM free of antibiotics and serum. For transfections in 30 mm dishes the amount of DNA and lipofectamine were scaled up 2.5 times, while in 100 mm dishes 8 µg DNA and 24 µl of transfection reagent were diluted in 800 µl of Optimem respectively. After 4 h, the transfection medium was changed to differentiation medium alone (DMEM supplemented with 0.1% horse serum, 0.1% fetal bovine serum, 4 mM glutamine) or with the appropriate differentiation stimulus. Nerve growth factor (NGF) was used at 100 ng/ml, dibutyryl-cyclic adenosine monophosphate (dbcAMP) was used at 0.1 mM or 0.5 mM, while glial cell-derived neurotrophic factor (GDNF) was used at 100 ng/ml in the presence of 10 µg/ml the co-receptor GDNF family receptor alpha chimera (GFRα-Fc). On addition of human Fc (Hu-Fc), CD6-Fc or ALCAM-Fc chimeras, they were used at a concentration of 1 µg/ml or 10 µg/ml

2.2.3.6 PC12 Neurite outgrowth analysis

Cells were fixed for 15 minutes in 4% paraformaldehyde (PFA) in phosphate buffered saline solution (PBS) at 3, 5 or 7 days after transfection depending on the

differentiation stimulus. Cells were then quenched with 50 mM NH4Cl in PBS pH 7.5 for 10 minutes, rinsed in PBS and permeabilised in 0.1% Triton X-100 for 5 min. After rinsing in PBS cells were incubated with 1:2000 DRAQ5 (BioStatus Ltd) a cell permeant DNA probe to stain nuclei for 30 minutes, washed in PBS several times and mounted in 10% mowiol 4-88 solution. Pictures were taken on a Zeiss LSM 510 confocal microscope using a 40x 1.3 NA Plan-NeoFluor oil-immersion objective. At least 10 random fields of view were selected per coverslip. An average of 48 cells were counted per condition in the original Dendra versus ALCAM-D neurite outgrowth experiments (see Chapter 5.1,) and in subsequent neurite outgrowth experiments a similar strategy was used. Cells were regarded as exhibiting neurite outgrowth if the longest neurite was at least two times the widest length of the soma. Data was analysed using 1-way ANOVA followed by a post-hoc Bonferroni's test on selected groups or using an unpaired t-test as appropriate.

2.2.4 Biochemical techniques

2.2.4.1 Preparation of cell and tissue lysates

Mouse brain was dissected and kept at 4°C in TNE lysis buffer (10 mM Tris-HCl pH 8, 150 mM NaCl, 1 mM EDTA, 1% NP40). Brain was homogenized in lysis buffer supplemented with a protease inhibitor cocktail (Roche). Ventral horn neuron or astrocyte cultures were plated on 100 mm dishes. After approximately 7 days *in vitro*, cells were washed in PBS, scraped in HBSS supplemented with protease inhibitors, and centrifuged at 170 x g for 5 min at 4°C. Cells were resuspended in TNE lysis buffer supplemented with protease inhibitors. Brain or cell homogenate was incubated with agitation for 30 min at 4°C, then centrifuged at 17,000 x g for 15 min. Supernatants were used immediately or snap frozen and kept at -80°C.

For signalling experiments, which involved analyzing phosphorylated proteins, a high sodium dodecyl sulphate (SDS) lysis buffer was used (2% SDS, 0.05 Tris-HCl pH 6.8). Cells starved of serum and neurotrophins for 5 hours were stimulated with 100 ng/ml NGF for the times indicated. Cells were washed once with PBS then 100 µl of high SDS lysis buffer at 100°C was added to the cells directly. Cells were not scraped but triturated slowly up and down using a p200 Gilson pipette, and then put in a tube on ice. Samples were then sonicated 3 times for 10 s for disaggregation. Samples supplemented with Laemmli sample buffer without SDS (60 mM Tris-HCl pH 6.8, 10% glycerol, 5% β-mercaptoethanol, 0.01% bromophenol blue) were then analysed by SDS-PAGE and western blot.

2.2.4.2 Protein concentration

The Bradford method was used to determine protein concentration (Bradford, 1976). A standard curve 0-10 µg of IgG was used with Biorad protein assay diluted in water and the samples were measured at 595 nm. Samples in high SDS lysis buffer were analysed using the BCA^{TM} protein assay (Thermoscientific).

2.2.4.3 Protein precipitation

Proteins were precipitated with 10% trichloroacetic acid (TCA) using 0.05% sodium deoxycholate as a carrier, centrifuged, washed with -20°C acetone and air dried before solubilisation in Laemmli sample buffer (60 mM Tris-HCl pH 6.8, 10% glycerol, 2% SDS, 5% β-mercaptoethanol, 0.01% bromophenol blue).

2.2.4.4 Sodium dodecyl sulphate polyacrylamide gel electrophoresis (SDS-PAGE)

Protein samples were prepared in Laemmli sample buffer, boiled for 3-5 min or left for 25 min at room temperature. For all SDS PAGE analysis NuPAGE 4-12% Bis-tris gels were run in Nupage MOPS running buffer unless otherwise stated.

2.2.4.5 Western blot analysis

After SDS-PAGE separation, protein was transferred to methanol-activated polyvinylidene fluoride (PVDF) membrane. After blocking for 45 min in 5% milk or 5% BSA in PBS with 0.01% Tween 20 (PBST) as appropriate, membranes were incubated with the primary antibody in the same blocking buffer for 1 hour at room temperature or overnight at 4°C. Bound primary antibodies were visualised by appropriate HRP-coupled secondary antibodies and enhanced chemiluminescence (ECL, Amersham Biosciences). In some experiments primary antibodies or serum were cross absorbed with purified protein, either 3 µg of CD6-Fc or 20 µg of ALCAM-C for 90 min in blocking solution before addition to the membrane.

2.2.4.6 Densitometric quantification of western blots

Quantification of phosphorylated protein by western blot was carried out using ImageJ software to measure band pixel intensity for the proteins of interest. The amount of phosphorylated protein was normalised according to the total protein in the sample (phosphorylated protein intensity multiplied by the ratio between the sample total protein and the average total protein per condition). Due to the limited transfection efficiency, the change in phosphorylation observed by western blot was expected to be small. To increase the power with which we could resolve differences statistically, we collaborated with Dr Gavin Kelly (LRI, Bioinformatics and Biostatistics Service). For this predicted intensity values were generated using a model that removed experiment and time-trend effects (i.e. variability introduced as an effect of the different cell preparations and times after NGF treatment). This allowed us to pool all the data obtained across all experiments and timepoints. We could then test whether there was a difference between the predicted values in our condition of interest i.e. if phosphorylation was different between ALCAM-D or Dendra-transfected cells. ANOVA was used to determine whether the difference between, the Dendra and ALCAM-D predicted phosphorylation values, was larger than that ascribable to noise.

2.2.4.7 Production of recombinant His_6-tagged ALCAM

BL21 bacteria transformed with ALCAM-His_6 constructs were grown in 2 litres 2YT (LRI media services) supplemented with 50 µg/ml kanamycin. At A600 of 0.6-0.8 1 mM isopropyl β-D-1-thiogalactopyranoside (IPTG) was added and bacteria were incubated for 6 h at 27°C to induce protein expression. The following steps were undertaken at 4°C or on ice. Samples were centrifuged for 15 minutes at 5,000 rpm (JA-10 Beckman), supernatant discarded and pellets washed in PBS-T. The samples were centrifuged again for 10 min at 10,000 rpm, discarding the supernatant. The bacterial pellet was then resuspended in Breaking Buffer (25 mM Tris/HCl pH 7.8, 300 mM KCl, 2 µg/ml pepstatin A, 1mM phenylmethylsulfonyl fluoride (PMSF) and β-mercaptoethanol) and passed through the French Press (1300 PSI; MaxiCell; 2 times). The bacterial lysate was centrifuged at 20,000 rpm (JA-20 Beckman) for 15 minutes.

The protein was then purified using a chromatographic method. Buffer A (50 mM Tris-HCl pH 7.8, 600 mM KCl, 4 mM β-mercaptoethanol and 20 mM imidazole) and Buffer B (50 mM Tris-HCl pH 7.8, 600 mM KCl, 4 mM β-mercaptoethanol and 500 mM imidazole) were prepared. For each litre of bacterial culture, 3 ml of Qiagen Ni-NTA 50% beads were used. Beads were washed with Buffer A, prior to adding the bacterial supernatant for 2 hours at 4°C on a rotor wheel. The bead suspension was then transferred to the column and allowed to pack. To elute the protein, a linear gradient of buffer B was run across the column (Biologic LP (BioRad), rate of 0.5 ml/min, fractions 0-25 buffer A, fraction 25-85 linear gradient buffer B, collection started at fraction 25). 10 µl of each fraction were treated with Laemmli sample buffer and analysed by SDS-PAGE. Gels was then stained with Coomassie Blue (0.1% coomassie blue stain, 50% methanol, 10% acetic acid), before destaining and drying, or transferred to methanol activated PVDF membrane for western blot analysis with anti-His_6 antibodies.

2.2.4.8 Production of recombinant atoxic fragment of the tetanus toxin (Hc)

TG1 bacteria transformed with the triple tagged Hc vector pGEX3T-TeNTHc were grown in 2YT with 100 µg/ml ampicillin at 37°C until A600 ~ 0.8, whereupon 1 mM of IPTG was added, and incubation was continued for 4 hours. Bacteria were harvested by centrifugation at 5000 rpm, washed in PBST. After a further centrifugation, pellets were resuspended in Resuspension Buffer (0.05% PBST, protease inhibitors (Roche) and 1 mg/ml lysozyme). Samples were frozen in liquid nitrogen then thawed in a hot water bath; this was repeated twice to lyse the cells. Samples were then centrifuged 28,000 rpm (Beckman Ti-70) at 4°C 20 min. Supernatant was incubated with 2 ml of 50% glutathione-agarose beads per litre of bacterial culture, for 2 hours with agitation at 4°C. As for His_6-tagged protein purification (section 2.2.4.7), the sample plus beads were added to a column, allowed time for packing of the beads and then washed with PBST. To reduce sample contamination by chaperones and unfolded protein, pre-warmed DNA-K elution buffer (10 mM $MgSO_4$, 50 mM Tris-HCl pH 7.4, 2 mM ATP) was added to the resin. Cleavage was carried out by adding Thrombin cleavage buffer (TCB - 50 mM Tris-HCl pH 8.0, 250 mM NaCl, 0.1% β-mercaptoethanol) supplemented with 30 units of thrombin per litre of bacterial culture for 30 minutes on a rotorary wheel at room temperature. The supernatant was decanted, resin washed with TCB supplemented with 0.05 mM PMSF and then with TCB containing 0.5 M NaCl. Protein was dialysed overnight at 4°C in dialysis buffer (20 mM Hepes-NaOH pH 7.5, 300 mM NaCl, 5% glycerol, 0.025 mM Dithiothreitol (DTT)).

2.2.4.9 Hc and BSA-conjugated MIONs

Amino-derivatised monocrystalline iron oxide nanoparticles (MION) were a kind gift of Prof. A. Moore, Harvard University, MA, USA. The beads were coupled to BSA or purified recombinant atoxic fragments of the tetanus toxin (Hc) as illustrated in Figure 2.4. The Hc fragment is tagged with a VSVG epitope and cysteine-rich tag (Lalli et al., 2003b), the latter of which is used to cross-link the peptide to the beads. MIONs were

initially incubated with 1 mM EDTA and 4 mM succinimidyl 4-[N-maleimidomethyl] cyclohexane-1-carboxylate (SMCC) for 30 minutes at room temperature followed by 2 hours at 4°C on a rotor wheel. This produces MIONs with maleimide-activated moieties that can react with sulfhydryls. MIONs were then purified through a pre-equilibrated PD10 column and divided into 2 batches, to label with 200 µg BSA or Hc previously treated with 1 mM Tris (2-carboxyethyl) phosphine (TCEP) for 30 min. Reaction mixes were incubated for 48 h at 4°C. The reaction was blocked by addition of 10 mM β-mercaptoethanol overnight. The Hc- or BSA-conjugated MIONs were purified by gel filtration using Sephacryl S100HR, using a flow rate 0.2 ml/min in PBS.

2.2.4.10 Membrane stripping experiment

For the membrane stripping experiment, ventral horn neuron cultures were scraped in HBSS containing protease inhibitors. Cells were diluted with equal volume of stripping buffer (0.2 M Na2CO3 (pH 11.2 with $NaHCO_3$), 2 M KCl, 4 mM EDTA, 0.05% saponin (Sigma)), or alternatively mixed with 4 M KCl up to a 1 M final concentration. Samples were incubated for 30 min at 4°C and centrifuged at 100,000 x g for 30 min. Proteins in supernatants were TCA precipitated (see 2.2.4.3) and pellets were resuspended in loading Laemmli sample buffer.

2.2.4.11 Deglycosylation experiment

I used the enzymatic protein deglycosylation kit (sigma EDEGLY) following manufacturers recommendations, then analyse ventral horn neuron culture protein samples by SDS-PAGE and western blot.

2.2.4.12 Immunoprecipitation experiments

PC12 cells 2 to 3 days after transfection with full-length ALCAM tagged with Dendra (ALCAM-D) or Dendra (see Figure 2.1) were maintained in differentiation medium treated with or without NGF. Cells were washed two times with PBS on ice before addition of IP Lysis buffer (150 mM NaCl, 1% Nonidet P-40, 50 mM Tris-HCl, pH 8)

supplemented with fresh EDTA-free protease inhibitors. After 10 minutes rocking at 4°C, cells were scraped on ice and clarified by centrifugation at 18,000 x g at 4°C for 15 minutes. The protein concentration was determined using the Biorad assay. 1 mg of protein was used per immunoprecipitate. Either Trueblot^{TM} anti-rabbit Ig IP beads (eBioscience) or Protein A-sepharose beads (Sigma) were used for ALCAM-D or tropomyosin receptor kinase A (TrkA) immunoprecipitation respectively. Cell lysates were precleared by incubation with beads alone for 30-60 minutes on a rotor wheel. Supernatants were transferred to new tubes and beads were sampled to analyse proteins that interact with the beads alone (preclear beads). Antibodies directed to ALCAM-D or TrkA (5 µg each) were added to the precleared supernatants for 1-2 hours on a rotor wheel. Subsequently, the appropriate beads (Trueblot for ALCAM-D and protein A for TrkA immunoprecipitations respectively) were added to the tube for a further 2-3 hours. Tubes were centrifuged, exhausted supernatant removed and a sample taken for western blotting. Preclear and immunoprecipitate beads were washed 3-5 times with IP buffer before elution of protein by direct addition of 30 µl of 2.5 x leammli sample buffer. Samples were run on a 4-12% NuPAGE, transferred to PVDF for further analysis of the membrane by standard western blotting. For experiments that utilised the Trueblot system, the appropriate Rabbit TrueblotTM:Horseradish Peroxidase (HRP) secondary antibody was used at 1:1000 (eBioscience).

The U251MG immunoprecipitation, carried out by my colleague in the laboratory Claire Thomas, was conducted using 0.5 mg of lysate. Either 10 µg of 4682 antibody or rabbit IgG was bound to Protein A beads in PBS and lysate was precleared with beads alone for 2 h with rotation. Beads washed in TNE lysis buffer were mixed with precleared lysate for 3 hours on the rotor wheel. Supernatant was sampled, the beads washed 5 times and the protein was eluted in 25 µl Laemmli sample buffer. Samples and beads were analysed by western blot.

2.2.4.13 Detergent resistant membrane preparation

PC12 cells transfected and differentiated in the presence of NGF for 3 days were washed with cold HBSS, excess wash was removed with a pipette before adding 1 ml 1% Triton X-100 in HBSS supplemented with EDTA free protease inhibitors (Roche) at 4°C. Cells were scraped on ice, then passed through a 25g needle 10 times, and left to solubilise on ice for 30 min. Samples (1 ml) were adjusted to 41% sucrose by adding pre-ground sucrose, vortexed and left to dissolve on a rotor wheel for 5-10 minutes. The samples were transferred to Beckman 9/16 x 3 ¾ inch tubes, and overlaid with 8.5 ml 35% sucrose then 2.5 ml 16% sucrose both dissolved in HBSS supplemented with protease inhibitors. Samples were then separated by centrifugation at 35,000 rpm in SW40 Ti (154,693 x g av., 217,874 x g max) for 18 hours at 4˚C with 0 deceleration. Twelve or thirteen 1 ml samples were collected, and the protein precipitated with 0.1% sodium deoxycholate and 800 µl 15% TCA for 15 min on ice (see 2.2.4.3). Samples were centrifuged at 13,000 rpm 15 minutes at 4°C, pellets washed with -20°C acetone, and centrifugation repeated for 10 min, then pellets were allowed to air dry before adding 25 µl of 2.5 x Laemmli sample buffer. pH was adjusted with Tris-base, and loaded on SDS-PAGE for analysis.

2.2.5 Visualisation and imaging techniques

2.2.5.1 Immunofluorescence

Ventral horn neurons or PC12 cells on coverslips were fixed in 4% PFA in PBS for 20 min, quenched with NH4Cl: pH 7.5 for 10 min and washed with PBS. Neurons or PC12 cells were permeabilised for 5 min with 0.1% Triton X-100 in PBS as necessary and were blocked in blocking solution (10% horse or goat serum according to the species of the secondary antibody to be used), 0.25% gelatin and 2% BSA). The cells were then incubated with primary antibodies for 30-60 min in blocking solution (see Table 3 for primary antibodies used in these studies). After washing, cells were incubated for

30 min with appropriate secondary antibodies diluted in blocking solution. After extensive washing, cells were mounted in 10% mowiol 4-88 solution. Cells were visualized using the Zeiss LSM 510 confocal laser scanning microscope using either the 63x 1.4 NA Plan-Apochromat or the 40x 1.3 NA Plan-NeoFluor oil-immersion objectives.

2.2.5.2 Conjugation of antibody

The goat anti-mouse ALCAM (AF1172 R&D Systems) antibody or the anti-$p75^{NTR}$CTD (Deinhardt et al., 2007) were labelled with the Alexa Fluor® 488 or 555 Monoclonal Antibody Labelling Kit (Invitrogen).

2.2.5.3 Internalisation assay

Ventral horn neuron cultures at 4°C or 37°C were exposed to the Alexa Fluor-conjugated primary antibody directed against the extracellular domain of the cell-surface molecule of interest (e.g. ALCAM or $p75^{NTR}$). Ventral horn neurons were washed in medium to remove unbound antibody then incubated at 37°C for 1-2 hours to allow for internalisation and transport of the complex. Neurons were acid washed (100 mM Citrate-NaOH pH 2, 140 mM NaCl) to remove the fraction of antibody remaining on the surface, then fixed, permeabilised and processed in the same way as for standard immunofluorescence as described in 2.2.5.1.

2.2.5.4 Measurement of axonal transport

Ventral horn neurons were incubated with 1:500 to 1:1000 ALCAM-Alexa®488 (αALCAM488) alone or in the presence of 40 nM Hc-AlexaFluor®555 (Hc-555) or anti-$p75^{NTR}$-AlexaFluor®555 (α$p75^{NTR}$555) in complete medium for 30 min at 37°C. Ventral horn neurons were then washed three times with imaging medium (Dulbecco's minimum essential medium without phenol red (DMEM-), riboflavin, folic acid and penicillin/streptomycin, supplemented with 30 mM Hepes-NaOH pH 7.4). In some

experiments, αALCAM488 was incubated in the presence of 75 nM of LysoTracker Red DND-99.

Ventral horn neurons were placed in a 37°C humidified chamber and an image taken every 5 s with a Zeiss LSM 510 confocal laser scanning microscope using a 63x 1.4 NA Plan-Apochromat oil-immersion objective. Carrier tracking was performed on time-lapse sequences using motion analysis software (AQM tracker). Only carriers that moved over 3 or more consecutive time points were analysed. Hc moves in the retrograde direction and this feature was used to determine the direction of transport in the axon during co-transport experiments. The distance covered by a carrier between two consecutive frames was used to calculate the speed (Bohnert and Schiavo, 2005). Speed distributions were plotted to show the relative frequency of single movements with identical speed and this was calculated per ventral horn neuron culture. In the speed distribution graphs, the mean relative frequency of carriers with a particular speed and the corresponding standard error of the mean (SEM) were plotted for all ventral horn neuron cultures analysed.

The frequency of carriers was calculated per axon, dividing the total number of carriers tracked during a time-lapse movie by its duration in seconds. The average carrier frequency was calculated for each ventral horn neuron culture. The frequency data analysed are represented as box and whisker plots, an example of which is described in Figure 2.5.

The proportion of carriers that paused during axonal transport was also quantified. An axonal carrier was defined as having paused if it moved more slowly than 0.01 μm/s between 2 consecutive frames in time-lapse sequences. This parameter was set according to the limitations imposed by the resolution of our live-cell imaging set-up i.e. smaller velocities are below the threshold of detection. The proportion of carriers that

paused was calculated by dividing the number of pausing carriers tracked by the total number of tracked carriers in a ventral horn neuron culture. The proportion of carriers that paused per ventral horn neuron culture are plotted on box and whisker diagrams similarly to the frequency analysis and as described in Figure 2.5.

Kymograph correspondent to the transport experiments were assembled with the aid of MetaMorph®. Kymographs are a way in which a dynamic process e.g. axonal transport can be represented in both time and space in a two-dimensional image. An example of an ALCAM transport experiment represented as a kymograph is shown in Figure 2.6, accompanied by a description as to how they are generated.

2.2.5.5 Measurement of axonal transport after binding on ice with or without the ALCAM ligand CD6

αALCAM488 was incubated at 4°C alone, or in the presence of either 1 µg/ml CD6-human Fc fusion protein or 1 µg/ml human Fc (Hu-Fc) in HBSS. Cells were then washed with imaging medium, then incubated for a further 30 min at 37°C. Cells were imaged and the data analysed as described in 2.2.5.4. In some cultures, neurons were exposed to both αALCAM488 and $\alpha p75^{NTR}555$. In these co-transport experiments the transport of either probe was used to assess axonal viability. If neither probe was transported, the axon was not considered in the frequency analysis.

For CD6-Fc exposed and control conditions, Gaussian curves, as a 'best-fit' for the instantaneous speeds observed for each axon, were generated with the help of Dr Gavin Kelly (LRI, Bioinformatics and Biostatistics Service). These curves were compared to the average speed distribution curves per ventral horn neuron culture and between the CD6 exposed and control conditions. No significant difference was detected between ventral horn neuron cultures, suggesting that transport did not differ between cell preparations isolated at different times.

2.2.6 Visualisation of axonal sprouting at skeletal muscle neuromuscular junctions (NMJ) in ALCAM$^{-/-}$ mice

2.2.6.1 Botulinum Neurotoxin A (BoNT/A) treatment of the extensor digitorum longus (EDL) and Levator auris longus (LAL)

Axonal sprouting in response to BoNT/A induced paralysis was compared in ALCAM$^{-/-}$ and their wild type littermates in two different skeletal muscles the EDL and LAL muscles. These experiments were undertaken with the help of Dr Bernadett Kalmar, a colleague in the laboratory, who carried out the BoNT/A intramuscular injections and removed the skeletal muscles from wild type and ALCAM$^{-/-}$ animals three weeks after the BoNT/A treatment.

For EDL muscles, animals were anaesthetised with isoflurane and their left leg shaved. A longitudinal incision was made in the leg, the skin pulled open to expose the muscle, the EDL muscle was identified beneath the tibialis anterior muscle. A 3D representation of the mouse hindlimb and location of the EDL is illustrated in Figure 2.7. The muscle was injected midway along its length with 1 µl of 1 pg/µl BoNT/A diluted in 2 mg/ml mouse serum albumin in PBS. The skin was then closed with sutures before returning the mice to their cages. Animals were sacrificed and muscles removed 3 weeks after BoNT/A injection, pinned in a slightly stretched position in a sylgard-coated petri dish and then fixed for 6 h in muscle fixative (4% Formaldehyde, 10% $CaCl_2$, 5% $MgCl_2$.6H2O, 1% $CdCl_2$.1/2H_2O, in Veronal Acetate buffer). As a control EDL muscles were also removed from the uninjected leg of some animals. The muscles were kept in 10% sucrose overnight and then mounted in Tissue-Tek® O.C.T.™ and cut into 40 nm sections using a Leica 4100 microtome at -20°C. Free-floating sections were processed using a combined silver-acetylcholinesterase stain, which allows for the simultaneous visualisation of nerve terminals and endplates (see 2.2.6.2)

For LAL muscles 2 µl of 0.25 pg/µl BoNT/A was injected subcutaneously on the left side of the head of each animal under isoflurane anaesthesia. After 3 weeks, both the left and right LAL muscles were removed, fixed for 2 hours in muscle fixative and transferred to 10% sucrose for 1 hour. The LAL muscle, as a whole mount preparation, was then stained using a combined acetylcholinesterase and silver stain as described in (Angaut-Petit et al., 1987).

2.2.6.2 Acetylcholinesterase and silver staining

Floating muscle sections washed in distilled water were cooled on ice and incubated for 20 min in cooled acetylcholine iodide solution (0.04% acetylcholine iodide, 59 mM sodium hydrogen maleate, 5 mM tri-sodium citrate, 3 mM copper sulphate, 0.45 mM potassium ferricyanide, 14% sucrose). Muscles were rinsed in distilled water and then immersed in potassium ferricyanide solution (7.6 mM potassium ferricyanide) for 10 min at room temperature to stain endplates. Following 3 washes in distilled water, sections were immersed in absolute ethanol for 2 washes of 30 min each and subsequently washed in distilled water for a further 30 minutes.

Nerve terminals were then stained by incubating sections in silver solution (0.1% $CaCO_3$, 0.05% $CuSO_4$.5H2O, 10% $AgNO_3$) for 20-30 minutes at 37°C. Muscles were rinsed briefly in distilled water before being immersed in reducer solution (1% hydroquinone, 10% Na_2SO_3). When axons became visible, the reaction was stopped by washing several times in water. Sections were mounted on polylysine slides using a paintbrush and allowed to dry overnight at 37°C. Finally the sections were cleared by immersion in histoclear before mounting in DPX mountant (BDH) for microscopical analysis. For LAL muscles the same staining protocol was followed but wholemount muscle preparations were used rather than muscle sections.

2.2.6.3 Quantification of axonal sprouting at NMJs

The number of sprouts per NMJ in BoNT/A injected muscles in wild type and ALCAM$^{-/-}$ littermates were counted. Uninjected muscles were also quantified as a control. Axonal sprouts were classified as silver stained processes that contacted the endplate region before extending beyond the acetylcholinesterase stained boundary. I also quantified nodal sprouts as those that branched from the axon immediately before entering the terminal. Examples of the terminal and nodal sprouts counted are shown in Figure 2.8. Counting was carried out blind to genotype, using HC PL FLUOTAR 20x/0.50 and PL FLUOTAR 40x/0.70 objectives on Leica DMR light microscope.

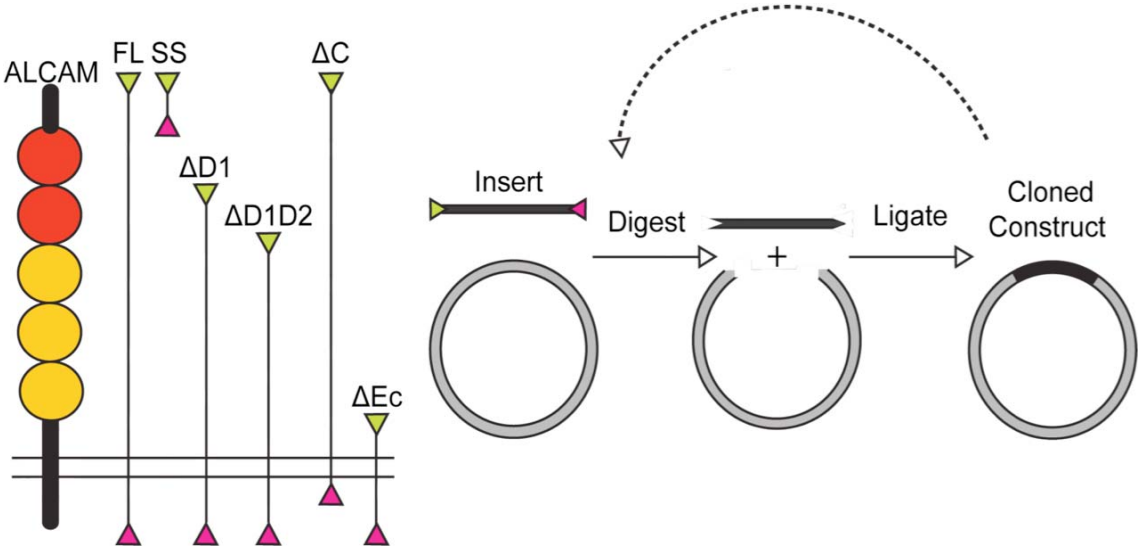

Figure 2.1 Cloning strategy for ALCAM Dendra (ALCAM-D) constructs

Forward primers (green arrowheads) and stop primers (pink arrowheads) were used to amplify DNA fragments by PCR. Full length ALCAM was amplified (FL) or ALCAM fragments; signal sequence (SS), ALCAM missing one or two of its most distal extracellular domains (ΔD1 or ΔD1D2 respectively), ALCAM lacking its cytoplasmic domain (ΔC), or ALCAM lacking its extracellular domain (ΔEc – was used to generate CD8-ALCAM chimera). Insert and vector are digested using appropriate restriction enzymes, purified and then ligated together. For constructs requiring ligation of two inserts, both fragments were ligated together at the same time or as a sequential process with firstly one digestion, ligation step and then a second digestion ligation step, as indicated by the dotted arrow.

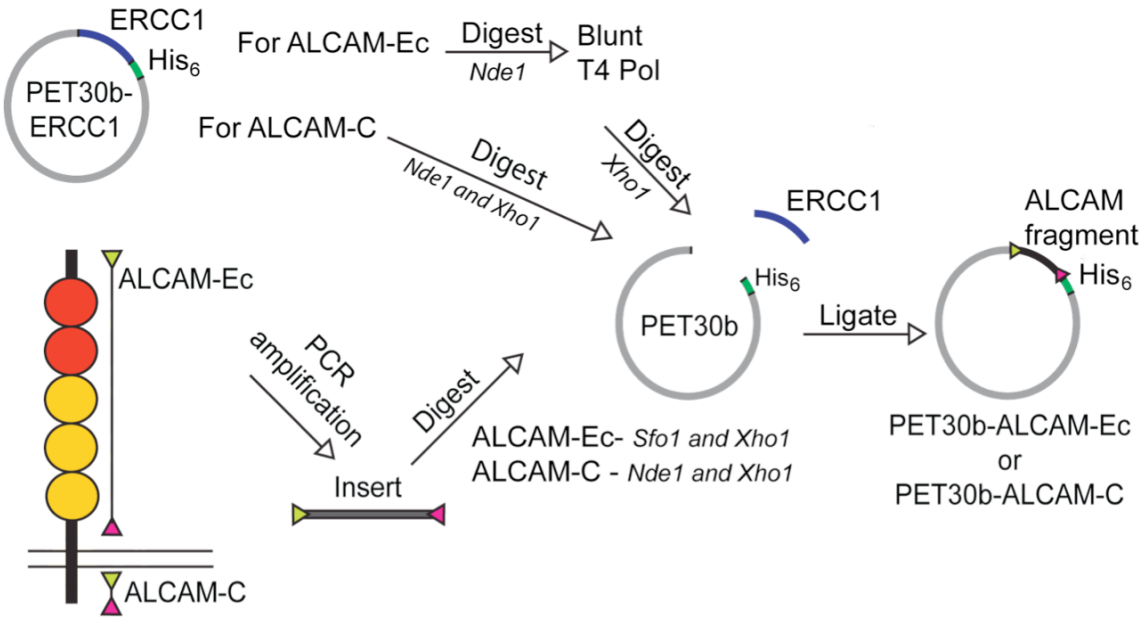

Figure 2.2 Cloning strategy for ALCAM-His_6 constructs

The strategy used to clone the His_6-tagged ALCAM extracellular domain (ALCAM-Ec) and cytoplasmic domain (ALCAM-C) is shown. Forward primers (green arrowheads) and stop primers (pink arrowheads) were used to amplify ALCAM DNA by PCR. The vector was digested using Nde1 and Xho1 to remove the ERCC1 insert either directly or sequentially. The ALCAM-Ec fragment could not be digested with Nde1, as there was an internal Nde1 restriction site within the ALCAM extracellular domain sequence. In the ALCAM-Ec start primer the Sfo1 blunt-end producing restriction site was used instead. Therefore, for the ALCAM-Ec construct the Nde1 digested vector had to undergo a sequential reaction with T4 polymerase (T4 Pol) to produce a blunt end before being digested with Xho1. The appropriate digested insert fragments were then incubated with their corresponding vector in a ligation reaction.

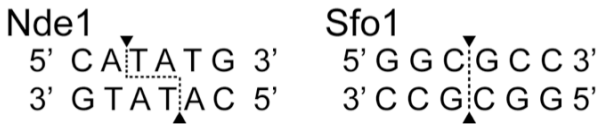

Figure 2.3 Nde1 and Sfo1 restriction sites

Arrowheads and dotted lines indicate where the enzymes Nde1 and Sfo1 cut their respective restriction sites. Nde1 cuts to give a 5' overhang, while the Sfo1 enzyme cuts resulting in a blunt-end.

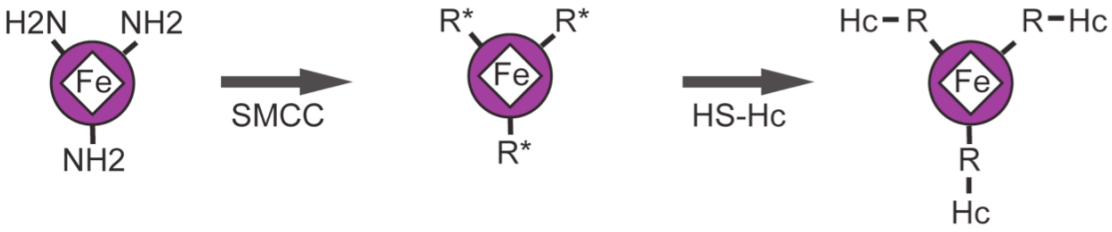

Figure 2.4 Coupling reaction of MION to protein

The amide groups on the MION beads (Fe) exposed to SMCC become activated maleimide intermediates which can react with the sulfhydryl groups on the Hc and BSA proteins. This results in a disulphide bond between the proteins and the bead. Previously this chemistry has been used in the lab to couple the Hc fragment with Alexa Fluor® dyes (Lalli and Schiavo, 2002).

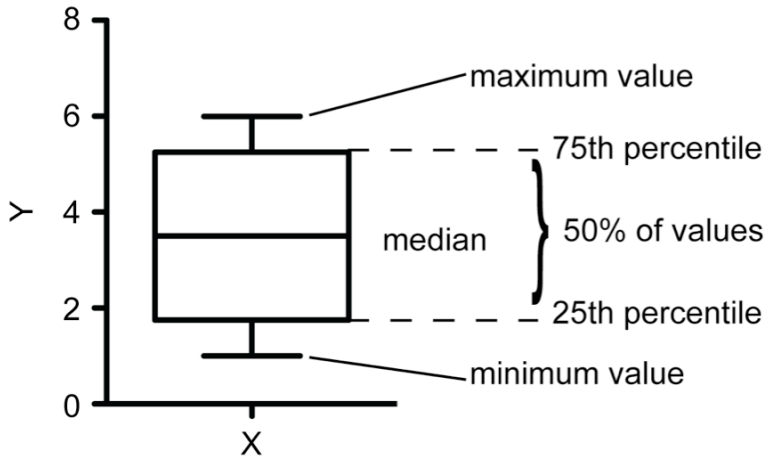

Figure 2.5 Example of box and whisker plot

The box spans the upper to lower quartiles (representing 50% of all data values). The line in the centre of the box is the 50th percentile or median, and the tips of the whiskers are the minimum and maximum values. The box and whisker plot is a non-parametric way of representing data without making assumptions of their underlying distribution. In this thesis, box and whisker diagrams have been used to represent ALCAM, Hc and $p75^{NTR}$ carrier frequency and the proportion of pausing carriers in transport experiments (Y-axis).

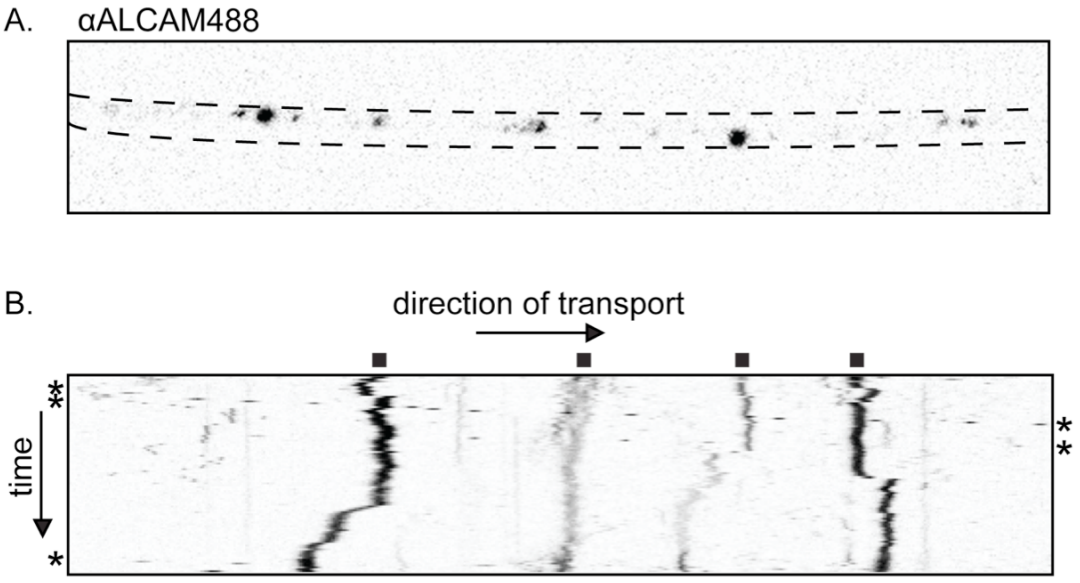

Figure 2.6 An example of a αALCAM488 movie kymograph

Panel (A) shows a frame from a time-lapse imaging experiment after black an white conversion and inversion, so that the black puncta represent the fluorescent carriers. The kymograph (B) is generated by drawing a region of interest along the length of the axon, as shown by the dotted line in (A). Consecutive lines from the region of interest in (A) are stacked vertically over time to create the kymograph. Actively transporting vesicles are represented as puncta moving diagonally across the kymograph. The asterisks indicate entrance and exit points of αALCAM488 vesicles. Stationary or oscillating vesicles appear as vertical stripes since they do not move over consecutive frames, indicated by the black boxes.

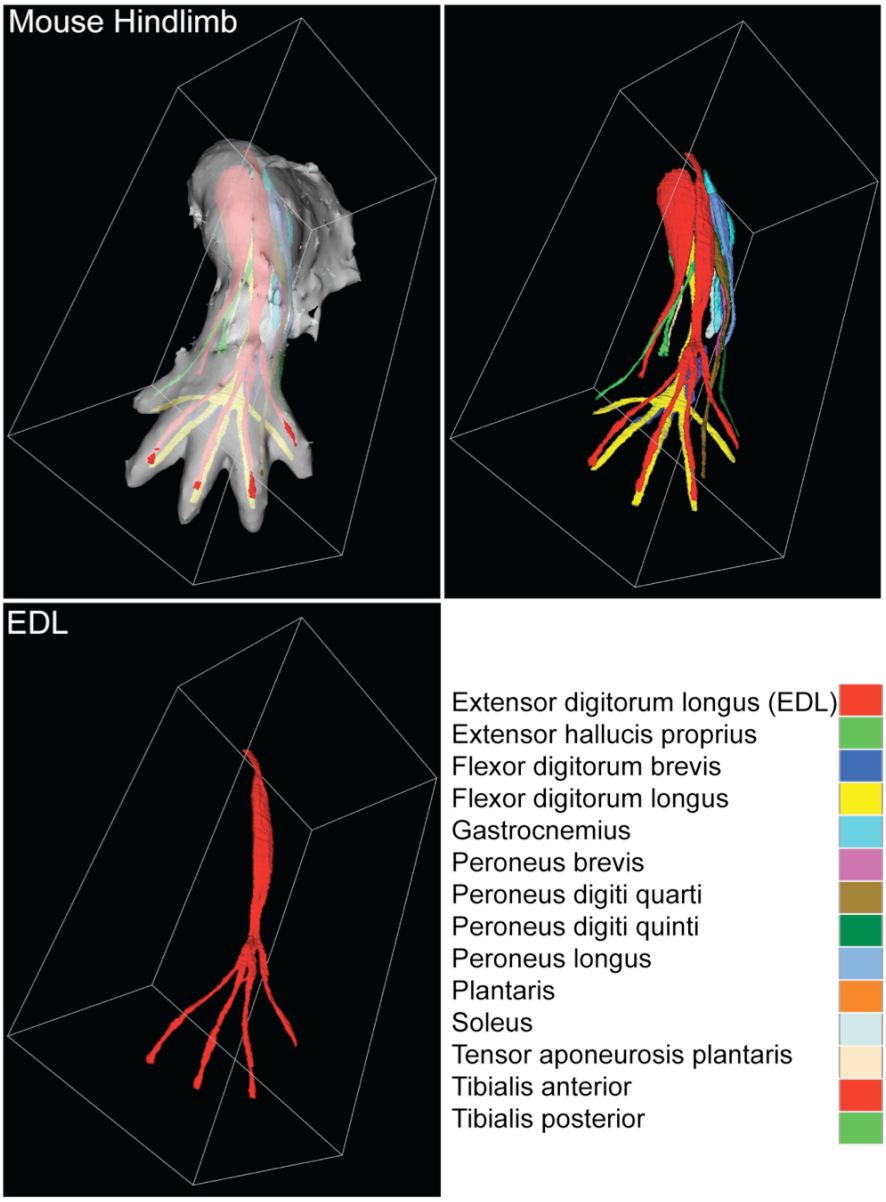

Figure 2.7 Mouse hindlimb muscles and tendons

Pictures were generated using the 3D mouse limb anatomy atlas http://www.nimr.mrc.ac.uk/3dlimb. A 3D reconstruction of the mouse hindlimb is shown. In the middle panel all muscles and tendons are represented and coloured as indicated in the lower panel. The EDL muscle alone, used in the nerve terminal sprouting study, is shown in the right panel. The overlying tibialis anterior muscle was cut away and the EDL muscle tendons exposed and the muscle removed.

Figure 2.8 An example of terminal and nodal sprouts from NMJ nerve terminal

Endplate and nerve terminals are visualised by the combined silver-acetylcholinesterase stain in a mouse skeletal muscle. Sprouting is induced in response to BoNT/A muscle paralysis. Terminal sprouts exiting the endplate region to contact the muscle fibre, indicated by the black arrows, were quantified. A nodal sprout that has branched from the nerve terminal before reaching the endplate region is also visible (white arrow) and were also counted in wild type and ALCAM$^{-/-}$ animals. Scale bar, 100 µm.

Chapter 3. ALCAM undergoes axonal retrograde transport with neurotrophin receptors

3.1 ALCAM is associated with Hc containing endosomes

As described in the introduction ALCAM was identified by mass spectrometry as a protein associated with the Hc-positive endosome in ventral horn neurons. In the first part of the study, I aimed to confirm the association between ALCAM and this axonal transport compartment using a variety of techniques.

Firstly, we purified membrane compartments associated with Hc by the same method previously used for the mass spectrometry proteomic screen. Mouse ventral horn cultures were exposed to magnetic nano-beads (MIONs) conjugated with Hc. These modified MIONs bind to the neuronal surface and are internalised into endosomal compartments, as shown in Figure 1.4 and in (Deinhardt et al., 2006b). Neurons were harvested, passed through a cell cracker to break their plasma membrane while keeping intracellular organelles intact and the resulting cell-free homogenate passed through a magnet. Organelles containing the MIONs were retained in the magnet. Subsequently, proteins associated with the nano-beads were eluted, separated by SDS-PAGE, transferred to PVDF and blotted for ALCAM. A typical western blot from one of these experiments is shown in Figure 3.1. Consistently ALCAM associated specifically with the Hc-conjugated MIONs and not with control BSA-conjugated MIONs. This verified biochemically the association between ALCAM and Hc containing organelles that was originally indicated in the proteomic screen.

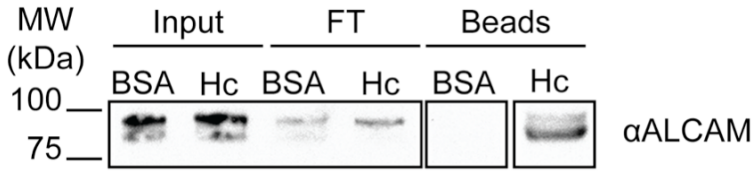

Figure 3.1 ALCAM associates with Hc MION beads

A typical SDS-PAGE and western blot following MION bead purification of the Hc endosomal compartment is shown. The membrane has been probed for ALCAM (αALCAM). Two ALCAM bands are present in the ventral horn culture lysate (Input). In samples eluted from MION (Beads), ALCAM is only associated with the Hc beads, not the BSA beads. ALCAM is depleted in the flow through (FT). Interestingly, although both ALCAM species are associated with the beads, the lower molecular weight, less abundant ALCAM band is enriched in association with Hc.

3.2 ALCAM undergoes retrograde transport in the Hc-transport organelle

I next investigated whether ALCAM underwent retrograde transport as previously observed with Hc, by visualisation of transport in live ventral horn neurons. To this end, I conjugated an antibody raised against the extracellular domain of ALCAM, to the fluorophore AlexaFluor®-488 (αALCAM488). The conjugated antibody can bind to the ALCAM extracellular domain at the plasma membrane and if the endogenous protein is internalised and transported, the conjugated antibody should also undergo internalisation and be transported. This method for following the destination of cell surface molecules has been extensively used to follow a variety of proteins. For example, an antibody directed towards the lumenal portion of synaptotagmin 1 was used to follow synaptic vesicle recycling in primary hippocampal neurons (Matteoli et al., 1992). The internalised antibody had a long half-life and did not alter the localisation or properties of the synaptic vesicles it labelled. Another group has used a monoclonal antibody to an extracellular loop of the chemokine receptor, CXCR4, to follow the internalisation of this protein and to monitor how this process is regulated (Signoret et al., 1997). However, both of these papers noted possible problems with the technique. In the study by M. Matteoli, evidence suggested that the antibodies could induce clustering of the endogenous protein in certain conditions, and this could alter its trafficking e.g. directing the protein into the degradative pathway. In (Signoret et al., 1997), it was found that the internalisation and trafficking properties of CXCR4 were altered when the protein was transfected into chinese hamster ovary (CHO) cells, although this was not the case when mink lung cells were used. This finding suggested not only that different cell lines have different basal rates of internalisation, but also that

following transfection anomalous trafficking can occur. Therefore studies using antibodies to track transfected proteins should be treated with caution.

To test whether the conjugated αALCAM488 retained the binding ability of the original antibody I conducted a competition assay. The binding of the conjugated antibody to ventral horn motor neurons alone was compared to that seen after pre-incubation with the unconjugated antibody. An experiment showing competition of αALCAM488 by the unconjugated antibody is shown in Figure 3.2 and confirmed that αALCAM488 bound to the same antigen as the original antibody. The specificity of the αALCAM488 probe was tested in transport experiments in ventral horn neurons isolated from ALCAM knockout ($ALCAM^{-/-}$) mice. As expected, αALCAM488 did not bind to neurons isolated from $ALCAM^{-/-}$ mice, as shown in Figure 3.3. This result illustrated that the αALCAM488 probe is specific for endogenous ALCAM.

Following characterisation of the αALCAM488 probe, I investigated whether internalisation and long-range transport of endogenous ALCAM occurred in primary ventral horn neurons. Neurons were incubated with the probe in the presence of Hc-555 for 30 min, washed in imaging medium and transport was visualised using time-lapse confocal microscopy in live neurons at 37°C. Onset of αALCAM488 transport occurred approximately one hour after initial exposure to the probe, when ALCAM-positive vesicles could be seen moving bi-directionally. ALCAM transport was predominantly retrograde, and this protein was often present in transport compartments also containing Hc, as shown in Figure 3.4. In 3 independent experiments, tracked αALCAM488 vesicles were classified as containing ALCAM alone or ALCAM in addition to Hc and 60% of ALCAM-positive carriers quantified also contained Hc (n = 84 ALCAM-positive carriers, 21 axons, 3 ventral horn cultures).

Tracking and speed displacement analysis of live-cell imaging experiments found no significant difference in the speed distribution of Hc and ALCAM carriers and, as seen in Figure 3.5, ALCAM is transported with a similar speed distribution as Hc. This is consistent with the observed partial colocalisation of ALCAM and Hc during retrograde transport, suggesting that the two probes share a transport route when travelling toward the cell body. Transported ALCAM has an increased relative frequency of carriers with speeds between -0.2 to 0.2 μm/s when compared to Hc and this could suggest ALCAM carriers have an increased tendency to pause.

The proportion of tracked ALCAM and Hc-positive vesicles that paused during transport was therefore quantified and is represented in Figure 3.6. A pausing carrier was defined as one that moved more slowly than 0.01 μm/s between 2 consecutive frames. There was no significant difference in the average proportion of carriers that paused containing ALCAM and/or Hc ($p = 0.0936$). Although the result did not reach significance, there is an increased tendency for ALCAM-positive vesicles to pause, shown as a shift towards more pausing carriers in the box and whisker plot Figure 3.6. This finding, along with the observed increase of low speed carriers observed in the speed distribution (Figure 3.5), suggests that ALCAM-positive carriers have an increased tendency to pause, when compared to Hc-positive compartments.

The frequency of ALCAM and Hc-positive carriers transported per min was quantified per axon imaged, and the average frequency per ventral horn culture is represented in Figure 3.7. The average frequency of αALCAM488 transported per min was comparable to the frequency of Hc-positive carriers per min in co-transport experiments.

In conclusion, ALCAM undergoes long-range axon transport toward the cell body, often in the presence of Hc. Furthermore, the speed and frequency of αALCAM488 transport

is comparable to Hc, suggesting ALCAM largely shares the same transport route (Lalli and Schiavo, 2002, Deinhardt et al., 2006b). Only axons that transported both ALCAM and Hc were analysed and because these probes are largely co-transported, differences in their transport kinetics, i.e. increased pausing of ALCAM-positive carriers, may be attributed to a pool of carriers that contained only one probe. This could suggest that the subset of ALCAM-positive carriers that did not contain Hc paused more often, and may represent another internalisation and transport route for ALCAM in neurons (for further discussion see 6.1.1).

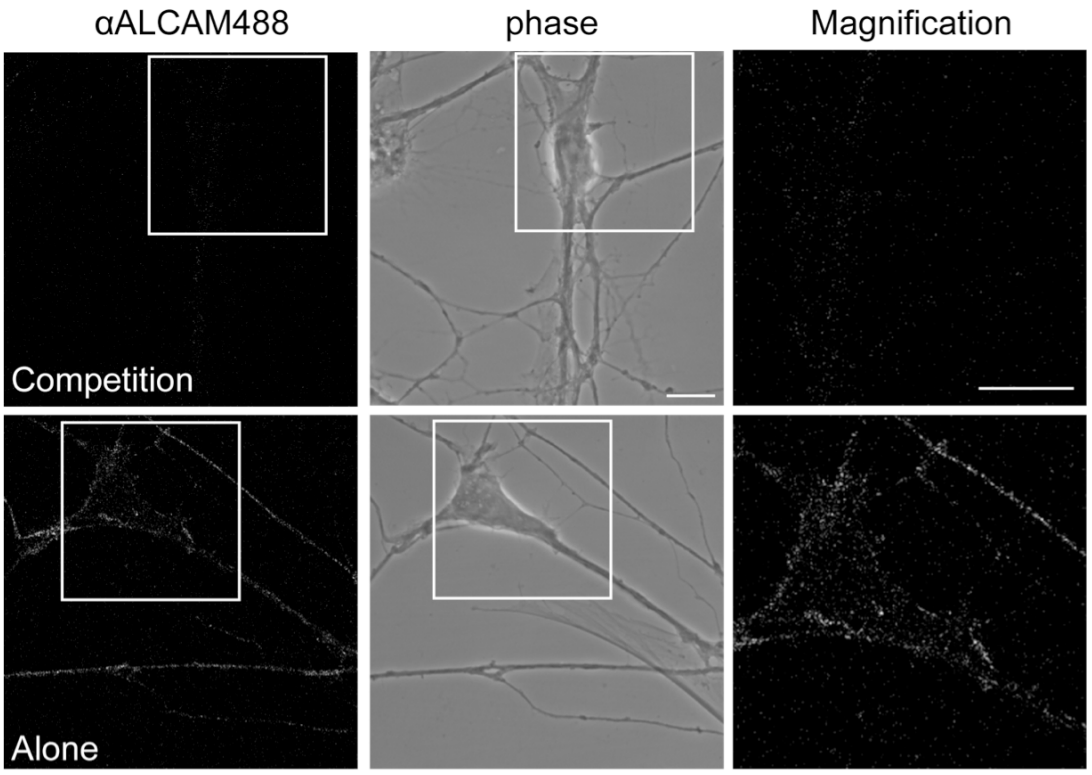

Figure 3.2 αALCAM488 binds to endogenous ALCAM on the surface of ventral horn culture cells

In the 'competition' condition, prior binding of endogenous ALCAM by the unconjugated antibody prevents αALCAM488 binding to the surface of cells, but exposure to the antibody alone gives a clear cell surface stain. The boxed area is shown at higher magnification on the right. αALCAM488 is shown to bind to neurites, as well as the cell body surface. Scale bar, 10μm.

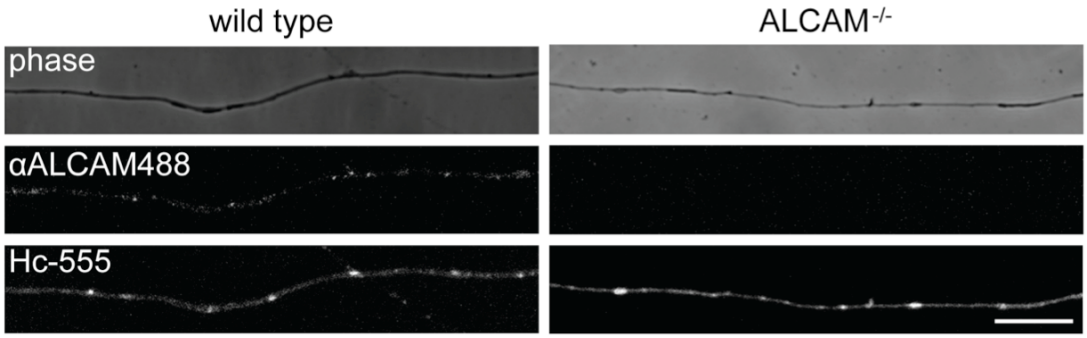

Figure 3.3 αALCAM488 does not bind to neurons in ALCAM$^{-/-}$ cultures

Ventral horn neuron cultures isolated form wild type and ALCAM$^{-/-}$ embryos were incubated with Hc-555 and αALCAM488. αALCAM488 did not bind to ALCAM$^{-/-}$ neurons, but did stain wild type axons. Hc-555 binding was not altered in neurons that did not express ALCAM when compared to wild type axons, and is illustrated in the lower panel where a similar Hc-555 signal is seen. Scale bar, 10μm.

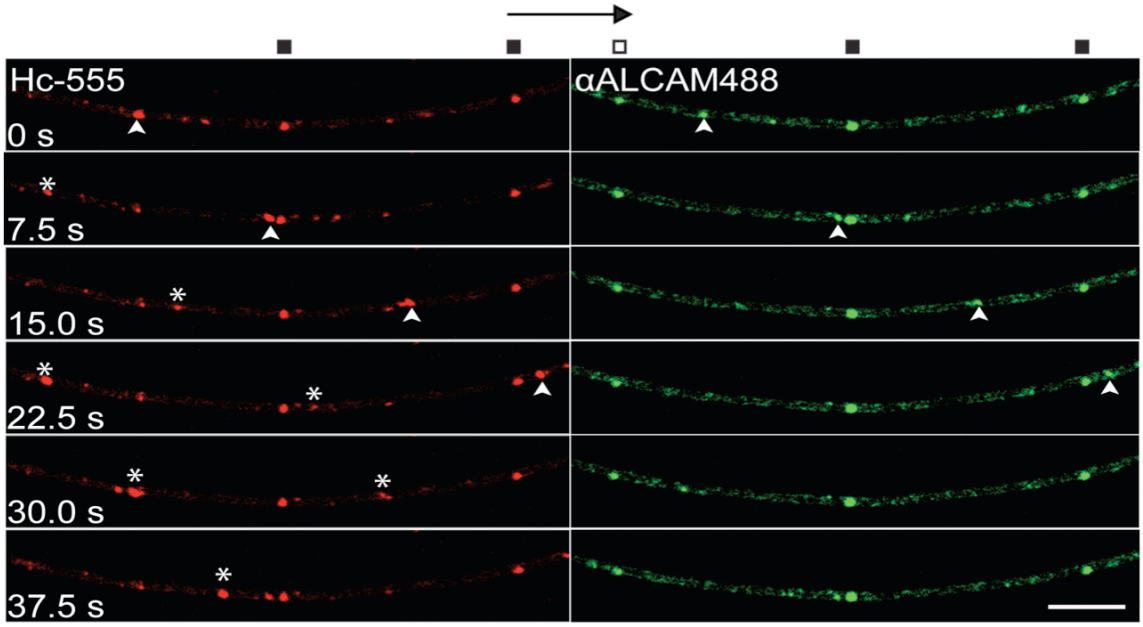

Figure 3.4 ALCAM undergoes retrograde transport and partially colocalises with Hc containing organelles

Consecutive frames from a transport movie obtained during live-cell imaging of Hc-555 and αALCAM488. The arrowhead indicates a retrograde transport vesicle containing Hc and ALCAM moving towards the cell body (black arrow). The two probes are not transported exclusively in the same carriers. The stars (*) indicate Hc-positive transport compartments that do not contain ALCAM. Stationary vesicles that contain both Hc and ALCAM are seen in the centre and right hand side of the axon, while another stationary vesicle contains ALCAM alone (indicated by black and white ■ respectively). Scale bar, 10 µm.

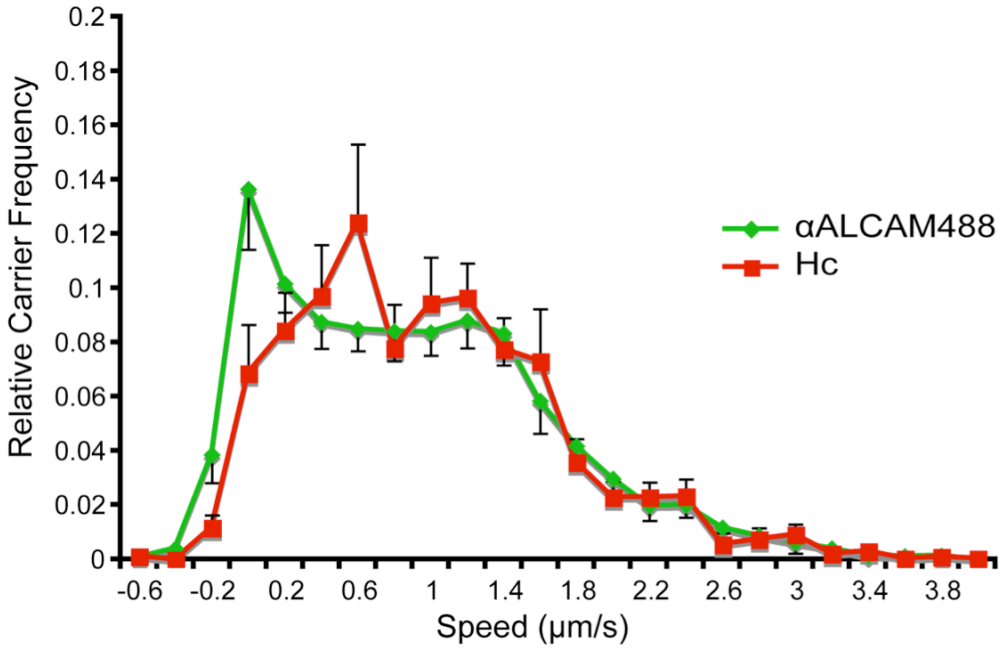

Figure 3.5 Speed distribution of αALCAM488 and Hc in co-transport experiments

The relative frequency of ALCAM-positive carriers with identical instantaneous velocities (speed µm/s) is plotted and is comparable to that of Hc-positive carriers recorded in the same experiments. The two probes have a similar speed distribution (n = 183 ALCAM and 231 Hc carriers, recorded in a total of 38 axons from 8 ventral horn cultures).

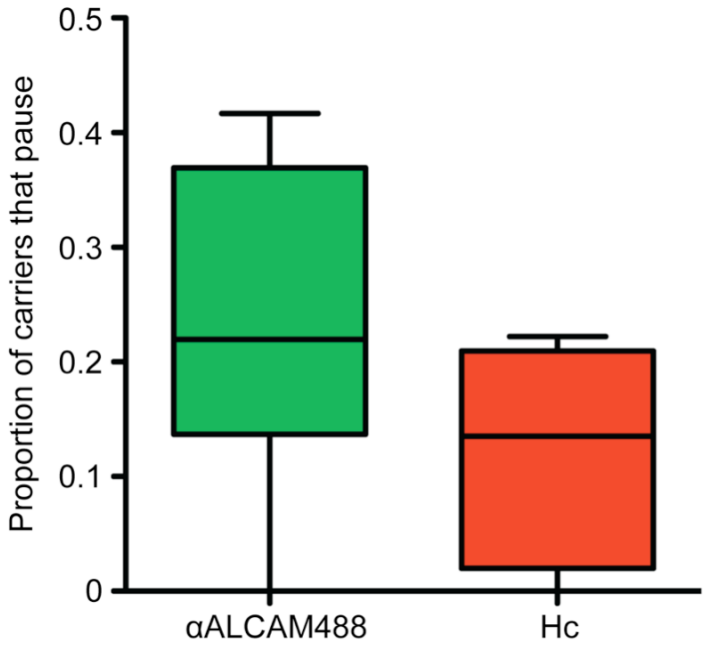

Figure 3.6 ALCAM-positive carriers show an increased tendency to pause

The box and whisker plot shows that a higher proportion of αALCAM488-positive carriers pause. Although not statistically significant, there is an increased tendency for αALCAM488-positive carriers to pause ($p = 0.0936$) when compared to Hc-positive organelles. Data was analysed using an unpaired t-test ($n = 8$ ventral horn cultures).

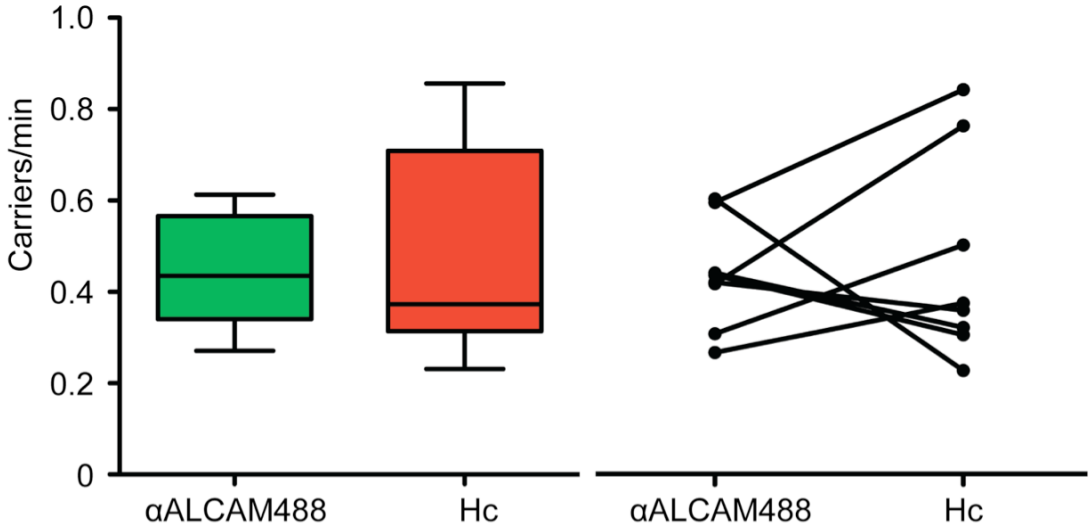

Figure 3.7 There is no significant difference in the frequency of ALCAM and Hc-positive carriers in co-transport experiments

The average frequency of αALCAM488 and Hc carriers per ventral horn neuron culture are represented in two ways; a box and whisker plot (left) or as paired αALCAM488 and Hc frequencies observed in the same axons (right). There is no significant difference in the average frequency of αALCAM488 or Hc-positive carriers per min in co-transport experiments. The range and maximum frequency is greater for Hc transport than for αALCAM488. Paired observations show that there is no consistent relationship between increased αALCAM488 and Hc transport frequencies. Data was analysed using an unpaired t-test (n = 8 ventral horn cultures).

3.3 ALCAM is transported in endosomes that contain neurotrophin receptors

Since ALCAM transport had shown substantial overlap with Hc, we next wanted to confirm more directly whether ALCAM was associated with the retrograde transport of neurotrophins and their receptors, or whether it was transported within a distinct subset of Hc-labelled endosomes that did not contain these molecules. I conducted experiments examining αALCAM488 transport in neurons that had been co-exposed to a fluorophore-conjugated antibody to the $p75^{NTR}$ receptor ($\alpha p75^{NTR}555$).

In these experiments, axonal retrograde transport compartments were seen which contained both, $p75^{NTR}$ and ALCAM, as well as endosomes that contained either protein exclusively (Figure 3.8). The incidence of co-transport was quantified and established that 64% of αALCAM488 vesicles tracked were also $\alpha p75^{NTR}555$-positive. Interestingly, we found that the frequency of $p75^{NTR}$ endosome transport was around 3 times higher than ALCAM containing compartments as shown in Figure 3.9.

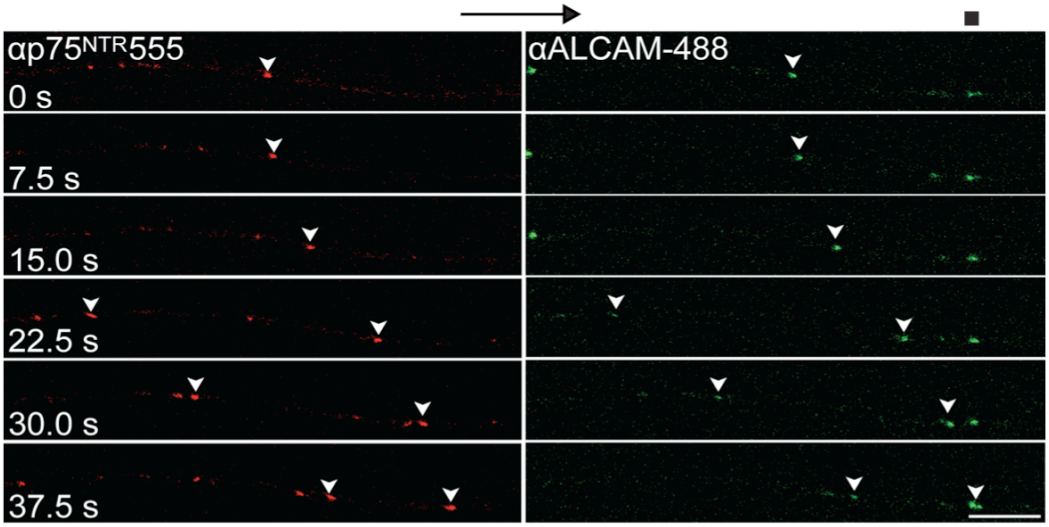

Figure 3.8 ALCAM is transported retrogradely in p75^{NTR}-positive endosomes

Consecutive frames from a live-cell imaging experiment with αp75^{NTR}555 and αALCAM488. The black arrow indicates the direction of transport towards the cell body. Arrowheads indicate retrogradely travelling endosomes that contain ALCAM and the neurotrophin receptor p75^{NTR}. An ALCAM static endosome that does not contain the p75^{NTR} is indicated by (■). Scale bar, 10µm.

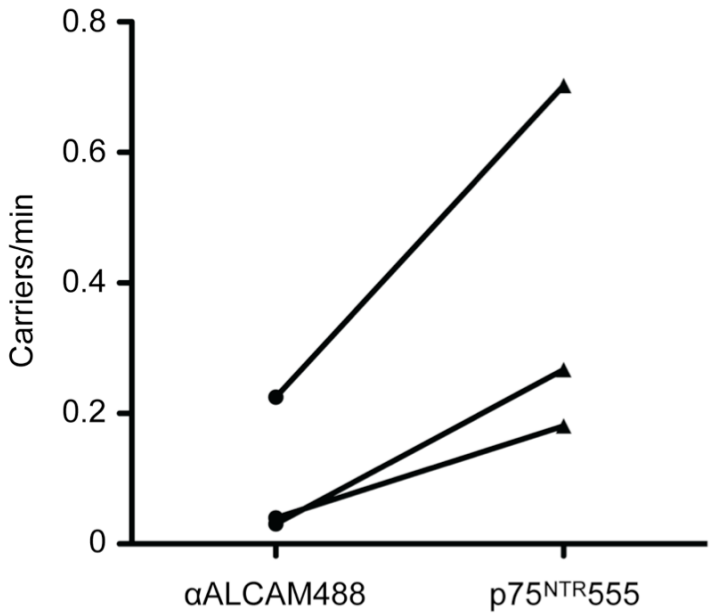

Figure 3.9 p75^{NTR} is transported more frequently than ALCAM

The frequency of p75^{NTR} and αALCAM488 carriers per min was calculated in 3 ventral horn neuron cultures and plotted as paired observations (each line represents the frequency of each probe matched in each culture experiment). Although not reaching statistical significance, p75^{NTR} is consistently transported at higher frequencies than ALCAM (around 4 fold more p75^{NTR} is transported). Data was analysed using an unpaired t-test, p = 0.1757 (n = 3 ventral horn cultures).

3.4 Does ALCAM play a role in the regulation of retrograde transport?

Considering ALCAM is retrogradely transported in the same compartment as Hc and $p75^{NTR}$, we investigated whether it has a role in regulation of this pathway or is merely a cargo in these endosomes. I isolated ventral horn cultures from $ALCAM^{-/-}$, $ALCAM^{+/-}$ and wild type litter mates and conducted live-cell imaging transport experiments after exposure to Hc-555 to investigate whether transport was altered when ALCAM was not expressed. As established earlier, αALCAM488 did not bind to $ALCAM^{-/-}$ neurons and was not transported in these cultures (Figure 3.3).

Analysis of these imaging experiments found that there was no difference in the transport of Hc between cultures lacking ALCAM and those that expressed ALCAM. The speed distribution profiles in Figure 3.10 show no alteration in the overall kinetics of Hc transport in ventral horn cultures isolated from wild type, $ALCAM^{+/-}$ or $ALCAM^{-/-}$ animals. Furthermore, there is no significant difference between the genotypes in the frequency of Hc-positive vesicles or the proportion of vesicles that pause (Figure 3.11). It is noted that in $ALCAM^{+/-}$ ventral horn cultures analysed one culture had a particularly high frequency of Hc carriers that is an outlier on the box and whisker plot (Figure 3.11). However, fewer $ALCAM^{+/-}$ cultures were analysed and considering that the other parameters quantified are the same, I concluded that Hc transport is not altered in heterozygote animals. In summary, Hc transport is normal in the absence of ALCAM, suggesting it does not play a regulatory role in this transport route.

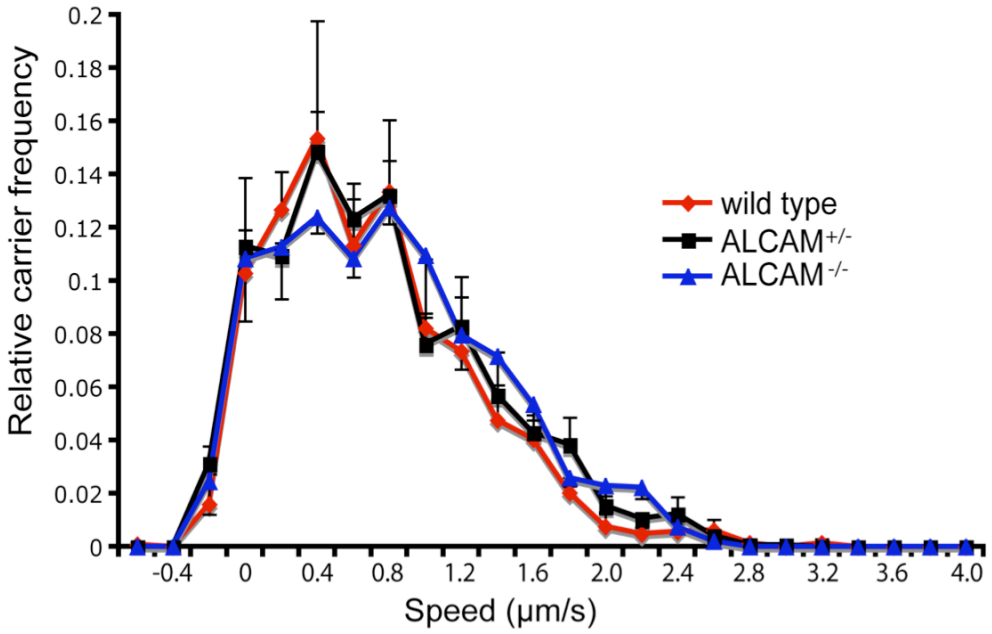

Figure 3.10 Hc transport is unaltered in ventral horn neurons with or without endogenous ALCAM

After tracking and speed displacement analysis of Hc transport, the speed distribution profiles were plotted for all three genotypes; wild type, ALCAM$^{+/-}$ and ALCAM$^{-/-}$. We found no difference in the speed distribution of Hc-555 retrograde transport in ventral horn neurons that did not express ALCAM when compared to the transport observed in neurons that did express ALCAM. wild type n = 92 Hc carriers, 22 axons, 4 ventral horn cultures; ALCAM$^{+/-}$ n = 100 Hc carriers, 17 axons, 3 ventral horn cultures; ALCAM$^{-/-}$ n = 101 Hc carriers, 22 axons and 4 ventral horn cultures.

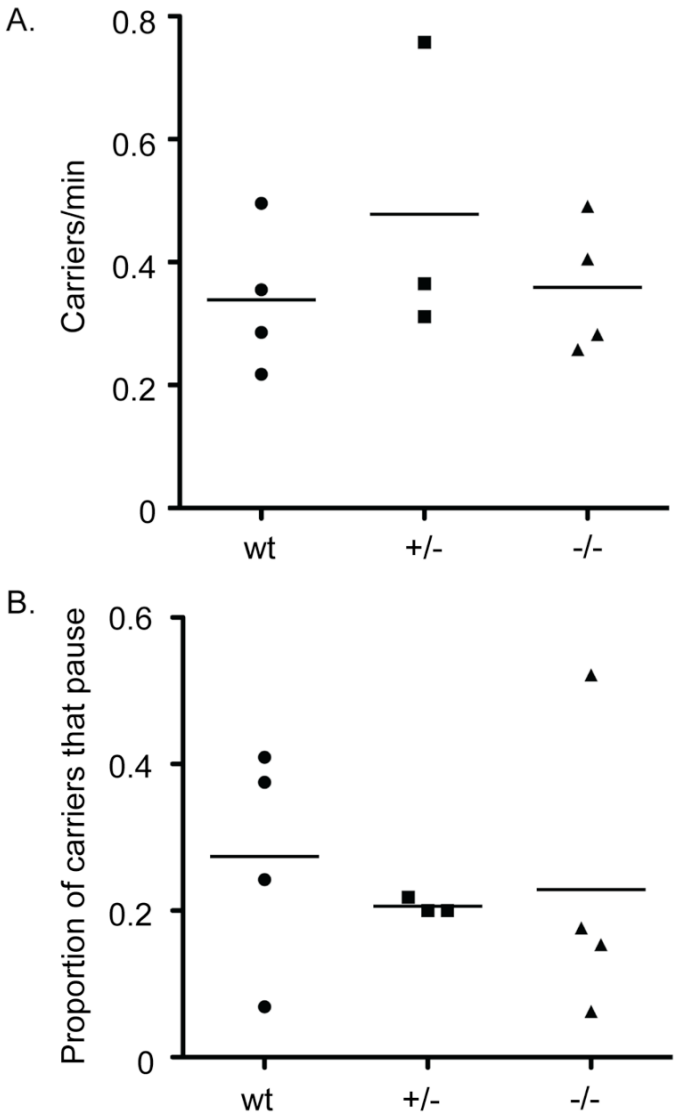

Figure 3.11 There is no significant difference in the frequency or pausing of Hc carriers in ALCAM$^{-/-}$ cultures

In the plots (A) the frequency of Hc carriers in wild type (wt), ALCAM$^{+/-}$(+/-), ALCAM$^{-/-}$(-/-) cultures is represented (line = median). There is no significant difference in the frequency of Hc carriers between the genotypes. Furthermore, in (B) there is no significant difference in the proportion of Hc-positive carriers that pause in ventral horn neurons that do or do not express ALCAM. All data was analysed using an unpaired t-test (n = 4 ventral horn cultures for wt and ALCAM$^{-/-}$ and 3 ventral horn cultures for ALCAM$^{+/-}$).

3.5 Can ALCAM transport be modulated?

As discussed in the Introduction, the CD6 glycoprotein is an endogenous binding partner of ALCAM and a soluble form of the protein has been shown to stimulate ALCAM internalisation in an ovarian cancer cell line (Piazza et al., 2005). I next examined whether exposure of ventral horn neuron cultures to CD6 could stimulate the retrograde transport of ALCAM.

3.5.1 The anti-ALCAM antibody cross reacts with the CD6-Fc chimera

Western blot analysis of ALCAM and its ligand CD6 revealed that the primary antibody used to detect ALCAM in my previous internalisation and transport experiments cross-reacted with the ALCAM ligand CD6. CD6-Fc, a chimeric protein consisting of the CD6 extracellular domain (Leu18-Gly396) fused to His_6 tagged Human IgG1 was obtained commercially. The problem was revealed in an experiment where mouse ventral horn culture lysates from cells incubated with GST or CD6-Fc, were analysed by western blot (Figure 3.12A). A novel band of 110-120 kDa molecular weight was recognised in samples exposed to CD6-Fc only. To check whether this novel band was due to cross-reaction of the anti-ALCAM antibody with CD6, the purified chimeric protein was analysed by western blot (Figure 3.12 B). A band was only detected in the presence of the anti-ALCAM primary antibody, suggesting that this antibody recognised the purified CD6-Fc protein. The datasheet specified that CD6-Fc should migrate at 116kDa, and this is the molecular weight of the band detected by the anti-ALCAM antibody. Endogenous ALCAM migrates at a lower molecular weight. This suggested that the antibody cross-reacted with the CD6-Fc protein directly rather than there being contamination of the chimeric protein sample with ALCAM.

In summary, I found that a primary antibody raised against the ALCAM extracellular domain also reacted with purified CD6-Fc, suggesting that the commercial ALCAM

polyclonal antibody also could recognise the CD6 antigen. This posed a potential problem considering that my previous studies made extensive use of this antibody in transport experiments, biochemical purification and western blots. Was the protein recognised in previous experiments endogenous ALCAM or CD6? I therefore needed to confirm that CD6 is not present in the nervous system and to establish whether CD6 is expressed in primary ventral horn neuron cultures.

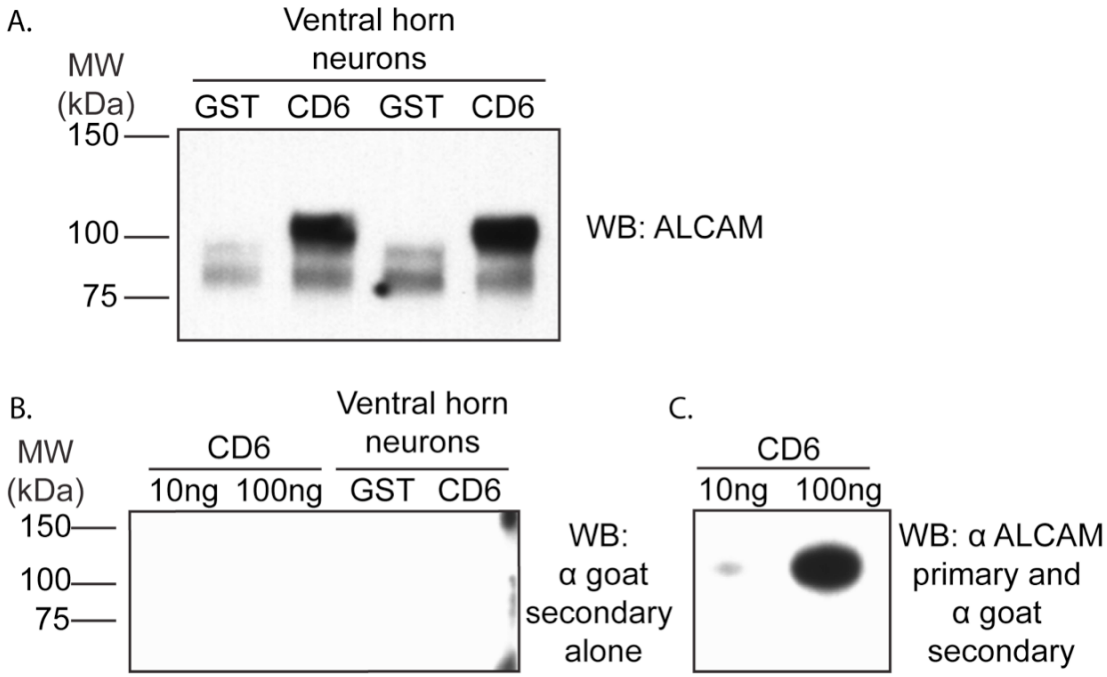

Figure 3.12 Anti-ALCAM antibody cross-reacts with soluble CD6-Fc

(A) Ventral horn neuron culture lysates of cells previously exposed to GST or CD6-Fc (CD6) were analysed by SDS-PAGE and probed for ALCAM by western blot (WB). A novel band appears in all conditions where CD6 has been added. In (B) and (C) purified CD6-Fc (10 and 100 ng) was analysed by western blot. The membrane was probed with an anti-goat secondary antibody alone (B) or after prior exposure to the anti-ALCAM primary antibody (C). Membranes exposed to the secondary antibody alone showed no reactivity, while CD6 protein was recognised by the anti-ALCAM primary antibody.

3.5.2 CD6 is not expressed in mouse ventral horn neuron cultures

Firstly I tested whether pre-absorption of the anti-ALCAM antibody with soluble CD6 altered the recognition of the ALCAM bands seen in ventral horn cultures. As shown in Figure 3.13, pre-absorption of the anti-ALCAM antibody with CD6 did not alter the recognition of both bands present in ventral horn cultures. This result suggested that the bands detected in primary ventral horn cultures represent endogenous ALCAM, rather than CD6.

Secondly, I isolated RNA from mouse ventral horn neuron cultures, synthesised the corresponding cDNA using the Superscript® Vilo Kit and tested for the presence of the CD6 transcript by PCR. No CD6 transcript could be amplified from mouse ventral horn neuron culture cDNA, suggesting that endogenous CD6 is not expressed in the spinal cord (Figure 3.14). However, CD6 could be amplified from whole embryo cDNA as a control. In summary, CD6 is not expressed in the ventral horn. This finding is consistent with reports claiming that CD6 expression is largely restricted to the immune system (gene expression atlas EMBL-EBI http://www.ebi.ac.uk/gxa/gene?gid= Q61003).

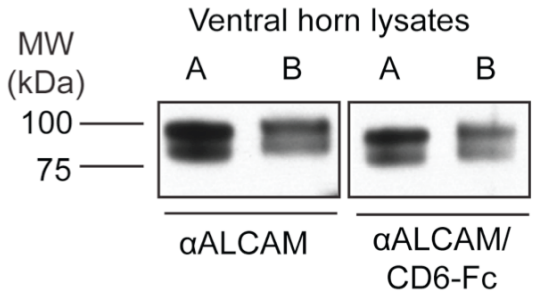

Figure 3.13 Ventral horn ALCAM species recognised are not altered by preabsorption with CD6-Fc

Ventral horn culture lysates from two independent experiments (A and B) were separated by SDS-PAGE, transferred to PVDF membrane and probed with the anti-ALCAM antibody (αALCAM) or the anti-ALCAM antibody cross-absorbed with 3 µg of CD6-Fc for 90 minutes before incubation with the membrane overnight (αALCAM/CD6-Fc). No significant change in the signal was detected after the absorption with CD6-Fc.

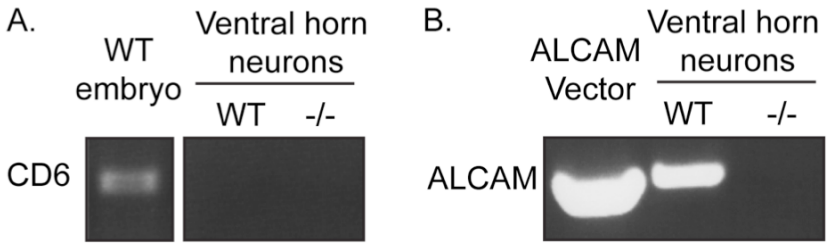

Figure 3.14 CD6 is not expressed in ventral horn cultures

In (A) a CD6 transcript was amplified from cDNA isolated from embryonic mouse brain but no equivalent CD6 band was seen in cDNA isolated from wild type (WT) and ALCAM$^{-/-}$ (-/-) ventral horn cultures. In (B) the ALCAM transcript amplified from 10ng of ALCAM containing vector plasmid is also present in WT but not the ALCAM$^{-/-}$ cDNA isolated from the same cultures, serving as a control for the integrity of the RNA.

3.5.3 Is the frequency of ALCAM transport modulated in the presence of CD6?

The discovery that the antibody cross-reacted with CD6-Fc created some methodological constraints when trying to investigate the effects of CD6 on ALCAM trafficking. Co-incubation of αALCAM488 and the soluble CD6-Fc chimera could produce large complexes of antibody and protein in solution that in turn could undergo macropinocytosis in neurons. If the internalised complexes underwent axonal transport, any transport visualised would then be composed of two carrier populations; those belonging to the characterised Hc-positive transport route, and potentially, a macropinocytosis-derived route.

Endocytosis is inhibited at low temperatures so I conducted transport experiments after an initial binding step on ice. Cells on ice were co-exposed to CD6-Fc and αALCAM488 that could interact with endogenous ALCAM on the cell surface. αALCAM488 could bind either, or both, endogenous ALCAM or the CD6-Fc bound to ALCAM on the membrane. Cells were then washed, removing large complexes in solution and leaving only membrane-bound antibody complexes, then incubated at 37°C for internalisation and transport. Following 60 min at 37°C, axonal transport could be visualised. As an additional control, soluble Human IgG Fc (Hu-Fc) was added to some of the cultures to investigate whether addition of a chimeric protein had any effect.

The time-lapse imaging movies were tracked and the carrier speed distribution and carrier frequency analysed. I found that addition of Hu-Fc had no effect on transport so data was pooled from experiments after exposure to αALCAM488 alone or in the presence of Hu-Fc (alone/with Hu-Fc). The overall speed distribution profiles of ALCAM transport in the presence or absence of CD6-Fc are similar (Figure 3.15). To analyse whether these profiles are statistically different, Dr Gavin Kelly (LRI,

Bioinformatics and Biostatistics Service) was consulted who conducted a curve-fitting analysis on the tracking data. Briefly, speed distributions were generated by fitting curves to the raw data from each axon, data pooled from the same ventral horn culture and data pooled from all ventral horn cultures analysed (for a full explanation see section 2.2.5.5 in Materials and Methods). There was no significant difference in the αALCAM488 speed distribution curves with or without prior exposure to CD6-Fc. The position of the speed distribution peaks, i.e. the modal speeds were not significantly different ($p=0.63$) between CD6-Fc exposed and control conditions. The spread of the speed distribution was also not significantly different ($p=0.64$). This suggests that the time in which ALCAM reaches the cell body from the periphery does not change in presence of its ligand, CD6.

A ligand could also alter the frequency at which its receptor is transported. I therefore quantified the frequency of ALCAM-positive carriers transported in the absence of CD6 or after exposure to CD6-Fc. As a control, I also conducted a subset of experiments on ventral horn cultures co-incubated with $\alpha p75^{NTR}555$ and αALCAM488 to establish whether CD6-Fc had a general effect on retrograde transport or whether the effect was specific to its binding partner ALCAM. Figure 3.16A represents the ALCAM-positive carrier frequency data collected from ventral horn neuron cultures exposed to αALCAM488 under control conditions (alone/in the presence of Hu-Fc) or after exposure to CD6-Fc. Neurons exposed to CD6-Fc show a tendency for increased αALCAM488 carrier frequency. Analysis of the proportion of αALCAM488-carriers that paused under control conditions or after exposure to CD6-Fc, revealed that carrier pausing was comparable between control and CD6 ligand stimulated conditions (Figure 3.16B).

In ALCAM and $p75^{NTR}$ co-transport experiments I could also estimate whether the presence of CD6 increased the number of axons that were transporting ALCAM. In these experiments, transport of either probe demonstrated the neuron was viable and capable of long-range transport, which allowed me to include neurons that transported $p75^{NTR}$ but not ALCAM in the analysis (i.e. axons with 0 carriers/min) and vice versa. The frequency of αALCAM488-carriers can be compared to $p75^{NTR}$-positive carrier frequency in Figure 3.17A in CD6 stimulated and unstimulated conditions. I found no significant difference between the retrograde transport frequency of $p75^{NTR}$-positive or ALCAM-positive endosomes in the presence of CD6-Fc or Hu-Fc. In Figure 3.17B, there is also a tendency towards an increased proportion of pausing ALCAM-positive carriers after exposure to CD6-Fc, although this was not statistically significant.

Although I did not reveal any effect of CD6 on ALCAM transport, there is a tendency toward higher ALCAM transport frequencies in the presence of CD6. In contrast, no consistent effect of CD6-Fc on the proportion of pausing ALCAM-positive carriers was found (compare Figure 3.16 and Figure 3.17). All the transport experiments in the presence of CD6 were complicated by the cross-reactivity of the anti-ALCAM antibody with CD6-Fc and because ALCAM was transported at very low frequencies, making the detection of a small effect difficult. Perhaps, further investigation of co-transport experiments with $\alpha p75^{NTR}555$ could establish if ALCAM-positive transport vesicles show increased pausing and/or frequency after exposure to an ALCAM ligand. I review this further in the Discussion, section 6.1.2.

An interesting observation in these experiments is that in the absence of Hc, ALCAM transport is much less frequent than was seen previously (Figure 3.7). In the Hc co-transport experiments, the mean ALCAM-positive and Hc-positive carrier frequency were 0.44 and 0.47 carriers per min respectively (n=9 ventral horn cultures). In the

ALCAM and $p75^{NTR}$ co-transport experiments ALCAM-positive and $p75^{NTR}$-positive carrier frequency was 0.10 and 0.38 carriers per min respectively, in control (alone/Hu-Fc) conditions (n=3 ventral horn cultures)(Figure 3.17A). These experiments were carried out at different times and on different cultures, however it suggests that exposure to Hc stimulates the internalisation and uptake of ALCAM in neurons. The ability of Hc to stimulate the transport of other proteins (i.e. $p75^{NTR}$) present in the Hc positive endosome has been reported previously (Deinhardt et al., 2007).

A soluble form of CD6 has been reported in human serum isolated from individuals with inflammatory conditions and has been suggested to have a biological role in the immune response as it can bind bacteria following infection (Sarrias et al., 2007). However, CD6 is not expressed in the nervous system, and therefore, it is unlikely that CD6 is a physiological ligand of ALCAM in neurons. I would suggest that the homologous ALCAM-ALCAM interaction is more likely to be important within the nervous system, acting between neurons themselves and between neurons and glia. Therefore, It is also worth considering several soluble forms of ALCAM have been described (Rosso et al., 2007, Ikeda and Quertermous, 2004) and could bind ALCAM in the nervous system *in vivo*. A schematic representing possible soluble binding partners for ALCAM is shown in Figure 3.18. Altogether my results suggest that ALCAM is loaded in a passive manner into axonal retrograde carriers, however I discuss the limitations of this experiment further in the Discussion, section 6.1.2.

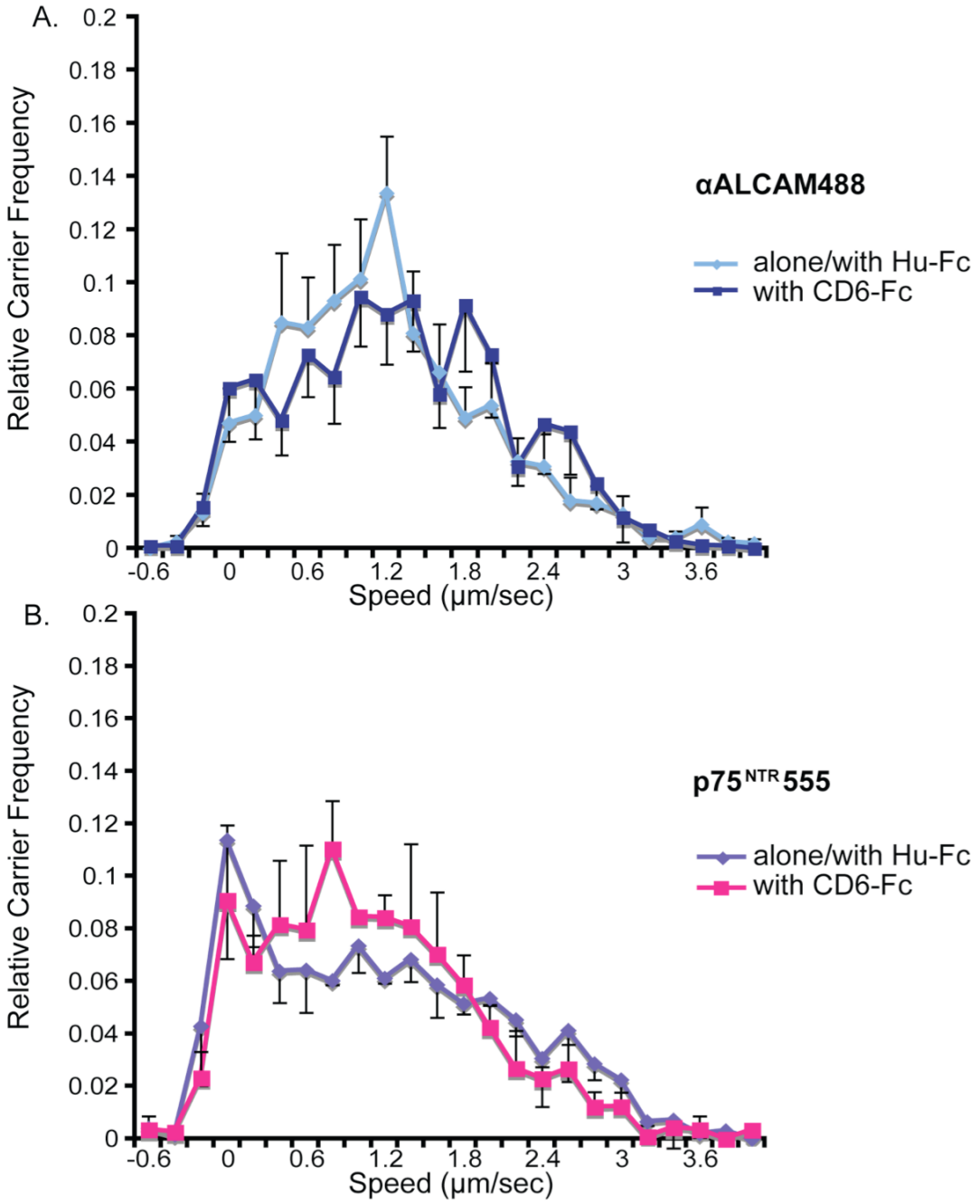

Figure 3.15 Speed distribution of ALCAM and p75^{NTR} transport does not change following exposure to CD6-Fc

ALCAM (A) and p75^{NTR} (B) speed distributions in ventral horn cultures were compared between control conditions (alone/Hu-Fc) or after exposure to CD6-Fc (with CD6-Fc). There is no significant change in the ALCAM or p75^{NTR} transport speed distribution after cells were exposed to CD6-Fc (**ALCAM**: alone/Hu-Fc n = 109 carriers, 32 axons, 9 cultures; CD6-Fc n = 214 carriers, 43 axons, 9 cultures; **p75^{NTR}**: alone/Hu-Fc n = 157 carriers, 21 axons, 3 cultures; for with CD6-Fc n = 111 carriers, 15 axons, 3 cultures).

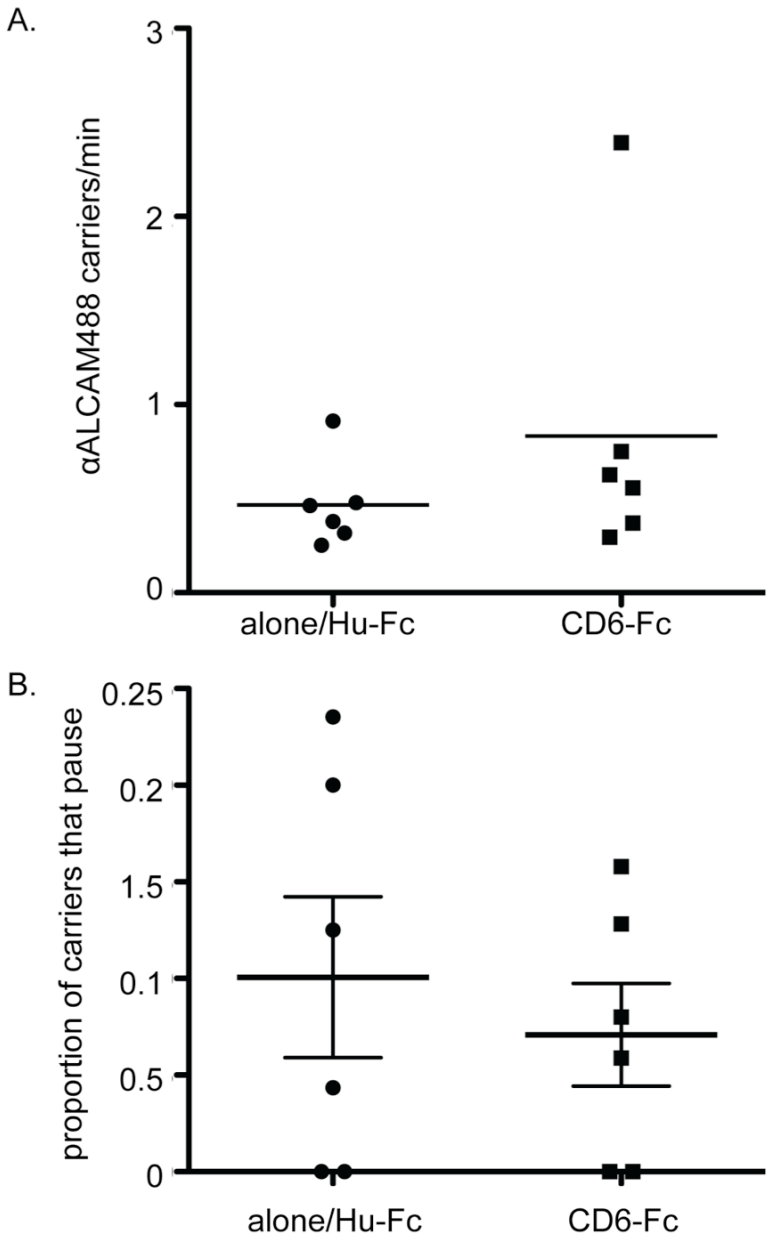

Figure 3.16 CD6 does not significantly alter ALCAM transport frequency

The frequency of ALCAM transport in ALCAM transport experiments with or without CD6-Fc is shown in (A) (n=6 ventral horn neuron cultures). The proportion of carriers that paused per ventral horn neuron culture is shown in (B), and is comparable between the alone/Human-Fc control condition or after addition of CD6-Fc.

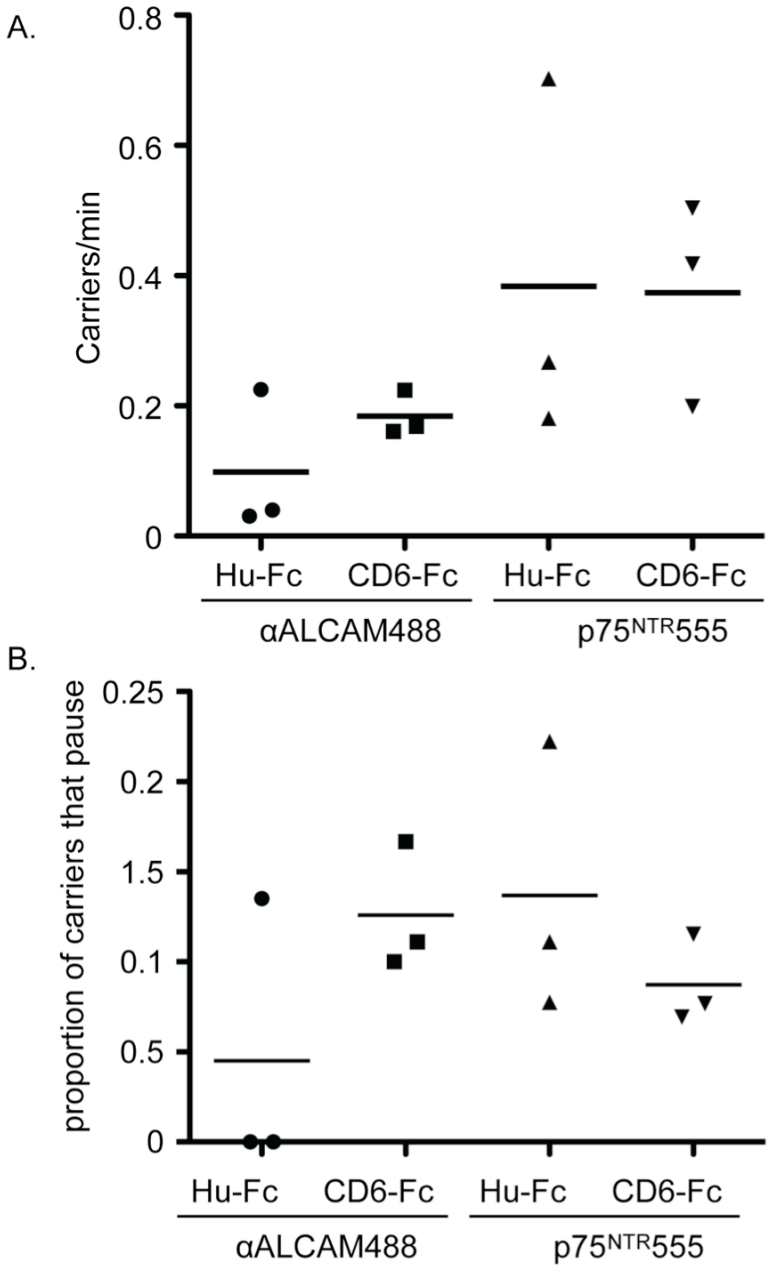

Figure 3.17 ALCAM and p75 ^{NTR} transport frequency is unaltered

A and B represent αALCAM488 and p75^{NTR}555 co-transport experiments after treatment with CD6-Fc or Hu-Fc (n=3 ventral horn cultures). In (A) neither the frequency of p75^{NTR} or ALCAM-positive carriers was significantly altered after incubation with CD6 (p = 0.9593 and 0.2647, respectively). Note that the frequency of p75^{NTR} retrograde transport is approximately 3 times greater than ALCAM transport. The proportion of ALCAM and p75^{NTR} carriers that pause after exposure to CD6-Fc or control Hu-Fc is shown in (B). ALCAM carriers have an increased tendency to pause after exposure to CD6 (p = 0.1779). Data was analysed using an unpaired t-test.

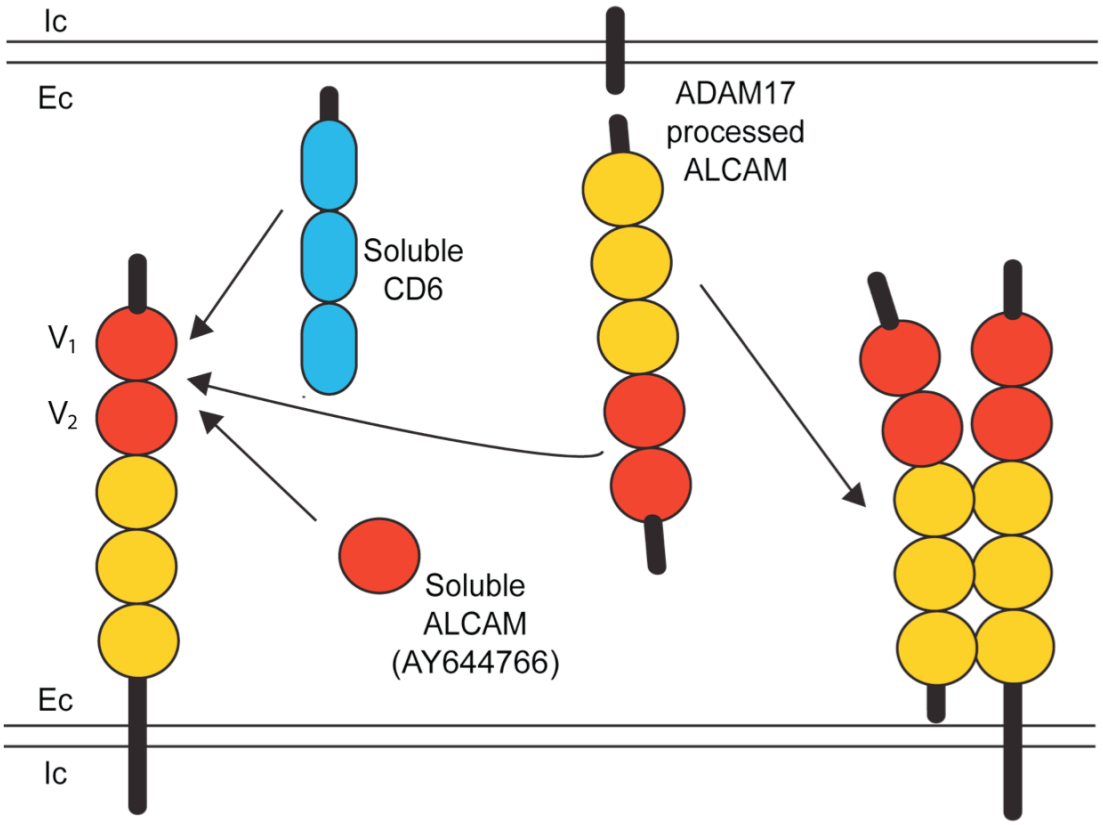

Figure 3.18 Schematic showing possible soluble proteins binding ALCAM

ALCAM is known to bind soluble CD6 (either CD6-Fc or endogenous) via its most distal extracellular domains (V_1). Theoretically, the most distal domains (V_1 and V_2) could also bind the soluble ALCAM fragment generated by alternative splicing, and the extracellular domain produced by ADAM17 cleavage in a *trans*-interaction. The cleavage product would also be able to bind in *cis* with membrane bound full length ALCAM, as shown on the right.

3.6 What is the fate of ALCAM-positive transport carriers?

ALCAM is internalised and transported in neurons from the axonal plasma membrane towards the cell body. My experiments suggest that endosomes transporting ALCAM toward the cell body may contain signalling molecules such as the neurotrophin receptor $p75^{NTR}$. Why is ALCAM transported to the cell body? ALCAM transport could have a role in neuronal homeostasis or the protein could merely be a passenger on the transport endosome. Alternatively, ALCAM could be transported back to the cell body to be targeted for degradation.

To address whether ALCAM containing endosomes are part of the degradative pathway, I conducted co-transport experiments of αALCAM488 with LysoTracker, an established marker of acidic compartments (113a abstract 653 1994). I found that ALCAM predominantly travelled independently of acidic compartments labelled by LysoTracker in neurons (see Figure 3.19 and Figure 3.20). Only 12% of the ALCAM positive organelles, both moving and stationary, were also positive for LysoTracker. This is consistent with experiments that have shown Hc, neurotrophin receptors and other retrograde cargoes are not transported in acidic compartments (Bohnert and Schiavo, 2005, Lalli and Schiavo, 2002). Furthermore, I did not see colocalisation of ALCAM with LysoTracker in the cell body as shown in Figure 3.21. This suggests that αALCAM488 does not enter acidic compartments after direct internalisation in the soma, or after having reached the cell body following axonal transport.

I also conducted immunofluorescence experiments on ventral horn cultures following 1-2 h of internalisation with αALCAM488 to determine whether ALCAM was targeted to lysosomes labelled with the lysosome marker LAMP2 (Cuervo and Dice, 1996). As seen in Figure 3.22, there is little colocalisation between αALCAM488 puncta and LAMP2 vesicle staining. This suggests that ALCAM endosomes are not primarily

targeted for degradation. However, it was noted that ALCAM puncta did not appreciably accumulate in cells. There are alternative explanations for the limited colocalisation observed between degradative pathway markers and ALCAM. ALCAM could be degraded very rapidly, the conjugated-antibody could dissociate from the protein, or the Alexa-Fluor® dye could quench once it reaches acidic organelles such as lysosomes. Considering ALCAM-positive puncta were not abundant in cells, it could be difficult to visualise rapid transient events using immunofluorescence techniques that only represent a snapshot in time. Furthermore, the fusion of endosomes and sharing of their content in the cell soma could lead to the dilution of ALCAM concentration and decrease its signal intensity below threshold. Although, I did not distinguish between these alternatives I did characterise the ALCAM-containing endosome further.

A type 1 glycoprotein, Coxsackievirus and adenovirus receptor (CAR) was one of the CAMs identified in the proteomic screen of the Hc-positive endosome (Table 1). CAR consists of two extracellular IgG domains, a transmembrane region and a cytoplasmic domain including a PDZ interaction motif. CAR has recently been shown to bind junctional adhesion molecule-like (JAML), and their interaction elicits cell-signalling events, important in the immune system for leukocyte migration and T-cell activation (Witherden et al., 2010, Verdino et al., 2010). As well as being identified in the Hc proteomic screen, CAR and the CAV-2 adenovirus have been shown to undergo axonal transport with Hc, neurotrophins and their receptors (Salinas et al., 2009). It was suggested that the CAV-2 virus utilises the innate transport of CAR and it was postulated that CAR transport could have a function in neurons. I conducted a co-transport experiment of ALCAM and Hc with CAV-2 in an attempt to further characterise which proteins are present in the ALCAM containing transport compartment.

Co-transport of ALCAM with CAV-2 was observed suggesting that ALCAM is transported along the same route as CAR (Figure 3.23). It is interesting to consider the similarities between the cell adhesion molecules, ALCAM and CAR. In the immune system the interactions of ALCAM and CAR with their respective ligands, CD6 and JAML, are important in T-cell activation. Furthermore, both ALCAM and CAR are retrogradely transported with neurotrophin receptors and Hc. Interestingly, ALCAM has also been identified as a virus receptor (Bartee et al., 2006). The virus K5 modulator of immune recognition (MIR2) binds to ALCAM and targets it for degradation. The axonal transport of cell surface glycoproteins could be a general homeostatic mechanism, by which cell surface proteins enter a pleitropic compartment, also containing neurotrophin receptors, to travel back toward the cell body. In turn, viruses hijack the endogenous transport route of glycoproteins to travel to the cell body, where they have access to the nucleus and other organelles important for their replication.

Another CAM previously shown to be associated with the Hc endosomal compartment in the proteomic screen was NCAM. To determine whether puncta containing both ALCAM and NCAM could be visualised, I conducted an internalisation experiment with αALCAM488 and αp75^{NTR}555 and then stained the intracellular domain of NCAM (NCAMic) using immunofluorescence. ALCAM is occasionally localised to puncta that contain NCAM in both neurites and soma, as shown in Figure 3.24 and Figure 3.25. In this experiment I cannot distinguish between NCAM present on the plasma membrane or present in internal vesicles. This may explain the limited colocalisation observed between NCAM and αALCAM488 because, following an acid wash, all the ALCAM visualised is internal. Another consideration is that the conjugated antibodies used to detect ALCAM and p75^{NTR} induce clustering, and internalisation. NCAM internalisation will not have been stimulated under these conditions. Instead, in these conditions the majority of NCAM staining will represent the protein on the plasma membrane. Despite

these limitations, I did observe some colocalisation of NCAM with ALCAM in cell soma and neurites in these experiments. In similar experiments, I also detected limited colocalisation of internalised αALCAM488 vesicles with antibody staining for another Ig superfamily member L1 (data not shown).

In conclusion, I found evidence that several cell adhesion molecules; CAR, ALCAM and NCAM are found in endosomes shared with neurotrophin receptors in ventral horn neurons.

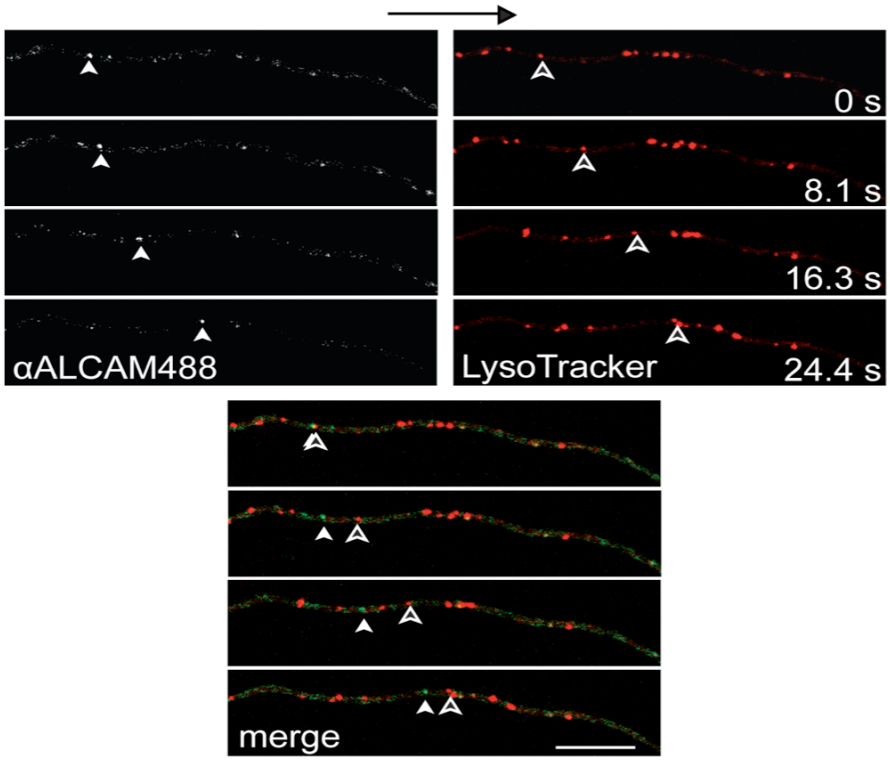

Figure 3.19 ALCAM is not transported in LysoTracker-positive acidic compartment

Consecutive frames from a co-transport experiment shows that both LysoTracker and αALCAM488 were transported along axons. However, they were predominantly not transported in the same compartment. The merged image shows that the carriers indicated by the white and black arrowheads are distinct carriers moving in the same direction back to the cell body (black arrow). Scale bar, 10 μm.

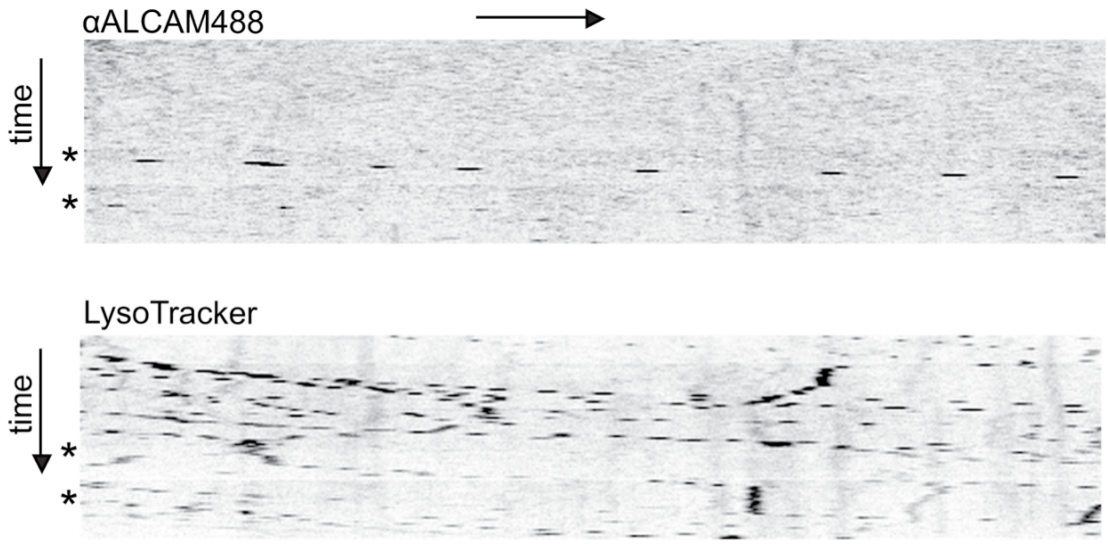

Figure 3.20 αALCAM488 and LysoTracker transport kymographs

A movie taken during a αALCAM488 and LysoTracker co-transport experiment is represented as two kymographs. The horizontal arrow indicates the direction of transport toward the cell body. The kymographs are generated by drawing a line along the axon and aligning the single line scans vertically over time (indicated by the vertical arrow). For a full explanation see Material and Methods, section 2.2.5.4 and Figure 2.6. Two αALCAM488 carriers are seen in the upper kymograph, their entry into the frame indicated by asterisks. There are many LysoTracker-positive transport compartments moving diagonally across the kymograph, however they do not colocalise with αALCAM488-positive vesicles.

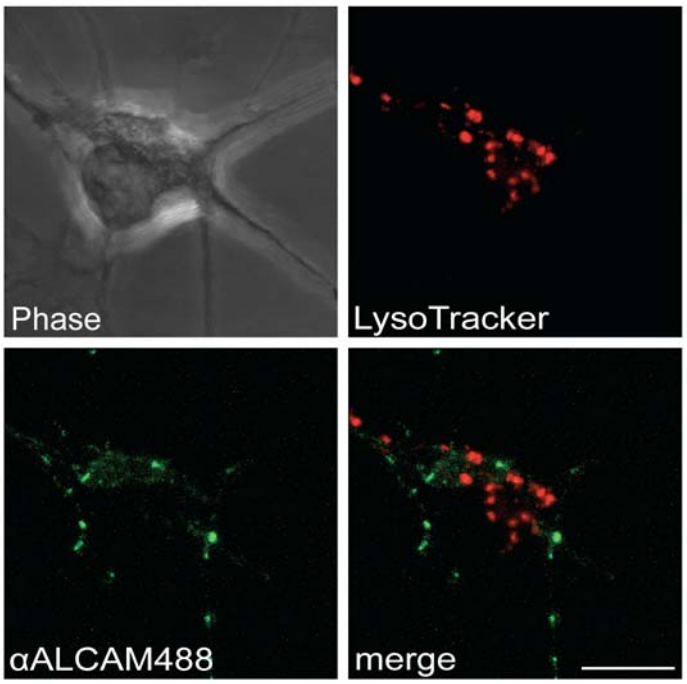

Figure 3.21 ALCAM does not colocalise with LysoTracker-positive organelles in the cell body

During transport experiments αALCAM488 and LysoTracker were not found in the same endosomal structures in the cell body. Scale bar, 10 μm

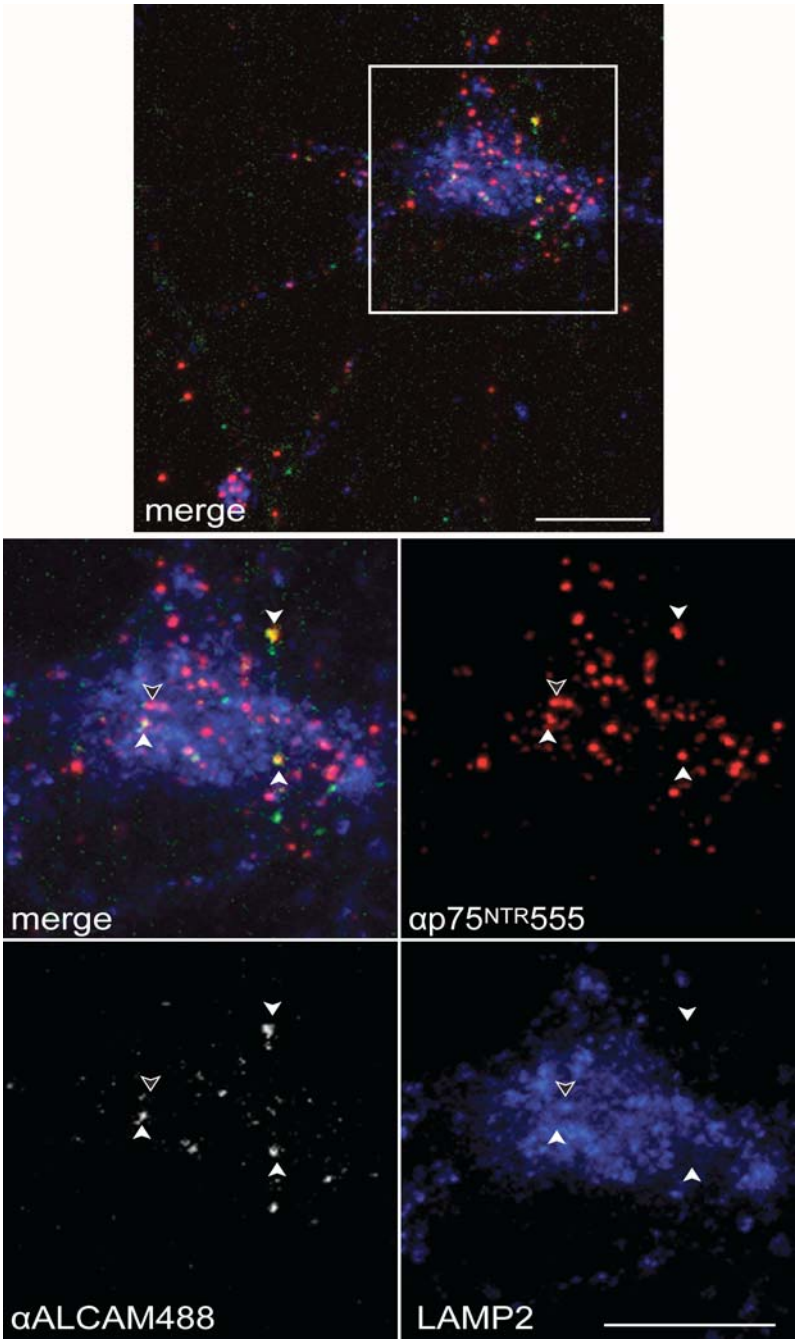

Figure 3.22 ALCAM does not enter LAMP2-positive degradative compartments in ventral horn neuron cell bodies

ALCAM colocalises with $p75^{NTR}$ in vesicles in the cell body however, there is little or no colocalisation of ALCAM with LAMP2. The boxed area is magnified in the lower panel where puncta containing both ALCAM and $p75^{NTR}$ but no LAMP2 are indicated by white arrowheads. The black arrowhead indicates a LAMP2 positive endosome that also contains $p75^{NTR}$. Scale bars, 10 μm.

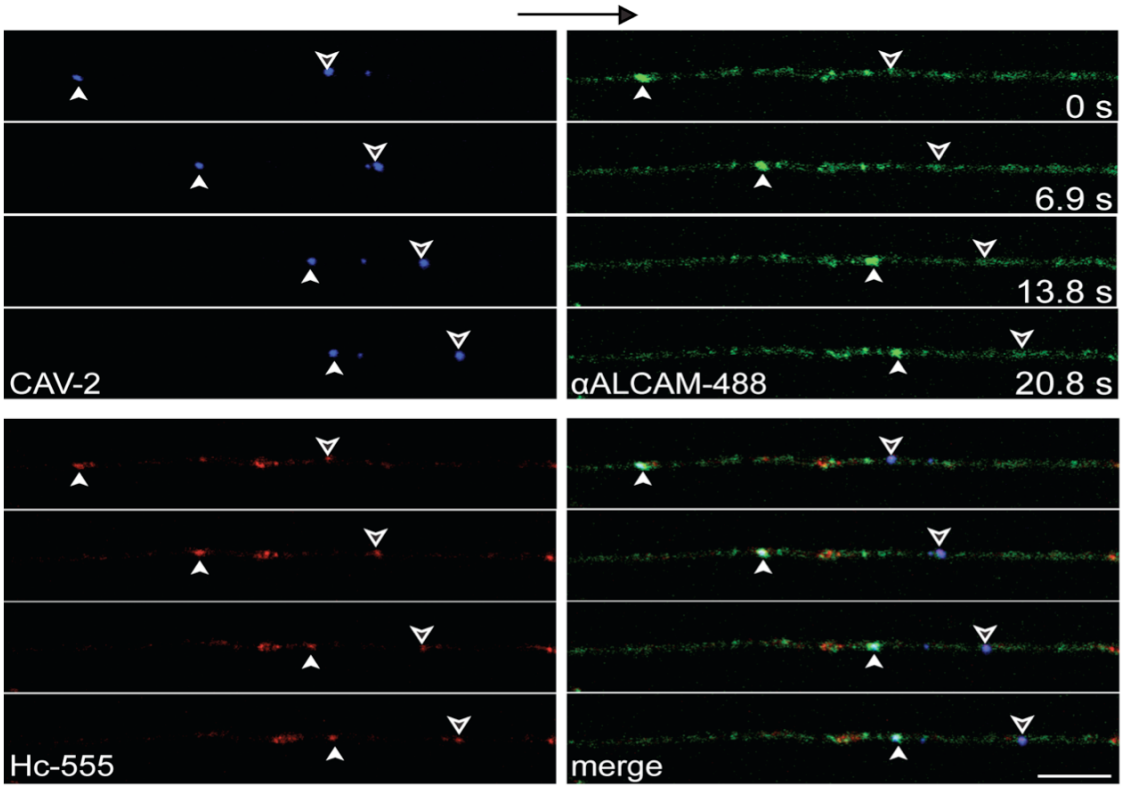

Figure 3.23 CAV-2 partially co-transports with ALCAM

Consecutive frames from a transport experiment after exposure to αALCAM488, Hc-555 and CAV-2 cy3, shows vesicles moving towards the cell body (black arrow). CAV-2 positive endosomes were seen to colocalise with ALCAM and Hc, indicated by white arrowheads. The black arrowheads indicate a carrier positive for CAV-2 and Hc, but not ALCAM. Scale bar, 10 µm.

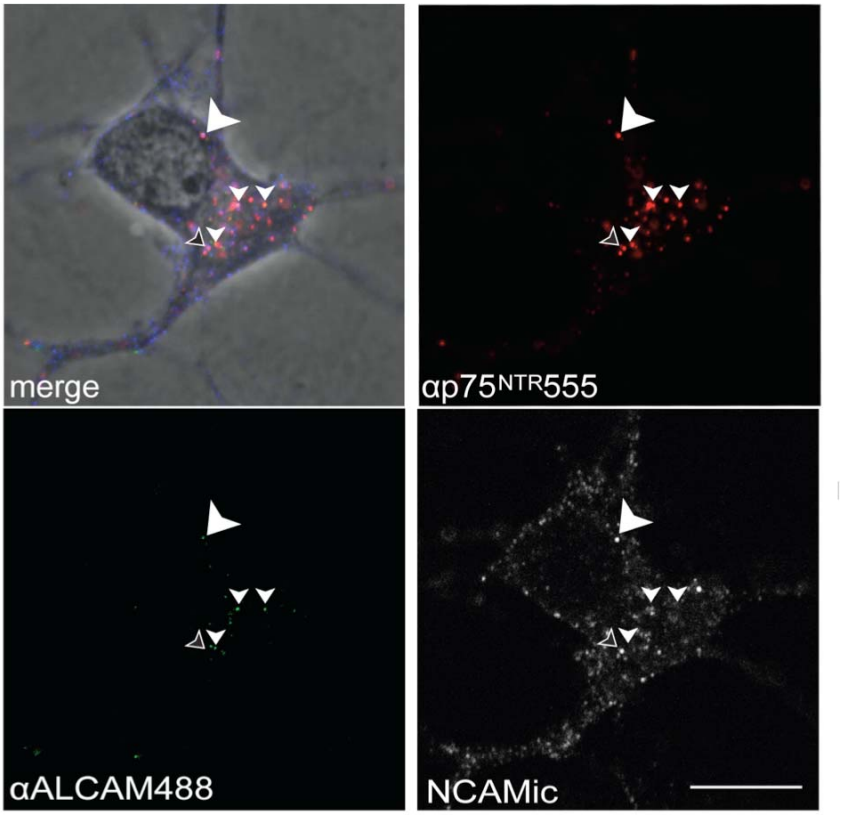

Figure 3.24 ALCAM shows limited colocalisation with NCAMic

Ventral horn neurons allowed to internalise αALCAM488 and p75^{NTR}555 were acid washed, and localisation of NCAM (NCAMIc) was assessed by immunofluorescence. Structures that contain ALCAM, NCAM and p75^{NTR} can be found in cell bodies after internalisation and immunofluorescence staining (indicated by the large arrowhead). There are also organelles that contain p75^{NTR} and NCAM but no ALCAM, an example is indicated by the black arrowhead. However, the predominant colocalisation is between ALCAM and p75^{NTR} (small white arrowheads).

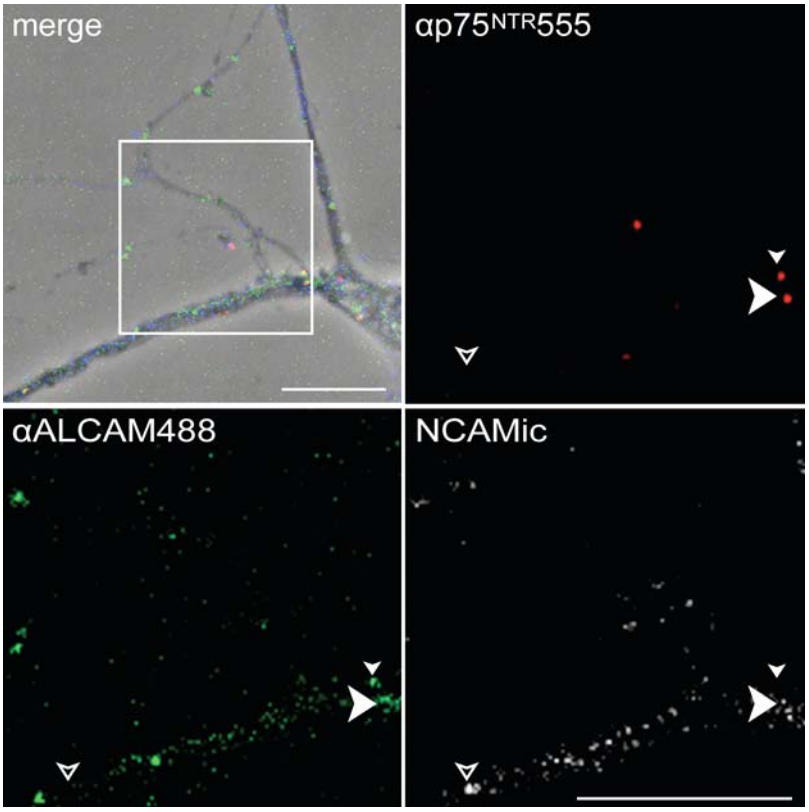

Figure 3.25 NCAM and ALCAM show partial colocalisation in neurites

The merged image shows neurites after ventral horn neuron internalisation of αALCAM488 and $p75^{NTR}$555 and staining for NCAM intracellular domain (NCAMic). The boxed region is magnified in the other panels where some, but not extensive, colocalisation between $p75^{NTR}$555 and αALCAM488 puncta with NCAMic is seen in neurites. The large white arrowhead indicates a compartment with all three molecules, although it is noted that they do not all have the same structure. An NCAMic positive cluster (black-filled arrowhead) does not associate with ALCAM or $p75^{NTR}$. The small white arrowhead indicates αALCAM488 and $p75^{NTR}$ colocalisation without NCAMic.

3.7 Summary

ALCAM was identified as a protein associated with the Hc-containing endosome by mass-spectrometry. I have verified the association of ALCAM with the Hc-positive compartment in ventral horn neurons, biochemically and by imaging co-transport experiments. In living neurons ALCAM undergoes constitutive axonal transport, and is often transported in the presence of the neurotrophin receptor $p75^{NTR}$. I found that exposure to the ALCAM ligand CD6 did not have a significant effect on the speed of ALCAM transport. Although I did not detect a significant change in ALCAM transport frequency, there was a consistent tendency for increased ALCAM carrier frequency after exposure to CD6. I found that ALCAM-containing organelles also contained other CAMs e.g. NCAM and CAR, perhaps suggesting CAMs travel via a general retrograde transport route. The function of ALCAM transport was not resolved in these experiments, but I did not find evidence to suggest that ALCAM transported to the cell body is primarily targeted for degradation.

Chapter 4. Characterisation of ALCAM in the nervous system

From live-cell imaging and biochemical studies we confirmed the association of ALCAM with Hc and found that ALCAM was retrogradely transported in mouse primary ventral horn neurons. In western blot analysis of the magnetically purified Hc compartment I found two distinct forms of ALCAM were expressed in ventral horn cultures and interestingly, the lower form was enriched in transport endosomes. To the best of my knowledge, this is the first demonstration that ALCAM can exist as two distinct species in the ventral horn. I aimed to further characterise ALCAM expression in the mouse nervous system, and attempted to determine the molecular differences between the two species.

4.1 ALCAM is differentially expressed in the mouse nervous system

I compared the expression of ALCAM in different tissue lysates isolated from whole CNS tissue, primary cell cultures and cell lines.

Initially I compared whole mouse brain lysate, purified brain synaptosomes, lysate from ventral horn neuron cultures that are commonly used in Hc internalisation and transport experiments, as well as a spinal cord astrocyte culture. I analysed ALCAM protein expression by western blot, probing the membrane with the same anti-ALCAM antibody used for the transport experiments *in vitro* (Figure 4.1). We found that only in mouse ventral horn neuron culture were two distinct forms of ALCAM expressed. In mouse whole brain lysate and purified synaptosomes a broad band with molecular weights varying between 90 and 100 kDa was recognised, which could consist of

several different ALCAM forms. Interestingly, purified spinal cord astrocytes expressed one form of ALCAM that migrated at the same molecular weight as the higher of the two ALCAM species observed in ventral horn neuron culture. We hypothesised that the existence of two ALCAM forms in these motor neuron enriched cultures is because they are composed of two distinct cell types, glia and neurons. Thus the high migrating form could be expressed on glial cells while the lower molecular weight species could be expressed on neurons. Consistent with this possibility, I found that the lower molecular weight ALCAM band was enriched in the Hc-containing axonal transport organelle isolated from primary ventral horn neurons (Chapter 3, Figure 3.1). Since the Hc-conjugated MIONs are predominantly internalised in neurons, the form of ALCAM associated with the Hc compartment should be that expressed on neural cells.

Another observation consistent with, but by no means proof of, our hypothesis is that the relative expression of the two ALCAM species varies in different primary cultures (Figure 4.2). Interestingly, this difference in intensity seems to correlate with the relative purity of neurons to glial cells in culture. The U251MG astrocytoma cell line only expressed the higher molecular weight form of ALCAM similarly to what was observed in primary astrocytes. As shown in Figure 4.2B, I also investigated ALCAM expression in the Pheochromocytoma (PC12) neural cell line and the MTLN3 rat mammary adenocarcinoma cell line by western blot. The MTLN3 cell line expressed a much lower molecular weight form, consistent with the predicted molecular weight of ALCAM, and could represent protein that has not undergone post-translational modification. In the PC12 neural cell line, the anti-ALCAM antibody used does not recognise a specific band but many proteins in the lysate. In summary, I found that ALCAM is expressed differently in different cell types and this may suggest that the protein undergoes differential post-translational modification according to cell type.

As outlined in the Introduction, Figure 1.6, human ALCAM has two reported isoforms, Q13740-1 and Q1370-2. Q1370-2 is attributed to differential splicing resulting in the loss of 13 amino acids in the juxta-membrane region. The equivalent region is conserved in the mouse sequence, which would suggest that the same isoform exists in mice. However, considering only 13 amino acids have been removed, this differential splicing event could not account for the 10 kDa molecular weight difference observed in ventral horn ALCAM species. Splicing is also thought to result in a soluble fragment of ALCAM comprising of the most extracellular variable Ig-domain only (Ikeda and Quertermous, 2004). Similarly this splicing event cannot account for the ALCAM forms expressed in ventral horn culture lysates.

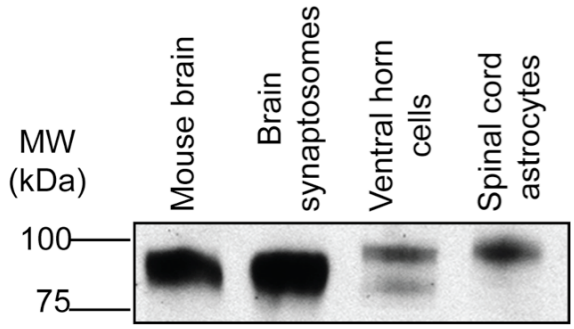

Figure 4.1 Distinct species of ALCAM are expressed in different tissues of the mouse nervous system

Cell culture and tissue lysate samples were separated by SDS-PAGE, transferred to PVDF membranes, and probed with the anti-ALCAM antibody. Mouse brain and synaptosome fraction purified from rat brain appear to have a similar ALCAM content. ALCAM appears as a broad band at around 90-100 kDa. ALCAM in ventral horn neuron culture is expressed in two distinct forms (Ventral horn cells), one migrating at around 100 kDa and a second migrating around 90 kDa. Primary spinal cord astrocytes express only the higher molecular weight ALCAM species.

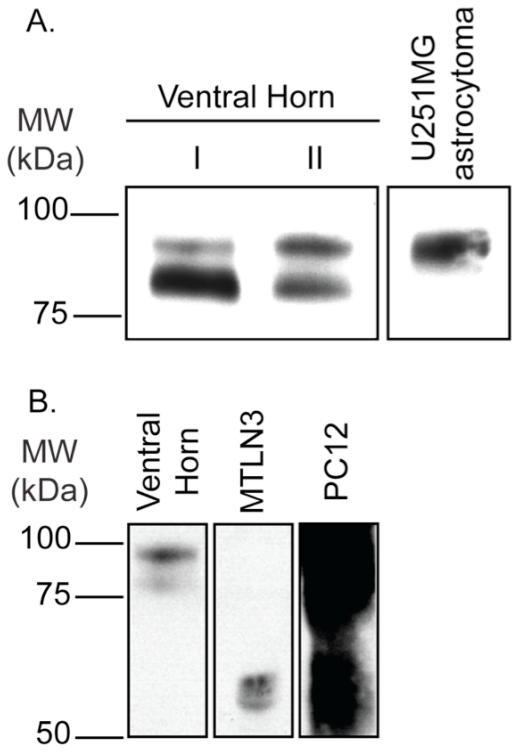

Figure 4.2 ALCAM expression varies in different cultures and cell lines

Primary cell cultures and cell lines extracts were separated by SDS-PAGE and analysed by western blot. In (A) the relative expression of the two ALCAM forms varies between ventral horn neuron primary cultures isolated from different litters as can be seen when comparing the relative intensities of the bands in experiment I and II. The U251MG astrocytoma cell line expressed the higher molecular weight form of ALCAM only. The expression of ALCAM in the MTLN3 and PC12 cell lines is analysed by western blot in (B). MTLN3 cells express a low molecular weight form of ALCAM, while the anti-ALCAM antibody does not recognise a specific band in PC12 cells. No explanation for this behaviour of the anti-ALCAM antibody is currently available.

4.2 ALCAM is glycosylated in ventral horn neuron cultures

Since two novel ALCAM forms were expressed in ventral horn cultures we wanted to characterise what could account for this difference. ALCAM can be N-glycosylated (Sekine-Aizawa et al., 1998) and has been identified as an O-glycosylated membrane protein expressed during neuronal differentiation (Sato et al., 2002). Therefore, we went on to examine if differential glycosylation could account for the two species observed.

We investigated this by exposing ventral horn neuron culture lysates to different deglycosylation enzymes (Tarentino et al., 1985, Lieberoth et al., 2009). We treated the samples either with PNGase-F that removes all N-type glycan modifications, neuraminidase (recombinant from *Arthrobacter ureafaciens*) to remove sialic acid chains, or with O-glycosidase (recombinant from *Streptococcus pneumonia*) to remove O-glycan chains. The latter enzyme required co-incubation with neuraminidase to remove sialic acids before the O-glycosidase could remove the O-glycans. Following the various deglycosylating treatments, the ventral horn neuron culture samples were analysed by western blot as shown in Figure 4.3.

Interestingly, ALCAM in ventral horn cultures continued to migrate as two distinct bands after all combinations of enzyme treatment. My findings suggest that ALCAM in ventral horn cultures is predominantly glycosylated on N-type glycan chains and the small shifts observed after neuraminidase and O-glycosidase treatments suggest that there are also minor sialic acid and O-type glycan chain modifications. Since ALCAM remained as two distinct species following all treatments, it demonstrated that differential glycosylation does not account for the two ventral horn ALCAM species.

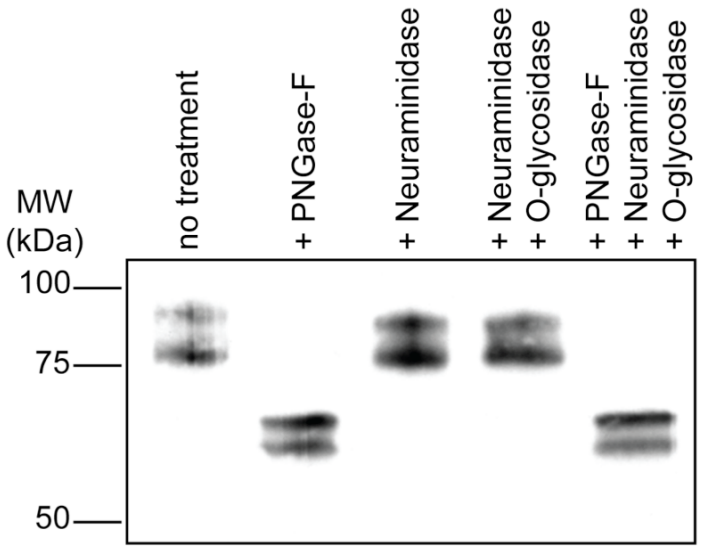

Figure 4.3 Ventral horn ALCAM species are not the result of differential glycosylation

Western blot analysis of ALCAM in ventral horn neuron culture extracts which have undergone deglycosylation treatments. In control conditions (no treatment) two ALCAM forms are observed. Upon treatment with PNGase-F there is a large shift in molecular weight due to the removal of N-type glycan chains, but the two bands remain distinct. Much smaller shifts are observed on treatment with Neuraminidase alone or in combination with O-glycosidase, removing sialic acid and O-type glycans respectively. When ventral horn lysate was treated with all three enzymes, ALCAM species continued to migrate as distinct bands illustrating that the two ALCAM forms are not due to differential glycosylation.

4.3 Ventral horn ALCAM species are not products of cleavage

ALCAM can undergo ectodomain shedding and membrane cleavage by the metalloprotease ADAM17 (Bech-Serra et al., 2006, Rosso et al., 2007). ADAM17 cleavage occurs in the juxtamembrane region (see Introduction, Figure 1.6). If this cleavage occurred in ventral horn neuron cultures it would produce a large soluble ectodomain fragment, corresponding to all 5 extracellular domains, and a short integral membrane fragment comprising of the transmembrane region and the cytoplasmic domain. Since the polyclonal antibody used in my previous experiments was raised to the extracellular domain of ALCAM, it would recognise the soluble ectodomain as well as the full-length protein.

To determine whether a cleavage event could account for the 2 forms of ALCAM seen in ventral horn cultures, I performed a membrane stripping experiment to remove proteins that did not directly interact with the membrane and separated the extracts into membrane and supernatant fractions. Cell samples were mixed with a high KCl salt wash or with stripping buffer, then analysed by SDS-PAGE and western blot. A typical western blot is shown in Figure 4.4. Both after high salt wash, and more stringent carbonate stripping, the two forms of ALCAM remained associated with the membrane pellet of ventral horn cultures. No evidence of ALCAM was found in the supernatant fraction in any condition. This suggests that both ventral horn ALCAM forms are integral membrane proteins, and ectodomain shedding does not account for the lower molecular weight form.

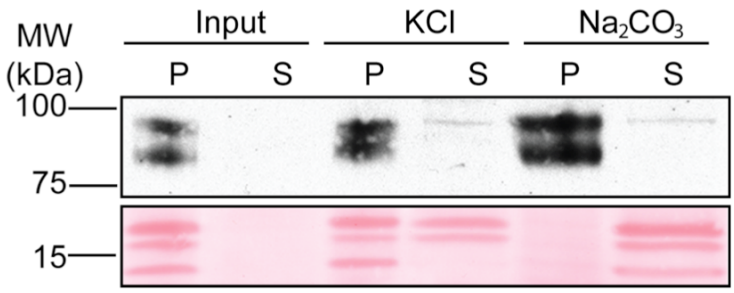

Figure 4.4 Both ventral horn ALCAM species are integral membrane proteins

Ventral horn culture lysate was separated into a membrane fraction (P) or supernatant (S) by centrifugation, either alone or after a 1 M KCl salt wash or 0.2 M Na_2CO_3 stripping step (Herreros et al., 2000). Samples were analysed by SDS-PAGE and western blot. Both ALCAM species associate to the membrane pellet (P) in control membranes (Input) and after salt wash and stripping treatments. The Ponceau (lower panel) shows that proteins associated with the membrane fraction in non--treated conditions (Input) move to the supernatant after high salt wash and carbonate stripping.

4.4 Production of an antibody to recognise the cytoplasmic domain of ALCAM

To further characterise the ventral horn ALCAM forms, I aimed to develop two new antibodies, one designed to recognise the extracellular domain and another the cytoplasmic domain. I hoped to investigate whether the two antibodies differentially recognised the two ventral horn ALCAM forms. We also hoped to use these antibodies to immunoprecipitate both ALCAM forms expressed in ventral horn neuron cultures, and then use mass spectrometry to identify the region of difference in the protein structure.

I designed pET vectors that contained either the whole extracellular domain of ALCAM or its cytoplasmic domain fused to a 6 Histidine sequence (His_6-tag) on their C-terminus (for full explanation see Materials and Methods 2.2.1.1 and Figure 2.2). The ALCAM-His_6 constructs were expressed in bacteria, and His-tagged proteins were purified on a nickel-resin column by affinity chromatography.

The relative purity of the ALCAM extracellular domain (ALCAM-Ec) and cytoplasmic domain (ALCAM-C) proteins can be visualised by Coomassie Blue stain (Figure 4.5). The ALCAM-Ec fragment was expressed at low yield and several contaminating bands are present in the eluate (Figure 4.5A). Furthermore, the western blot reveals that the majority of the His_6-tagged protein in the eluate has a molecular weight that is too small to comprise of the full extracellular domain. Considering there are already several commercial antibodies to the extracellular domain and in view of these problems with protein expression and purification, I decided not to pursue the production of an antibody directed to the extracellular domain further.

In SDS-PAGE, ALCAM-C migrated at 12kDa, a higher molecular weight than 3976 Da predicted by ApE (Universal) (Figure 4.5). However, the western blot shows that the majority of the purified protein is His_6-tagged. Since protein migration depends on protein charge and SDS binding, it was reasonable to assume that the predominant protein seen in the coomassie gel was the tagged cytoplasmic domain of ALCAM. The P3 fraction contained the fewest contaminating bands and so this fraction was used for rabbit immunisation. We sent 1.7 mg of purified ALCAM-C in PBS to BioGenes GmbH (Köpenicker Straße 325, D-12555 Berlin, Germany) who then immunised 2 rabbits, 4682 and 4683 with the purified protein fragment. The rabbits went through a sequence of immunisation boosts and bleeds and their serum was tested. BioGenes conducted an Elisa titre test on antigen-coated plates to test sera binding to ALCAM-C. The serum titer for rabbit 4682 was 1:100,000, while the titer for rabbit 4683 was 1:25,000.

I tested the serum of rabbits 4682 and 4683 in western blot and the results are shown in Figure 4.6. Both sera 4682 and 4683 recognised the purified ALCAM-C protein and did not detect an unrelated His_6-tagged protein (KNA). Sera 4682 and 4683 detection of ALCAM-C was competed by pre-absorption of the sera with soluble ALCAM-C protein. These results suggested both sera specifically recognised the ALCAM cytoplasmic domain antigen and not the His_6-tag. When tested on ventral horn culture lysates, the serum from rabbit 4682 was more reactive than serum 4683. Furthermore some bands recognised in ventral horn lysate were at an appropriate molecular weight to be endogenous ALCAM. Some putative ALCAM bands were partially or completely competed by prior incubation with ALCAM-C, suggesting that this serum could recognise endogenous ALCAM expressed in ventral horn cultures (Figure 4.6; highlighted by the arrow and star). Considering the much lower titer of 4683 and its weaker immunoreactivity with ventral horn culture extracts I decided to pursue the immunisation regime with rabbit 4682 only. We also added a purification step whereby

the serum was passed over an ALCAM-C antigen column to specifically enrich for the antibodies directed against the ALCAM cytoplasmic domain. Purified 4682 antibody (4682 IgG) was pooled, aliquoted and frozen in 30% glycerol at -20°C.

The purified 4682 antibody was tested on ventral horn neuron culture lysates isolated from wild type, ALCAM$^{+/-}$ and ALCAM$^{-/-}$ embryos to see which of the recognised bands would be lost in ALCAM$^{-/-}$ lysates (Figure 4.7). I found that 4682 IgG recognised a band at the molecular weight of ALCAM that was lost in cells isolated from ALCAM$^{-/-}$ ventral horn neuron cultures. This result demonstrated that antibody 4682 recognised endogenous ALCAM. Interestingly, the western blot suggests that two forms of ALCAM may be recognised, similarly to the pattern revealed by the goat anti-ALCAM antibody. However, the 4682 IgG immunoreactive bands were not well resolved. This suggests that the ALCAM species present in ventral horn cultures are recognised by the 4682 antibody and therefore that they both contain the cytoplasmic domain. This is consistent with the membrane stripping experiment where both species were shown to be integral membrane proteins. An interesting outcome of this western blot analysis is that there appears to be a gene dosage effect in heterozygote animals. If the ALCAM signal is normalised to the total loaded (Tubulin) it appears that less ALCAM is present in ALCAM$^{+/-}$ when compared to wild type.

I also tested whether rabbit 4682 IgG recognised overexpressed ALCAM in PC12 cells using both western blot and immunofluorescence analysis as shown in Figure 4.8 and Figure 4.9. ALCAM-D is full length ALCAM tagged with the fluorescent protein Dendra on its C-terminus and is described in Material and Methods, section 2.2.1 and Chapter 5, section **5.1**. As expected, 4682 IgG recognised overexpressed ALCAM in western blot (Figure 4.8), where it detected bands overlapping with those recognised by the antibody to the Dendra tag. By immunofluorescence, antibody 4682 recognised

ALCAM-D in the overexpressing cell, which colocalised with the Dendra signal (Figure 4.9). Antibody 4682 can therefore recognise overexpressed ALCAM in PC12 cells. 4682 IgG also recognised additional bands around 100 kDa that could represent endogenous ALCAM in PC12 cells (Figure 4.8), but their specificity has not been confirmed. Furthermore, in immunofluorescence (Figure 4.9) I only saw a minimal membrane localised stain in non-transfected cells, suggesting that either ALCAM expressed in PC12 cells is not recognised by the 4682 antibody or that ALCAM is expressed at very low levels in this cell line. Considering ALCAM has not been reported to display nuclear localisation, it is likely that the 4682 nuclear staining observed in Figure 4.9 is non-specific.

In these experiments, a potential accumulation of 4682 IgG ALCAM signal was detected in neurite tips of differentiating PC12 cells. Kidins220, a scaffold protein for neurotrophin receptors, has been shown to localise to neurite tips in NGF-differentiated PC12 cells (Bracale et al., 2007). I therefore tested whether ALCAM colocalised with Kidins220 at neurite tips. As can be seen in the merged image in Figure 4.9, there is little evidence for the colocalisation of ALCAM with Kidins220 on the same structures, though they can be present in the same neurite. Since the accumulation of 4682 IgG in neurite tips was not found in all differentiated cells (both transfected and untransfected), it could suggest that the accumulation of ALCAM at tips is a transient event related to a stage of differentiation (distinct from that when Kidins220 accumulates). However, the difference observed could also be unrelated to differentiation and simply due heterogeneity in protein content and distribution between PC12 cells. My experiments did not distinguish between these hypotheses.

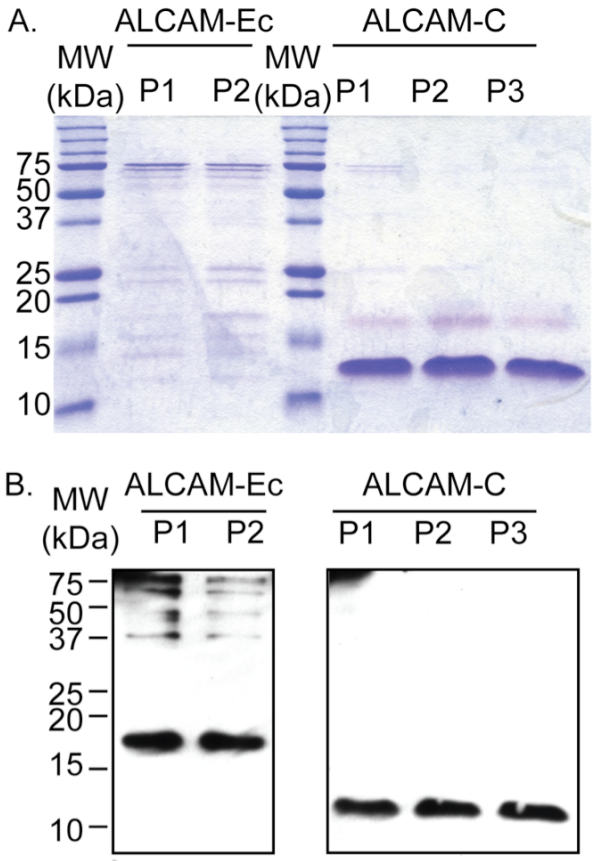

Figure 4.5 ALCAM His-tagged construct purification

The extracellular domain protein fragment (ALCAM-Ec) was eluted into 2 samples and the cytoplasmic domain (ALCAM-C) was collected as 3 samples. Two µg of each sample was run on two 15% Bis-Acrylamide SDS-PAGE in parallel, one gel was stained with Coomassie Blue (A), and the other was transferred to PVDF and western blotted with rabbit anti-His_6 (B). The expression and purification of ALCAM-Ec was not efficient, there is little protein in the eluate and it is contaminated with several additional bands (A). Furthermore, the molecular weight of this His-tagged fragment is very different from the expected molecular weight (17 kDa vs. 56 kDa using ApE (Universal)) (B). In contrast the ALCAM-C purification worked well, with significant yield of recombinant protein present in the eluate, as shown in the Coomassie Blue stain. Crucially, the majority of protein produced is His_6-tagged (B).

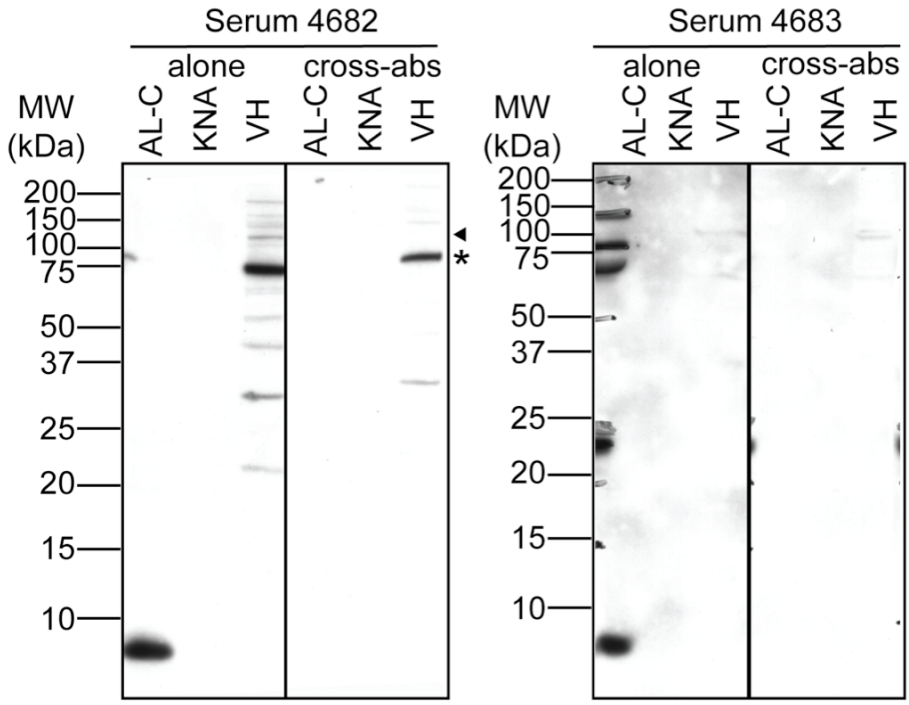

Figure 4.6 Sera 4682 and 4683 recognise the purified ALCAM-C protein but serum 4682 also clearly recognises endogenous protein in ventral horn neuron lysates

Purified ALCAM-C (AL-C), KNA (an unrelated His_6-tagged protein) and ventral horn neuron culture lysate (VH) were analysed by western blot with serum 4682 or 4683. Both sera recognise purified ALCAM-C and not KNA. Following pre-absorption of the sera with purified ALCAM-C (cross-abs), the ability of both 4682 and 4683 to recognise ALCAM-C is lost. Serum 4682 detects several bands in ventral horn lysate. One band migrates at an appropriate molecular weight to be ALCAM and is competed by pre-absorption with ALCAM-C (arrow). Other bands present in ventral horn neuron culture are partially competed by preabsorption indicated by (*). Serum 4683 is much less immunoreactive with ventral horn proteins. Note that the bands on the top left of the 4683 western blot are actually ladder proteins.

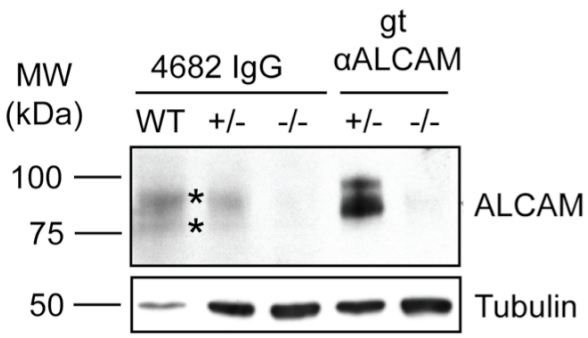

Figure 4.7 4682 IgG recognises a specific ALCAM band that is lost in knockout ventral horn neuron cultures

Lysate from ventral horn neuron cultures isolated from ALCAM$^{-/-}$ mice were analysed by western blot. 4682 IgG recognises bands that are not present in ventral horn neuron cultures isolated from ALCAM$^{-/-}$ mice around 90-80 kDa. The two bands indicated by stars (*) are not well resolved. When compared to the commercial goat antibody against ALCAM (gt αALCAM) it can be seen that the interaction of 4682 IgG is weaker. Comparison of the 4682 IgG signal relative to the Tubulin loading control suggests there is a gene dosage effect and less ALCAM is present in ALCAM$^{+/-}$ cultures.

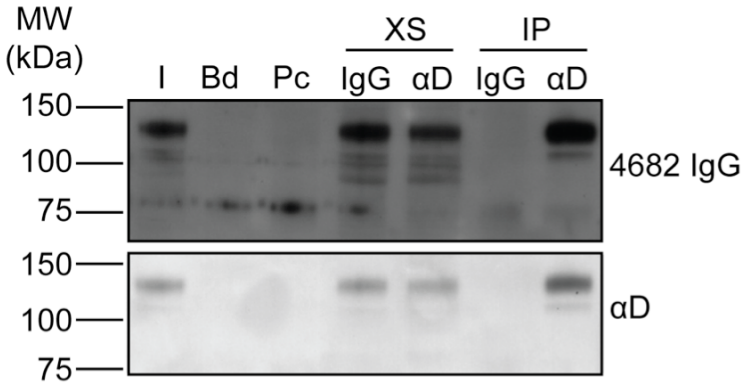

Figure 4.8 4682 IgG recognised ALCAM-D expressed in PC12 cells

4682 IgG recognised a band at 130 kDa corresponding to ALCAM-D in the PC12 lysate (I) and in the immunoprecipitate (IP) with the anti-Dendra (αD) antibody. However it does not recognise any bands in the control rabbit IgG (IgG) immunoprecipitate. After immunoprecipitation ALCAM-D has been partially depleted from the exhausted supernatant (XS) in the anti-Dendra immunoprecipitated sample, but not the control IgG sample. An overlapping 130 KDa band is recognised by the anti-Dendra antibody using the Trueblot™ system, as seen in the lower panel.

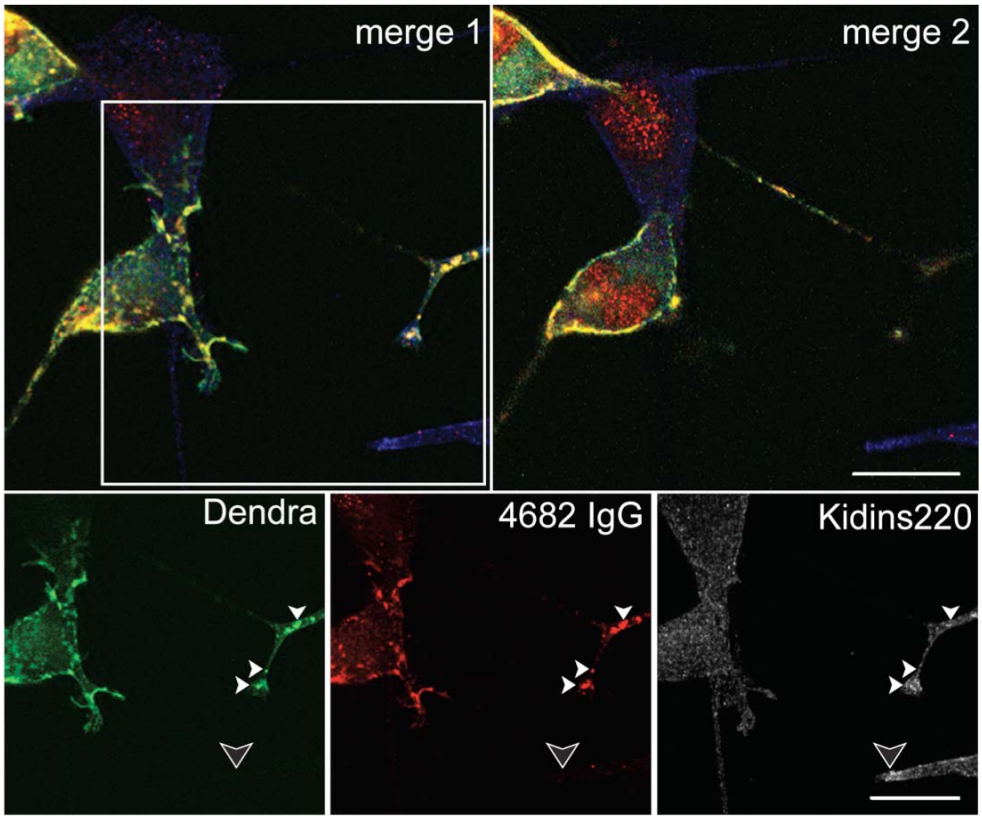

Figure 4.9 Immunofluorescence showing colocalisation of ALCAM-D and 4682 IgG signal

PC12 cells transfected with fluorescently tagged ALCAM (ALCAM-D) and differentiated with NGF were stained with 4682 IgG and an antibody directed towards Kidins220 a membrane scaffold for neurotrophin receptors. Merge 1 and merge 2 are at different depths in the cell (Z planes). Merge 1 is near the substrate surface, while merge 2 is a slice through the cell body. The yellow signal in the merged image shows that ALCAM-D (green) expressed in PC12 cells is recognised by 4682 IgG (red). This illustrates that the cytoplasmic domain of overexpressed ALCAM-D is recognised by 4682 IgG. The boxed region is magnified in the lower panel. Dendra and 4682 IgG are shown to colocalise in punctate structures in the neurite (white arrowheads). Kidins220 also localises to neurite tips of NGF differentiated PC12 cells but it is not present in the ALCAM-positive puncta. Kidins220 is also present in the non-transfected neurite (black arrowhead). The 4682 IgG nuclear stain (merge 2) is unspecific and of equal intensity in transfected and untransfected cells. Scale bar, 20 µm

4.5 Immunoprecipitation of ALCAM using antibody 4682

The 4682 IgG was next tested in immunoprecipitation experiments. However, it became apparent that there were problems in using this 4682 antibody to immunoprecipitate ALCAM. Unfortunately, 4682 IgG alone migrated at the molecular weight of endogenous ALCAM as shown in Figure 4.10. Given the anomalous migration of this band in SDS-PAGE it was hypothesised that it was due to a particularly strong disulphide bond interaction between the two antibody heavy chains that did not dissociate at room temperature in Laemmli sample buffer. Boiling the IP samples and therefore forcing the reduction of these disulphide bonds, shifted the antibody bands so that they migrated at around 50 kDa. The disadvantage of this procedure was that boiling samples decreased the yield of ALCAM resolved by western blot.

An immunoprecipitation experiment with U251MG astrocytoma cell line carried out under the modified conditions i.e. boiling samples for 5 minutes before SDS-PAGE separation, is shown in Figure 4.11. After boiling, the antibody bands no longer migrated between 100 and 75 KDa, but shifted to around 50 kDa (Figure 4.11, lower panel). Unfortunately, the western blot also shows that immunoprecipitation of ALCAM using antibody 4682 is very inefficient (compare input and 4682 immunoprecipitate signals in Figure 4.11). Considering the amount of ALCAM protein expressed in primary cultures, the low efficiency of immunoprecipitation and the difficultly of getting large amounts of primary culture extracts, we did not proceed with our initial plan of sending immunoprecipitated samples for a mass-spectrometry analysis.

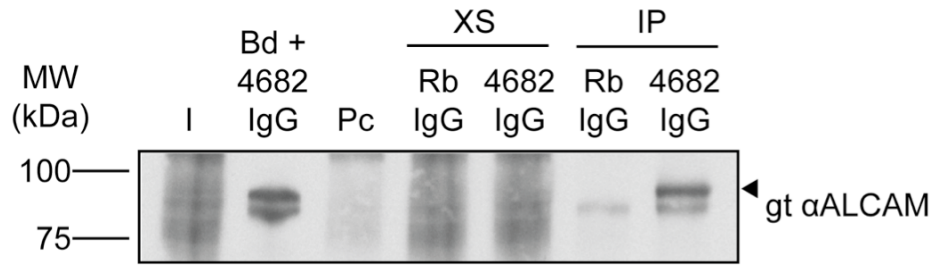

Figure 4.10 Immunoprecipitation of ALCAM using the 4682 antibody

The western blot shows an immunoprecipitation experiment with PC12 cells using the 4682 antibody (4682 IgG) and purified rabbit immunoglobulin (Rb IgG) as a control. As shown previously goat anti-ALCAM (gt αALCAM) recognises many proteins in PC12 cell lysate input (I) and in the exhausted supernatant (XS) after the immunoprecipitation. Prior to immunoprecipitation, lysates were precleared with beads and found limited evidence of protein that bound to the beads alone (Pc). A specific band associated with the 4682 IgG immunoprecipitation (IP) migrated at the level of endogenous ALCAM, but similar bands were recognised in the prebound 4682 IgG beads alone (Bd+4682 IgG).

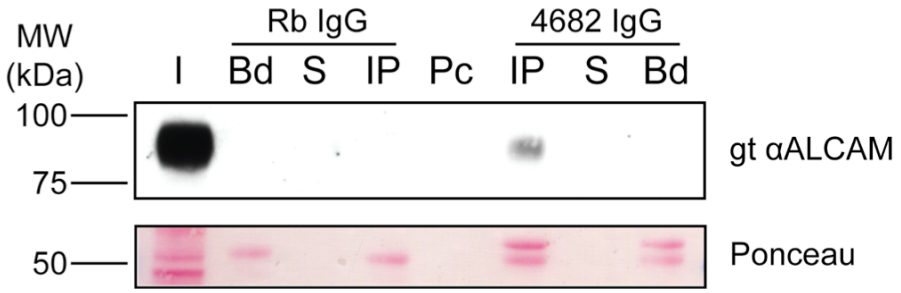

Figure 4.11 Immunoprecipitation of ALCAM from U251MG astrocytoma cell line

ALCAM is expressed in the U251MG total lysate (Input,I) detected with the goat anti-ALCAM antibody (gt αALCAM). ALCAM is specifically immunoprecipitated (IP) with 4682 IgG and not with the control rabbit IgG (Rb IgG). Samples were boiled so that the antibody bands migrated around 50 KDa, as seen in the Ponceau stained membrane in IP and antibody-conjugated beads (Bd) samples. No ALCAM can be seen in the supernatant (S) after either the IgG bead or 4682 IgG bead incubation. There is no explanation for this anomalous result.

Experiment conducted by Claire Thomas

4.6 Summary

ALCAM expression in the mouse nervous system was investigated in order to characterise the novel forms of ALCAM revealed in the magnetically purified Hc-endosome. The results showed that ALCAM is differentially expressed in different areas of the mouse nervous system, primary cells and cell lines. ALCAM appears as a broad band in mouse brain and purified synaptosomes in contrast to ventral horn neuron cultures that express ALCAM in two distinct forms. We hypothesise that the higher molecular weight species is expressed on glial cells and the lower molecular weight species is expressed on neurons. Primary astrocyte cultures and the astrocytoma cell line only express the higher migrating form consistent with our hypothesis. The lower migrating putative neural ALCAM species is specifically enriched in the Hc compartment that should be specifically present in neurons. I hypothesise that ALCAM is recognised as a broad band in brain lysates and synaptosomes because both are composed of multiple neuron and glia subtypes that may express different forms of ALCAM. In contrast, ventral horn neuron cultures produce a unique co-culture system, enriched for motor neurons and containing a restricted number of glia types, in which distinct forms of ALCAM can be resolved.

I attempted to characterise what could account for the difference in molecular weight between the two ALCAM species. I found that both ALCAM bands are glycosylated but differences in glycosylation did not account for the difference in their molecular weight. Furthermore, both ALCAM forms are integral membrane proteins, and both are recognised by antibody 4682 IgG directed toward the ALCAM cytoplasmic domain.

I produced and characterised a novel antibody, 4682 IgG, directed toward the mouse ALCAM cytoplasmic domain that specifically recognised ALCAM in primary cultures. It also recognised overexpressed ALCAM in PC12 cells by immunofluorescence and

western blot. Unfortunately, we found that the antibody was not efficient at immunoprecipitating ALCAM from primary ventral horn neuron or PC12 culture extracts. Therefore, I did not pursue further analysis of the two forms by mass-spectrometry, which may have provided useful information on the difference between the two ALCAM species. This strategy could be pursued further by optimising the immunoprecipitation protocol with other anti-ALCAM antibodies.

Chapter 5. The role of ALCAM in neurite outgrowth and neurotrophin signalling

ALCAM is transported in neurotrophin-associated endosomes and it has been proposed that this compartment has a signalling role in neurons (reviewed in Cosker et al., 2008, and Zweifel et al., 2005)). It is therefore possible that ALCAM may contribute to neurotrophin signalling during the development and maintenance of the nervous system. As described in the Introduction, section 1.5, the role of ALCAM in the nervous system has been examined in several animal models. In chick and fish, interfering with ALCAM-dependent adhesion using antibodies directed towards the extracellular domain, can disrupt neuron outgrowth, fasciculation and neuromuscular junction formation (Fournier-Thibault et al., 1999, Ott et al., 2001, Avci et al., 2004). Furthermore, zebrafish show aberrant retinal ganglion cell (RGC) differentiation and axon outgrowth following morpholino knockdown of Neurolin A and B, the zebrafish orthologs of ALCAM (Diekmann and Stuermer, 2009). However, ALCAM$^{-/-}$ mice have a limited neurological phenotype, suggesting that other proteins can functionally compensate for the loss of ALCAM during development in higher vertebrates (Weiner et al., 2004). In this chapter, I investigated the role of ALCAM in neurite outgrowth, and whether it cooperated with neurotrophin signalling.

5.1 ALCAM overexpression potentiates neurite outgrowth in response to NGF

Full-length ALCAM was cloned and tagged with the fluorescent protein Dendra to its cytoplasmic domain (ALCAM-D) (for full explanation see Materials and Methods, section 2.2.1 and Figure 2.1). Dendra is a monomeric fluorescent protein derived from *Dendronepthya sp*. that can undergo photoconversion from green to red fluorescent states (Gurskaya et al., 2006). It is not only capable of stable photoconversion with UV-violet light, similar to earlier generation photoactivatable fluorescent proteins, but also by visible blue light which is less phototoxic to cells (Gurskaya et al., 2006). ALCAM-D was transfected into PC12 cells that could be differentiated in the presence of NGF. Examples of Dendra or ALCAM-D transfected cells are shown in Figure 5.1 and Figure 5.2 respectively. I found ALCAM-D was expressed on the surface of PC12 cells in culture where it was recognised by an antibody directed towards the ALCAM extracellular domain (Figure 5.2). Interestingly, ALCAM was found in clusters on the plasma membrane and in internal puncta that were not stained by the antibody to the extracellular domain in non-permeabilising conditions. ALCAM-D photoconverted by a 405 nm laser was used to follow the protein in transfected cells. This permitted visualisation of the protein under conditions that did not require antibody binding and therefore, clustering of ALCAM on the plasma membrane. I found that the majority of ALCAM in PC12 cells was slowly diffusing, and puncta did not undergo vectorial long-range transport, as shown in Figure 5.3 and Figure 5.4.

A study that analysed PC12 cell gene expression profiles after 12 h treatment with the differentiation stimuli, NGF or dbcAMP, found that ALCAM transcript levels increased between 2 and 3 fold in both conditions (Ng et al., 2009). Further evidence that regulation of ALCAM expression is coupled to neuronal differentiation came from a

study that identified ALCAM as a protein whose glycosylation was induced upon Neuro2A cell differentiation (Sato et al., 2002). Since ALCAM expression is modulated upon differentiation and that it is involved in axonal outgrowth during development in chick and fish, I wanted to investigate whether ALCAM played a role in neurotrophin-induced differentiation in PC12 cells.

The percentage of cells that displayed neurite outgrowth at both 1 and 3 days after transfection with ALCAM-D or Dendra and treatment with NGF was calculated (Figure 5.5). Neurite outgrowth was quantified by counting the number of cells whose longest neurite was at least two times or more the length of the cell body at its widest point. I found that ALCAM-D expression significantly increased the percentage of PC12 cells that displayed neurite outgrowth. This suggested that ALCAM overexpression in PC12 cells cooperated with NGF-signalling during differentiation.

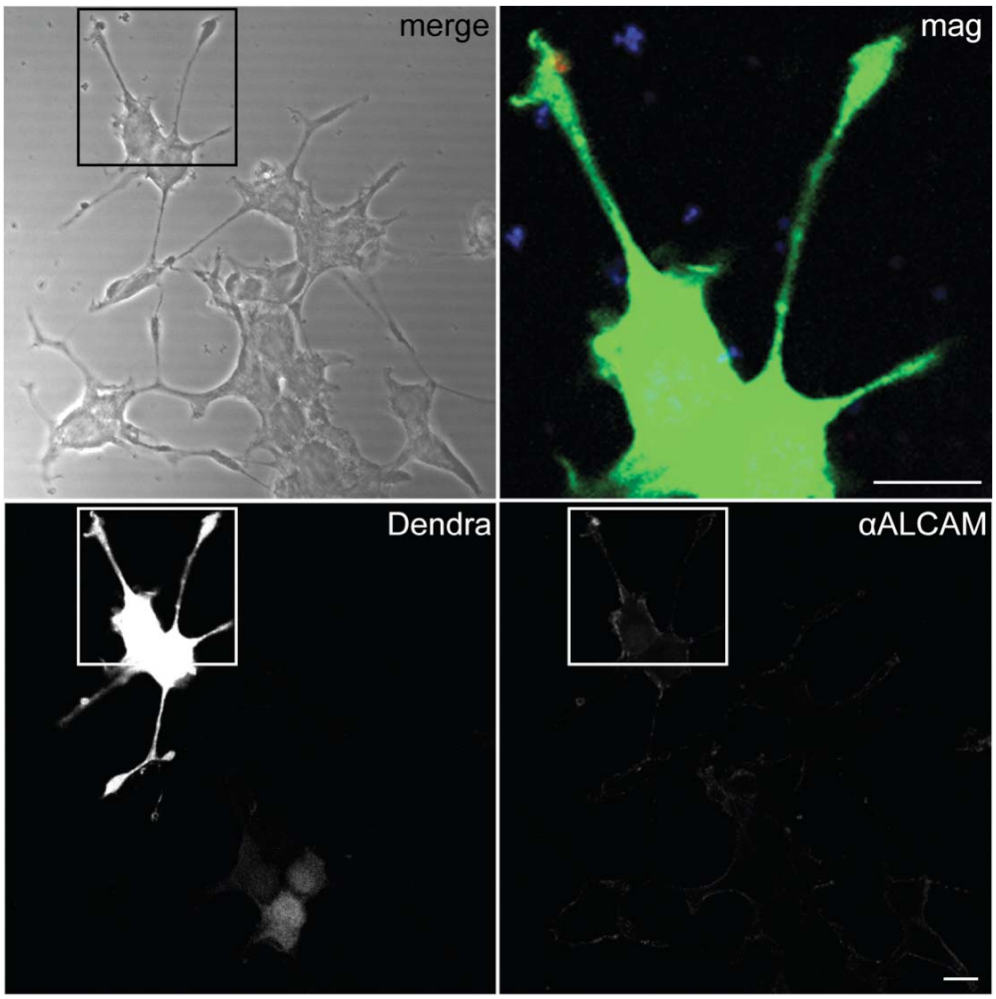

Figure 5.1 NGF differentiated PC12 cells transfected with Dendra

Immunofluorescence showing differentiated PC12 cells transfected with Dendra. Cells transfected and kept in differentiation medium with 100 ng/ml NGF have clearly visible neurite extensions 3 days after transfection. The boxed region is magnified in the upper right panel (mag) and Dendra can be seen present throughout the cell cytoplasm. An anti-ALCAM antibody (αALCAM) shows weak interaction with both the untransfected and transfected PC12 plasma membrane and could reflect low levels of endogenous ALCAM. Scale bar, 10 μm.

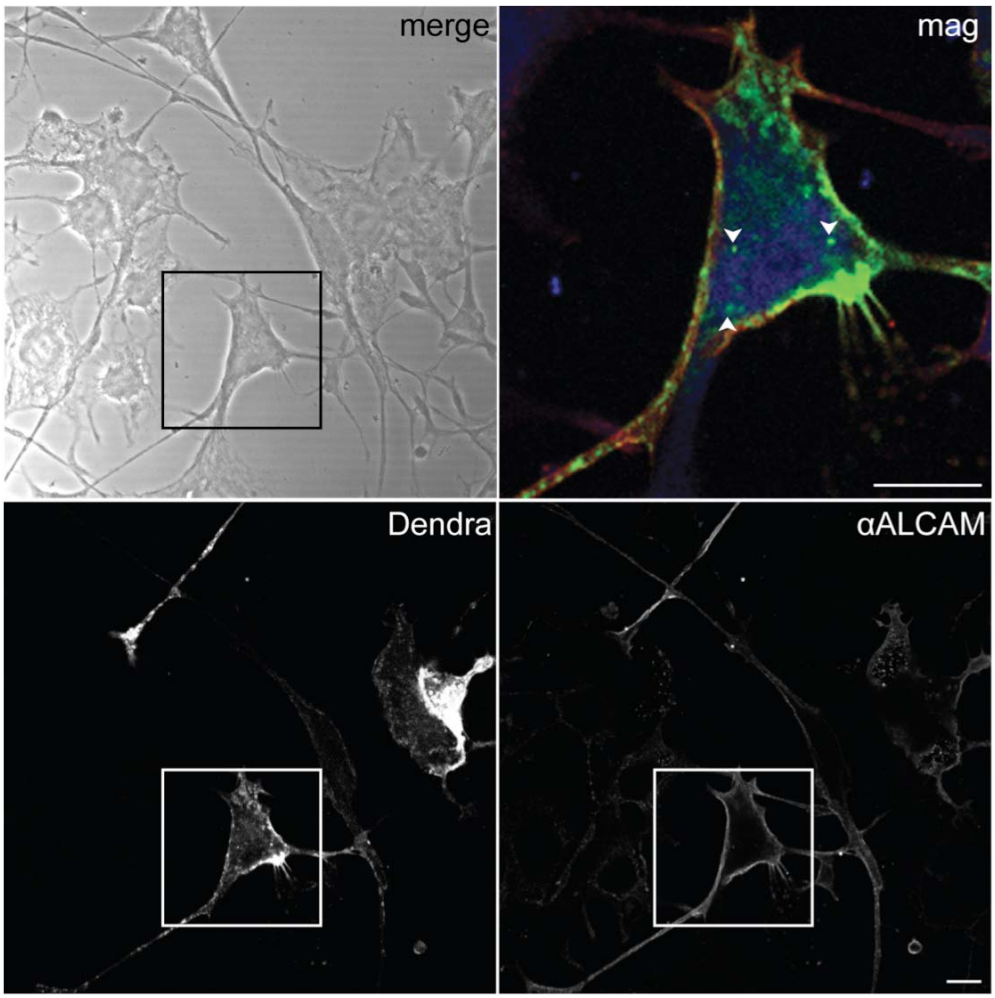

Figure 5.2 NGF differentiated PC12 cells transfected with ALCAM-D

Immunofluorescence showing PC12 cells transfected with ALCAM-D and differentiated in the presence of 100 ng/ml NGF for 3 days. ALCAM-D is predominantly seen on the plasma membrane (Dendra). In non-permeabilising conditions ALCAM-D on the surface of the cell is recognised by the anti-ALCAM antibody (αALCAM). The boxed area is enlarged in the upper right panel (mag) and shows that ALCAM-D is present on internal vesicular structures (arrowheads), as well as on the plasma membrane. Staining is similar to that observed with 4682 IgG in Chapter 4, Figure 4.8. Scale bar, 10 µm.

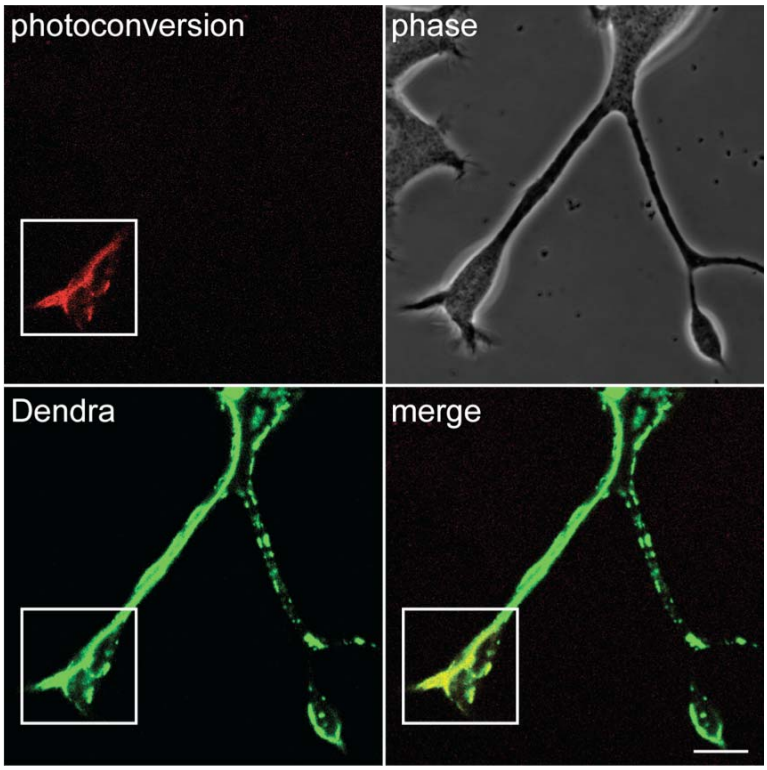

Figure 5.3 Photoactivation of ALCAM-D

ALCAM-D could be photoconverted from green to red channel by irradiating the boxed region with 10% 405 nm laser power for 5 iterations. Scale bar,10 μm.

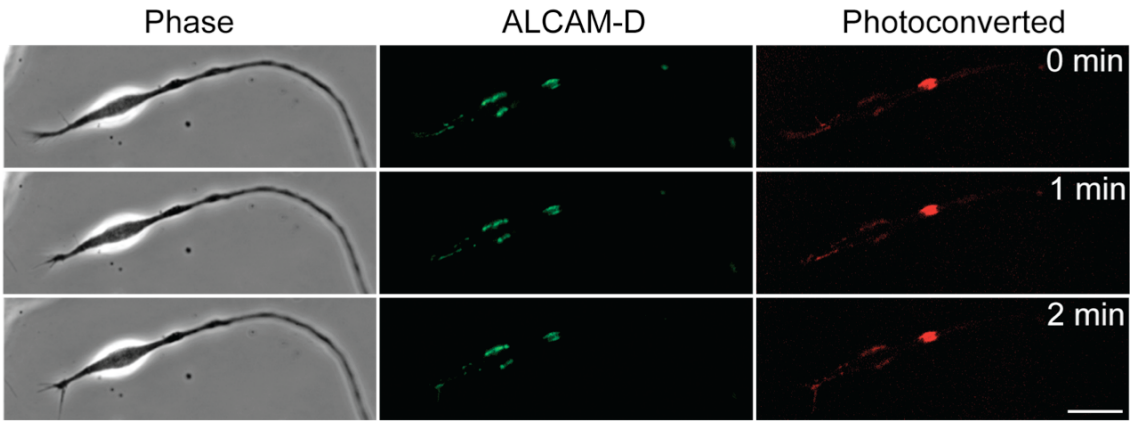

Figure 5.4 ALCAM-D is predominantly static on the surface of PC12 cells

Frames from a live-cell imaging experiment of PC12 cells transfected with ALCAM-D. Over two minutes no movement of ALCAM-D along the surface of a differentiated PC12 cell neurite could be detected. Scale bar, 10 µm.

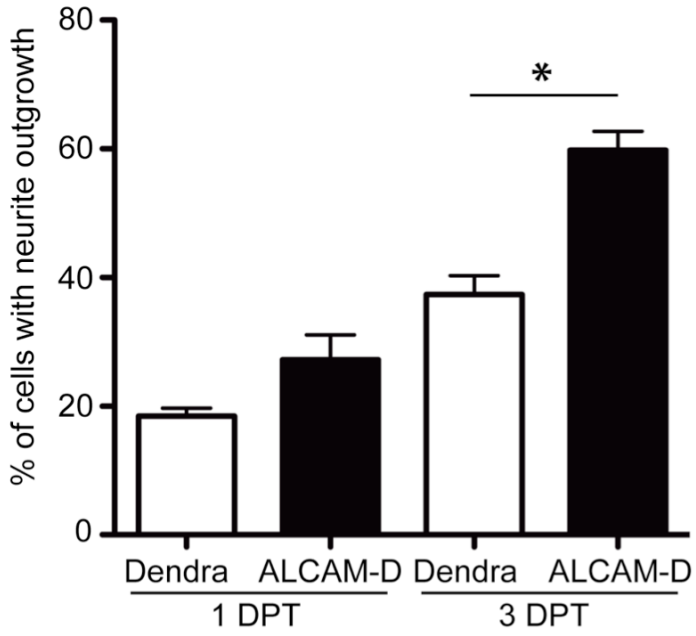

Figure 5.5 ALCAM-D significantly increased the percentage of PC12 cells that displayed neurite outgrowth

PC12 cells were differentiated with NGF after transfection with Dendra or ALCAM-D for 1 or 3 days post transfection (DPT). The percentage of cells whose longest neurite was at least two times the length of the soma was calculated (% of cells with neurite outgrowth). ALCAM-D significantly potentiated the percentage of cells that displayed neurite outgrowth at 3 days post transfection ($p=0.0059$). Data analysed using unpaired t-test. (n = 3 experiments, error bars = SEM).

5.2 ALCAM's extracellular domain is necessary and sufficient for potentiation of neurite outgrowth in PC12 cells

I next investigated which domains of ALCAM were important for its ability to potentiate NGF-induced neurite outgrowth. For this I designed and cloned four ALCAM constructs that lacked different functional domains, similar to those used previously to investigate the role of human ALCAM in cancer (van Kempen et al., 2001). Constructs were generated similarly to the full-length ALCAM-D, (for a full explanation see Material and Methods, 2.2.1 and Figure 2.1).

A schematic illustrating all the Dendra-tagged ALCAM constructs is shown in Figure 5.6. I generated two extracellular domain truncation mutants; ΔD1-ALCAM-D, lacked the more distal variable immunoglobulin (V_1) domain, and ΔD1D2-ALCAM-D lacked the two V_1V_2 domains. These two constructs lack one or both of the variable immunoglobulin domains that are required for trans-binding in both homophilic and heterophilic interactions (van Kempen et al., 2001, Bowen et al., 1997). The signal sequence of 27 amino acids was fused to the start of the truncated domains because it is required for protein folding and delivery onto the plasma membrane. A construct generated that lacked this signal sequence was found to accumulate in the endoplasmic reticulum (ER) (data not shown). I also generated ΔC-ALCAM-D that lacked the short cytoplasmic domain after amino acid 553. Lastly, I produced a chimeric protein consisting of the ALCAM transmembrane and cytoplasmic domain and the extracellular portion of CD8 (a kind gift of Prof. M. Seaman, University of Cambridge). CD8 is a type 1 transmembrane glycoprotein expressed in T-cells that has been used to generate reporter constructs to test whether cytoplasmic domains of proteins of interest contain targeting information (Seaman, 2004). The CD8 luminal and transmembrane portions have no intrinsic role in trafficking and therefore can be fused

to specific cytoplasmic tails to investigate their targeting and localisation. The CD8-ALCAM-D construct would address whether the ALCAM transmembrane and cytoplasmic domains had intrinsic neurite outgrowth potentiating ability.

I transfected these constructs into PC12 cells and differentiated them for 3 days in 100 ng/ml NGF. Figure 5.7 shows PC12 cells expressing the various proteins. All the ALCAM constructs were localised on the plasma membrane and all cells retained the ability to differentiate.

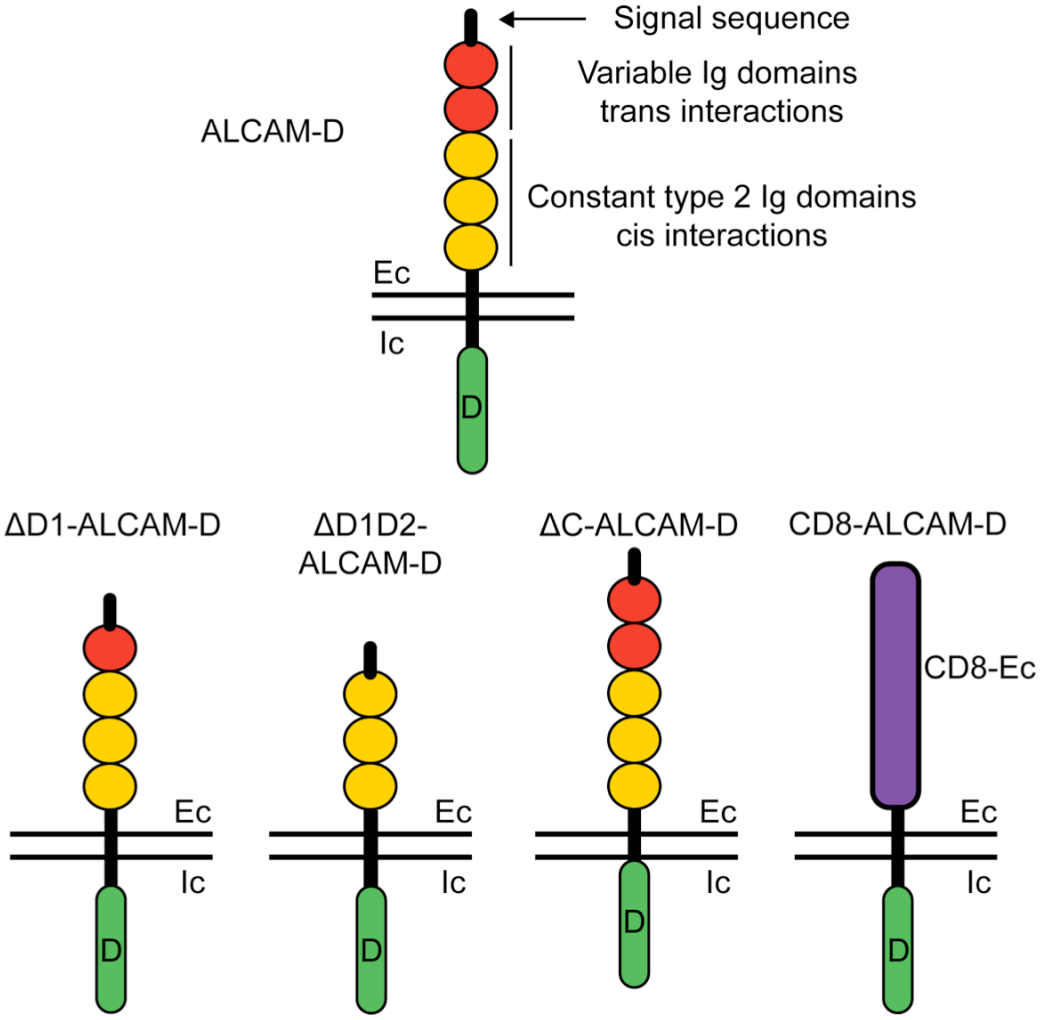

Figure 5.6 Schematic illustrating the truncated ALCAM proteins generated

Full length ALCAM-D comprises the signal sequence required for translocation in the ER lumen and sorting on the plasma membrane, followed by two variable immunoglobulin domains (V_1 and V_2) required for binding in *trans*, three membrane constant type-2 proximal domains ($C_1C_2C_3$) required for *cis*-interactions followed by a trans-membrane region, and a carboxy terminal cytoplasmic domain. The carboxy terminal was tagged with Dendra (D). ALCAM truncation and chimeric proteins are represented below. Ec extracellular; Ic intracellular.

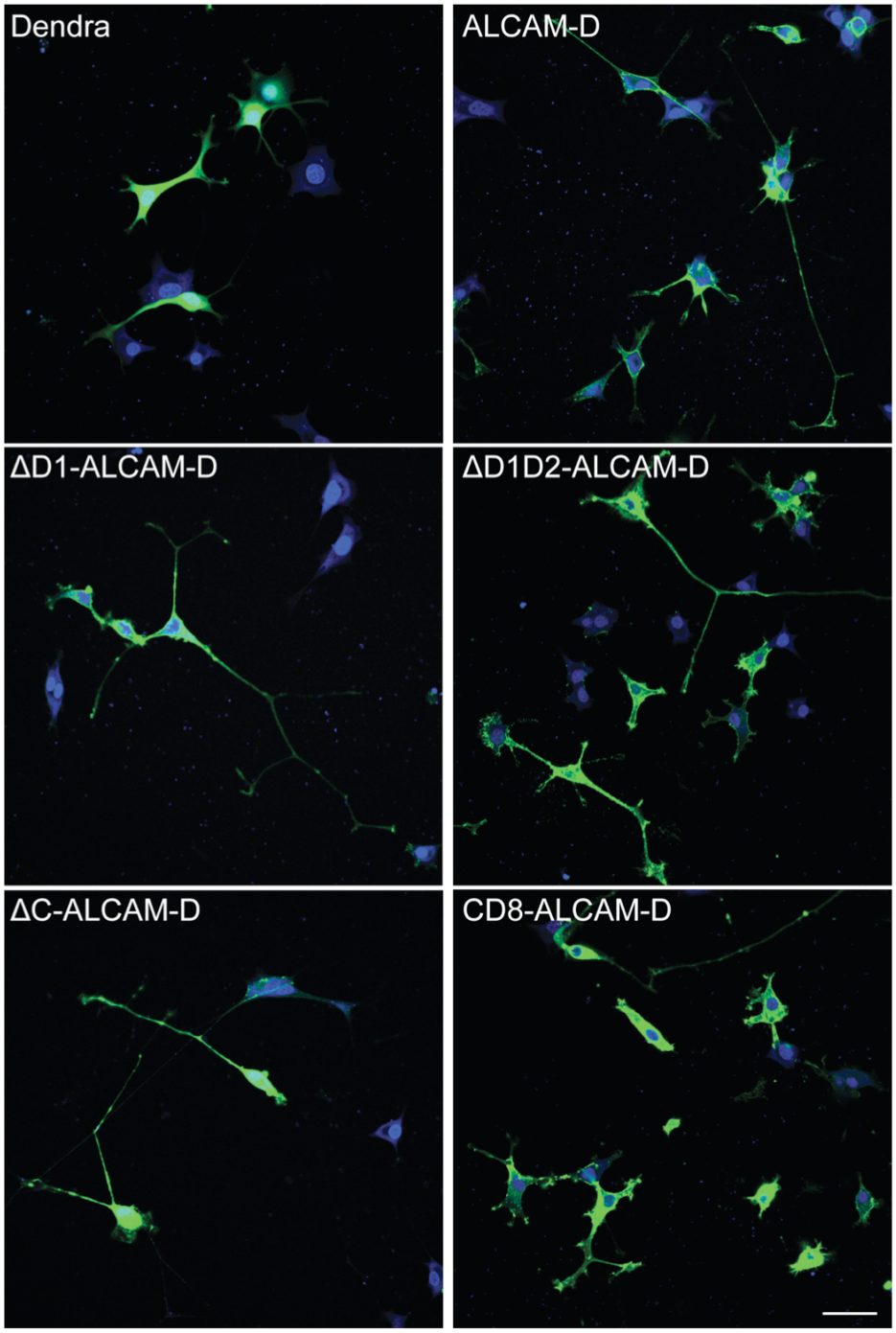

Figure 5.7 NGF differentiated PC12 cells expressing ALCAM fluorescent constructs

Images show that ALCAM-D truncation mutants were expressed at similar levels and localised to the plasma membranes of PC12 cells in culture. Cells transfected with the ALCAM-D constructs were still capable of differentiating in response to NGF exposure. Nuclei are stained with DRAQ5 in blue. Scale bar, 40μm.

5.2.1 ALCAM extracellular domains engaged in *cis* and *trans* interactions contribute to potentiating NGF-induced neurite outgrowth in PC12 cells.

Quantification of neurite outgrowth was carried out 3 days after transfection and differentiation with NGF for PC12 cells transfected with the ALCAM constructs and is shown in Figure 5.8. Truncations of the most distal extracellular domains (V_1 and V_2) decreased the ability of transfected ALCAM to potentiate NGF-induced neurite outgrowth. The effect of losing both domains was additive because cells that expressed ALCAM lacking V_1V_2 showed less neurite outgrowth than those without V_1. This suggests that binding of ALCAM in *trans* contributes to the potentiation of neurite outgrowth seen in transfected PC12 cells. Interestingly, the truncations did not abolish this potentiation completely. Indeed, ΔD1-ALCAM-D and ΔD1D2-ALCAM-D increased neurite outgrowth in response to NGF above control Dendra transfected cells. This suggests that *cis* interactions within the membrane maintained in these mutants also contribute to the potentiation effect.

Interestingly, an ALCAM construct that lacked the cytoplasmic domain (ΔC-ALCAMD) potentiated neurite outgrowth to the same extent as the full-length protein. This could suggest that ALCAM does not contribute to neurotrophin signalling by direct downstream signalling. As described in the Introduction, section 1.5, the cytoplasmic tail of ALCAM is the least conserved region when compared to its $V_1V_2C_1C_2C_3$ family members, MCAM and BCAM, which suggests the cytoplasmic region has not been under strong selective pressure during evolution. The other family members have much larger cytoplasmic regions with known interaction motifs, while the ALCAM cytoplasmic domain has no known motifs and interactions have only been demonstrated for ubiquitin and actin (Thelen et al., 2008, Te Riet et al., 2007). The latter interaction has been shown to contribute to ALCAM adhesion (Zimmerman et al.,

2004). However, it is not possible to conclude that the cytoplasmic domain is not required for neurite outgrowth potentiation from my findings because PC12 cells may express endogenous ALCAM (reviewed in Discussion, section 6.3.3). In PC12 cells transfected with ΔC-ALCAM-D, endogenous ALCAM could compensate for the truncation mutant through *cis*-interactions by transmitting any relevant signals or cytoskeletal alterations required to cause the increase in neurite outgrowth observed.

The CD8-ALCAM-D chimera comprised of the CD8 ectodomain fused to the juxta-membrane, trans-membrane and cytoplasmic domain of ALCAM was incapable of increasing neurite outgrowth. This result corroborated the findings obtained with the other constructs. Firstly, that the ectodomain of ALCAM was required to potentiate NGF-induced neurite outgrowth, and secondly, that the cytoplasmic domain did not contribute to this effect. Importantly, this also illustrated that the observed potentiation of neurite outgrowth was not a general response to the overexpression of a cell surface plasma membrane protein.

These results are particularly interesting considering the proposed segregation of function within the extracellular domains of ALCAM discussed in the Introduction, section 1.5 and (van Kempen et al., 2001). Swart and colleagues have previously shown that ALCAM has two functional modules; domains V_1V_2 are responsible for binding in *trans* while domains $C_1C_2C_3$ are responsible for binding in *cis*-interactions. Manipulations of these two modules can have cooperating and opposing effects. Expression of a ΔN-ALCAM (equivalent to my ΔD1D2 construct) was found to interfere with homophilic cell adhesion by altering ALCAM avidity. Furthermore, it was found that cells expressing this dominant negative form of ALCAM showed increased ability to metastasise while displaying decreased metalloprotease activity (van Kempen et al., 2004). Cells treated with a soluble form of ALCAM, comprising of the V_1 domain alone,

also showed inhibition of metalloprotease activity but showed decrease in migration and metastasis (van Kilsdonk et al., 2008). It is suggested that metalloprotease activation relies on an intact ALCAM network, which is inhibited by both ΔN-ALCAM and soluble ALCAM. However, the difference in migration and metastasis is thought to occur because ΔN-ALCAM expression causes upregulation of L1-CAM, while soluble ALCAM does the opposite (van Kilsdonk et al., 2008). The mechanism behind the differential effects on L1-CAM expression is not yet understood. These studies demonstrate that manipulations of ALCAM binding and analysis of the effects caused by the overexpression of ALCAM truncation forms are complex to interpret.

ALCAM can be expressed on the sending and receiving cell, and can function bidirectionally, both in *cis* and in *trans*. In my experiments disruption of clustering, requiring both *trans* and *cis* interactions, abrogates the potentiation of neurite outgrowth seen on overexpression of full-length ALCAM.

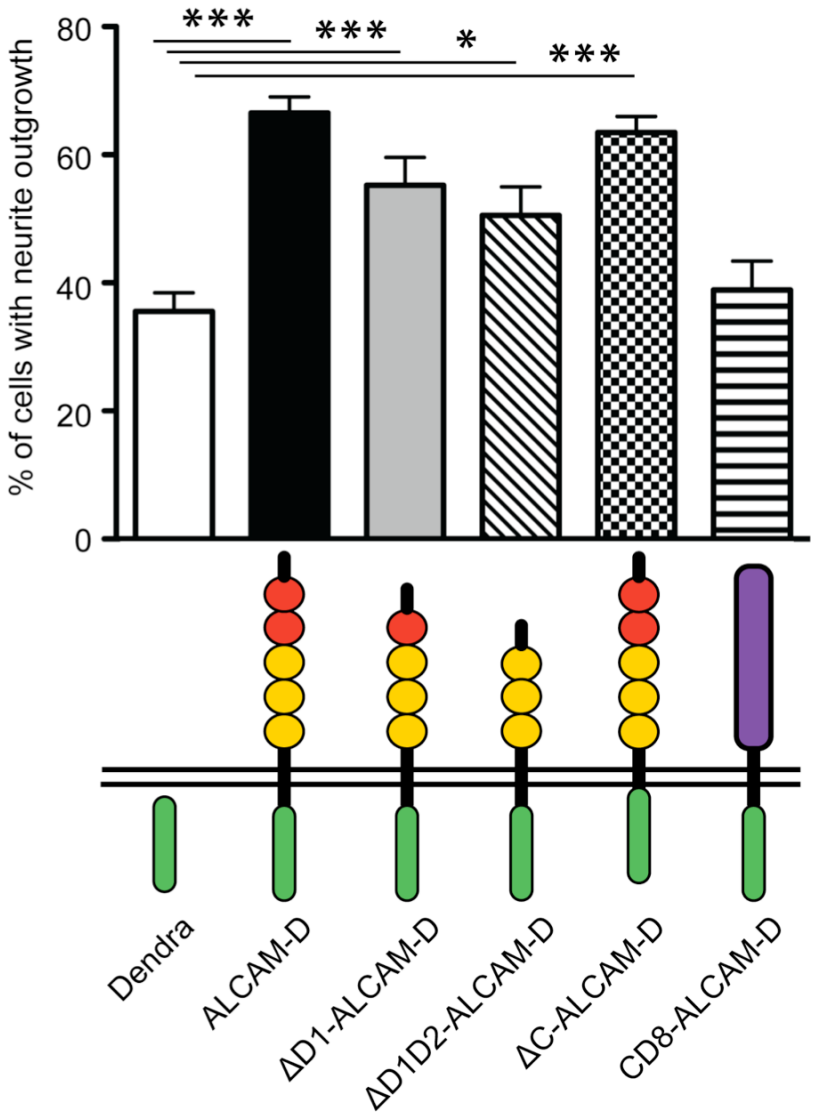

Figure 5.8 Potentiation of NGF-induced differentiation of PC12 cells requires the extracellular domains of ALCAM

Quantification of PC12 cells with neurites at least two times the length of the soma (% of cells with neurite outgrowth) transfected with a variety of ALCAM mutants and differentiated with 100 ng/ml NGF for 3 days. Truncations ΔD1-ALCAM-D and ΔD1D2-ALCAM-D inhibited the potentiating effect of ALCAM on neurite outgrowth, however both constructs were still capable of potentiating NGF-induced differentiation above control levels. ΔC-ALCAM-D, lacking the cytoplasmic domain, was capable of potentiating neurite outgrowth equivalently to expressing full length ALCAM-D. CD8-ALCAM-D, that lacked the entire ALCAM extracellular domain did not potentiate neurite outgrowth above control Dendra transfected cells. Data analysed using 1 way ANOVA with Bonferroni's Multiple Comparison Test; * $p<0.05$ *** $p<0.001$ (n = 3 to 8 experiments, error bars = SEM).

5.2.2 The ALCAM extracellular domain is sufficient to potentiate neurite outgrowth in PC12 cells

To complement the truncation studies I next tested whether addition of the soluble ALCAM ectodomain could potentiate the NGF-induced differentiation in PC12 cells. ALCAM-Fc was added to the NGF-differentiation medium at either 1 µg/ml or 10 µg/ml. As a control, the chimeric protein human immunoglobulin IgG1 (Hu-Fc) was added to differentiation medium at the same concentrations tested. Neurite outgrowth of Dendra expressing PC12 cells was measured 3 days after transfection.

Addition of soluble ALCAM-Fc at 1 µg/ml was found to significantly potentiate neurite outgrowth in response to NGF (Figure 5.9). This complements my previous findings (Figure 5.8), suggesting that the extracellular domain was necessary to potentiate neurite outgrowth in response to NGF. Furthermore, this is consistent with PC12 cells expressing endogenous ALCAM with which the ALCAM-Fc can bind. However, I cannot exclude that ALCAM-Fc may also bind another unidentified, heterophilic binding partner on the surface of PC12 cells, through which it could modulate neurotrophin signalling.

It is noted that ALCAM-Fc at 10 µg/ml did not significantly potentiate neurite outgrowth in response to NGF above control levels. However, this can be attributed to an anomalous increase in neurite outgrowth seen in the presence of 10 µg/ml Human-Fc. The explanation for this was not investigated further, however upon addition of 10 µg/ml of soluble protein (ALCAM-Fc or Human-Fc) cell adhesion was compromised and cells were often lost during staining and mounting. This could explain why potentiation of neurite outgrowth at this concentration did not reach significance.

I went on to test whether addition of the heterophilic ALCAM ligand, CD6, would have the same effect as addition of soluble ALCAM-Fc. In axonal transport experiments (Chapter 3; Figure 3.16 and Figure 3.17), addition of CD6-Fc showed a tendency towards increasing the retrograde transport frequency of ALCAM-positive carriers but did not alter their average speed. I tested whether addition of 1 µg/ml CD6-Fc or Hu-Fc would alter NGF-induced neurite outgrowth in PC12 cells transfected with ALCAM-D or Dendra. Quantification of neurite outgrowth found no evidence to suggest that the soluble CD6-Fc could potentiate neurite outgrowth in response to NGF in either Dendra or ALCAM-D expressing cells three days after transfection (Figure 5.10). Interestingly, this suggests that though CD6 can increase internalisation in cancer cell lines and shows a tendency towards modulating ALCAM transport frequency, the same stimulus has no effect on neurite outgrowth.

Remarkably, the different effects of CD6-Fc and ALCAM-Fc illustrate that even though both ligands bind the variable immunoglobulin domains in *trans*, they have different physiological properties. Importantly, ALCAM-Fc should also be capable of binding endogenous ALCAM in *cis* and therefore would more closely replicate the overexpression of the full-length protein (for schematic representation of binding configurations of soluble ALCAM refer to Chapter 3, Figure 3.18). My findings therefore suggest that the ability of ALCAM to potentiate neurotrophin signalling requires binding in *cis*.

Lastly, it is noted that overall decreased levels of neurite outgrowth were observed following addition of soluble proteins to the differentiation medium (Figure 5.10). In these experiments neurite outgrowth was displayed in around 40% of cells compared to 60% observed in the original experiments involving transfection of full-length protein (compare Figure 5.5 and Figure 5.8 to Figure 5.9 and Figure 5.10). This suggests that

addition of soluble proteins to the medium, especially at higher concentrations, may interfere with adhesion and differentiation.

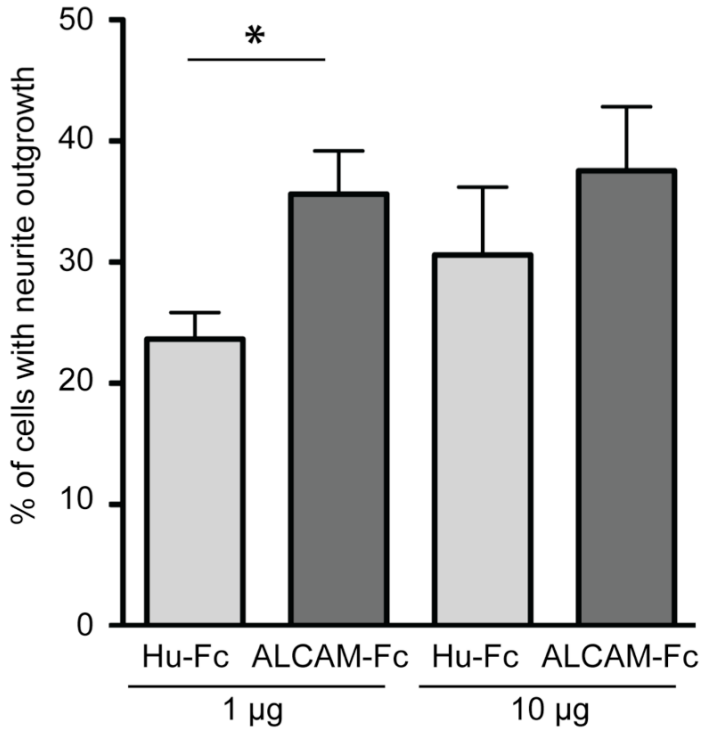

Figure 5.9 Addition of soluble ALCAM potentiates NGF-induced neurite outgrowth in PC12 cells

The histogram shows quantification of the percentage of cells whose longest neurite was two times or greater than the length of the soma (% of cells with neurite outgrowth) three days after transfection in response to 100 ng/ml NGF in the presence of soluble ALCAM-Fc or human-Fc (Hu-Fc). Neurite outgrowth was quantified in Dendra-transfected cells. A significant difference was found between the percentages of cells displaying neurite outgrowth after exposure to 1 µg ALCAM-Fc when compared to 1 µg Hu-Fc (P=0.0285). There is no significant difference between ALCAM-Fc and Hu-Fc at the higher concentration used (10 µg). Data analysed using unpaired t-test; * $p < 0.05$ (n = 4 experiments, error bars = SEM).

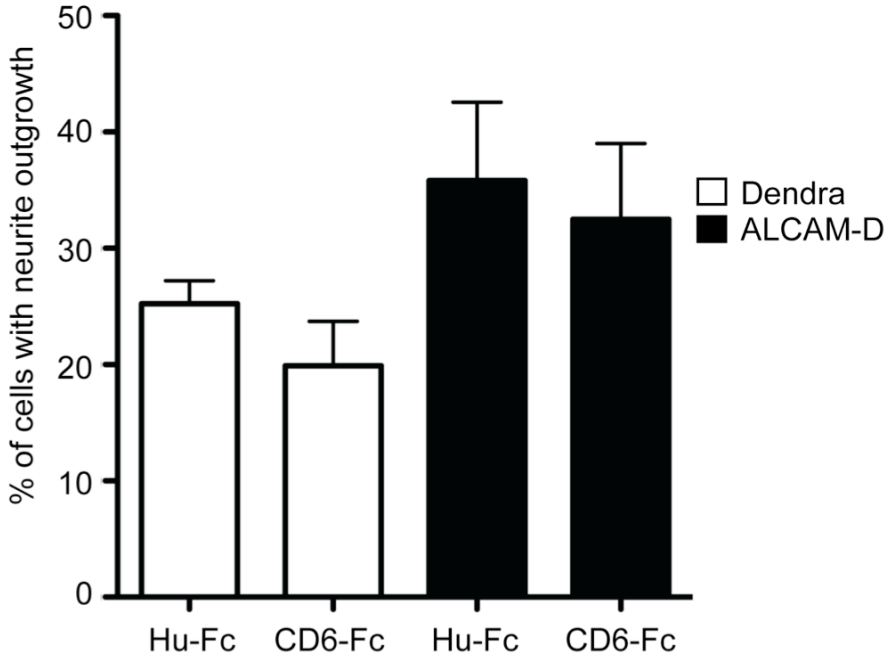

Figure 5.10 Addition of the soluble ALCAM ligand CD6 does not potentiate neurite outgrowth in PC12 cells

The histogram shows the percentage of cells that displayed neurite outgrowth (those that had neurites at least two times the length of the soma) in response to NGF in the presence of 1 µg/ml human-Fc (Hu-Fc) or soluble CD6-Fc three days after transfection. There is no significant potentiation of neurite outgrowth in the presence of CD6-Fc in either Dendra or ALCAM-D transfected cells. Data analysed using unpaired t-test analysis (n = 3 experiments, error bars = SEM).

5.3 ALCAM overexpression potentiates specific differentiation stimuli in PC12 cells

I next examined whether ALCAM overexpression was having a general potentiative effect on neurite outgrowth or whether it was specific to the differentiation stimulus. I compared neurite outgrowth in PC12 cells expressing Dendra or ALCAM-D in various differentiation conditions. Cells were analysed in the presence of NGF as a positive control and after serum withdrawal but in the absence of a specific differentiation stimulus. PC12 cell neurite outgrowth was investigated in response to glial cell line-derived neurotrophic factor (GDNF), a growth factor that is not in the neurotrophin family, and to dibutyryl cAMP (dbcAMP), a cyclic AMP analogue known to induce neurite differentiation in a variety of cell lines (Ng et al., 2009). Figure 5.11 shows transfected PC12 cells in each of these conditions.

Quantification of neurite outgrowth in ALCAM-D and Dendra-expressing PC12 cells in various conditions found that ALCAM overexpression only significantly potentiated NGF-induced differentiation (Figure 5.12). In the absence of differentiation stimuli, ALCAM-D expression had no effect on neurite outgrowth, suggesting that ALCAM does not initiate differentiation per se, but can either potentiate the stimulus itself or the process of neurite extension once it has been initiated. Interestingly, ALCAM did not potentiate neurite outgrowth in PC12 cells in response to dbcAMP at either concentration tested. This demonstrates that ALCAM potentiation of neurite outgrowth is not a general effect on differentiation but is specific to the stimulus. Analogues of cAMP act intracellularly where they mimic an increased concentration of the secondary messenger cAMP and therefore act downstream of membrane signalling. Along with the previous experiments using truncation mutants, this finding suggests that ALCAM potentiation of neurite outgrowth may occur at the level of the plasma membrane. In

this experiment the dbcAMP treatment essentially bypassed the requirement of extracellular receptor activation, by directly activating the signalling cascade required for neurite outgrowth, downstream of ALCAM.

Interestingly, there is a trend to suggest that ALCAM-D transfection could potentiate neurite outgrowth in response to GDNF, although the difference between ALCAM-D and Dendra-transfected PC12 cells is not significant. This could suggest that the mechanism by which ALCAM potentiates growth factor signalling is more influential in the NGF than GDNF signalling pathways. Alternatively, it could be merely a methodological issue. GDNF is a weak inducer of neurite outgrowth in comparison to NGF (around 20% or 50% of cells respectively). Perhaps with more experiments the smaller percentage difference may become significant.

PC12 cells do not express the GDNF co-receptor, GFRα, that cooperates with RET and/or NCAM in activating differentiation signalling (see Introduction, section 1.4, and (Paratcha et al., 2003)). To induce neurite outgrowth in these experiments it is necessary to add a soluble form of GFRα to the GDNF differentiation medium. I therefore also tested whether ALCAM-D could replace the requirement for soluble GFRα in these experiments. However no neurite outgrowth was observed in response to GDNF without GFRα but in the presence of ALCAM-D (data not shown). This suggests that ALCAM does not interact with RET or NCAM directly in a similar way to the co-receptor GFRα.

In summary, these experiments analysing PC12 neurite outgrowth suggest that ALCAM potentiates neurotrophin signalling and that this requires the ALCAM extracellular domain. Furthermore, ALCAM itself appears not to directly activate downstream signalling cascades, but acts as a modifier, altering specific differentiation signals at the membrane.

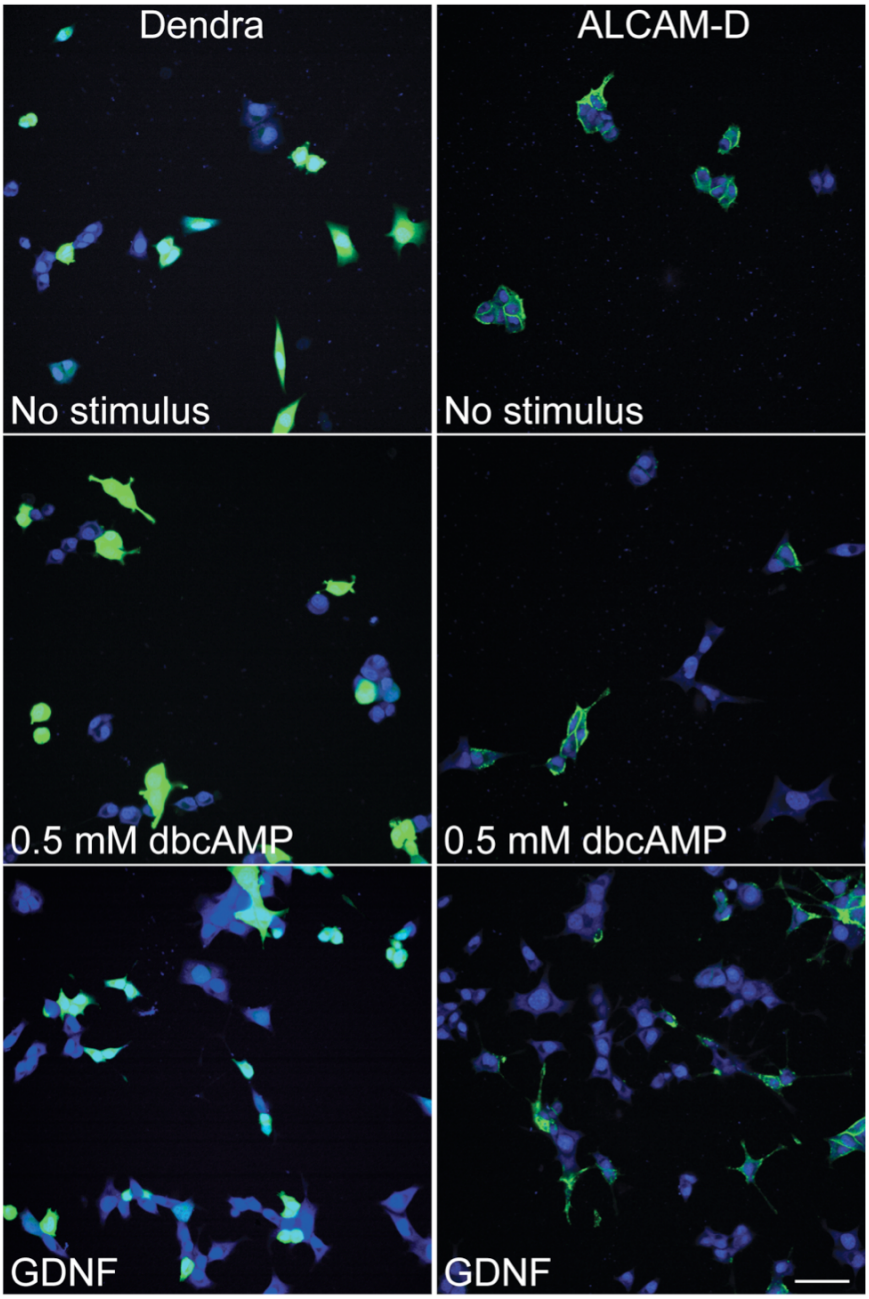

Figure 5.11 Analysis of neurite outgrowth in response to a variety of differentiation signals in PC12 cells expressing Dendra or ALCAM-D

PC12 cells transfected with Dendra or ALCAM-D are shown in the different treatment conditions. In the absence of differentiation stimuli (no stimulus), very few neuritic protrusions are seen. On dbcAMP and GDNF treatment some transfected cells have neuritic extensions, however the differentiation is less extensive than following NGF treatment (compare to Figure 5.7). Nuclei are stained with DRAQ5 in blue. Scale bar, 40 µm.

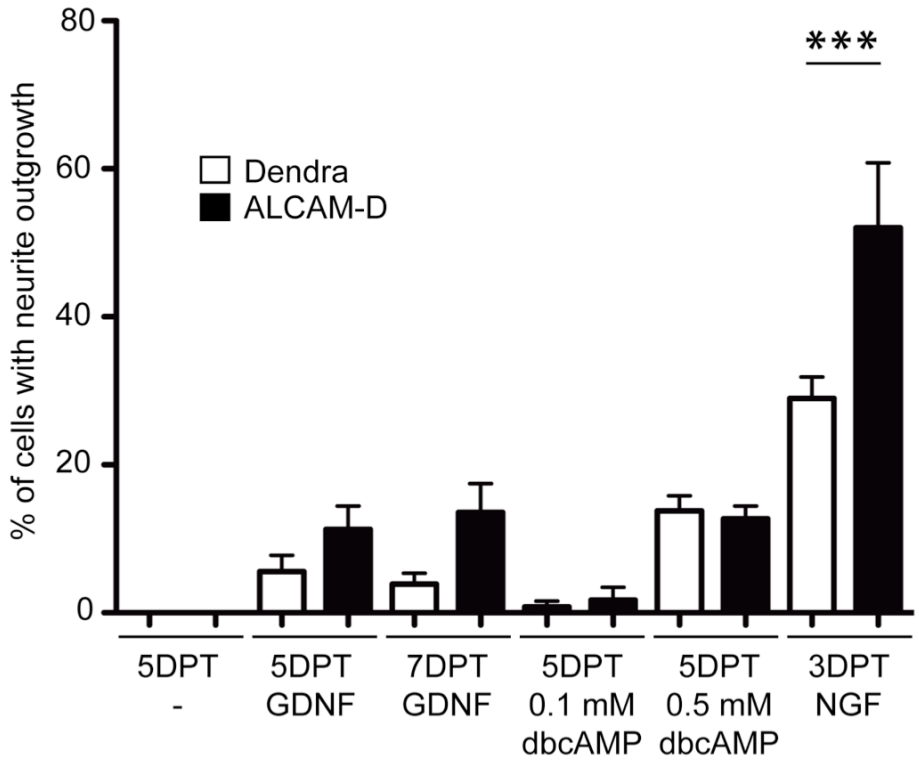

Figure 5.12 ALCAM-D potentiates specific PC12 differentiation stimuli

The histogram summarises the quantification of neurite outgrowth (cells with neurites two times or greater in length than the soma) in experiments investigating the PC12 cell response to the presence or absence of specific differentiation stimuli. ALCAM-D did not induce neuronal differentiation in the absence of differentiation stimuli (-). ALCAM-D did not potentiate differentiation induced by exposure to dbcAMP 5 days after transfection (5DPT) at either 0.1 mM or 0.5 mM. PC12 cells transfected with ALCAM-D differentiated with GDNF showed a tendency for increased neurite outgrowth at both time points tested (5DPT or 7DPT), but this was not statistically significant. ALCAM-D transfection significantly potentiated neurite outgrowth in response to NGF 3 days after transfection (3DPT). Data analysed using 1 way ANOVA with Bonferroni's Multiple Comparison Test; $p<0.001$ (n = 4 experiments, error bars = SEM).

5.4 ALCAM overexpression potentiates TrkA phosphorylation in response to NGF

I then went on to assess whether ALCAM-D overexpression directly alters the neurotrophin-signalling pathway in PC12 cells. Differentiated ALCAM-D or Dendra transfected PC12 cells were starved of serum and neurotrophins for 5 hours and then treated with NGF. Activation of the neurotrophin signalling pathway was assessed by western blotting for phosphorylated components of the NGF-signalling cascade. Cells were harvested in boiling high SDS buffer, to inactivate proteases and phosphatases. Samples were run on SDS-PAGE, transferred to PVDF membranes and analysed by western blot to compare the levels of specific phosphorylated proteins after NGF treatment. I analysed the levels of phosphorylation of the NGF receptor, TrkA, and the MAPK, ERK1/2 (Figure 5.13). The intensity of phosphorylated protein (TrkA or ERK1/2) was normalised to the total amount of protein per sample, and phosphorylation levels were normalised to activation 3 min after NGF treatment in Dendra cells (see Materials and Methods). The time course represented in Figure 5.14 shows that NGF increased phosphorylation of TrkA and ERK1/2 peaking at 3 minutes and 15 minutes respectively. ALCAM-D cells had increased TrkA and ERK1/2 phosphorylation at all timepoints, consistent with the downstream increase in neurite outgrowth observed in PC12 cells.

However, upon Lipofectamine transfection, ALCAM-D or Dendra is only expressed in ~30-40% of PC12 cells and therefore we assumed that we would only be able to observe a small change in phosphorylation by western blot because of the contribution of non-transfected cells to the sample. Furthermore, the phosphorylation intensities obtained varied between experiments i.e. due to different cell preparations, as well as between the different time points after NGF exposure. This variability decreased the

power with which I could assess the small differences in phosphorylation by conventional statistical tests.

To take these issues into account we consulted with Dr Gavin Kelly, a statistician (LRI, Bioinformatics and Biostatistics Service). The raw intensity data values were transformed on a log scale (to reflect relative differences rather than absolute values), and a model that assumed the individual phosphorylation intensities had dependencies on experiment and timepoint after NGF treatment was fitted. This model was used to produce individual intensity values with the experiment and time-trend effect removed for TrkA and ERK1/2 phosphorylation and these values are shown on the box plot (Figure 5.15). This allowed us to pool individual phosphorylation values across all timepoints and all experiments, so that we could analyse whether there was an effect of transfection. ANOVA was used to determine whether the difference between the Dendra and ALCAM-D predicted phosphorylation intensity values was larger than that ascribbable to noise. The difference between TrkA predicted phosphorylation intensities is significantly different between Dendra and ALCAM-D conditions ($p=0.00038$), but is not significant for ERK1/2 ($p=0.19$). The ANOVA also indicates that phosphorylation was significantly different between experiments and between timepoints after NGF stimulation ($p<1^{e-6}$).

In summary, my results show that ALCAM-D significantly increased TrkA phosphorylation intensity. I also found a significant effect on phosphorylation with time after NGF stimulation, as well as between experiments. The ERK1/2 phosphorylation observed was much more variable than TrkA phosphorylation. ERK1/2 is downstream of many stimuli (e.g. cell stress), which are more problematic to control between experiments. This variation limited our ability to resolve an effect of ALCAM-D on ERK1/2 phosphorylation (reviewed further in the Discussion, section 6.3.1).

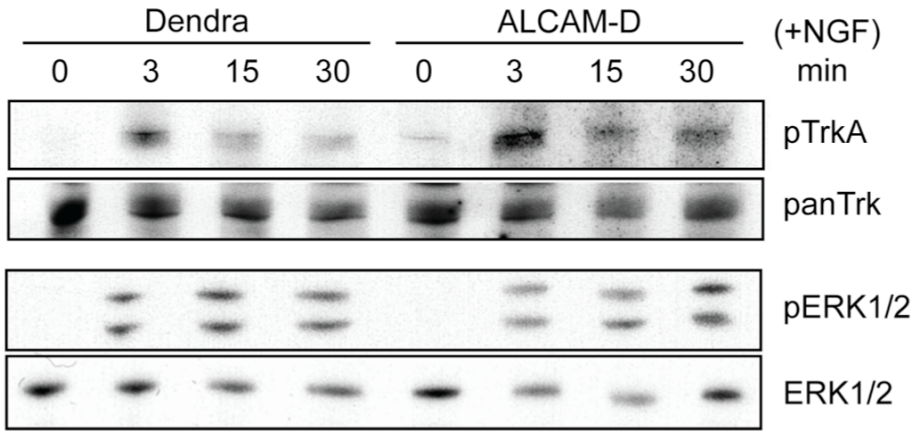

Figure 5.13 TrkA and ERK1/2 phosphorylation in PC12 cells stimulated with NGF

A typical western blot showing phosphorylated TrkA and ERK1/2 at 0, 3, 5 and 30 minutes after addition of 100 ng/ml NGF. ALCAM-D expressing PC12 cells show higher TrkA phosphorylation than Dendra-expressing cells in response to NGF. ERK1/2 is also phosphorylated after addition of NGF.

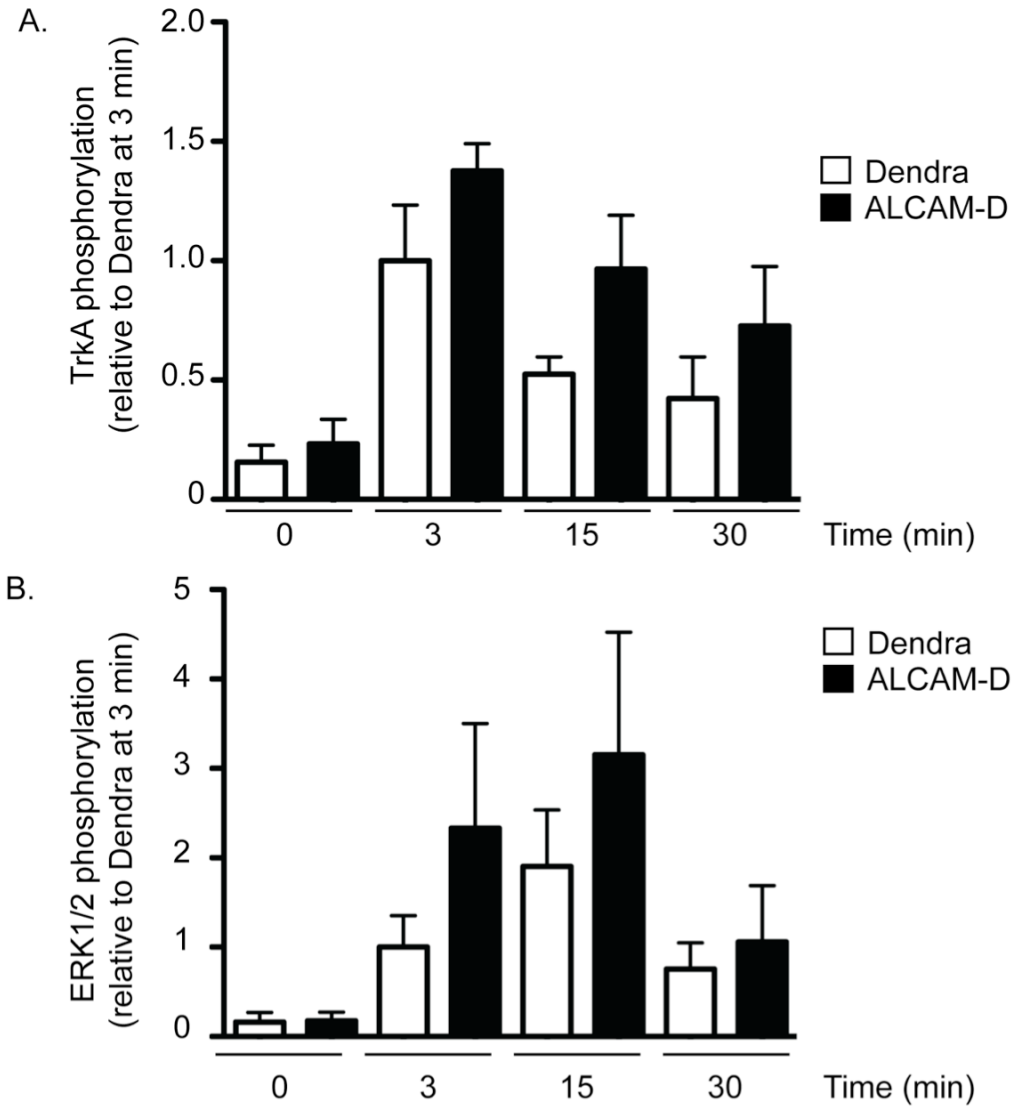

Figure 5.14 ALCAM-D expressing PC12 cells showed increased TrkA and ERK1/2 phosphorylation in response to NGF

The histograms represent protein phosphorylation levels for TrkA and ERK1/2 (n=4 experiments). For each experiment, phosphorylated levels were adjusted to the total TrkA or ERK1/2 per sample. Phosphorylation was then normalised to the average phosphorylation intensity of Dendra cells 3 minutes after NGF exposure across all experiments analysed. ALCAM-D expression shows a tendency towards potentiation of TrkA and ERK1/2 phosphorylation at all time points after exposure to NGF. Using 1 way ANOVA TrkA phosphorylation is significantly different ($p = <0.0004$) but not between transfection conditions using Bonferroni's Multiple Comparison Test (n = 4 experiments).

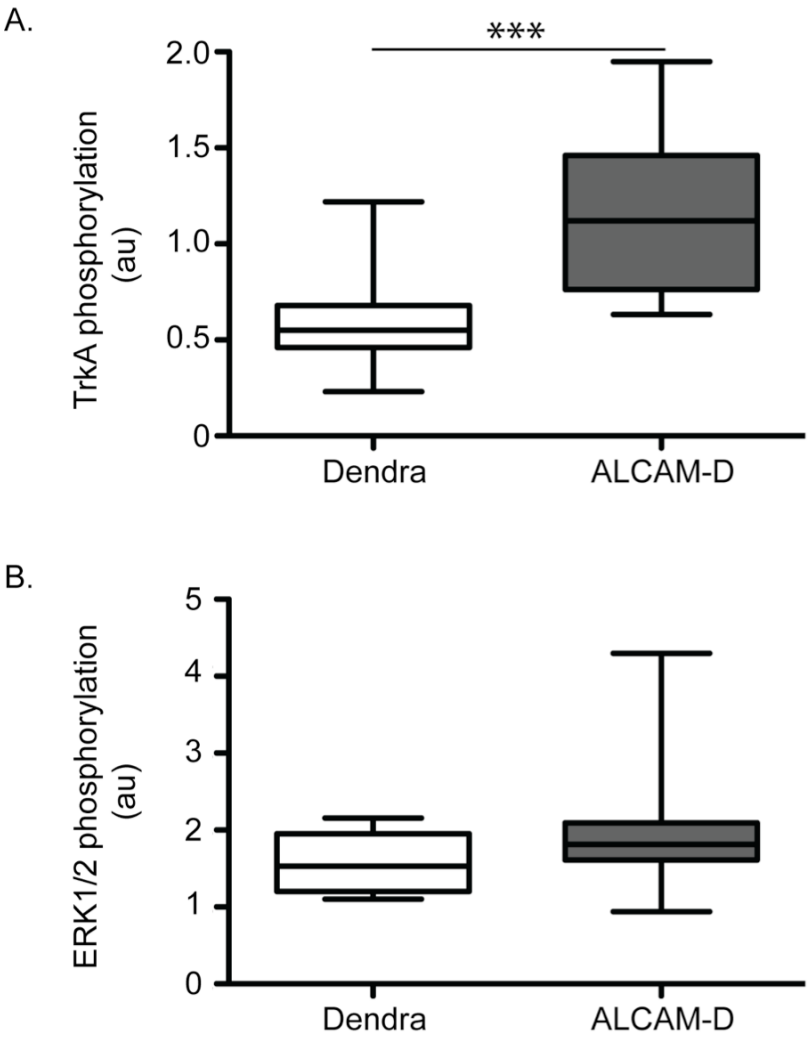

Figure 5.15 ALCAM-D significantly increased TrkA phosphorylation

Box and whisker plots of TrkA and ERK1/2 phosphorylation (au - arbitrary units) after adjustment to remove variability attributed to different experiments and timepoints after NGF stimulation. A significant increase in TrkA phosphorylation in ALCAM-D transfected cells is shown in comparison to Dendra transfected cells (A) (*** $p<0.001$). In contrast, no significant difference in ERK1/2 phosphorylation intensity in Dendra and ALCAM-D transfected cells is observed (B). Data was analysed with the help of Dr Gavin Kelly, using ANOVA to compare the predicted phosphorylation values in Dendra versus ALCAM-D transfected conditions for TrkA and Erk1/2 across all experiments and timepoints (n = 4 experiments).

5.4.1 ALCAM-D does not directly interact with TrkA

ALCAM overexpression could alter NGF signalling through interactions with the NGF receptor TrkA. To test whether ALCAM directly interacted with the neurotrophin receptor I tried to co-immunoprecipitate the two proteins in various conditions, using endogenous protein in primary ventral horn cultures, and transfected ALCAM-D in PC12 cells after differentiation. As explained in Chapter 4, section 4.5, the immunoprecipitation of endogenous ALCAM was inefficient in the conditions tested. However, I identified conditions in which immunoprecipitation of overexpressed ALCAM-D was possible.

I did not find any evidence of an interaction between ALCAM and TrkA when either protein was immunoprecipitated. As can be seen in Figure 5.16, ALCAM-D immunoprecipitated by the Dendra antibody was not associated with TrkA. Furthermore, immunoprecipitation of endogenous TrkA revealed no evidence of association with endogenous or overexpressed ALCAM in PC12 cells. This would suggest that the way in which ALCAM overexpression modulates TrkA-NGF signalling is not due to direct transactivation of TrkA.

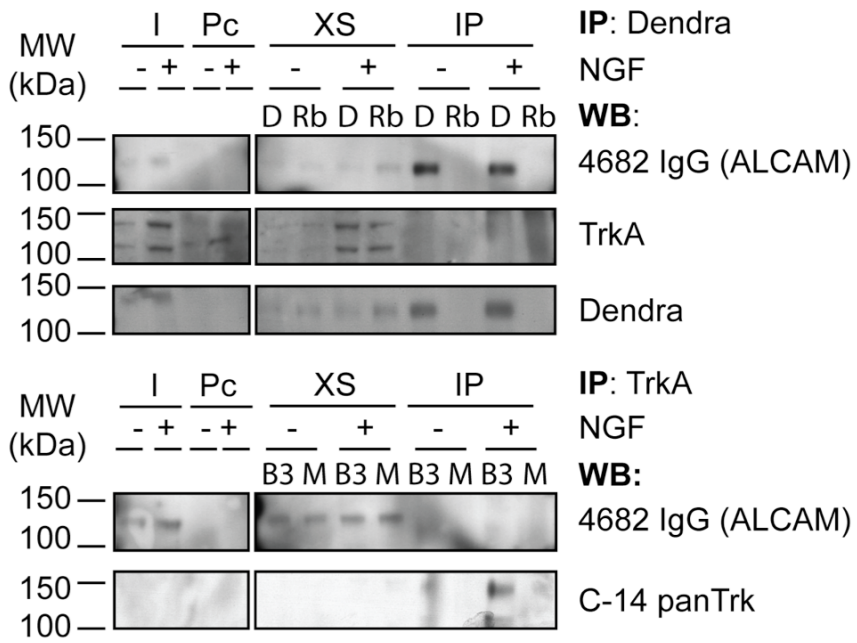

Figure 5.16 ALCAM and TrkA do not directly interact

PC12 cells transfected with ALCAM-D, undifferentiated or differentiated with NGF (NGF – or + respectively) were used in an immunoprecipitation experiment. Cell lysates (I) were pre-cleared with beads alone (Pc), then immunoprecipitated with antibodies directed against ALCAM-D (IP Dendra) or to TrkA (IP TrkA). Samples of cell lysates (I) and exhausted supernatant (XS) after removal of IP beads are also shown. In IP Dendra samples ALCAM-D was immunoprecipitated with the anti-Dendra antibody (D) but not the control Rabbit IgG (Rb), and is recognised by western blotting (WB) with 4682 IgG antibody for ALCAM or Dendra. However there is no evidence for association of TrkA with the ALCAM-D immunoprecipitate (IP). In IP TrkA, it can be seen that TrkA was successfully immunoprecipitated by a monoclonal antibody (B3) but not by an unrelated monoclonal (M). It can be seen that more TrkA was pulled down in the differentiated (+ NGF) condition. However there is no evidence of ALCAM-D also being pulled down with TrkA when the membrane was probed with 4682 IgG directed to ALCAM.

5.4.2 ALCAM-D modulates the association of p75^{NTR} to detergent resistant membranes

A possible way in which ALCAM could indirectly alter NGF receptor signalling would be by altering the association of neurotrophin receptors to detergent-resistant membranes (DRMs), also known as lipid rafts. TrkA and p75^{NTR} have been shown to localise to lipid rafts, and this relates to their signalling function (Limpert et al., 2007, Gil et al., 2007). For example, it has been found that on laminin binding to ganglioside GM1, TrkA residence in DRMs is altered, leading to potentiation of TrkA signalling and neurite outgrowth (Ichikawa et al., 2009). Furthermore, the cell adhesion molecule NCAM has different signalling partners and subsequent downstream signalling, depending on whether it is present in DRMs or detergent-soluble membranes (reviewed in Maness and Schachner, 2007). To determine whether ALCAM could affect neurotrophin receptor localisation I isolated DRMs from PC12 cells transfected with ALCAM-D or Dendra differentiated with NGF for 3 days.

Detergent resistant membranes were isolated and analysed by western blot for markers of lipid rafts, neurotrophin receptors and ALCAM (Figure 5.17). Lipid rafts were successfully isolated from both ALCAM-D and Dendra-expressing cells, shown by fractions 2-5 containing Thy-1.1, a GPI-anchored protein which accumulates in DRMs (Madore et al., 1999). ALCAM-D was present in the non-raft associated membrane fractions. Over several experiments, we saw no major alteration in Thy-1.1 DRM distribution between PC12 cells expressing ALCAM-D or Dendra. Furthermore, there was no difference in the distribution of full length TrkA in cells that overexpressed ALCAM-D or Dendra. This suggests that the increase in TrkA phosphorylation (seen in Figure 5.13 and Figure 5.14) was not due to an alteration in the amount of TrkA associated with DRMs.

However, the distribution of the other PC12 neurotrophin receptor $p75^{NTR}$ was shifted toward those DRM fractions containing Thy1.1 in ALCAM-D cells. The alteration in the membrane localisation of $p75^{NTR}$ could affect its downstream signalling. Interestingly, a second band was observed around 25 kDa in the $p75^{NTR}$ western blot, although its membrane association is not altered between ALCAM-D and Dendra-transfected conditions. The lower band was not recognised by an antibody to the $p75^{NTR}$ extracellular domain consistent with the idea that it could be the $p75^{NTR}$ C-terminal fragment (data not shown). It is also noted that an unknown band migrating at 50 kDa recognised by TrkA antibodies, (both α phosphoTrk and α panTrk), and which changes its distribution between ALCAM-D and Dendra expressing cells. A possible explanation for the 50 kDa band, is that it represents the truncated C-terminal domain of the TrkA receptor which has been shown to be constitutively active (Diaz-Rodriguez et al., 1999). Perhaps ALCAM overexpression alters the activity of the proteases responsible for neurotrophin receptor cleavage. A recent paper found that $p75^{NTR}$ processing by γ-secretase generates an intracellular fragment capable of potentiating TrkA signalling in PC12 cells (Ceni et al., 2010). In turn, if there were alterations in processing it could explain how ALCAM overexpression influences TrkA signalling indirectly (see Discussion, section 6.3.2).

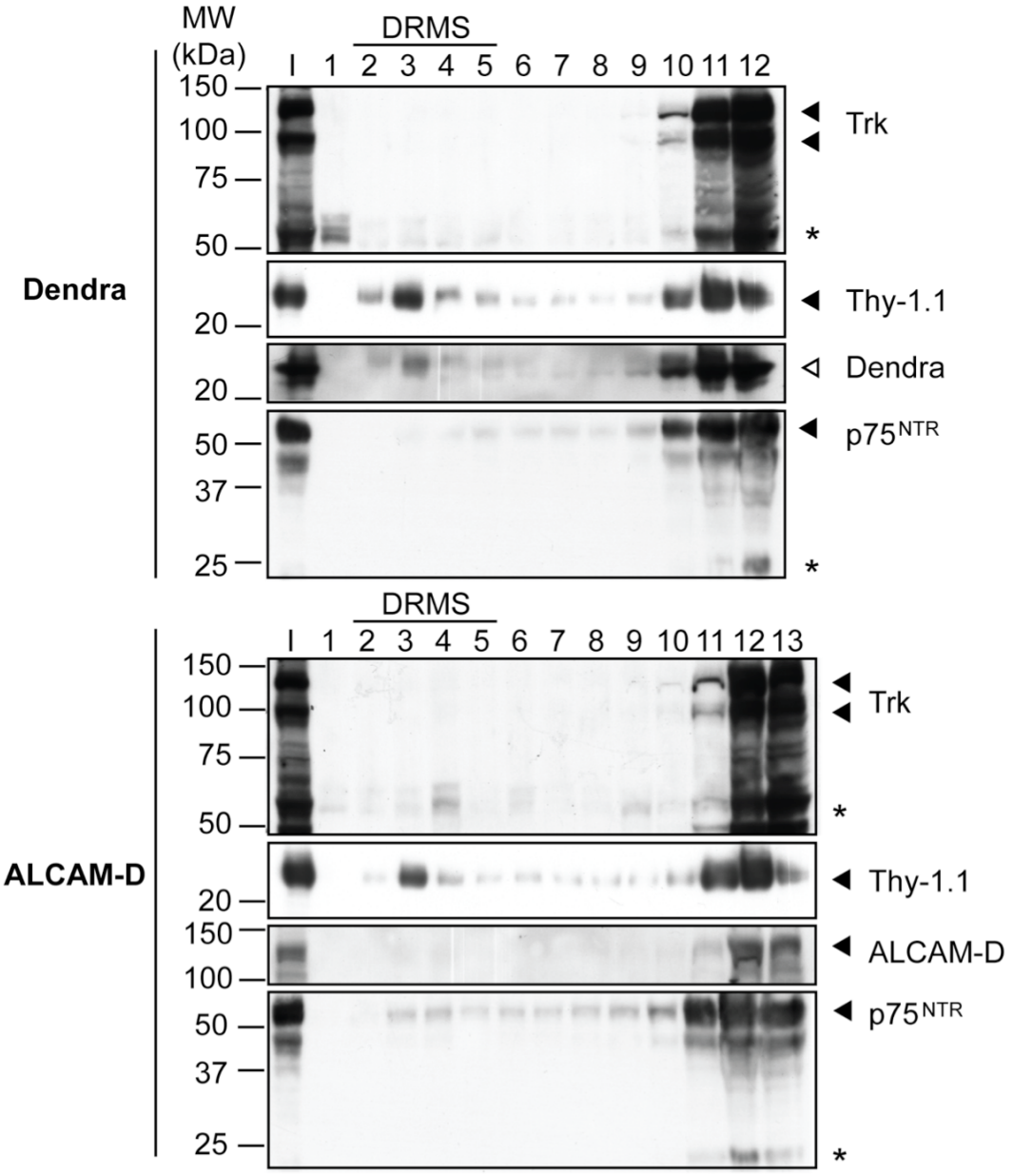

Figure 5.17 DRMs are not altered in ALCAM-D expression

PC12 Dendra and PC12 ALCAM-D cell lysates (I) and detergent-resistant membrane (DRM) fractions were separated (1-12/13) and analysed by western blot. Thy1.1 is present in DRMs and is not altered between Dendra and ALCAM-D transfected cells. Both Dendra at 26 KDa and ALCAM-D at 130 kDa are detected in soluble membrane fractions (10-12/13). TrkA is detected in soluble membrane fractions in both Dendra and ALCAM-D expressing cells. The distribution of $p75^{NTR}$ is shifted toward DRMs in ALCAM-D expressing cells. The asterisks highlight unknown bands detected by the Trk and $p75^{NTR}$ antibodies. Similar results were obtained in 2 experiments.

5.5 The role of ALCAM in nerve terminal sprouting *in vivo* at the mouse neuromuscular junction (NMJ)

Since overexpression of ALCAM potentiated NGF-induced neurite outgrowth in a neural cell line, we next examined the potential role of ALCAM in axonal outgrowth *in vivo*. To do this I investigated whether ALCAM$^{-/-}$ mice displayed decreased axonal outgrowth in response to an insult that normally induces sprouting of nerve terminals at the NMJ. As described in the Introduction section 1.5, ALCAM$^{-/-}$ animals have a mild neurological phenotype and it was hypothesised that upregulation of proteins with related functions compensated for the loss of ALCAM during development. In the adult nervous system axonal outgrowth occurs in response to injury, for example nerve transection (for example Moscoso et al., 1998). Since ALCAM is expressed in the immune system, we wanted to avoid using a procedure that caused inflammation because recovery could be affected by loss of ALCAM in immune cells e.g. macrophages, as well as in the neurons themselves. Nerve crush injury has been associated with macrophage invasion (Omura et al., 2005). However, muscle paralysis is known to be a potent inducer of nerve terminal sprouting (Angaut-Petit et al., 1990) but has not been reported to involve an immune response.

In this study muscle paralysis was induced by intramuscular injection of botulinum toxin type A (BoNT/A). In response to muscle paralysis nerve terminals sprout from the axon terminal to neighbouring regions of the muscle in an attempt to functionally innervate the inactive muscle fibres (de Paiva et al., 1999). During the early phase of recovery, when nerve stimulation again elicits muscle contraction, it has been shown that areas where the nerve sprouts contact the muscle fibre are the only sites of synaptic vesicle turnover and are responsible for neurotransmission (de Paiva et al., 1999). The process of nerve terminal sprouting is then followed by their retraction and removal

once the original terminals reacquire full functionality and become capable of vesicle turnover.

I analysed the sprouting response to BoNT/A injection in the extensor digitorum longus (EDL) hindlimb muscle in adult wild type and ALCAM$^{-/-}$ littermates. Electrophysiological recordings performed by Jim Dick in the laboratory were used to determine if the BoNT/A treatment was effective in producing complete muscle paralysis. An *in vivo* assessment of isometric twitch and tetanic force was performed in an anaesthetised wild type mouse following BoNT/A treatment of the EDL hindlimb muscle, using the contralateral untreated limb as a control. As can be seen in Figure 5.18, seven days after BoNT/A treatment the EDL muscle was completely paralysed.

To examine the extent of nerve terminal sprouting, animals were sacrificed 3 weeks after BoNT/A treatment, the EDL muscles in the BoNT/A treated leg and the contralateral untreated leg were removed, fixed and sectioned. Then axons and neuromuscular junctions were visualised using a combined acetylcholinesterase silver staining protocol (modified from Namba et al., 1967). Terminal sprouts, extending from within the endplate region into surrounding muscle, and nodal sprouts, where axons branched immediately before entering the endplate, were quantified. Examples of terminal and nodal sprouts observed in response to BoNT/A treatment are shown in Figure 5.19. Quantification of endplate sprouting was conducted blind to the genotype on a light microscope.

The same analysis was also conducted on the levator auris longus (LAL) muscle, which has been used extensively in the study of the response to BoNT/A-induced paralysis (Angaut-Petit et al., 1987, Angaut-Petit et al., 1990). The LAL muscle does not require sectioning and was stained as a whole mount preparation using the same combined cholinesterase silver stain. We sacrificed the animals 3 weeks after injection

of 0.5 pg of BoNT/A subcutaneously into the head and sprouting was quantified by the same method as for the EDL.

I found that loss of ALCAM *in vivo* had no effect on the nerve terminal sprouting in response to BoNT/A observed after 3 weeks. There was no difference in the percentage of endplates with nerve terminal sprouts (terminal and/or nodal) in either EDL or LAL muscles (Figure 5.20). The number of sprouts in untreated EDL and LAL muscles was also comparable between wild type and ALCAM$^{-/-}$ mice. Furthermore, as illustrated by the frequency distribution of the number of sprouts quantified, the ability of motor axons to extend more than one sprout from an endplate did not differ between wild type or ALCAM$^{-/-}$ littermates (Figure 5.21). In summary, no difference in nerve terminal sprouting at the NMJ was detected in ALCAM$^{-/-}$ animals either in normal conditions or in response to BoNT/A induced paralysis. The ALCAM$^{-/-}$ animals may have compensatory mechanisms similar to those proposed to exist during development that allowed the animals to respond normally to BoNT/A induced muscle paralysis. Alternatively these *in vivo* results may suggest that the increased neurite outgrowth seen in vitro in PC12 cells are due to ALCAM overexpression, rather than reflecting a function of the endogenous protein. Knockdown of ALCAM in PC12 cells is necessary to determine whether endogenous ALCAM has a role in neurite outgrowth in PC12 cells. I will discuss these issues further in the Discussion, section 6.3.3.

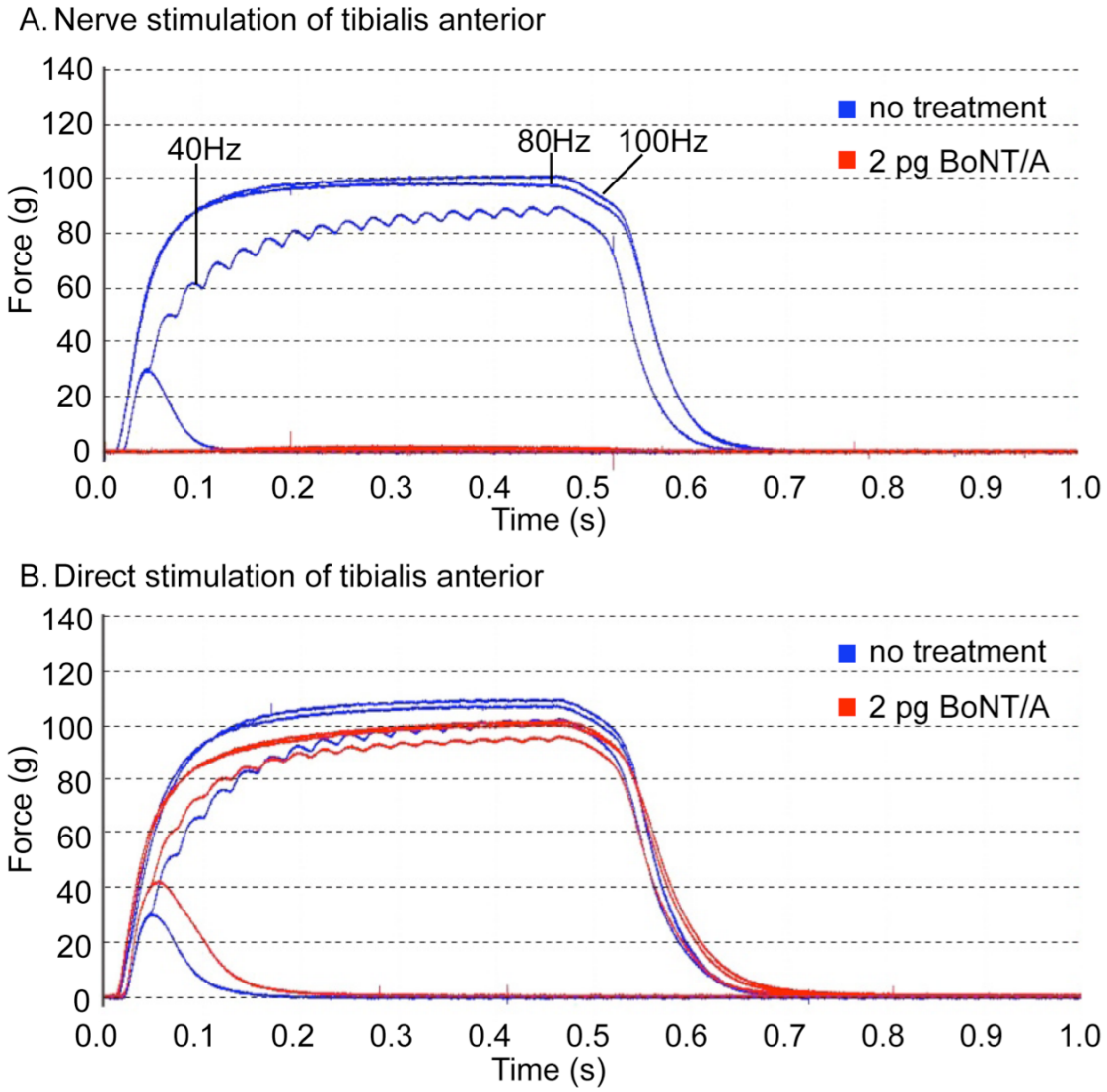

Figure 5.18 BoNT/A caused complete paralysis one week after injection

Injection of 2 pg of BoNT/A into the mouse hindlimb caused complete paralysis in EDL muscles as illustrated by electrophysiological recording. Four stimuli were used; a single 10 volt stimulation for 0.05 s (twitch tension), or successive stimulations at 40 Hz, 80 Hz and 100 Hz (tetanic stimulation). Indirect stimulation via the nerve is shown in A while direct stimulation of the muscle directly is shown in B. The injected muscle (red trace) does not contract in response to nerve stimulation, however the untreated leg (blue trace) showed both a twitch response to the single stimulation (single peak trace) and sustained contraction on tetanic stimulation at high frequency stimulations (broad trace). The lower panel shows that the muscle was still functional because it responds to direct electrical stimulation of the muscle. The experiment confirmed that the dose of the toxin used was sufficient to completely prevent signal transduction from nerve to muscle i.e. induce muscle paralysis 7 days after treatment. Performed by J Dick.

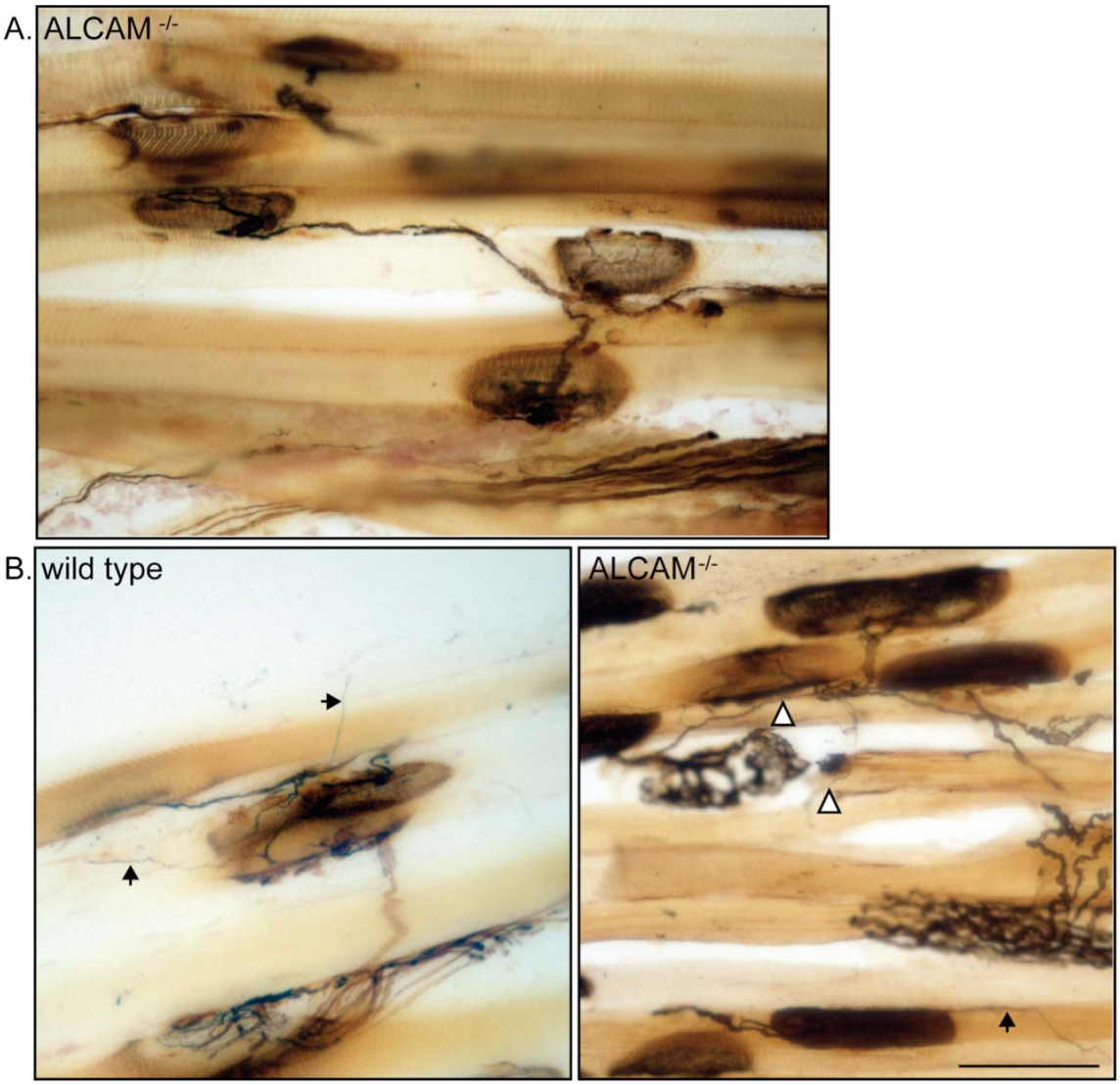

Figure 5.19 Nerve terminal sprouts were observed in EDL muscles 3 weeks after BoNT/A injection

Nerve terminals labelled by silver can be seen contacting endplates labelled by acetylcholinesterase. No nerve terminal sprouts are seen in an ALCAM$^{-/-}$ uninjected EDL muscle in image (A). Terminal sprouts were defined as a neurite branch that extended beyond the cholinesterase stained region after entering the endplate (black arrows) and are seen in wild type and ALCAM$^{-/-}$ muscles in (B). Nodal sprouts, defined as those that branched from the axon immediately before it reached the endplate, were also quantified (white arrowhead). Scale bar 50 μm.

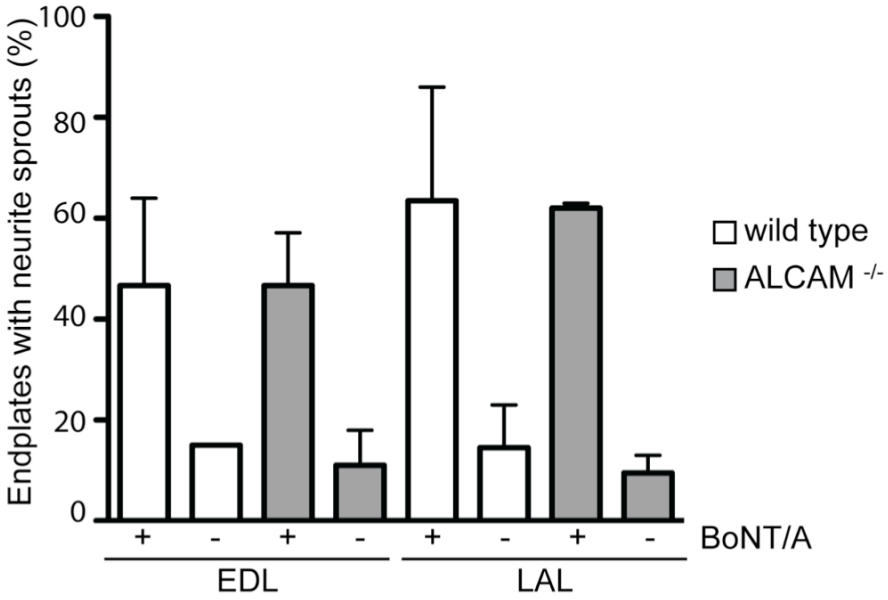

Figure 5.20 Loss of ALCAM did not alter sprouting in response to BoNT/A

The percentage of endplates that possessed terminal or nodal sprouts in BoNT/A treated (+ BoNT/A) and control muscles (- BoNT/A) were quantified in EDL and LAL muscles of wild type and ALCAM$^{-/-}$ mice and is represented as a histogram. In EDL muscles approximately 50% of endplates possessed sprouts in BoNT/A treated muscles in both wild type and ALCAM$^{-/-}$ animals, while only ~10% of endplates in untreated muscles had sprouts. In the LAL muscle a similar pattern was seen with no difference between wild type and ALCAM$^{-/-}$ animals. Both showed a sprouting response after BoNT/A treatment (For EDL muscles n = 3 litters, 3 wild type and ALCAM$^{-/-}$ BoNT/A treated muscles, 1 wild type and 2 ALCAM$^{-/-}$ untreated muscles; average of 47 endplates counted per muscle. For LAL muscle analysis n = 2 litters and 2 wild type and 2 ALCAM$^{-/-}$ muscles with and without BoNT/A treatment; average of 30 endplates counted per muscle). Data was analysed by 1 way ANOVA and the means are significantly different ($p = 0.0303$). There was a significant increase in sprouting in injected versus uninjected muscles but there was no difference between wild type and ALCAM$^{-/-}$ muscles (error bars = SEM).

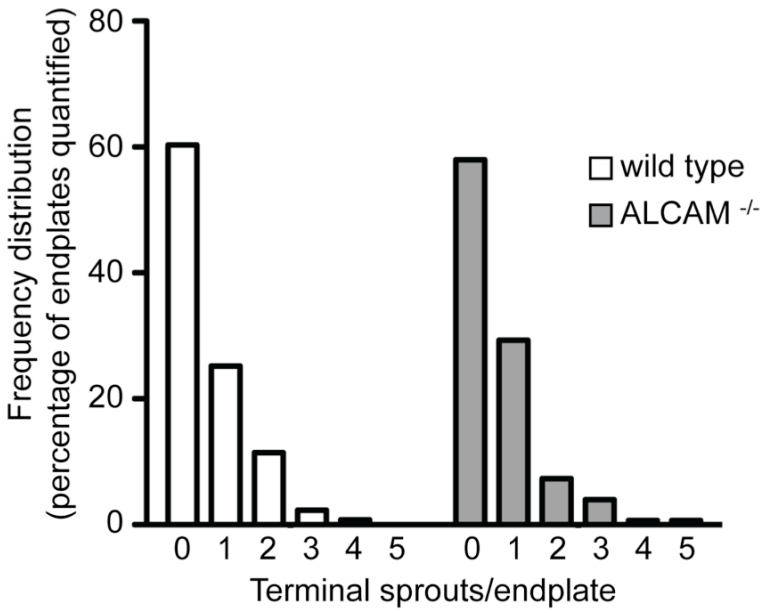

Figure 5.21 The frequency distribution of the number of sprouts per endplate is comparable in EDL muscles of ALCAM$^{-/-}$ and wild type littermates

The percentage of endplates with 0 to 5 sprouts is plotted for BoNT/A treated EDL muscles from wild type and ALCAM$^{-/-}$ animals. There is no apparent change in the frequency distribution of endplates with more than one sprout. (n = 3 animals per genotype; total of 131 neuromuscular junctions in wild type animals and 150 neuromuscular junctions in ALCAM$^{-/-}$ animals were quantified).

5.6 Summary

In this chapter, I have shown that ALCAM can potentiate neurite outgrowth in PC12 cells. Through the use of a soluble ALCAM extracellular domain and a variety of truncation mutants, I demonstrated that the ability of ALCAM to potentiate neurite outgrowth upon NGF-induced differentiation was dependent on its extracellular domain. The ALCAM cytoplasmic tail and transmembrane region was ineffective in inducing neurite outgrowth. Since PC12 cells express endogenous ALCAM, which could compensate for truncation of the cytoplasmic domain, it was not possible to determine whether the cytoplasmic domain was necessary to potentiate NGF-induced neurite outgrowth. Overexpression of the extracellular domain truncation mutants were capable of disrupting the extracellular ALCAM network, and ALCAM function, even in the presence of endogenous ALCAM. CD6-Fc binding in *trans* was incapable of potentiating neurite outgrowth and suggests that binding in *cis* is required for ALCAM to potentiate NGF stimulated differentiation. My findings suggest that ALCAM does not take part in direct signal transduction via its cytoplasmic domain upon ligand binding. Instead the difference observed between CD6-Fc and ALCAM-Fc suggests that the *cis* interaction and resulting increased avidity is required to potentiate neurite outgrowth.

ALCAM did not cause neurite outgrowth when overexpressed in the absence of other differentiation signals, suggesting that ALCAM is a modifier rather an initiator of the process. Interestingly, ALCAM did not potentiate all differentiation stimuli, it did not potentiate outgrowth in response to the downstream messenger dbcAMP and this again suggests that ALCAM does not directly activate downstream signalling cascades that could cooperate with other downstream stimuli. My results indicate that ALCAM potentiates specific membrane initiated differentiation signals. I found that ALCAM also

alters GDNF induced differentiation suggesting it may not be TrkA specific and ALCAM potentiation may extend to other growth factor receptors.

I attempted to determine the mechanism by which ALCAM-D potentiated neurite outgrowth. There was a consistent increase in the phosphorylation of TrkA after ALCAM-D transfection. No direct interaction between TrkA and ALCAM was identified by immunoprecipitation experiments suggesting that it was not due to direct transactivation of the receptor. Following isolation of DRMs, it appeared that ALCAM-D did not localise to DRMs, and did not alter the overall distribution of Thy-1.1, or full-length TrkA. The distribution of $p75^{NTR}$ was however shifted toward DRMs, which could alter $p75^{NTR}$ function. Considering ALCAM has already been shown to be involved in regulation of metalloprotease activity in cancer cell lines (van Kilsdonk et al., 2008, Lunter et al., 2005), it would be interesting to investigate whether ALCAM overexpression alters metalloprotease activity in neural cells, especially considering that anomalous smaller TrkA and $p75^{NTR}$ forms were observed (discussed further in the Discussion, section 6.3.2).

There is no difference in neurite sprouting in response to BoNT/A-induced muscle paralysis in animals that did not express ALCAM. My results suggest that ALCAM does not play a role in nerve terminal sprouting in response to paralysis of LAL and EDL muscles *in vivo*. I propose that the ALCAM network at the plasma membrane can influence growth factor signalling at the level of the receptor-ligand interaction. Currently we have not determined whether this is a property of ALCAM expressed at endogenous levels or a PC12 specific mechanism. Possible explanations that warrant further investigation will be considered further in the Discussion.

Chapter 6. Discussion

6.1 ALCAM undergoes retrograde transport in ventral horn neurons.

6.1.1 Characterisation of the ALCAM retrograde transport endosome

The results presented in this thesis show that endogenous ALCAM on the surface of ventral horn neurons undergoes axonal retrograde transport and is transported in endosomes that also contain the atoxic fragment of the tetanus toxin (Hc). ALCAM is not associated with a distinct subset of Hc-positive endosomes but is co-transported with known retrograde cargoes entering this axonal compartment, such as the cell adhesion molecule CAR and the neurotrophin receptor $p75^{NTR}$. Considering the substantial percentage of ALCAM-containing endosomes that also contained Hc and $p75^{NTR}$ (60% and 64% respectively), my results strongly suggest that the ALCAM transport compartment associates with the same motor proteins and Rab GTPases characterised previously for Hc-positive endosomes. Transport of Hc depends on the retrograde motor cytoplasmic dynein, as well as myosin Va (Lalli et al., 2003b). On expression of GFP-Rab5 and GFP-Rab7, Rab5 was found to localise on stationary or oscillating structures in the axon while Rab7 was found on long-range bi-directional moving puncta (Deinhardt et al., 2006b). This is particularly interesting since my results showed that the ALCAM transport speed distribution had two distinct peaks. This suggested that there are two types of ALCAM carriers, one slow moving with frequent pauses and a second faster retrograde transport carrier. It would be interesting to investigate this further in co-transport experiments in neurons expressing GFP-Rab5 and GFP-Rab7. I hypothesise that ALCAM vesicles with slow transport kinetics would associate with Rab5, while those with faster transport would instead associate with Rab7. Perhaps the ALCAM transport observed with slower kinetics in neurons, could

be comparable to the short range ALCAM recycling reported in ovarian cancer cell lines (Piazza et al., 2005).

The slow ALCAM transport component was not observed in the experiments assessing the effect of the ALCAM ligand CD6-Fc on transport. This may, however, be accounted for by methodological differences between these experiments and the original Hc co-transport experiments. Firstly, the initial experiments were conducted in the presence of the atoxic Hc fragment, which is capable of modifying transport of other retrograde cargoes. Indeed, in the absence of neurotrophins, $p75^{NTR}$ can be directed to the retrograde route by Hc (Deinhardt et al., 2007), and Hc triggers Trk signalling in the absence of neurotrophins (Gil et al., 2003). This suggests that ALCAM sorting to the retrograde transport route could have been altered in the presence of Hc. Secondly, in the CD6-Fc experiments ventral horn neurons were exposed to the fluorescently labelled antibody against ALCAM (αALCAM488) on ice before moving to 37°C for internalisation and transport. Hypothetically this could result in a wave of internalisation that would saturate the sorting machinery so that a homogeneous population of antibody labelled carriers were at a similar stage of trafficking while being imaged. In contrast, in the initial experiments the probes were internalised throughout the incubation period allowing antibody-labelled endosomes at both early and late stages of internalisation and trafficking to be imaged simultaneously. It would be interesting to perform ALCAM transport experiments on ventral horn neurons isolated from the same mouse litter in the presence or absence of Hc and after exposure to the probes at both 37°C and 4°C. This could resolve whether either of these working hypotheses account for the difference observed or whether it was merely due to the biological variability of different neuronal cultures. It would also be interesting to analyse my co-transport experiments in more detail, by separating the transport information of ALCAM-positive Hc-positive endosomes from those that were ALCAM-positive but Hc-negative. This

could reveal whether the speed distribution of ALCAM endosomes that also contained Hc had different transport dynamics from those that did not.

6.1.2 Modulation of ALCAM transport

I used αALCAM488 to follow transport of the endogenous protein in living ventral horn neurons. This involved antibody binding to ALCAM at the plasma membrane, which would cause clustering of the protein on the cell surface. This strategy for following protein transport may alter the subsequent trafficking route of the protein of interest as discussed in Chapter 3.2. It would have been interesting to follow photoactivated ALCAM-D in transfected neurons to determine if ALCAM clustering is a pre-requisite for its subsequent internalisation and transport. Although this would involve the overexpression of a tagged protein it would have allowed me to address whether transport was altered in response to stimuli that induce clustering, such as addition of ALCAM ligands or antibody cross-linking. Initial experiments examining ALCAM-D transport in differentiated PC12 cells yielded limited information because I found no evidence of vectorial transport of ALCAM along neurites. It would have been interesting to follow ALCAM-D transport in primary ventral horn neurons, however this strategy was hampered by the low efficiency of ALCAM-D expression after electroporation and the poor health of the electroporated neurons.

In my experiments I did not detect a significant effect of CD6-Fc on the speed or frequency of αALCAM488-endosome transport. This could suggest that ALCAM transport is not modulated by ligand engagement. However, there were some practical issues in performing these experiments that may have made detection of small differences difficult. As described in Chapter 3, section 3.5.1, the αALCAM488 cross-reacted with CD6-Fc and therefore these experiments had to be conducted with the constraint of incubating the neurons at 4°C. This additional manipulation may have contributed to the low frequency of ALCAM transport observed in these cultures and

this in turn made it difficult to get substantial numbers of carriers to analyse. Another factor that probably contributed to the low transport frequency observed in these experiments is that they were performed in the absence of Hc. However, this was necessary because it was unclear whether Hc modifies ALCAM transport and, if this was the case, the effect of ALCAM ligand stimulation may have been masked. Considering ALCAM is transported at low frequency and that sampling from each culture is low (only a few axons can be imaged during an individual experiment), the data analysis was inherently variable between different cultures. This made the detection of small differences difficult using statistical methods. Furthermore, my strategy assumed that αALCAM488 would be able to bind ALCAM molecules bound to CD6-Fc directly or to endogenous ALCAM associated in *cis* with ALCAM-CD6-Fc complexes. However, if this was not the case e.g. αALCAM488 and CD6-Fc competed for ALCAM binding, then the αALCAM488 probe would not have been capable of detecting the pool of carriers that contained ALCAM-ligand complexes.

Although there is certainly not a large ligand-dependent effect on ALCAM transport as there is for $p75^{NTR}$ after exposure to neurotrophins (Deinhardt et al., 2007), several observations suggest that further examination of a ligand-dependent modulation of ALCAM transport is warranted. There was a consistent tendency towards an increase in the frequency of ALCAM carriers after exposure to CD6. It would be interesting to examine whether addition of ALCAM-Fc would alter αALCAM488 transport. Considering ALCAM-Fc and CD6-Fc have differential effects on neurite outgrowth, the ligands could also affect ALCAM transport differently. Furthermore, mimicking homophilic binding may be more physiologically relevant when examining the effect of ligand stimulation in neurons because CD6 is not expressed in the central nervous system but ALCAM is (discussed previously in Chapter 3, section 3.5.3).

6.1.3 The fate of ALCAM after axonal retrograde transport

The biological reason for retrograde transport of ALCAM was not resolved in my experiments. However, following axonal transport to the neural cell body it is known that other retrograde transport cargoes can be degraded, be transcytosed to the dendrite/cell body plasma membrane via recycling endosomes or secreted as exosomes (reviewed in von Bartheld, 2004).

6.1.3.1 Is transported ALCAM degraded?

ALCAM vesicles showed little colocalisation with lysosomal markers, both in living neurons during transport or in immunofluorescence of ALCAM puncta in the cell body. However, my conclusions rely on the assumption that the αALCAM488 probe does not dissociate from the endogenous protein, nor lose fluorescence once in acidic compartments. In support of my findings, studies on other endocytosed CAMs in neurons have shown they do not primarily colocalise with degradative compartments, using both fluorescently tagged proteins and antibody-based approaches (Yap et al., 2008, Diestel et al., 2007). NCAM localised to both Rab4 and Rab11 labelled endosomes, as well as those containing transferrin, suggesting that NCAM is targeted to recycling endosomes and then back to the plasma membrane (Diestel et al., 2007). Yap and colleagues (2008) found that NgCAM endocytosed in the dendritic/cell body compartment traffics via endosomes containing neuron-enriched endosomal protein of 21 kDa (NEEP21) before being transcytosed to the axonal plasma membrane. It would be interesting to investigate the nature of the ALCAM-containing compartment in the soma further. Since ALCAM puncta in ventral horn neurons are not as numerous as NgCAM or NCAM puncta reported in these papers, it may be necessary to stimulate internalisation e.g. in the presence of Hc or an ALCAM ligand. This would increase the number of ALCAM-containing puncta in the soma necessary for proper quantification of colocalisation with endosomal markers (e.g. Rab proteins) by immunofluorescence. Preliminary experiments however, did not show a significant colocalisation with Rab21-

positive compartments that have been previously associated with integrin recycling endosomes (Pellinen et al., 2006).

As discussed in the Introduction section 1.5, an independent investigation in neurons has reported endocytosis of DM-GRASP, the chick orthologue of ALCAM (Thelen et al., 2008), however, with conclusions that partially contrast with my results. Thelen and collaborators (2008) found that the cytoplasmic tail of DM-GRASP could bind ubiquitin, and was also a site for ubiquitination. They found that DM-GRASP was mono-ubiquitinated on the plasma membrane and suggested that internalised DM-GRASP in retinal ganglion cells (RGCs) was degraded after internalisation. In contrast, I found no evidence of ALCAM being targeted to degradative compartments in neurons. There are several reasons why Thelen et al (2008) have drawn different conclusions on the fate of internalised ALCAM/DM-GRASP from those presented here. Firstly, they assumed that DM-GRASP was targeted for degradation because they found DM-GRASP in large vesicles in cells overexpressing ubiquitin. Only vesicle size was used to indicate that the DM-GRASP-containing puncta after ubiquitin overexpression were of a degradative nature. In contrast, I used lysosomal markers, including LysoTracker in transport experiments and LAMP2 in immunofluorescence studies. Secondly, their experiments analysing the degradation of DM-GRASP were conducted on DM-GRASP transfected undifferentiated Neuro2A cells, while the DM-GRASP immunoprecipitation of ubiquitin was performed in transfected HEK cells. In sharp contrast, I examined the transport and destination of endogenous ALCAM in primary ventral horn neurons. In fact, in the study by Thelen et al (2008), it was observed that DM-GRASP accumulated in the central domain of RGC growth cones 15 minutes after antibody-stimulated internalisation, and interestingly, DM-GRASP-positive puncta decreased by 30 minutes. Although, DM-GRASP degradation could account for this observation,

another interesting possibility consistent with my findings is that DM-GRASP underwent long-range axonal transport.

Thelen et al (2008) concluded that the mono-ubiquitination was not responsible for internalisation because endocytosis of DM-GRASP was unaffected upon overexpression of ubiquitin. However, the effect of ubiquitin depletion was not tested in these experiments, and therefore, they cannot exclude the possibility that endogenous levels of ubiquitin are sufficient for steady state endocytosis of ALCAM/DM-GRASP. To date it has not been demonstrated whether the internalisation, transport or degradation of ALCAM is altered upon depletion of ubiquitin, or expression of ALCAM forms incapable of being ubiquitinated. Mono-ubiquitination of ALCAM would be a particularly interesting phenomenon to investigate in more detail because ALCAM lacks any known endocytosis motifs in its cytoplasmic tail, but mono-ubiquitination has been shown to regulate the endocytosis of NCAM in cortical neurons (Diestel et al., 2007).

6.1.3.2 Does ALCAM undergo transcytosis?

Considering the evidence showing that NCAM and NgCAM/L1 can be recycled back to the plasma membrane, it would be interesting to investigate if ALCAM can undergo recycling and transcytosis. I attempted to examine transcytosis of ALCAM in ventral horn cultures in compartmentalised chambers but the results of these experiments were inconclusive. Microfluidic devices currently produced in our laboratory have two channels separated by microgrooves (adapted from Park et al., 2006). These microgrooves do not allow cells to cross but are permissive for axon growth and therefore there is separation between the neuronal cell bodies in one channel and the axons in the other. In these experiments the αALCAM488 probe was allowed to internalise in the axonal compartment and be transported via the axon to the cell body. The cell body compartment was then incubated with the appropriate secondary antibody so, if ALCAM reached the cell surface, it would be labelled. Motor neurons are

a notoriously sensitive neural cell type to handle and in my experiments very few axons crossed the microgrooves to the axonal side in the microfluidic devices. I believe that to investigate this further, it would be necessary to characterise ALCAM transport in another neural cell type that can be cultured in this compartmentalised system e.g. dorsal root ganglia (DRG). L1/NgCAM accumulates on the axon plasma membrane and therefore the ratio of NgCAM fluorescence on the axon versus in the dendritic/soma compartment is used as a read-out for transcytosis efficiency (Yap et al., 2008). ALCAM is expressed on the neuron cell body, neurites and the axon, which means that I could not use the relative accumulation of ALCAM in the central compartment as a read-out of transcytosis efficiency.

Transcytosis of ALCAM is however an attractive hypothesis to account for ALCAM's retrograde transport in a non-degradative endosome. It has been shown that neurotrophins, their receptors and various toxins and viruses undergo transcytosis (reviewed in von Bartheld, 2004, Rind et al., 2005). I observed extensive colocalisation of ALCAM with $p75^{NTR}$ in the soma, and this could suggest that ALCAM is sorted with this neurotrophin receptor to the plasma membrane of the soma and/or dendrites after reaching the cell body. After transcytosis, a protein can be reinserted into the plasma membrane to function similarly as it did in the origin membrane (reviewed in von Bartheld, 2004). Alternative possible fates include, that the protein is used as a vehicle to release its ligand into the extracellular environment (either directly or by receptor ectodomain shedding), or secretion of the protein into the extracellular medium e.g. L1 can undergo ectodomain shedding and secretion in exosomes (Stoeck et al., 2006). There is evidence that ALCAM can be released in exosomes from lung endothelial cells (King et al., 2008). ALCAM transcytosis is a legitimate and interesting hypothesis to test since ALCAM has several properties that are consistent with this possibility: (i) it can be cleaved, (ii) it has been found in exosomes, and (iii) it is known to interact with

other proteins that undergo transcytosis e.g. NgCAM (DeBernardo and Chang, 1996) and $p75^{NTR}$ (unpublished results from our laboratory).

6.2 ALCAM expression in the nervous system

In ventral horn neuron cultures, ALCAM is expressed as two distinct forms that are both membrane-bound and glycosylated. To the best of my knowledge, this is the first report showing the existence of two distinct ALCAM forms within the nervous system. I propose that these two forms in ventral horn neuron cultures are comprised of a higher migrating glial form, equivalent to that seen in U251MG cultures, and a smaller neural form, which is associated with the Hc axonal retrograde transport compartment.

Alternative forms of ALCAM have been reported previously, but these can be attributed to differential glycosylation or membrane cleavage. In Fournier-Thibault et al (1999) neural ALCAM isolated from the spinal cord migrated on SDS-PAGE at a lower molecular weight than that observed in muscle lysates and epithelial cells. Pourquie and colleagues (1992), reported that ALCAM/BEN has at least 3 distinct forms: a heavy 110 kDa epithelial form, an intermediate 100 kDa haematopoietic form and a 95 kDa neural form. However, all three forms collapsed into a 75 kDa band after deglycosylation with PNGase-F and therefore the difference in protein migration is attributed to differential glycosylation. The two novel ALCAM forms observed in this study in ventral horn neuron cultures cannot be attributed to differential glycosylation.

Unfortunately, it was not possible to determine what accounts for the difference in migration of the two forms of ventral horn ALCAM. To address this, I plan to investigate if two transcripts are amplified by RT-PCR from RNA of ventral horn neuron cultures. It would be particularly interesting to establish whether the neural and glial ALCAM forms differ in their primary sequence, and whether this could reflect differences in function. Other important CAMs expressed in the nervous system express specific isoforms in

neurons and glia. For example, differential splicing of L1 in neurons results in inclusion of a sequence that is responsible for L1 endocytosis in growth cones, while the GPI-anchored form of NCAM is expressed in glia (reviewed in Maness and Schachner, 2007). Optimisation of ALCAM immunoprecipitation using different antibodies would also be warranted in order to determine whether the two forms associate with different proteins. Antibodies directed toward human ALCAM have been shown to immunoprecipitate the native protein. Based on the high degree of conservation of ALCAM in vertebrates, it is reasonable to hypothesis that these antibodies could be exploited to immunoprecipitate mouse ALCAM.

I did not find evidence of ALCAM cleavage in ventral horn cultures or ALCAM-D PC12 cells. For example, I did not detect a membrane bound C-terminal fragment as a product of cleavage in cell lysates or evidence of the ectodomain in the cell culture medium by western blot analysis (data not shown). However, in previous work examining ALCAM cleavage, ALCAM ectodomain fragments have been immunoprecipitated from cell lysates and culture medium (Rosso et al., 2007). Therefore, if ALCAM immunoprecipitation were optimised I would conduct these experiments again. Furthermore, it would be interesting to examine whether ALCAM cleavage and ectodomain shedding would be stimulated by neurotrophin stimulation in PC12 cells and ventral horn neurons, in analogy to the EGF-dependent cleavage observed in ovarian cancer cells (Rosso et al., 2007).

6.3 ALCAM potentiates NGF-induced neurite outgrowth

My results showed that ALCAM significantly potentiates neurite outgrowth in response to NGF in PC12 cells. Analysis of NGF-induced differentiation after transfection of truncation mutants or after addition of soluble ALCAM-Fc, revealed that this effect was dependent on the ALCAM extracellular domain. Expression of the transmembrane and

cytoplasmic domain alone had no effect on NGF-induced differentiation. Importantly, ALCAM alone did not induce PC12 differentiation, remarkably suggesting that ALCAM acts as a modifier of other signals and not as an initiator of neurite outgrowth. ALCAM's role in neurite outgrowth was specific to the stimuli used. ALCAM overexpression increased NGF-differentiation of PC12 cells only but did not potentiate dbcAMP-mediated neurite outgrowth. This suggests that ALCAM does not activate an intracellular signalling cascade directly because ALCAM overexpression did not synergise with dbcAMP stimulation. In contrast, ALCAM overexpression showed only a non-significant potentiation of GDNF-dependent neurite outgrowth, further supporting the specificity of its effect on neurite outgrowth.

In light of these results, the findings presented in this thesis are compatible with the model of ALCAM function proposed by Prof. G Swart and colleagues and shown schematically in the Introduction, Figure 1.8. Indeed, truncation of the N-terminal of ALCAM abrogated the potentiation of neurite outgrowth seen upon overexpression of the full-length protein. This suggests that intact ALCAM binding can increase growth factor signalling and this is partially inhibited when *trans* binding is interrupted. The soluble ligand CD6-Fc that is only capable of *trans* binding, and in this respect behaves similarly to the isolated V_1 domain alone, disrupted the endogenous ALCAM network resulting in no potentiation of neurite outgrowth. However, ALCAM-Fc, which is capable of *cis* as well as *trans*-interactions, was able to potentiate neurite outgrowth. This suggested that it is binding in *cis* and clustering on the membrane that is important in ALCAM mediated potentiation of NGF signalling. Previous work *in vitro* and *in vivo* has shown that ALCAM is involved in neurite outgrowth in many neuron types (DeBernardo and Chang, 1995, Avci et al., 2004, Ott et al., 2001), however my work, as outlined above, has provided molecular information on how this process may occur.

A critical difference between my studies and previous work is that I examined neurite outgrowth within cells overexpressing various forms of ALCAM, whereas previous studies have looked at the effect of ALCAM/DM-GRASP substrates on neuron outgrowth (Kawauchi et al., 2003, DeBernardo and Chang, 1995). Interestingly Avci and colleagues (2004), found that RGCs on a DM-GRASP/laminin substrate showed increased neurite outgrowth when compared to RGCs on laminin alone. In this study, the authors also showed that a DM-GRASP/polylysine substrate did not promote neurite outgrowth. Interestingly, I found that transfection of ALCAM did not potentiate neurite outgrowth alone but required a differentiation stimulus, e.g. NGF. In this context, my interpretation of the findings of Avci et al (2004) is that the laminin substrate has acted as the initiator of differentiation, similarly to NGF, and ALCAM has potentiated the subsequent neurite outgrowth as a modifier of the differentiation signal. If ALCAM can cooperate with laminin functioning as an initiator, it suggests that ALCAM cooperates with integrin signalling as has already been shown with other CAMs (Chen et al., 2010). Avci et al (2004) did not investigate whether NgCAM modulated integrin signalling directly, but this would be interesting to examine further considering my finding that ALCAM can potentiate NGF-signalling and differentiation.

Since, my analysis of neurite outgrowth was restricted to ALCAM transfected cells, my results shed light on a cell-autonomous function for ALCAM in neurite outgrowth rather than a non-cell autonomous function as a substrate as previously described by others. Since ALCAM-D was only transfected in around 30% of cells, most cells with which these transfected cell came into contact with would have been untransfected. Therefore the differences in the neurite outgrowth observed is likely to be the result of ALCAM expression within the transfected cell analysed, rather than the result of interactions in *trans* from an adjacent cell. However, it is possible, although less likely,

that the alterations in neurite outgrowth were influenced by secretion of the ALCAM ectodomain into the medium, which could therefore function similarly to ALCAM-Fc.

My experiments did not address whether ALCAM internalisation and transport related to ALCAM's role in neurite outgrowth. In a previous study it was claimed that endocytosis of DM-GRASP was required for RGC preference for DM-GRASP substrates, but this study only showed that a general clathrin inhibitor abolished RGC preference for DM-GRASP/laminin substrates (Thelen et al., 2008). This approach did not formally prove that DM-GRASP endocytosis is important for RGC axon growth preference because the inhibitor used abolished general endocytosis and therefore the recycling of many plasma membrane proteins.

6.3.1 Modulation of NGF-signalling

I also examined whether ALCAM modulated the NGF signalling response by looking at the phosphorylation levels of TrkA and ERK1/2 in control and ALCAM-D transfected PC12 cells. ALCAM overexpression significantly increased the phosphorylation of the TrkA receptor. Unfortunately, I did not observe a statistically significant increase in ERK1/2 phosphorylation. However, this kinase is downstream of many other stimuli including stress factors and these are hard to control experimentally, as described in Chapter 5, section 5.4. I decided to analyse the phosphorylation of ERK1/2 because this signalling cascade is thought to be responsible for PC12 differentiation in response to NGF and I had seen a potentiation of neurite outgrowth in ALCAM-D transfected cells. However, different kinases are responsible for distinct responses downstream of NGF (reviewed in Klesse and Parada, 1999). It would be interesting to investigate whether the signalling cascade mediated through PI3K and Akt, which is responsible for PC12 cell survival, is also modified in ALCAM overexpressing cells.

6.3.2 Possible mechanisms by which ALCAM could potentiate NGF-induced differentiation

I was unable to determine the precise mechanism by which ALCAM overexpression potentiates NGF-induced differentiation and TrkA phosphorylation in PC12 cells. I could not detect a direct interaction between TrkA and ALCAM by immunoprecipitation. Alternatively, ALCAM could potentiate NGF-signalling by altering the stoichiometry of neurotrophin receptor complexes on the plasma membrane. Therefore, I also investigated whether ALCAM interacts with $p75^{NTR}$ or sortilin, the $p75^{NTR}$ co-receptor, but no direct interactions were detected in ALCAM immunoprecipitations (data not shown). However, in view of the overall low immunoprecipitation efficiency, I can only tentatively conclude that ALCAM does not interact with these proteins.

To clarify if NGF receptor activation is required as proposed or whether ALCAM interacts directly with NGF, it would be necessary to analyse the effect of ALCAM transfection on neurite outgrowth in PC12 cells that lack NGF receptors (e.g. knockdown of $p75^{NTR}$ or using PC12nnr that lack TrkA). Alternatively I could use a pharmacological approach and assess ALCAM potentiation of NGF-induced neurite outgrowth in the presence of the inhibitor K252a, to inhibit tyrosine kinase activity. I did not find evidence to suggest that ALCAM can bind to NGF directly by immunoprecipitation (data not shown) but perhaps a cell surface binding and interference experiment similar to that described in Piazza et al (2005) could be undertaken. Comparison of NGF binding to cells expressing ALCAM (but not TrkA or $p75^{NTR}$) would need to be compared to cells that are null for all three proteins. Cells would need to be exposed to fluorescently labelled NGF-Fc prior to fluorescence-activated cell sorting analysis (FACs analysis).

Several alternative mechanisms could account for the potentiation of NGF-induced differentiation observed in this thesis. These include altered membrane localisation of

neurotrophin receptors, which I investigated in experiments that isolated detergent resistant membranes (DRMs - also referred to as lipid rafts) from ALCAM-D expressing cells. ALCAM transfection did not alter the association of Thy1.1 (a marker for DRMs), full length TrkA or its phosphorylated form within DRMs. ALCAM-D was found in detergent soluble membranes, but its expression appeared to alter the distribution of $p75^{NTR}$ toward Thy1.1-containing fractions. This could have functional consequences for $p75^{NTR}$-dependent NGF signalling by changing the association of $p75^{NTR}$ with TrkA, its proximity to other effectors or its localisation to specific membrane subdomains.

Another possible mechanism by which ALCAM overexpression could potentiate neurotrophin signalling is by altering the regulated proteolysis of membrane receptors. TrkA , $p75^{NTR}$ and ALCAM are all processed by ADAM17, and regulated proteolysis has been associated with altering signal cascade activation (Diaz-Rodriguez et al., 1999, Ahmed et al., 2006, Rosso et al., 2007). Subsequently $p75^{NTR}$ can undergo γ-secretase cleavage in endosomes (Urra et al., 2007) to generate an intracellular domain capable of potentiating TrkA signalling in response to NGF. The $p75^{NTR}$ intracellular domain is generated in response to NGF treatment in PC12 cells and it was shown that $p75^{NTR}$ cleavage induced by TrkA activity, in turn potentiated TrkA signalling (Ceni et al., 2010). Therefore, if ALCAM could increase $p75^{NTR}$ cleavage it could also potentiate TrkA signalling. It would be interesting to examine whether $p75^{NTR}$ cleavage is altered upon NGF stimulation in Dendra or ALCAM-D transfected cells by western blot. If this cleavage were confirmed, it would be interesting to test if potentiation of neurite outgrowth in response to ALCAM overexpression was altered following inhibition of ADAM17 or γ-secretase. This experiment would determine if the potentiation of NGF-signalling upon ALCAM overexpression required protease activity. To determine which ADAM17 substrate mediated this effect, it would be required to see whether potentiation of NGF-induced neurite outgrowth was inhibited in PC12 cells

transfected with $p75^{NTR}$, TrkA and ALCAM mutants resistant to cleavage. I am aware that a possible explanation for the potentiation of NGF-signalling observed is that ALCAM overexpression could upregulate ADAM17 activity and in turn this could lead to an increase in cleavage of other ADAM17 substrates like $p75^{NTR}$ and TrkA. Although this could mean that the effects observed in this study are a consequence of overexpression, rather than a property of endogenous ALCAM, it could still be physiologically important considering that ALCAM is found overexpressed in several forms of cancer (Ofori-Acquah and King, 2008).

It should be noted that several of the Hc endosome cell-surface proteins have properties relating to ectodomain shedding and metalloprotease regulation. Firstly, one metalloprotease itself, ADAM10, was found in this proteomic screen. Secondly, ALCAM has been shown to regulate metalloprotease activity e.g. matrix metalloprotease MMP-2 and membrane type 1 matrix metalloprotease MT1-MMP (van Kilsdonk et al., 2008, Lunter et al., 2005). Furthermore, another of the IgCAMs identified in this Hc-containing compartment is CD147, also known as extracellular matrix metalloproteinase (MMP) inducer (EMMPRIN) (see Introduction, Table.1). As well as these metalloprotease regulators, several of the Hc-endosome cargoes are known to undergo metalloprotease cleavage e.g. TrkA, $p75^{NTR}$ and NCAM (Diaz-Rodriguez et al., 1999, Urra et al., 2007, Hinkle et al., 2006). This could suggest that regulation of metalloprotease activity is an important process in these retrograde carriers. This possibility is consistent with growing evidence suggesting that membrane proteolysis often happens on endosomes and this can relate to their signalling function (Urra et al., 2007).

6.3.3 Issues relating to ALCAM depletion

All my experiments examining the role of ALCAM in NGF-dependent neurite outgrowth in PC12 cells used overexpression of ALCAM. To determine whether the potentiation

of NGF-signalling observed is a property of endogenous ALCAM it is necessary to perform ALCAM knockdown experiments. By western blot and immunofluorescence I could not detect any endogenous ALCAM expressed in PC12 cells. However, I amplified an ALCAM transcript from PC12 cDNA by PCR. This result was in agreement with previous findings that demonstrated that the ALCAM transcript significantly increased in PC12 cells upon differentiation by NGF and dbcAMP (Ng et al., 2009). It is therefore likely that endogenous ALCAM was expressed in PC12 cells in my neurite outgrowth experiments, limiting the conclusions I could draw from my studies. For example, I could not conclude whether the cytoplasmic domain was required for potentiation of neurite outgrowth when I overexpressed ALCAM lacking the C-terminal tail because endogenous ALCAM may have been sufficient in transmitting signals in these cells.

I attempted to knockdown ALCAM in PC12 cells but using immunofluorescence and western blot analysis I could not determine whether the protein had been depleted. It would be necessary to establish the efficiency of ALCAM knockdown using RT-PCR if I were to repeat these experiments. Furthermore, the interpretation of ALCAM knockdown experiments can be further complicated by mechanisms compensating for loss of ALCAM in knockdown cells. In Lunter et al (2005) ALCAM depletion decreased basal metalloprotease activity, however it had no effect on concanavalin A stimulated metalloprotease activity, a stimulator of the proteolytic cascade that bypasses the need for cell-matrix interactions. In contrast, ALCAM N-terminal truncation mutants (ΔN-ALCAM) inhibited both basal and concanavalin A stimulated metalloprotease activity in this study. This suggests that pharmacological stimulation can restore metalloprotease activity and relieve its dependence on ALCAM in ALCAM knockdown cells. In contrast, ALCAM truncation mutants inhibit metalloprotease activity under basal and stimulated conditions, suggesting that in the presence of a defective ALCAM network

metalloprotease activity remained ALCAM-dependent in both conditions. This suggests that ALCAM acts as a conditional switch in regulation of this pathway; if ALCAM is present a functional network is required to activate the metalloprotease cascade, but in the absence of ALCAM cells can compensate and activate metalloproteases via different mechanisms.

ALCAM is expressed in many different tissues during development (reviewed in Swart, 2002). I found ALCAM expressed in all cell types tested including PC12 cells, U251MG, primary ventral horn cultures, primary astrocytes, brain and muscle lysates. Undifferentiated Neuro2A cells have been used in previous studies as a cell system that lacks endogenous ALCAM (Thelen et al., 2008). However, upon differentiation with retinoic acid ALCAM was identified as a protein that became modified with a disialic acid epitope in Neuro2A cells (Sato et al., 2002). This suggests that once differentiated, these cells express ALCAM, and I confirmed this by amplifying the ALCAM transcript from differentiated Neuro2A cDNA (data not shown). Since my experiments were looking at the role of ALCAM in differentiation I could not use Neuro2A cells as an ALCAM null system. An alternative way to analyse the effect of ALCAM on neurite outgrowth in a null system would have been to express my constructs in ALCAM$^{-/-}$ ventral horn neurons. However, primary ventral horn neurons are notoriously difficult to transfect and as already described, electroporation of ventral horn neurons was unsuccessful.

6.4 Nerve terminal sprouting *in vivo* in response to BoNT/A was unaffected in ALCAM$^{-/-}$ animals

I found that ALCAM$^{-/-}$ and wild type mice showed comparable nerve terminal sprouting in response to BoNT/A induced paralysis at the neuromuscular junction (NMJ) *in vivo*.

Although this suggests that ALCAM is not involved in this process, there are several considerations to be taken into account when interpreting this result. Firstly, the precise mechanism by which BoNT/A-induced sprouting at the NMJ occurs is unknown. It has been suggested that the muscle secretes factors that induce sprouting, such as insulin-like growth factors (IGF) (Caroni and Schneider, 1994). Since I have shown that ALCAM exhibits specificity in modulating growth factor signalling and no phenotype was observed *in vivo*, this could suggest that the growth factors involved in sprouting after BoNT/A-induced paralysis activate pathways that are not potentiated by ALCAM.

Another possible reason why absence of ALCAM did not alter the sprouting response in ALCAM$^{-/-}$ animals, is that upregulation of other CAMs may have compensated for the loss of ALCAM function. As described in the Introduction section 1.4, the IgCAM family is very large and there is known functional redundancy between its members. For example in cell lines, interference with endogenous ALCAM function can upregulate L1 expression (van Kilsdonk et al., 2008). Interestingly, the $V_1V_2C_1C_2C_3$ family member BCAM is also localised to the neuromuscular junction (Nishimune et al., 2008) and therefore it may compensate for ALCAM function in the knockout animals. It would have been interesting to investigate whether ALCAM$^{-/-}$ ventral horn cultures showed increased L1 or BCAM expression in western blot analysis from ventral horn cultures, brain and muscle lysates.

Although NCAM and L1 have proven important functions in the nervous system, animals in which these genes have been knocked out have surprisingly mild phenotypes (see Introduction 1.4). Despite NCAM being expressed on muscle, motor neurons and terminal Schwann cells, NCAM$^{-/-}$ mice were found to have surprisingly normal NMJs (Moscoso et al., 1998). Only an in-depth electrophysiological analysis found subtle alterations in NMJ function (Polo-Parada et al., 2001). The knockout mice

have abnormal synaptic vesicle recycling, which results in increased transmission failures at high stimulation frequencies. Behaviourally, this cellular phenotype manifests as poor performance on a rota-rod test at high speeds when compared to wild type animals (Polo-Parada et al., 2001). Perhaps in-depth electrophysiological analysis of ALCAM$^{-/-}$ animals could reveal similar subtle changes in NMJ function.

As outlined above, the relatively mild phenotype of NCAM$^{-/-}$ mice is proposed to be a consequence of functional redundancy between members of the IgCAM superfamily and the upregulation of proteins with related function during development (Moscoso et al., 1998). NCAM expression is restricted to the NMJ in adulthood but is re-expressed along nerves and muscle fibres in response to injury. Many genes expressed during development of the peripheral nervous system are not re-expressed after injury and therefore, Chipman and collaborators (2010) investigated whether a role for NCAM in synaptic stability could be revealed after injury when compensation by upregulation of other proteins may not occur. The authors analysed the recovery of NMJ function at 1, 3 and 6 months after a tibial nerve crush in NCAM$^{-/-}$ mice. They found that NCAM$^{-/-}$ animals re-innervate normally after nerve injury. However, it was revealed that 3 and 6 months after injury the reinnervated NMJ axons retracted in NCAM$^{-/-}$ mice, which in turn resulted in a progressive muscular atrophy. This study revealed that NCAM is required to maintain synaptic function after reinnervation and suggested NCAM has a role in long-term stability and maintenance of the NMJ that only becomes evident after injury when expression of other proteins cannot compensate for loss of its function. Interestingly, ALCAM is also dynamically regulated during NMJ formation and is upregulated in response to injury (described in the introduction section 1.5 and see Fournier-Thibault et al., 1999). ALCAM, therefore, may have a similar role to NCAM in maintenance of the NMJ. It would be interesting to conduct a similar study on ALCAM$^{-/-}$ mice examining the long-term stability of the NMJ after nerve injury. In this thesis the

NMJ was only examined at a relatively short period (three weeks), after induction of BoNT/A-induced paralysis. Taking into account the changes observed in NCAM$^{-/-}$ animals months after reinnervation, it would be interesting to also look at later time points after BoNT/A treatment, to establish if there would be long-term deficits in NMJ stability after recovery from muscle paralysis.

Retinal ganglion cells in ALCAM$^{-/-}$ animals show misprojections from the temporal part of the retina to the superior colliculus (Buhusi et al., 2009). Since ALCAM is also expressed in a population of motor neurons, I think that it would also be interesting to map whether there is aberrant patterning of motor neurons and interneurons circuits in the spinal cord of ALCAM$^{-/-}$ animals. Behavioural monitoring of the ALCAM$^{-/-}$ mice showed that some adult knockout mice showed subtle hind limb clasping defects, which could suggest they had abnormal connectivity of neurons in their spinal cord which control these reflexes. The mistargeting of RGCs in ALCAM$^{-/-}$ mice reported by Buhusi et al (2009) was not observed in all animals analysed e.g. of 14 mice analysed 11 had abnormal projections as well as normal, one had only abnormal projections while 2 were equivalent to wild type. This supports my observation of an abnormal clasping phenotype in only some ALCAM$^{-/-}$ mice, possibly because there is variability in the patterning defects observed, and perhaps normal connectivity exists in parallel to the aberrant circuits in many animals. A possible way to analyse whether motor neurons have aberrant projections in the spinal cord of ALCAM$^{-/-}$ mice would be to conduct a similar retrograde tracing study as reported by Buhusi et al (2009). Injecting tagged tetanus toxin, cholera toxin or viruses into muscles of ALCAM$^{-/-}$ animals could reveal if the neurons had an abnormal circuitry within the spinal cord, which could account for their abnormal clasping reflex.

6.5 Concluding remarks

In this thesis, I have characterised the cell adhesion molecule ALCAM as a novel cargo of retrograde axonal transport in primary ventral horn neurons. I have shown that ALCAM is transported in a non-degradative compartment with other cell adhesion molecules and neurotrophin receptors. However, further work on the fate of ALCAM once it reaches the neuron cell body is required. I reported two novel ALCAM forms expressed in the nervous system that are likely to represent glial and neural isoforms. Importantly, my findings revealed a novel role for ALCAM in neurite outgrowth as a modulator of growth factor signalling. ALCAM overexpression potentiates NGF differentiation signalling and neurite outgrowth in PC12 cells. Molecular characterisation of ALCAM's ability to potentiate neurite outgrowth revealed that the ALCAM extracellular domain is necessary and sufficient to increase PC12 differentiation in response to NGF. A model for ALCAM function initially proposed in cancer cells (Swart et al., 2005) is consistent with my findings of ALCAM function in neurons. An intact ALCAM network can potentiate neurite outgrowth and the effect is predominantly dependent on *cis*-interactions. I propose that ALCAM can modulate specific growth factor signalling, although I did not determine the mechanism responsible for this phenomenon. I saw an alteration in $p75^{NTR}$ membrane localisation in detergent-resistant membranes, which could influence $p75^{NTR}$ signalling ability. An attractive hypothesis to test is that ALCAM regulates ADAM17 metalloprotease activity and therefore $p75^{NTR}$ cleavage. An increase in the cleavage and in turn in the concentration of the soluble $p75^{NTR}$ intracellular domain could potentiate TrkA signalling. Unfortunately, due to problems knocking down ALCAM and probable compensation by upregulation of proteins with related functions *in vivo*, I was unable to prove that ALCAM expressed at endogenous levels also contributes to growth factor

signalling. In the Discussion, I have described several ways in which to address some of these problems.

The data presented in this thesis illustrates the complicated and intimate relationship between cell adhesion molecules and classical receptors at the membrane. Over recent years, work on signalling molecules at the membrane has shown that the boundaries between cell adhesion molecules and receptors are increasingly blurred. My results are consistent with work on other IgCAM family members that have been shown to cooperate with integrin and growth factor signalling. I have characterised the role of ALCAM in neurite outgrowth in molecular detail unlike previous studies. My results suggest that ALCAM is not merely a permissive substrate for neuron outgrowth, but that it can act cell-autonomously to potentiate neurotrophin signalling.

The finding that ALCAM overexpression can potentiate growth factor signalling may have important implications for the study of cancer. ALCAM is found upregulated in many forms of cancer (Ofori-Acquah and King, 2008) where it has been correlated with disease progression and poor prognosis. My results show that overexpressed ALCAM potentiated neurotrophin signalling in neural cells. This implies that ALCAM overexpression in cancer, as well as regulating metalloprotease activity and adhesion, could have an additional role potentiating growth factor signalling. Importantly, it has been demonstrated that NGF and TrkA are overexpressed in epithelial ovarian cancer cells (Campos et al., 2007), which also overexpress ALCAM (Rosso et al., 2007). Therefore, overexpression of ALCAM in epithelial ovarian cancer may be of particular physiological importance because it could potentiate TrkA signalling, which has been linked to increased vascular endothelial growth factor (VEGF) expression and tumour progression in this cancer. Furthermore, Swart et al (2005) performed a gene expression profile analysis of ALCAM-positive metastatic melanoma cell lines versus

ALCAM-negative non-metastatic cell lines. The authors found that ALCAM overexpression not only correlated with the upregulation of the plasminogen activation cascade, but also the overexpression of several growth factors including bFGF, PDGF-A and VEGF that may suggest that ALCAM could also play a role in these growth factor signalling cascades. In the future, it would be interesting to explore whether ALCAM overexpression cooperates with these growth factor signalling pathways, to promote tumour growth and progression in these cancers.

Reference List

(1994) The American Society for Cell Biology 34th annual meeting. San Francisco, California, December 10-14, 1994. Abstracts. *Mol Biol Cell,* 5 Suppl, 1A-573A.

AHMED, Z., MAZIBRADA, G., SEABRIGHT, R. J., DENT, R. G., BERRY, M. & LOGAN, A. (2006) TACE-induced cleavage of NgR and p75NTR in dorsal root ganglion cultures disinhibits outgrowth and promotes branching of neurites in the presence of inhibitory CNS myelin. *FASEB J,* 20, 1939-41.

ALOE, L. (2004) Rita Levi-Montalcini: the discovery of nerve growth factor and modern neurobiology. *Trends Cell Biol,* 14, 395-9.

ANDERSON, A. A., KENDAL, C. E., GARCIA-MAYA, M., KENNY, A. V., MORRIS-TRIGGS, S. A., WU, T., REYNOLDS, R., HOHENESTER, E. & SAFFELL, J. L. (2005) A peptide from the first fibronectin domain of NCAM acts as an inverse agonist and stimulates FGF receptor activation, neurite outgrowth and survival. *J Neurochem,* 95, 570-83.

ANGAUT-PETIT, D., MOLGO, J., COMELLA, J. X., FAILLE, L. & TABTI, N. (1990) Terminal sprouting in mouse neuromuscular junctions poisoned with botulinum type A toxin: morphological and electrophysiological features. *Neuroscience,* 37, 799-808.

ANGAUT-PETIT, D., MOLGO, J., CONNOLD, A. L. & FAILLE, L. (1987) The levator auris longus muscle of the mouse: a convenient preparation for studies of short- and long-term presynaptic effects of drugs or toxins. *Neurosci Lett,* 82, 83-8.

ANTONUCCI, F., ROSSI, C., GIANFRANCESCHI, L., ROSSETTO, O. & CALEO, M. (2008) Long-distance retrograde effects of botulinum neurotoxin A. *J Neurosci,* 28, 3689-96.

ARCE, V., GARCES, A., DE BOVIS, B., FILIPPI, P., HENDERSON, C., PETTMANN, B. & DELAPEYRIERE, O. (1999) Cardiotrophin-1 requires LIFRbeta to promote survival of mouse motoneurons purified by a novel technique. *J Neurosci Res,* 55, 119-26.

ASCANO, M., RICHMOND, A., BORDEN, P. & KURUVILLA, R. (2009) Axonal targeting of Trk receptors via transcytosis regulates sensitivity to neurotrophin responses. *J Neurosci,* 29, 11674-85.

AVCI, H. X., ZELINA, P., THELEN, K. & POLLERBERG, G. E. (2004) Role of cell adhesion molecule DM-GRASP in growth and orientation of retinal ganglion cell axons. *Dev Biol,* 271, 291-305.

BARTEE, E., MCCORMACK, A. & FRUH, K. (2006) Quantitative membrane proteomics reveals new cellular targets of viral immune modulators. *PLoS Pathog,* 2, e107.

BECH-SERRA, J. J., SANTIAGO-JOSEFAT, B., ESSELENS, C., SAFTIG, P., BASELGA, J., ARRIBAS, J. & CANALS, F. (2006) Proteomic identification of desmoglein 2 and activated leukocyte cell adhesion molecule as substrates of ADAM17 and ADAM10 by difference gel electrophoresis. *Mol Cell Biol,* 26, 5086-95.

BILSLAND, L. G., SAHAI, E., KELLY, G., GOLDING, M., GREENSMITH, L. & SCHIAVO, G. (2010) Deficits in axonal transport precede ALS symptoms in vivo. *Proc Natl Acad Sci U S A*.

BOHNERT, S. & SCHIAVO, G. (2005) Tetanus toxin is transported in a novel neuronal compartment characterized by a specialized pH regulation. *J Biol Chem,* 280, 42336-44.

BOILLEE, S., VANDE VELDE, C. & CLEVELAND, D. W. (2006) ALS: a disease of motor neurons and their nonneuronal neighbors. *Neuron,* 52, 39-59.

BOWEN, M. A., BAJORATH, J., D'EGIDIO, M., WHITNEY, G. S., PALMER, D., KOBARG, J., STARLING, G. C., SIADAK, A. W. & ARUFFO, A. (1997) Characterization of mouse ALCAM (CD166): the CD6-binding domain is conserved in different homologs and mediates cross-species binding. *Eur J Immunol,* 27, 1469-78.

BOWEN, M. A., PATEL, D. D., LI, X., MODRELL, B., MALACKO, A. R., WANG, W. C., MARQUARDT, H., NEUBAUER, M., PESANDO, J. M., FRANCKE, U. & ET AL. (1995) Cloning, mapping, and characterization of activated leukocyte-cell adhesion molecule (ALCAM), a CD6 ligand. *J Exp Med,* 181, 2213-20.

BRACALE, A., CESCA, F., NEUBRAND, V. E., NEWSOME, T. P., WAY, M. & SCHIAVO, G. (2007) Kidins220/ARMS is transported by a kinesin-1-based mechanism likely to be involved in neuronal differentiation. *Mol Biol Cell,* 18, 142-52.

BRADFORD, M. M. (1976) A rapid and sensitive method for the quantitation of microgram quantities of protein utilizing the principle of protein-dye binding. *Anal Biochem,* 72, 248-54.

BRADY, S. T., RICHARDS, B. W. & LEOPOLD, P. L. (1993) Assay of vesicle motility in squid axoplasm. *Methods Cell Biol,* 39, 191-202.

BUHUSI, M., DEMYANENKO, G. P., JANNIE, K. M., DALAL, J., DARNELL, E. P., WEINER, J. A. & MANESS, P. F. (2009) ALCAM regulates mediolateral retinotopic mapping in the superior colliculus. *J Neurosci,* 29, 15630-41.

CAMPOS, X., MUNOZ, Y., SELMAN, A., YAZIGI, R., MOYANO, L., WEINSTEIN-OPPENHEIMER, C., LARA, H. E. & ROMERO, C. (2007) Nerve growth factor and its high-affinity receptor trkA participate in the control of vascular endothelial growth factor expression in epithelial ovarian cancer. *Gynecol Oncol,* 104, 168-75.

CARONI, P. & SCHNEIDER, C. (1994) Signaling by insulin-like growth factors in paralyzed skeletal muscle: rapid induction of IGF1 expression in muscle

fibers and prevention of interstitial cell proliferation by IGF-BP5 and IGF-BP4. *J Neurosci,* 14, 3378-88.

CASSENS, C., KLEENE, R., XIAO, M. F., FRIEDRICH, C., DITYATEVA, G., SCHAFER-NIELSEN, C. & SCHACHNER, M. (2010) Binding of the receptor tyrosine kinase TrkB to the neural cell adhesion molecule (NCAM) regulates phosphorylation of NCAM and NCAM-dependent neurite outgrowth. *J Biol Chem,* 285, 28959-67.

CASTELLANI, V., DE ANGELIS, E., KENWRICK, S. & ROUGON, G. (2002) Cis and trans interactions of L1 with neuropilin-1 control axonal responses to semaphorin 3A. *EMBO J,* 21, 6348-57.

CASWELL, P. T., VADREVU, S. & NORMAN, J. C. (2009) Integrins: masters and slaves of endocytic transport. *Nat Rev Mol Cell Biol,* 10, 843-53.

CENI, C., KOMMADDI, R. P., THOMAS, R., VEREKER, E., LIU, X., MCPHERSON, P. S., RITTER, B. & BARKER, P. A. (2010) The p75NTR intracellular domain generated by neurotrophin-induced receptor cleavage potentiates Trk signaling. *J Cell Sci,* 123, 2299-307.

CHEN, M. M., LEE, C. Y., LELAND, H. A., LIN, G. Y., MONTGOMERY, A. M. & SILLETTI, S. (2010) Inside-out regulation of L1 conformation, integrin binding, proteolysis, and concomitant cell migration. *Mol Biol Cell,* 21, 1671-85.

CHEN, X. J., LEVEDAKOU, E. N., MILLEN, K. J., WOLLMANN, R. L., SOLIVEN, B. & POPKO, B. (2007) Proprioceptive sensory neuropathy in mice with a mutation in the cytoplasmic Dynein heavy chain 1 gene. *J Neurosci,* 27, 14515-24.

CHEVALIER-LARSEN, E. S., WALLACE, K. E., PENNISE, C. R. & HOLZBAUR, E. L. (2008) Lysosomal proliferation and distal degeneration in motor neurons expressing the G59S mutation in the p150Glued subunit of dynactin. *Hum Mol Genet,* 17, 1946-55.

CHIPMAN, P. H., FRANZ, C. K., NELSON, A., SCHACHNER, M. & RAFUSE, V. F. (2010) Neural cell adhesion molecule is required for stability of reinnervated neuromuscular junctions. *Eur J Neurosci,* 31, 238-49.

COHEN, N. R., TAYLOR, J. S., SCOTT, L. B., GUILLERY, R. W., SORIANO, P. & FURLEY, A. J. (1998) Errors in corticospinal axon guidance in mice lacking the neural cell adhesion molecule L1. *Curr Biol,* 8, 26-33.

COSKER, K. E., COURCHESNE, S. L. & SEGAL, R. A. (2008) Action in the axon: generation and transport of signaling endosomes. *Curr Opin Neurobiol,* 18, 270-5.

CREMER, H., LANGE, R., CHRISTOPH, A., PLOMANN, M., VOPPER, G., ROES, J., BROWN, R., BALDWIN, S., KRAEMER, P., SCHEFF, S. & ET AL. (1994) Inactivation of the N-CAM gene in mice results in size reduction of the olfactory bulb and deficits in spatial learning. *Nature,* 367, 455-9.

CUERVO, A. M. & DICE, J. F. (1996) A receptor for the selective uptake and degradation of proteins by lysosomes. *Science,* 273, 501-3.

DE PAIVA, A., MEUNIER, F. A., MOLGO, J., AOKI, K. R. & DOLLY, J. O. (1999) Functional repair of motor endplates after botulinum neurotoxin type A poisoning: biphasic switch of synaptic activity between nerve sprouts and their parent terminals. *Proc Natl Acad Sci U S A,* 96, 3200-5.

DE VOS, K. J., CHAPMAN, A. L., TENNANT, M. E., MANSER, C., TUDOR, E. L., LAU, K. F., BROWNLEES, J., ACKERLEY, S., SHAW, P. J., MCLOUGHLIN, D. M., SHAW, C. E., LEIGH, P. N., MILLER, C. C. & GRIERSON, A. J. (2007) Familial amyotrophic lateral sclerosis-linked SOD1 mutants perturb fast axonal transport to reduce axonal mitochondria content. *Hum Mol Genet,* 16, 2720-8.

DE VOS, K. J., GRIERSON, A. J., ACKERLEY, S. & MILLER, C. C. (2008) Role of axonal transport in neurodegenerative diseases. *Annu Rev Neurosci,* 31, 151-73.

DEBERNARDO, A. P. & CHANG, S. (1995) Native and recombinant DM-GRASP selectively support neurite extension from neurons that express GRASP. *Dev Biol,* 169, 65-75.

DEBERNARDO, A. P. & CHANG, S. (1996) Heterophilic interactions of DM-GRASP: GRASP-NgCAM interactions involved in neurite extension. *J Cell Biol,* 133, 657-66.

DEINHARDT, K., BERNINGHAUSEN, O., WILLISON, H. J., HOPKINS, C. R. & SCHIAVO, G. (2006a) Tetanus toxin is internalized by a sequential clathrin-dependent mechanism initiated within lipid microdomains and independent of epsin1. *J Cell Biol,* 174, 459-71.

DEINHARDT, K., REVERSI, A., BERNINGHAUSEN, O., HOPKINS, C. R. & SCHIAVO, G. (2007) Neurotrophins Redirect p75NTR from a clathrin-independent to a clathrin-dependent endocytic pathway coupled to axonal transport. *Traffic,* 8, 1736-49.

DEINHARDT, K., SALINAS, S., VERASTEGUI, C., WATSON, R., WORTH, D., HANRAHAN, S., BUCCI, C. & SCHIAVO, G. (2006b) Rab5 and Rab7 control endocytic sorting along the axonal retrograde transport pathway. *Neuron,* 52, 293-305.

DIAZ-RODRIGUEZ, E., CABRERA, N., ESPARIS-OGANDO, A., MONTERO, J. C. & PANDIELLA, A. (1999) Cleavage of the TrkA neurotrophin receptor by multiple metalloproteases generates signalling-competent truncated forms. *Eur J Neurosci,* 11, 1421-30.

DIEKMANN, H. & STUERMER, C. A. (2009) Zebrafish neurolin-a and -b, orthologs of ALCAM, are involved in retinal ganglion cell differentiation and retinal axon pathfinding. *J Comp Neurol,* 513, 38-50.

DIESTEL, S., SCHAEFER, D., CREMER, H. & SCHMITZ, B. (2007) NCAM is ubiquitylated, endocytosed and recycled in neurons. *J Cell Sci,* 120, 4035-49.

DILLON, A. K., FUJITA, S. C., MATISE, M. P., JARJOUR, A. A., KENNEDY, T. E., KOLLMUS, H., ARNOLD, H. H., WEINER, J. A., SANES, J. R. & KAPRIELIAN, Z. (2005) Molecular control of spinal accessory motor neuron/axon development in the mouse spinal cord. *J Neurosci,* 25, 10119-30.

DODGE, J. C., TRELEAVEN, C. M., FIDLER, J. A., HESTER, M., HAIDET, A., HANDY, C., RAO, M., EAGLE, A., MATTHEWS, J. C., TAKSIR, T. V., CHENG, S. H., SHIHABUDDIN, L. S. & KASPAR, B. K. (2010) AAV4-mediated Expression of IGF-1 and VEGF Within Cellular Components of the Ventricular System Improves Survival Outcome in Familial ALS Mice. *Mol Ther,* 18, 2075-84.

EL-KADI, A. M., BROS-FACER, V., DENG, W., PHILPOTT, A., STODDART, E., BANKS, G., JACKSON, G. S., FISHER, E. M., DUCHEN, M. R., GREENSMITH, L., MOORE, A. L. & HAFEZPARAST, M. (2010) The legs at odd angles (Loa) mutation in cytoplasmic dynein ameliorates mitochondrial function in SOD1G93A mouse model for motor neuron disease. *J Biol Chem,* 285, 18627-39.

FOURNIER-THIBAULT, C., POURQUIE, O., ROUAUD, T. & LE DOUARIN, N. M. (1999) BEN/SC1/DM-GRASP expression during neuromuscular development: a cell adhesion molecule regulated by innervation. *J Neurosci,* 19, 1382-92.

GIL, C., CHAIB-OUKADOUR, I. & AGUILERA, J. (2003) C-terminal fragment of tetanus toxin heavy chain activates Akt and MEK/ERK signalling pathways in a Trk receptor-dependent manner in cultured cortical neurons. *Biochem J,* 373, 613-20.

GIL, C., CUBI, R. & AGUILERA, J. (2007) Shedding of the p75NTR neurotrophin receptor is modulated by lipid rafts. *FEBS Lett,* 581, 1851-8.

GIMFERRER, I., CALVO, M., MITTELBRUNN, M., FARNOS, M., SARRIAS, M. R., ENRICH, C., VIVES, J., SANCHEZ-MADRID, F. & LOZANO, F. (2004) Relevance of CD6-mediated interactions in T cell activation and proliferation. *J Immunol,* 173, 2262-70.

GUNAWARDENA, S., HER, L. S., BRUSCH, R. G., LAYMON, R. A., NIESMAN, I. R., GORDESKY-GOLD, B., SINTASATH, L., BONINI, N. M. & GOLDSTEIN, L. S. (2003) Disruption of axonal transport by loss of huntingtin or expression of pathogenic polyQ proteins in Drosophila. *Neuron,* 40, 25-40.

GURSKAYA, N. G., VERKHUSHA, V. V., SHCHEGLOV, A. S., STAROVEROV, D. B., CHEPURNYKH, T. V., FRADKOV, A. F., LUKYANOV, S. & LUKYANOV, K. A. (2006) Engineering of a monomeric green-to-red photoactivatable fluorescent protein induced by blue light. *Nat Biotechnol,* 24, 461-5.

HAFEZPARAST, M., KLOCKE, R., RUHRBERG, C., MARQUARDT, A., AHMAD-ANNUAR, A., BOWEN, S., LALLI, G., WITHERDEN, A. S., HUMMERICH, H., NICHOLSON, S., MORGAN, P. J., OOZAGEER, R., PRIESTLEY, J. V., AVERILL, S., KING, V. R., BALL, S., PETERS, J., TODA, T., YAMAMOTO, A., HIRAOKA, Y., AUGUSTIN, M., KORTHAUS, D., WATTLER, S., WABNITZ, P., DICKNEITE, C., LAMPEL, S., BOEHME, F., PERAUS, G., POPP, A., RUDELIUS, M., SCHLEGEL, J., FUCHS, H., HRABE DE ANGELIS, M., SCHIAVO, G., SHIMA, D. T., RUSS, A. P., STUMM, G., MARTIN, J. E. & FISHER, E. M. (2003) Mutations in dynein link motor neuron degeneration to defects in retrograde transport. *Science,* 300, 808-12.

HANZ, S. & FAINZILBER, M. (2006) Retrograde signaling in injured nerve--the axon reaction revisited. *J Neurochem,* 99, 13-9.

HASSAN, N. J., BARCLAY, A. N. & BROWN, M. H. (2004) Frontline: Optimal T cell activation requires the engagement of CD6 and CD166. *Eur J Immunol,* 34, 930-40.

HENDRY, I. A., STOCKEL, K., THOENEN, H. & IVERSEN, L. L. (1974) The retrograde axonal transport of nerve growth factor. *Brain Res,* 68, 103-21.

HER, L. S. & GOLDSTEIN, L. S. (2008) Enhanced sensitivity of striatal neurons to axonal transport defects induced by mutant huntingtin. *J Neurosci,* 28, 13662-72.

HERREROS, J., LALLI, G., MONTECUCCO, C. & SCHIAVO, G. (2000) Tetanus toxin fragment C binds to a protein present in neuronal cell lines and motoneurons. *J Neurochem,* 74, 1941-50.

HEUMANN, R., SCHWAB, M. & THOENEN, H. (1981) A second messenger required for nerve growth factor biological activity? *Nature,* 292, 838-40.

HINKLE, C. L., DIESTEL, S., LIEBERMAN, J. & MANESS, P. F. (2006) Metalloprotease-induced ectodomain shedding of neural cell adhesion molecule (NCAM). *J Neurobiol,* 66, 1378-95.

HUBSCHMANN, M. V., SKLADCHIKOVA, G., BOCK, E. & BEREZIN, V. (2005) Neural cell adhesion molecule function is regulated by metalloproteinase-mediated ectodomain release. *J Neurosci Res,* 80, 826-37.

IBANEZ, C. F. (2007) Message in a bottle: long-range retrograde signaling in the nervous system. *Trends Cell Biol,* 17, 519-28.

ICHIKAWA, N., IWABUCHI, K., KURIHARA, H., ISHII, K., KOBAYASHI, T., SASAKI, T., HATTORI, N., MIZUNO, Y., HOZUMI, K., YAMADA, Y. & ARIKAWA-HIRASAWA, E. (2009) Binding of laminin-1 to monosialoganglioside GM1 in lipid rafts is crucial for neurite outgrowth. *J Cell Sci,* 122, 289-99.

IKEDA, K. & QUERTERMOUS, T. (2004) Molecular isolation and characterization of a soluble isoform of activated leukocyte cell adhesion molecule that modulates endothelial cell function. *J Biol Chem,* 279, 55315-23.

IVASKA, J. & HEINO, J. (2010) Interplay between cell adhesion and growth factor receptors: from the plasma membrane to the endosomes. *Cell Tissue Res,* 339, 111-20.

KAMIGUCHI, H. & LEMMON, V. (2000) IgCAMs: bidirectional signals underlying neurite growth. *Curr Opin Cell Biol,* 12, 598-605.

KAMIGUCHI, H., LONG, K. E., PENDERGAST, M., SCHAEFER, A. W., RAPOPORT, I., KIRCHHAUSEN, T. & LEMMON, V. (1998) The neural cell adhesion molecule L1 interacts with the AP-2 adaptor and is endocytosed via the clathrin-mediated pathway. *J Neurosci,* 18, 5311-21.

KAWAUCHI, D., KOBAYASHI, H., SEKINE-AIZAWA, Y., FUJITA, S. C. & MURAKAMI, F. (2003) MuSC is involved in regulating axonal fasciculation of mouse primary vestibular afferents. *Eur J Neurosci,* 18, 2244-52.

KIERAN, D., HAFEZPARAST, M., BOHNERT, S., DICK, J. R., MARTIN, J., SCHIAVO, G., FISHER, E. M. & GREENSMITH, L. (2005) A mutation in dynein rescues axonal transport defects and extends the life span of ALS mice. *J Cell Biol,* 169, 561-7.

KING, J., SYKLAWER, E., CHEN, H., RESMONDO, J., MCDONALD, F., STEVENS, T., SHEVDE, L., OFORI-ACQUAH, S., MOORE, T. & BAUER, N. (2008) Lung Endothelial Cells Express ALCAM on Released Exosomes/Microparticles. *Microsc Microanal 14(Suppl 2),,* 14, 1520-1521.

KLESSE, L. J. & PARADA, L. F. (1999) Trks: signal transduction and intracellular pathways. *Microsc Res Tech,* 45, 210-6.

KOMATSU, M., WAGURI, S., CHIBA, T., MURATA, S., IWATA, J., TANIDA, I., UENO, T., KOIKE, M., UCHIYAMA, Y., KOMINAMI, E. & TANAKA, K. (2006) Loss of autophagy in the central nervous system causes neurodegeneration in mice. *Nature,* 441, 880-4.

LALLI, G., BOHNERT, S., DEINHARDT, K., VERASTEGUI, C. & SCHIAVO, G. (2003a) The journey of tetanus and botulinum neurotoxins in neurons. *Trends Microbiol,* 11, 431-7.

LALLI, G., GSCHMEISSNER, S. & SCHIAVO, G. (2003b) Myosin Va and microtubule-based motors are required for fast axonal retrograde transport of tetanus toxin in motor neurons. *J Cell Sci,* 116, 4639-50.

LALLI, G. & SCHIAVO, G. (2002) Analysis of retrograde transport in motor neurons reveals common endocytic carriers for tetanus toxin and neurotrophin receptor p75NTR. *J Cell Biol,* 156, 233-9.

LAMONTE, B. H., WALLACE, K. E., HOLLOWAY, B. A., SHELLY, S. S., ASCANO, J., TOKITO, M., VAN WINKLE, T., HOWLAND, D. S. & HOLZBAUR, E. L. (2002) Disruption of dynein/dynactin inhibits axonal transport in motor neurons causing late-onset progressive degeneration. *Neuron,* 34, 715-27.

LEVI-MONTALCINI, R. & HAMBURGER, V. (1951) Selective growth stimulating effects of mouse sarcoma on the sensory and sympathetic nervous system of the chick embryo. *J Exp Zool,* 116, 321-61.

LIEBEROTH, A., SPLITTSTOESSER, F., KATAGIHALLIMATH, N., JAKOVCEVSKI, I., LOERS, G., RANSCHT, B., KARAGOGEOS, D., SCHACHNER, M. & KLEENE, R. (2009) Lewis(x) and alpha2,3-sialyl glycans and their receptors TAG-1, Contactin, and L1 mediate CD24-dependent neurite outgrowth. *J Neurosci,* 29, 6677-90.

LIMPERT, A. S., KARLO, J. C. & LANDRETH, G. E. (2007) Nerve growth factor stimulates the concentration of TrkA within lipid rafts and extracellular signal-regulated kinase activation through c-Cbl-associated protein. *Mol Cell Biol,* 27, 5686-98.

LUNTER, P. C., VAN KILSDONK, J. W., VAN BEEK, H., CORNELISSEN, I. M., BERGERS, M., WILLEMS, P. H., VAN MUIJEN, G. N. & SWART, G. W. (2005) Activated leukocyte cell adhesion molecule (ALCAM/CD166/MEMD), a novel actor in invasive growth, controls matrix metalloproteinase activity. *Cancer Res,* 65, 8801-8.

MADORE, N., SMITH, K. L., GRAHAM, C. H., JEN, A., BRADY, K., HALL, S. & MORRIS, R. (1999) Functionally different GPI proteins are organized in different domains on the neuronal surface. *EMBO J,* 18, 6917-26.

MANESS, P. F. & SCHACHNER, M. (2007) Neural recognition molecules of the immunoglobulin superfamily: signaling transducers of axon guidance and neuronal migration. *Nat Neurosci,* 10, 19-26.

MARETZKY, T., SCHULTE, M., LUDWIG, A., ROSE-JOHN, S., BLOBEL, C., HARTMANN, D., ALTEVOGT, P., SAFTIG, P. & REISS, K. (2005) L1 is sequentially processed by two differently activated metalloproteases and presenilin/gamma-secretase and regulates neural cell adhesion, cell migration, and neurite outgrowth. *Mol Cell Biol,* 25, 9040-53.

MATTEOLI, M., TAKEI, K., PERIN, M. S., SUDHOF, T. C. & DE CAMILLI, P. (1992) Exo-endocytotic recycling of synaptic vesicles in developing processes of cultured hippocampal neurons. *J Cell Biol,* 117, 849-61.

MECHTERSHEIMER, S., GUTWEIN, P., AGMON-LEVIN, N., STOECK, A., OLESZEWSKI, M., RIEDLE, S., POSTINA, R., FAHRENHOLZ, F., FOGEL, M., LEMMON, V. & ALTEVOGT, P. (2001) Ectodomain shedding of L1 adhesion molecule promotes cell migration by autocrine binding to integrins. *J Cell Biol,* 155, 661-73.

MOISES, T., DREIER, A., FLOHR, S., ESSER, M., BRAUERS, E., REISS, K., MERKEN, D., WEIS, J. & KRUTTGEN, A. (2007) Tracking TrkA's trafficking: NGF receptor trafficking controls NGF receptor signaling. *Mol Neurobiol,* 35, 151-9.

MOSCOSO, L. M., CREMER, H. & SANES, J. R. (1998) Organization and reorganization of neuromuscular junctions in mice lacking neural cell

adhesion molecule, tenascin-C, or fibroblast growth factor-5. *J Neurosci,* 18, 1465-77.

NAMBA, T., NAKAMURA, T. & GROB, D. (1967) Staining for nerve fiber and cholinesterase activity in fresh frozen sections. *Am J Clin Pathol,* 47, 74-7.

NEIIENDAM, J. L., KOHLER, L. B., CHRISTENSEN, C., LI, S., PEDERSEN, M. V., DITLEVSEN, D. K., KORNUM, M. K., KISELYOV, V. V., BEREZIN, V. & BOCK, E. (2004) An NCAM-derived FGF-receptor agonist, the FGL-peptide, induces neurite outgrowth and neuronal survival in primary rat neurons. *J Neurochem,* 91, 920-35.

NELISSEN, J. M., PETERS, I. M., DE GROOTH, B. G., VAN KOOYK, Y. & FIGDOR, C. G. (2000) Dynamic regulation of activated leukocyte cell adhesion molecule-mediated homotypic cell adhesion through the actin cytoskeleton. *Mol Biol Cell,* 11, 2057-68.

NG, E. L. & TANG, B. L. (2008) Rab GTPases and their roles in brain neurons and glia. *Brain Res Rev,* 58, 236-46.

NG, Y. P., WU, Z., WISE, H., TSIM, K. W., WONG, Y. H. & IP, N. Y. (2009) Differential and synergistic effect of nerve growth factor and cAMP on the regulation of early response genes during neuronal differentiation. *Neurosignals,* 17, 111-20.

NISHIMUNE, H., VALDEZ, G., JARAD, G., MOULSON, C. L., MULLER, U., MINER, J. H. & SANES, J. R. (2008) Laminins promote postsynaptic maturation by an autocrine mechanism at the neuromuscular junction. *J Cell Biol,* 182, 1201-15.

NUTI, E., CASALINI, F., AVRAMOVA, S. I., SANTAMARIA, S., FABBI, M., FERRINI, S., MARINELLI, L., LA PIETRA, V., LIMONGELLI, V., NOVELLINO, E., CERCIGNANI, G., ORLANDINI, E., NENCETTI, S. & ROSSELLO, A. (2010) Potent arylsulfonamide inhibitors of tumor necrosis factor-alpha converting enzyme able to reduce activated leukocyte cell adhesion molecule shedding in cancer cell models. *J Med Chem,* 53, 2622-35.

OFORI-ACQUAH, S. F. & KING, J. A. (2008) Activated leukocyte cell adhesion molecule: a new paradox in cancer. *Transl Res,* 151, 122-8.

OMURA, T., OMURA, K., SANO, M., SAWADA, T., HASEGAWA, T. & NAGANO, A. (2005) Spatiotemporal quantification of recruit and resident macrophages after crush nerve injury utilizing immunohistochemistry. *Brain Res,* 1057, 29-36.

OTT, H., DIEKMANN, H., STUERMER, C. A. & BASTMEYER, M. (2001) Function of Neurolin (DM-GRASP/SC-1) in guidance of motor axons during zebrafish development. *Dev Biol,* 235, 86-97.

PARATCHA, G., LEDDA, F. & IBANEZ, C. F. (2003) The neural cell adhesion molecule NCAM is an alternative signaling receptor for GDNF family ligands. *Cell,* 113, 867-79.

PARK, J. W., VAHIDI, B., TAYLOR, A. M., RHEE, S. W. & JEON, N. L. (2006) Microfluidic culture platform for neuroscience research. *Nat Protoc,* 1, 2128-36.

PELLINEN, T., ARJONEN, A., VUORILUOTO, K., KALLIO, K., FRANSEN, J. A. & IVASKA, J. (2006) Small GTPase Rab21 regulates cell adhesion and controls endosomal traffic of beta1-integrins. *J Cell Biol,* 173, 767-80.

PERLSON, E., JEONG, G. B., ROSS, J. L., DIXIT, R., WALLACE, K. E., KALB, R. G. & HOLZBAUR, E. L. (2009) A switch in retrograde signaling from survival to stress in rapid-onset neurodegeneration. *J Neurosci,* 29, 9903-17.

PERLSON, E., MADAY, S., FU, M. M., MOUGHAMIAN, A. J. & HOLZBAUR, E. L. (2010) Retrograde axonal transport: pathways to cell death? *Trends Neurosci,* 33, 335-44.

PIAZZA, T., CHA, E., BONGARZONE, I., CANEVARI, S., BOLOGNESI, A., POLITO, L., BARGELLESI, A., SASSI, F., FERRINI, S. & FABBI, M. (2005) Internalization and recycling of ALCAM/CD166 detected by a fully human single-chain recombinant antibody. *J Cell Sci,* 118, 1515-25.

POLO-PARADA, L., BOSE, C. M. & LANDMESSER, L. T. (2001) Alterations in transmission, vesicle dynamics, and transmitter release machinery at NCAM-deficient neuromuscular junctions. *Neuron,* 32, 815-28.

POURQUIE, O., CORBEL, C., LE CAER, J. P., ROSSIER, J. & LE DOUARIN, N. M. (1992) BEN, a surface glycoprotein of the immunoglobulin superfamily, is expressed in a variety of developing systems. *Proc Natl Acad Sci U S A,* 89, 5261-5.

PULS, I., OH, S. J., SUMNER, C. J., WALLACE, K. E., FLOETER, M. K., MANN, E. A., KENNEDY, W. R., WENDELSCHAFER-CRABB, G., VORTMEYER, A., POWERS, R., FINNEGAN, K., HOLZBAUR, E. L., FISCHBECK, K. H. & LUDLOW, C. L. (2005) Distal spinal and bulbar muscular atrophy caused by dynactin mutation. *Ann Neurol,* 57, 687-94.

RIND, H. B., BUTOWT, R. & VON BARTHELD, C. S. (2005) Synaptic targeting of retrogradely transported trophic factors in motoneurons: comparison of glial cell line-derived neurotrophic factor, brain-derived neurotrophic factor, and cardiotrophin-1 with tetanus toxin. *J Neurosci,* 25, 539-49.

ROSSO, O., PIAZZA, T., BONGARZONE, I., ROSSELLO, A., MEZZANZANICA, D., CANEVARI, S., ORENGO, A. M., PUPPO, A., FERRINI, S. & FABBI, M. (2007) The ALCAM shedding by the metalloprotease ADAM17/TACE is involved in motility of ovarian carcinoma cells. *Mol Cancer Res,* 5, 1246-53.

SAFFELL, J. L., WILLIAMS, E. J., MASON, I. J., WALSH, F. S. & DOHERTY, P. (1997) Expression of a dominant negative FGF receptor inhibits axonal growth and FGF receptor phosphorylation stimulated by CAMs. *Neuron,* 18, 231-42.

SALINAS, S., BILSLAND, L. G., HENAFF, D., WESTON, A. E., KERIEL, A., SCHIAVO, G. & KREMER, E. J. (2009) CAR-associated vesicular transport of an adenovirus in motor neuron axons. *PLoS Pathog,* 5, e1000442.

SALINAS, S., BILSLAND, L. G. & SCHIAVO, G. (2008) Molecular landmarks along the axonal route: axonal transport in health and disease. *Curr Opin Cell Biol,* 20, 445-53.

SALINAS, S., SCHIAVO, G. & KREMER, E. J. (2010) A hitchhiker's guide to the nervous system: the complex journey of viruses and toxins. *Nat Rev Microbiol,* 8, 645-55.

SARRIAS, M. R., FARNOS, M., MOTA, R., SANCHEZ-BARBERO, F., IBANEZ, A., GIMFERRER, I., VERA, J., FENUTRIA, R., CASALS, C., YELAMOS, J. & LOZANO, F. (2007) CD6 binds to pathogen-associated molecular patterns and protects from LPS-induced septic shock. *Proc Natl Acad Sci U S A,* 104, 11724-9.

SATO, C., MATSUDA, T. & KITAJIMA, K. (2002) Neuronal differentiation-dependent expression of the disialic acid epitope on CD166 and its involvement in neurite formation in Neuro2A cells. *J Biol Chem,* 277, 45299-305.

SAXENA, S., BUCCI, C., WEIS, J. & KRUTTGEN, A. (2005) The small GTPase Rab7 controls the endosomal trafficking and neuritogenic signaling of the nerve growth factor receptor TrkA. *J Neurosci,* 25, 10930-40.

SCHAEFER, A. W., KAMEI, Y., KAMIGUCHI, H., WONG, E. V., RAPOPORT, I., KIRCHHAUSEN, T., BEACH, C. M., LANDRETH, G., LEMMON, S. K. & LEMMON, V. (2002) L1 endocytosis is controlled by a phosphorylation-dephosphorylation cycle stimulated by outside-in signaling by L1. *J Cell Biol,* 157, 1223-32.

SCHECTERSON, L. C. & BOTHWELL, M. (2010) Neurotrophin receptors: Old friends with new partners. *Dev Neurobiol,* 70, 332-8.

SCHMID, R. S. & MANESS, P. F. (2008) L1 and NCAM adhesion molecules as signaling coreceptors in neuronal migration and process outgrowth. *Curr Opin Neurobiol*.

SEAMAN, M. N. (2004) Cargo-selective endosomal sorting for retrieval to the Golgi requires retromer. *J Cell Biol,* 165, 111-22.

SEKINE-AIZAWA, Y., OMORI, A. & FUJITA, S. C. (1998) MuSC, a novel member of the immunoglobulin superfamily, is expressed in neurons of a subset of cranial sensory ganglia in the mouse embryo. *Eur J Neurosci,* 10, 2810-24.

SIGNORET, N., OLDRIDGE, J., PELCHEN-MATTHEWS, A., KLASSE, P. J., TRAN, T., BRASS, L. F., ROSENKILDE, M. M., SCHWARTZ, T. W., HOLMES, W., DALLAS, W., LUTHER, M. A., WELLS, T. N., HOXIE, J. A. & MARSH, M. (1997) Phorbol esters and SDF-1 induce rapid endocytosis and down modulation of the chemokine receptor CXCR4. *J Cell Biol,* 139, 651-64.

SILLETTI, S., MEI, F., SHEPPARD, D. & MONTGOMERY, A. M. (2000) Plasmin-sensitive dibasic sequences in the third fibronectin-like domain of L1-cell adhesion molecule (CAM) facilitate homomultimerization and concomitant integrin recruitment. *J Cell Biol,* 149, 1485-502.

SILLETTI, S., YEBRA, M., PEREZ, B., CIRULLI, V., MCMAHON, M. & MONTGOMERY, A. M. (2004) Extracellular signal-regulated kinase (ERK)-dependent gene expression contributes to L1 cell adhesion molecule-dependent motility and invasion. *J Biol Chem,* 279, 28880-8.

SKONIER, J. E., BOWEN, M. A., ARUFFO, A. & BAJORATH, J. (1997) CD6 recognizes the neural adhesion molecule BEN. *Protein Sci,* 6, 1768-70.

STOECK, A., KELLER, S., RIEDLE, S., SANDERSON, M. P., RUNZ, S., LE NAOUR, F., GUTWEIN, P., LUDWIG, A., RUBINSTEIN, E. & ALTEVOGT, P. (2006) A role for exosomes in the constitutive and stimulus-induced ectodomain cleavage of L1 and CD44. *Biochem J,* 393, 609-18.

SWART, G. W. (2002) Activated leukocyte cell adhesion molecule (CD166/ALCAM): developmental and mechanistic aspects of cell clustering and cell migration. *Eur J Cell Biol,* 81, 313-21.

SWART, G. W., LUNTER, P. C., KILSDONK, J. W. & KEMPEN, L. C. (2005) Activated leukocyte cell adhesion molecule (ALCAM/CD166): signaling at the divide of melanoma cell clustering and cell migration? *Cancer Metastasis Rev,* 24, 223-36.

TARENTINO, A. L., GOMEZ, C. M. & PLUMMER, T. H., JR. (1985) Deglycosylation of asparagine-linked glycans by peptide:N-glycosidase F. *Biochemistry,* 24, 4665-71.

TE RIET, J., ZIMMERMAN, A. W., CAMBI, A., JOOSTEN, B., SPELLER, S., TORENSMA, R., VAN LEEUWEN, F. N., FIGDOR, C. G. & DE LANGE, F. (2007) Distinct kinetic and mechanical properties govern ALCAM-mediated interactions as shown by single-molecule force spectroscopy. *J Cell Sci,* 120, 3965-76.

THELEN, K., GEORG, T., BERTUCH, S., ZELINA, P. & POLLERBERG, G. E. (2008) Ubiquitination and endocytosis of cell adhesion molecule DM-GRASP regulate its cell surface presence and affect its role for axon navigation. *J Biol Chem,* 283, 32792-801.

THOENEN, H. & SENDTNER, M. (2002) Neurotrophins: from enthusiastic expectations through sobering experiences to rational therapeutic approaches. *Nat Neurosci,* 5 Suppl, 1046-50.

URRA, S., ESCUDERO, C. A., RAMOS, P., LISBONA, F., ALLENDE, E., COVARRUBIAS, P., PARRAGUEZ, J. I., ZAMPIERI, N., CHAO, M. V., ANNAERT, W. & BRONFMAN, F. C. (2007) TrkA receptor activation by nerve growth factor induces shedding of the p75 neurotrophin receptor followed by endosomal gamma-secretase-mediated release of the p75 intracellular domain. *J Biol Chem,* 282, 7606-15.

VAN KEMPEN, L. C., MEIER, F., EGEBLAD, M., KERSTEN-NIESSEN, M. J., GARBE, C., WEIDLE, U. H., VAN MUIJEN, G. N., HERLYN, M., BLOEMERS, H. P. & SWART, G. W. (2004) Truncation of activated leukocyte cell adhesion molecule: a gateway to melanoma metastasis. *J Invest Dermatol,* 122, 1293-301.

VAN KEMPEN, L. C., NELISSEN, J. M., DEGEN, W. G., TORENSMA, R., WEIDLE, U. H., BLOEMERS, H. P., FIGDOR, C. G. & SWART, G. W. (2001) Molecular basis for the homophilic activated leukocyte cell adhesion molecule (ALCAM)-ALCAM interaction. *J Biol Chem,* 276, 25783-90.

VAN KILSDONK, J. W., WILTING, R. H., BERGERS, M., VAN MUIJEN, G. N., SCHALKWIJK, J., VAN KEMPEN, L. C. & SWART, G. W. (2008) Attenuation of melanoma invasion by a secreted variant of activated leukocyte cell adhesion molecule. *Cancer Res,* 68, 3671-9.

VERDINO, P., WITHERDEN, D. A., HAVRAN, W. L. & WILSON, I. A. (2010) The molecular interaction of CAR and JAML recruits the central cell signal transducer PI3K. *Science,* 329, 1210-4.

VERHOEVEN, K., DE JONGHE, P., COEN, K., VERPOORTEN, N., AUER-GRUMBACH, M., KWON, J. M., FITZPATRICK, D., SCHMEDDING, E., DE VRIENDT, E., JACOBS, A., VAN GERWEN, V., WAGNER, K., HARTUNG, H. P. & TIMMERMAN, V. (2003) Mutations in the small GTP-ase late endosomal protein RAB7 cause Charcot-Marie-Tooth type 2B neuropathy. *Am J Hum Genet,* 72, 722-7.

VILAR, M., CHARALAMPOPOULOS, I., KENCHAPPA, R. S., SIMI, A., KARACA, E., REVERSI, A., CHOI, S., BOTHWELL, M., MINGARRO, I., FRIEDMAN, W. J., SCHIAVO, G., BASTIAENS, P. I., VERVEER, P. J., CARTER, B. D. & IBANEZ, C. F. (2009) Activation of the p75 neurotrophin receptor through conformational rearrangement of disulphide-linked receptor dimers. *Neuron,* 62, 72-83.

VON BARTHELD, C. S. (2004) Axonal transport and neuronal transcytosis of trophic factors, tracers, and pathogens. *J Neurobiol,* 58, 295-314.

WATSON, F. L., HEERSSEN, H. M., BHATTACHARYYA, A., KLESSE, L., LIN, M. Z. & SEGAL, R. A. (2001) Neurotrophins use the Erk5 pathway to mediate a retrograde survival response. *Nat Neurosci,* 4, 981-8.

WATSON, F. L., HEERSSEN, H. M., MOHEBAN, D. B., LIN, M. Z., SAUVAGEOT, C. M., BHATTACHARYYA, A., POMEROY, S. L. & SEGAL, R. A. (1999) Rapid nuclear responses to target-derived neurotrophins require retrograde transport of ligand-receptor complex. *J Neurosci,* 19, 7889-900.

WEINER, J. A., KOO, S. J., NICOLAS, S., FRABOULET, S., PFAFF, S. L., POURQUIE, O. & SANES, J. R. (2004) Axon fasciculation defects and retinal dysplasias in mice lacking the immunoglobulin superfamily adhesion molecule BEN/ALCAM/SC1. *Mol Cell Neurosci,* 27, 59-69.

WHITTARD, J. D., SAKURAI, T., CASSELLA, M. R., GAZDOIU, M. & FELSENFELD, D. P. (2006) MAP kinase pathway-dependent phosphorylation of the L1-

CAM ankyrin binding site regulates neuronal growth. *Mol Biol Cell,* 17, 2696-706.

WIENCKEN-BARGER, A. E., MAVITY-HUDSON, J., BARTSCH, U., SCHACHNER, M. & CASAGRANDE, V. A. (2004) The role of L1 in axon pathfinding and fasciculation. *Cereb Cortex,* 14, 121-31.

WILLIAMSON, T. L. & CLEVELAND, D. W. (1999) Slowing of axonal transport is a very early event in the toxicity of ALS-linked SOD1 mutants to motor neurons. *Nat Neurosci,* 2, 50-6.

WISCO, D., ANDERSON, E. D., CHANG, M. C., NORDEN, C., BOIKO, T., FOLSCH, H. & WINCKLER, B. (2003) Uncovering multiple axonal targeting pathways in hippocampal neurons. *J Cell Biol,* 162, 1317-28.

WITHERDEN, D. A., VERDINO, P., RIEDER, S. E., GARIJO, O., MILLS, R. E., TEYTON, L., FISCHER, W. H., WILSON, I. A. & HAVRAN, W. L. (2010) The junctional adhesion molecule JAML is a costimulatory receptor for epithelial gammadelta T cell activation. *Science,* 329, 1205-10.

XIA, C. H., ROBERTS, E. A., HER, L. S., LIU, X., WILLIAMS, D. S., CLEVELAND, D. W. & GOLDSTEIN, L. S. (2003) Abnormal neurofilament transport caused by targeted disruption of neuronal kinesin heavy chain KIF5A. *J Cell Biol,* 161, 55-66.

YAP, C. C., WISCO, D., KUJALA, P., LASIECKA, Z. M., CANNON, J. T., CHANG, M. C., HIRLING, H., KLUMPERMAN, J. & WINCKLER, B. (2008) The somatodendritic endosomal regulator NEEP21 facilitates axonal targeting of L1/NgCAM. *J Cell Biol,* 180, 827-42.

YE, H., KURUVILLA, R., ZWEIFEL, L. S. & GINTY, D. D. (2003) Evidence in support of signaling endosome-based retrograde survival of sympathetic neurons. *Neuron,* 39, 57-68.

ZHANG, Y., MOHEBAN, D. B., CONWAY, B. R., BHATTACHARYYA, A. & SEGAL, R. A. (2000) Cell surface Trk receptors mediate NGF-induced survival while internalized receptors regulate NGF-induced differentiation. *J Neurosci,* 20, 5671-8.

ZHAO, C., TAKITA, J., TANAKA, Y., SETOU, M., NAKAGAWA, T., TAKEDA, S., YANG, H. W., TERADA, S., NAKATA, T., TAKEI, Y., SAITO, M., TSUJI, S., HAYASHI, Y. & HIROKAWA, N. (2001) Charcot-Marie-Tooth disease type 2A caused by mutation in a microtubule motor KIF1Bbeta. *Cell,* 105, 587-97.

ZIMMERMAN, A. W., JOOSTEN, B., TORENSMA, R., PARNES, J. R., VAN LEEUWEN, F. N. & FIGDOR, C. G. (2006) Long-term engagement of CD6 and ALCAM is essential for T-cell proliferation induced by dendritic cells. *Blood,* 107, 3212-20.

ZIMMERMAN, A. W., NELISSEN, J. M., VAN EMST-DE VRIES, S. E., WILLEMS, P. H., DE LANGE, F., COLLARD, J. G., VAN LEEUWEN, F. N. & FIGDOR, C. G. (2004) Cytoskeletal restraints regulate homotypic ALCAM-mediated

adhesion through PKCalpha independently of Rho-like GTPases. *J Cell Sci,* 117, 2841-52.

ZWEIFEL, L. S., KURUVILLA, R. & GINTY, D. D. (2005) Functions and mechanisms of retrograde neurotrophin signalling. *Nat Rev Neurosci,* 6, 615-25.